CARDIFF UNIVERSITY

Investigating the Effects of Processing, Morphology and Functionalisation on the Properties of Epoxy Nanocomposites

Perminder Sangha
Doctor of Philosophy

Mechanics, Materials and Advanced Manufacturing Engineering
School of Engineering

2021

Summary

The exceptional mechanical properties of graphene make it an attractive choice for use in composite materials. In order to achieve optimised mechanical performance, good graphene dispersion and interfacial interactions between graphene and matrix must be achieved. As graphene has a tendency to preferentially interact with itself and form into agglomerates which are not bonded with the matrix material, leaving the production of good quality graphene nanocomposites challenging. This industrially led project performed in conjunction with Haydale Ltd, aims to further understand this behaviour and how processing parameters can be used to optimise overall properties.

Plasma-functionalisation, performed through bespoke plasma treatment HDPlas®, has been utilised to attach chemically reactive, oxygen-based functional groups to the surface of the studied graphene. This has been performed at varied intensities to understand the improvement to both interfacial bonding and dispersion of graphene within epoxy resin. Dispersion state has been further examined through investigation of various high-shear mixing methods and durations, and changes have been correlated to mechanical performance with tensile and flexural tests. A range of methods to characterise dispersion state have been explored to assess the efficacy of each method and suitability of use as a quality control process. Furthermore, DMA analysis has been employed to understand the effect of graphene, functionalisation and dispersion state on the cure behaviour and thermomechanical properties of the produced graphene / epoxy composite. The relationship between all of these factors has been assessed to produce an optimised mixing and manufacturing procedure.

Investigations into the ‘shelf-life’ of dispersion state have also been performed, in order to assess any re-agglomeration behaviour after mixing. The use of various storage conditions have been investigated to assess the ability to preserve dispersion state.

This work has shown a strong correlation between manufacturing parameters, dispersion state and mechanical properties and proposing an effective numerical method of predicting de-agglomeration. A full review of quality control methods determined macroscale techniques, which are easily incorporated into production lines, can successfully demonstrate dispersion state. The presence of functionalisation has been proven to improve mechanical properties and aid dispersion. The presence of graphene has been shown to alter the epoxy curing process, negatively impacting thermomechanical properties. Finally, storing materials at low temperatures was found to be most effective at preserving dispersion state.

Table of Contents

Table of Figures

Table of Tables

Abbreviations

3RM	Three Roll Mill
CFRP	Carbon Fibre Reinforced Plastic
C=O	Carbonyl
COOH	Carboxyl
EM	Electron Microscopy
FLG	Few Layer Graphene
GNP	Graphene Nanoplatelet
OH	Hydroxyl
OHM	Overhead Mixing
PSD	Particle Size Distribution
SEM	Scanning Electron Microscopy
SM	Speedmix
TEM	Transmission Electron Microscopy
XPS	X-Ray Photoelectron Spectroscopy
XRD	X-Ray Diffraction

Glossary of Terms

-H	Denotes high intensity plasma functionalisation has been performed, will follow either GNP or FLG
-S	Denotes standard intensity plasma functionalisation has been performed, will follow either GNP or FLG
-U	Denotes no plasma functionalisation has been performed and the material is unfunctionalised, will follow either GNP or FLG
Agglomerate	A collection of randomly orientated graphene stacks which are held together by weak Van-der-Waals forces
Cohesion strength	The total strength, in Pa, of the internal interactions which hold an agglomerate together. This value is dependent on the size of the agglomerate and the dimensions of the graphene stacks.
Composite	A material comprised of two or more separate components
Crosslinking	The process of forming covalent bonds between polymer chains
Crystallisation	The process by which a solid forms with a crystalline structure. This can occur in uncured epoxy resins and can be triggered by temperature change, moisture or contamination. This is usually reversible through exposure to elevated temperatures
Cure cycle	The pre-determined sequence of temperature and time periods that the epoxy resin is exposed to during cure
Dispersion	Description of the distribution and level of de-agglomeration of graphene within epoxy

Erosion	Describes the mechanism of de-agglomeration where applied shear stress < cohesive stress. The shearing of small sections from the agglomerate surface
Exfoliation	The act of separating the graphene layers in stacked graphite
Filler loading	The proportion of composite material which is comprised of graphene fillers. This is expressed as a percentage of the overall cured composite weight
Functional group	A group of atoms with distinct chemical properties. In this work, oxygen based functional groups have been attached to the graphene surface to increase overall surface energy, promoting de-agglomeration and interactions with epoxy resin
Functionalisation	Modifying a material surface to alter the chemical characteristics, plasma treatments have been used in this project
Glass transition temperature (Tg)	The range of temperatures where a polymeric material changes from exhibiting hard glassy properties to soft rubbery properties
HDPlas®	The bespoke plasma treatment performed by Haydale Ltd
High-shear mixer	Mixing techniques which primarily use high-shear forces to mix and combine materials
Homogeneous	For a composition to be the same throughout
Hybrid composite	A composite material which is comprised of long fibres, graphene and polymer matrix
Interface	The area between the graphene surface and epoxy resin
Masterbatch	The incorporation of high filler loadings of graphene into epoxy for storage purposes. This allows safe handling and storage of graphene by eliminating the risk of inhalation by encasing the powders into the epoxy resin

Morphology	In reference to the various graphene powders investigated which differ by dimension, i.e. GNP or FLG
Planar size	The longest length of one singular sheet of graphene of a given morphology
Quality control	A repeatable measurement which can be performed to ensure a level of performance is shown by a material
Rupture	Describes the mechanism of de-agglomeration where applied shear stress > cohesive stress. Fast and unpredictable break down of agglomerates
Shelf-life	The period of time over which a materials properties can be confidently assumed to be consistent
Stacking	The natural layered formation of graphene sheets
Stoichiometry	The relationship between the quantities of reactants and products during a chemical reaction, in this case, the relationship between the amount of epoxy resin and hardener used during cure
Van-der-Waals	The distance-dependent interactions found between atoms and molecules. This work sees Van-der-Waals forces act as attractive forces responsible for the formation of graphene agglomerates

Acknowledgments

I would like to acknowledge the funding support provided by Haydale Ltd, KESS2 and ESF, without which this project would not have been able to have taken place. Knowledge Economy Skills Scholarships (KESS2) is a pan-Wales higher level skills initiative led by Bangor University on behalf of the HE sector in Wales. It is part funded by the Welsh Government's European Social Fund (ESF) convergence programme for West Wales and the Valleys.

My appreciation and thanks goes to my supervisors Mark, Rhys, Sam and industrial supervisor Matt, for all the support and encouragement given through this process. I'd like to extend this thanks further to all of the staff and technicians at Cardiff University and Haydale who have helped along the way.

Finally, a big thank you to my family and friends, without whom I would not have been able to finish this process.

1 Introduction

1.1 Background

Since its isolation in 2004, graphene has received much attention both scientifically and commercially due to a plethora of remarkable material capabilities, leading to the apt nickname of 'wonder material'. It has been found to possess excellent electrical, thermal and mechanical properties – with monolayer graphene boasting an intrinsic strength of 130GPa (Lee et al., 2008) and stiffness of over 1TPa (Young et al., 2012). In an attempt to harness these properties for structural purposes, increased interest has turned to graphene nanocomposites. Epoxy resins have been identified as an ideal matrix material, due to their good mechanical performance and chemical resistance alongside low weight and cost.

Graphene-based nanocomposites have begun to emerge commercially, with the sports and leisure sector, textile, electronics and biomedical industries all beginning to incorporate graphene into their products. For example, the bicycle manufacturer Dassi has innovated a composite frame constructed from carbon fibre infused with graphene/epoxy matrix (Figure 1.1). This has allowed for significant improvements to fracture toughness, whilst maintaining strength and stiffness (Dassi, 2019).

Figure 1.1: Dassi INTERCEPTOR^{TM} graphene road bike, manufactured with graphene infused epoxy resin matrix, combined with carbon fibres (Dassi, 2020)

It is well documented that the quality of graphene dispersion into the epoxy matrix is instrumental to the overall composite performance. Good dispersion relies on obtaining minimal agglomeration, homogeneous graphene distribution and good interfacial properties. The main challenge in achieving good dispersion is caused by the natural tendency of graphene to preferentially interact with itself rather than the matrix material and form into agglomerates. Agglomeration is undesirable as the impressive mechanical properties begin to diminish due to the weak Van-der-Waals forces which bind them together, leaving graphene to perform as an inclusion rather than reinforcement. These effects can be minimised during the manufacturing process, through methods such as altering graphene surface chemistry to improve interfacial properties and high energy mixing to de-agglomerate and evenly distribute through the epoxy matrix.

1.2 Purpose

This project has been funded through the Knowledge Economy Skills Scholarships (KESS2) and European Social Funds (ESF), who form links between SMEs and higher education institutions within Wales to collaborate on industry led research projects. This work has been performed in conjunction with technology solutions company Haydale Ltd, who have developed the patented plasma functionalisation technology HDPlas® which is used with many nanomaterials including graphene. Haydale materials are used in a variety of sectors ranging from medical, to aerospace, to sports and leisure and are developed in a way to best suit customer needs. The versatility in the final use of these materials has highlighted space to further understand the influence of processing parameters. As dispersion state is closely linked to mechanical properties, this relationship has been explored, concentrating on how the presence of functionalisation can aid this process and enhance mechanical properties. Special attention has been paid to ensure the mixing and characterisation methods used are commonplace within an industrial setting to allow for easy adoption into Haydale’s manufacturing practices.

Two different graphene powders were used in this study; graphene nanoplatelets (GNP) and few layer graphene (FLG). GNPs have higher aspect ratio, planar size and graphene layers, whereas FLGs are much smaller, with all dimensions over the nanoscale. GNPs are commonly used to enhance mechanical properties alone, whereas FLGs are an ideal addition within the matrix of long fibre composites, as their small planar size can easily infiltrate fibre tows.

Functionalisation is the process of altering a materials surface chemistry to promote chemical interaction. Each graphene underwent HDPlas® treatment, where oxygen based functional groups were attached onto the graphene powder surface. This treatment undermines Van-der-Waals forces responsible for agglomeration and improves graphene / epoxy interfacial properties. Two treatments of varied intensity were performed on each flake morphology; standard and high. The initial aim was to increase the proportion of functional groups present, however it emerged that for GNPs this resulted in changes to the proportions of bonding groups.

1.3 Aims

The research project can be summarised into 3 main deliverables.

- Producing and characterising dispersion state
- Investigating the link between dispersion and mechanical properties
- Following changes to dispersion state over time to gauge dispersion 'shelf-life'

Creating 'good dispersion' is a step taken in the majority of research studies centred around graphene / epoxy composites. As this description is subjective to each researcher, there is scope to fully assess and more accurately describe this relationship to optimise composite performance.

High-shear mixing methods have been used over extended mixing times and the resultant levels of de-agglomeration and exfoliation assessed to improve efficiency of the mixing process. The changes to dispersion state have been tracked using a variety of quantification methods, spanning over the macro, micro and nano scale. Currently, there is no standardised method of describing dispersion within nanocomposite materials, with many researchers opting to use electron microscopy (EM) to visualise dispersion. Whilst this remains the most accurate way of determining agglomerate size, EM is expensive, time consuming and representative of a very small amount of material, rendering it inappropriate for use in a production line. This work aims to compare the efficacy of different sizing methods to develop a quick method of measuring dispersion state, which can be easily adopted into a quality control procedure.

Tensile, flexural and DMA testing were carried out to measure the changes in physical properties with relation to mixing method and time, to further optimise the mixing process. The improvement to interfacial properties after plasma treatment was assessed, as well as the differences in performance with relation to flake size.

Finally, the dispersion state has been assessed over time to determine the changes to dispersion state over long time scales. It has been documented in studies that even after a 'good dispersion' has been achieved there is potential for graphene to re-agglomerate (Vilaverde et al., 2015). Factors thought to prolong dispersion state such as; low temperature, high filler loading and functionalisation were investigated over a 4 week period. This behaviour is important to understand when assessing shelf-life and relaying long-term processing needs.

2 Literature Review

2.1 Introduction to Materials

2.1.1 Graphene

Graphene refers to a single layer of carbon atoms and has been described as the world's first 2D material, which were previously thought impossible to exist as they were believed to be thermodynamically unstable (Geim and Novoselov, 2007). Since isolation, extensive research has been performed to better understand graphene material properties leading to a spectrum of desirable properties being unearthed. Graphene holds intriguing thermal, electrical and mechanical properties, opening a broad spectrum of potential applications. These properties follow-on from the unique hexagonal arrangement of sp^2 carbon atoms, which form each graphene sheet, depicted in figure 2.1. Each carbon atom possesses 4 valence electrons which bond covalently to 3 other carbon atoms, with one pair double-bonded with an additional pi-bond. Sigma bonds are the strongest of the covalent bonds, due to their high electron density and therefore short bond length (0.142nm) (Cooper et al., 2012).

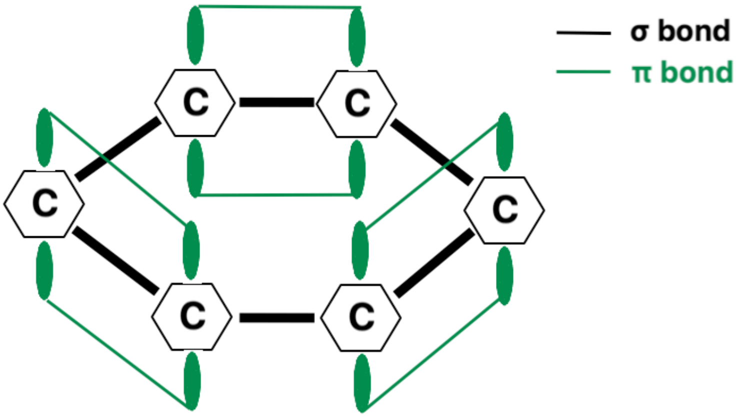

Figure 2.1 : Atomic bond structure of sp^2 hybridised graphene

There are numerous methods to produce graphene, generally categorised into either top-down or bottom-up processes, where the former refers to the exfoliation of graphene from bulk graphite and the latter to firstly growing multilayer graphene epitaxially. This can be followed by a second method to isolate or exfoliate into a small number of layers. Perhaps the most famous top-down method is mechanical exfoliation through micromechanical cleavage. This is the practice of using force to separate layers of graphene from graphite and describes the method first used by Geim, Novoselov and researchers at Manchester University, where 'Scotch Tape' was used to pull apart graphene sheets. Exfoliation can easily be achieved due to graphene layers being held together by weak Van-Der-Waal forces. This method produces high quality crystals with large planar size, however it is difficult to scale up production leaving this approach to be predominantly used in research environments (Geim, 2011). This process is commonly used with graphite, thicker graphene type materials and graphene oxide. The chemical oxidation and reduction of graphene however, is an effective top-down production method with high yield and low cost. This technique involves the initial oxidation of graphite which increases the interlayer spacing of the graphene sheets, reducing the strength of the Van-der-Waals forces holding them together (figure 2.2). This aids subsequent mixing by making exfoliation easier to achieve, mixing is commonly performed in a polar solvent through mechanical stirring or ultrasonication. The graphene oxide sheets are then chemically reduced to remove the oxygen functional groups and achieve the resultant graphene (Chua and Pumera, 2013)(Avouris and Dimitrakopoulos, 2012). The Hummers method expands on these principles through the use of potassium permanganate, sodium nitrate and sulphuric acid to perform the oxidation. This method is popular as the reactions can be performed in a singular container. Many researchers have further improved upon the Hummers method with various modified Hummers methods, in order to either; make the process scalable (Lavin-Lopez *et al.*, 2016), make the procedure more 'green' (Chen *et al.*, 2013) or alter and improve physical properties (Zaaba *et al.*, 2017)(Sohail *et al.*, 2017). Graphene functionalisation can be simultaneously achieved during the oxidation stage of this process.

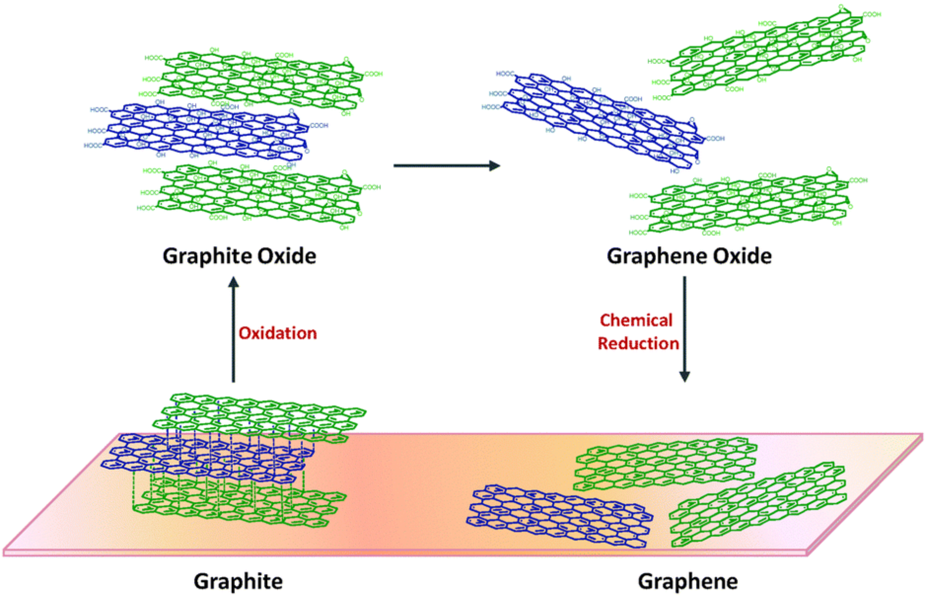

Figure 2.2: Top-down method of graphene production through the oxidation and reduction method (Chua and Pumera, 2013)

Chemical vapour deposition (CVD) is a common bottom-up method of graphene production, allowing production of high quality graphene with great control. This method is used for the production of mono, or few layer graphene and involves the growth of flakes upon a substrate such as copper or silicon. This is achieved in two stages, firstly by releasing carbon atoms from a precursor such as methane through either high temperature or pressure, before emitting into a vacuum chamber and deposited onto the substrate through condensation. This process is capable of producing large flakes with few layers and has the potential to be scaled up to produce larger quantities. This method allows greater control over graphene layers and planar size and eliminates the use of any acids or solvents. However, the large energy inputs required leave this method with high running costs (Kalita and Tanemura, 2017). Graphene can also be epitaxially produced from a SiC substrate, this method involves exposing etched SiC to a high temperature and high pressure environment. Over a period of time, the non-carbon atoms evaporate and carbides begin to break down and reconfigure into graphene. This technique produces high quality graphene sheets that are highly compatible for use in electronics, but has a very low yield (Tan, Wang and Guo, 2018)(Saeed *et al.*, 2020). .

Whilst the methods described above are generally the most popular approaches taken to produce graphene, there are notable alternative techniques. Arc-discharge deposition is a commonly used method in the production of carbon nanotubes (CNTs), which can be modified to produce graphene. This technique passes a high current through a two graphitic electrodes of high purity, the anode and cathode are placed in close proximity and within a suitable medium. As the current passes through the graphitic electrodes, carbon begins to evaporate from the surface and is deposited (Sharma, Sharma and Sharma, 2015). Subrahmanyam et al determined that by performing arc-discharge within a mixture of hydrogen and helium, the deposited carbon was prevented from forming into CNTs as the dangling carbon edge atoms bonded with the hydrogen contained in the atmosphere, resulting in the production of graphene (Subrahmanyam *et al.*, 2009) . Electrochemical exfoliation is a similarly performed technique which uses a graphitic substance, in the form of rods, sheets or foils, as both the anode and cathode. The current passed through the system causes electrochemical reactions to occur at the anode and cathode, which provide enough driving force to break the Van-der-Waals forces within the graphite and causing exfoliation of graphene (Liu *et al.*, 2019).

Finally, graphene sheets can be synthesised organically through a series of reactions, creating pristine sp^2 graphene. This method allows high controllability of the morphology, size and edge structure of the final synthesis graphene (Wei and Liu, 2010). The advantages and disadvantages of the discussed manufacturing methods detailed in table 2.1.

Table 2.1: Advantages and disadvantages of common methods of graphene production

Method	Pros	Cons
Mechanical exfoliation of graphite	- High quality of graphene - Large planar size achievable	- Very low yield
Chemical oxidation and reduction	- Low cost - Equipment required is easy to use - Suited to large scale industrial use - Functionalisation can be simultaneously achieved - Reduction can be performed thermally, eliminating use of chemicals	- Time consuming process - Preparation conditions can be difficult to control
Chemical Vapour Deposition (CVD)	- High quality - High yield - Good control of graphene layers	- Substrates can be costly - Transfer process is difficult & may lead to the introduction of defects
Epitaxial growth	- High quality	- Low yield - Large quantities of expensive SiC required to scale up production - Difficult to transfer graphene from SiC
Arc discharge	- Equipment simple to use - Can be scaled-up - High purity graphene - Can simultaneously add functional groups to graphene	- Method simultaneously produces CNTs, therefore an additional process required to remove graphene
Electrochemical exfoliation	- Easy method to perform with simple setup - Can be modified to functionalise graphene surface simultaneously	- Only certain combinations of solvent and graphite are compatible. May increase environmental impact

Organic synthesis	- High control over graphene morphology - Pristine graphene can be produced	- Difficult to prevent side reactions occurring with increased graphene size

2.1.2 Plasma Functionalisation

The low processability of graphene and epoxy is a key obstacle to the commercialisation of the final composite material. Graphene has high surface energy due to its small size, leaving a tendency to preferentially interact with itself forming into agglomerates held together by weak van der Waals forces. Additionally, this results in poor interfacial interactions between the graphene and epoxy when combined (Atif and Inam, 2016)(Li *et al.*, 2018). These two factors result in the degradation of overall composite mechanical performance whereby the graphene agglomerates behave as defects, promoting sites for crack initiation and propagation, reducing composite strength, modulus and toughness. Functionalisation is utilised to counteract this behaviour by altering the graphene surface chemistry to improve the chemical affinity with the epoxy matrix, promoting good dispersion and interfacial interactions, whilst preventing re-agglomeration (Boaretti et al., 2020). Functionalisation is industrially desirable as it aids the initial mixing process and maintains dispersion state over time, enhancing the mechanical performance of the overall composite.

Plasma is defined as ionised gas, created when high levels of energy are input into a gaseous system allowing electrons to break away from their host nucleus. This results in a mixture of positively charged ions and negatively charged electrons which possess high free energy (Dey et al., 2016). In this functionalisation process, plasma is directed at the sp^2 bonded graphene structure. High levels of energy is supplied into the system exciting the carbon atoms allowing electrons to jump out of the valence band and into the conduction band and become sp^3 bonds, making them more readily available to bond to atoms in the atmosphere (McEvoy et al., 2013). This has been performed in an oxygen rich atmosphere resulting with hydroxyl (OH), carbonyl (C=O) and carboxyl (COOH) groups covalently bonding to the graphene edges and defect sites (Felten et al., 2005). This has been demonstrated to increase surface energy and aid dispersion when mixed with epoxy resins (Valentini et al., 2005) (Lu et al., 2010) (Johnson, Dobson and Coleman, 2015). Additionally, oxygen functional groups have potential to form interactions with epoxy chains (Alam, Wan and McNally, 2017)(Naebe et al., 2014)(Williams et al., 2013), which is highly desirable when creating a good interface with the epoxy matrix. As plasma functionalisation is a surface technique, graphene powder is simultaneously ball milled to ensure the breakdown of agglomerates and ensure a higher proportion of treated powder.

Functionalisation can be alternatively achieved electrochemically or through acid treatments (Rooyanian et al., 2018)(Georgakilas et al., 2012)(Xia et al., 2016). However plasma treatment is advantageous as it is a dry process producing no hazardous waste like acid treatments, making it an environmentally friendly alternative. Plasma treatment is a versatile technique which is compatible with a variety of materials. The type and proportion of functional groups can also be tailored based through adjustment of gas used and processing parameters. Haydale Ltd have also demonstrated that large quantities of materials can be functionalised at a time (Williams et al., 2013)(Ma et al., 2010).

2.1.3 Epoxy Resin

Epoxy resins are a thermosetting polymer, meaning the material cures irreversibly into the hardened state. The epoxy system investigated in this research was a two part system consisting of bisphenol A (DGEBA) type epoxy resin and cycloaliphatic polyamine hardener. The bisphenol A resin used in this project consists of two epoxide rings, as illustrated in figure 2.3, these groups are reactive and determine the amount of crosslinking which can occur (Hamerton *et al.*, 2014).

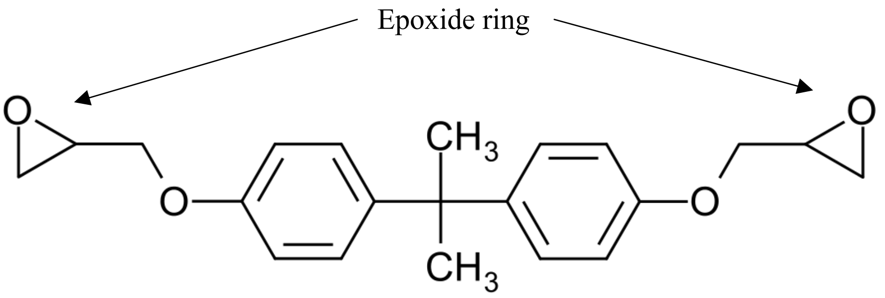

Figure 2.3: Chemical structure of DGEBA epoxy resin

The two amine groups found within the hardener structure (figure 2.4) form bonds with the resin epoxide rings during the curing process. These chemical reactions result in the formation of a highly crosslinked network, the density of which closely relates to the properties of the final material. Post-cure is generally required to further facilitate crosslinking of epoxy systems, this is achieved by exposing the material to elevated temperatures for extended periods of time. The temperature and length of cure time is specific to each epoxy system and the parameters are advised on the material data sheet. High crosslink density is desirable as it correlates to increased stiffness, strength and glass transition temperature (Fiore and Valenza, 2013)(Nixon, Cahill and Jolanki, 2012).

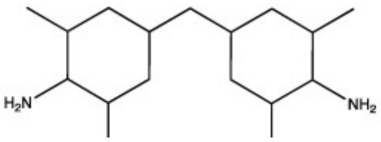

Figure 2.4 : Chemical structure of cycloaliphatic polyamine hardener

Epoxy resins show many desirable physical properties which make them an ideal matrix material for graphene powders. They have high stiffness to weight ratios, in addition to good resistance to chemicals and corrosion, leaving them suitable for structural and environmental applications (Massingill and Bauer, 2000). Epoxy resins do exhibit brittle behaviour as a result of their highly crosslinked structure, which could result in catastrophic failure. The addition of graphene powder can improve the overall stiffness, strength, and fracture toughness, whilst maintaining low weight. Additionally, the epoxy resin investigated in this research has low viscosity, owed to the low number of epoxide rings within each epoxy monomer, easing material processability during mixing and material fabrication.

The functional groups attached to the graphene surface during plasma treatment are capable of interacting and bonding with the epoxy resin. Carboxyl (COOH) and hydroxyl (OH) groups have the potential to bond covalently to the epoxy resin, carboxyl groups are able to open the epoxide ring and form an ester bond and additional hydroxyl group. This is desirable as they are able to form further bonds or strong polar interactions with oxide surfaces. Hydroxyl groups are also able to interact with the epoxy resin and form an ester linkage (Eitan *et al.*, 2003). It is favourable to select a resin system which is able to form attractive polar interactions with the filler surface chemistry, in order to maintain some interfacial interaction in case covalent bonding in not achieved. The promotion of graphene / epoxy interfacial interactions are highly favourable as they improve the overall composite properties.

2.1.4 Graphene Nanocomposites

Transportation based industry such as automotive and aerospace have already begun to incorporate carbon-fibre reinforced plastics (CFRP) within their products. An example of this is the Airbus A350 XWB aircraft, which is manufactured with 53% carbon based composite materials (figure 2.5), resulting in 25% reduction in operating costs, fuel burn and CO_2 emissions. (A350 XWB Family - Passenger aircraft - Airbus, 2020). This highlights the commercial interest in composite materials and creates space to improve upon readily used CFRP.

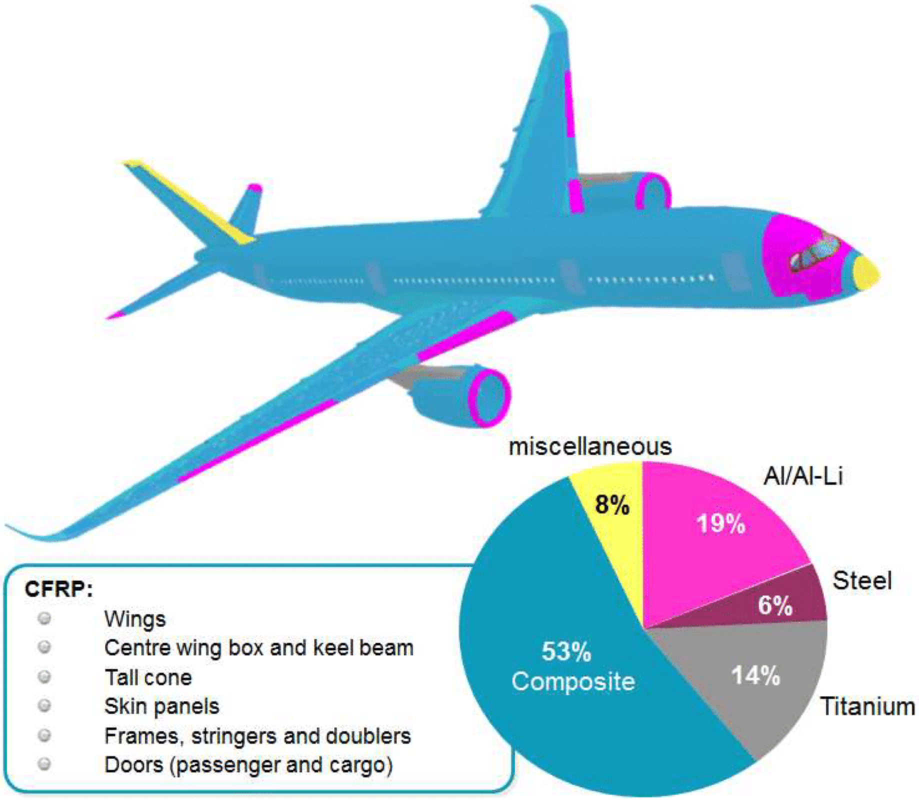

Figure 2.5 : Breakdown of materials used to manufacture Airbus A350 XWB (Bachmann, Hidalgo and Bricout, 2017)

The role of graphene in composite materials is generally explored in two ways;

- Composites where graphene is the only reinforcing constituent
- Hybrid composites where graphene is incorporated as part of the matrix material to be used with long fibres

Instances where graphene provides sole reinforcement, large planar sizes and few layers are preferred to achieve good stress transfer over the graphene / epoxy interface, giving improvements to material strength and stiffness. These materials are yet to emerge commercially for structural applications due to the key challenges faced with achieving good dispersion and stress transfer over the graphene / epoxy interface. This has left measured mechanical properties to be much lower than those mathematically predicted and generally overall producing small improvements to the matrix properties. The largest and most substantial improvements are seen with fracture toughness measurements, these trends are discussed in more detail in section 2.5.

Hybrid composites describe the inclusion of graphene into traditional long fibre composites. Long fibres are manufactured from a variety of materials, such as carbon, ceramics and metals. Graphene is included into hybrid composites to improve both matrix properties and interlaminar shear strength (Ali Charfi *et al.*, 2020). These innovative materials have begun to emerge industrially. Automotive manufacturer BAC have launched the Mono R sportscar, which has been manufactured with Haydale produced graphene enhanced carbon fibre composite materials (figure 2.6). These have been utilised in the production of body panels and wheel arches, improving mechanical performance and reducing the weight of the vehicle (Haydale, 2019). The incorporation of graphene into regular fibre composites can improve strength, stiffness and fracture toughness of the overall composite (Topkaya, Çelik and Kilickap, 2020)(Watson *et al.*, 2017)(Wang, Soutis and Gresil, 2021). Topkaya et al demonstrated the incorporation of 0.2% by weight of GNPs to carbon-fibre reinforced plastics (CFRP), improved tensile strength and modulus by 8.06% and 7.12%, respectively, compared with that of the CFRP without the addition of GNPs (Topkaya, Çelik and Kilickap, 2020). Additionally, Hawkins et al determined the addition of just 0.1% GNPs by weight to CFRP, resulted with an 11.4% improvement to fracture toughness upon that on the CFRP with no GNPs (Hawkins and Haque, 2014).

© Tom Ziora

Figure 2.6: BAC Mono R supercar with Haydale Ltd graphene infused CFRP materials incorporated within the body panels and wheel arches

Hybrid composites are fabricated through two difference approaches, the first is where graphene is directly applied to the fibres before infusing with the matrix material to ensure the improvement of fibre / matrix interfacial properties (Qin *et al.*, 2020). The second approach begins with the incorporation of the graphene into the matrix material, which is then utilised as it would be in conventional fibre composite materials. These methods include resin infusion techniques, pre-preg production and wet lay-up. Manufacturing the hybrid composites in this way ensures the enhancement to the matrix material, these methods are discussed further in section 2.4.4. Resins intended to be used in processes described in the second approach, where graphene is incorporated within the epoxy resin, will be explored in this project. As the failure of fibre composites generally begins with the matrix material, improvements to strength are imperative.

2.2 Graphene Characterisation

2.2.1 Nomenclature

Graphene is defined as one atomic layer of sp^2 bonded carbon, however in engineering purposes the term can apply to a wide variety of structures. The research reported in this thesis is focussed on few layer graphene and graphene nanoplatelet powders, which are depicted in figure 2.7 and defined as follows (Iso, 2017);

- Few Layer Graphene (FLG), two-dimensional material consisting of 3-10 well defined stacked graphene layers. The quoted number of layers for FLG powder examined during this work is 1-4, meaning there is likely a mix of monolayer, bi-layer and tri-layer graphene (meaning one, two and three graphene layers respectively) but the term FLG has been used for clarity.

- Graphene Nanoplatelet (GNP), where nanoplatelet refers to possession of one dimension measuring in the nanoscale and the remaining two being significantly larger.

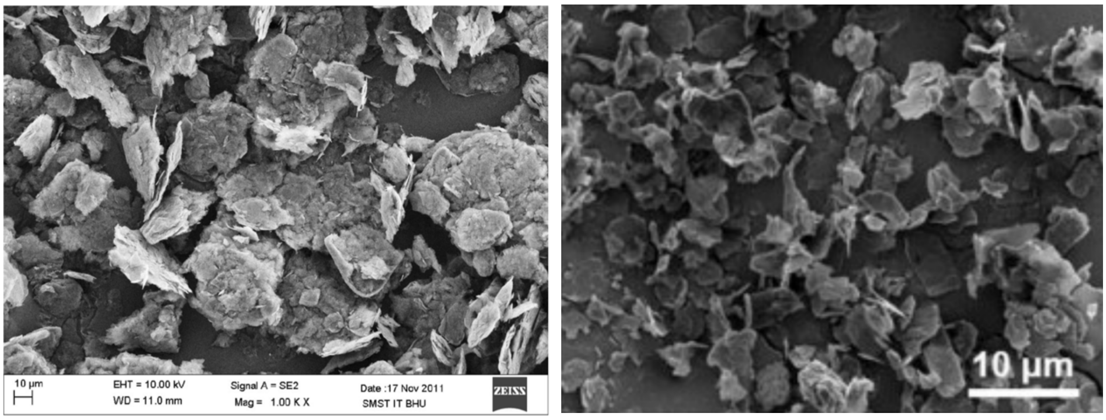

Figure 2.7: SEM images depicting (left) Graphene Nanoplatelets (GNPs) (Singh, Srivastava and Prakash, 2015) (right) Few Layer Graphene (FLGs) (Castarlenas *et al.*, 2014)

2.2.2 Graphene as Reinforcement

Good dispersion state and interfacial properties are essential to effectively enhance composite performance. The success of which is influenced by graphene morphology which refers to number of stacked layers, planar size, surface texture and functionalisation. Graphene flakes with high aspect ratio, where planar dimensions are larger than thickness, are more desirable when enhancing mechanical performance (Hussein and Kim, 2018). Fewer layers are preferred as Van-der-Waals forces responsible for graphene stacking are weak, leading to poor transfer of stress between layers. This decreases the efficiency to dissipate load across stacks, resulting with reduction in composite performance with increased layers (Androulidakis et al., 2017)(Eqra, Janghorban and Manesh, 2015)(Young et al., 2012)(Gong et al., 2012).

The effective transfer of load from epoxy matrix to graphene is integral to the enhancement of material properties (Laurenzi et al., 2014). In order to effectively facilitate this, good interfacial bonding must be attained and the graphene planar dimensions must exceed a critical length. This principle is illustrated in figure 2.8 in relation to short fibre composites, demonstrating interfacial elastic stress-transfer. Under loading, the bond between the fibre ends and matrix diminishes, leaving the applied stress to build up along the length of the fibre and increase towards the centre. If the fibre is of sufficient length, the full applied stress can develop across the fibre resulting in reinforcement. The critical length (lc) of reinforcement is defined as the distance over which this maximum stress is reached and can be calculated using equation 1

$$l_c = \frac{\sigma_f d}{2\tau_c} \tag{1}$$

Where σ_f is the tensile strength of the fibre, d is the fibre diameter and τ_c is the fibre / matrix bond strength or the shear yield strength of the matrix (whichever value is smaller)(Callister and Rethwisch, 2011).

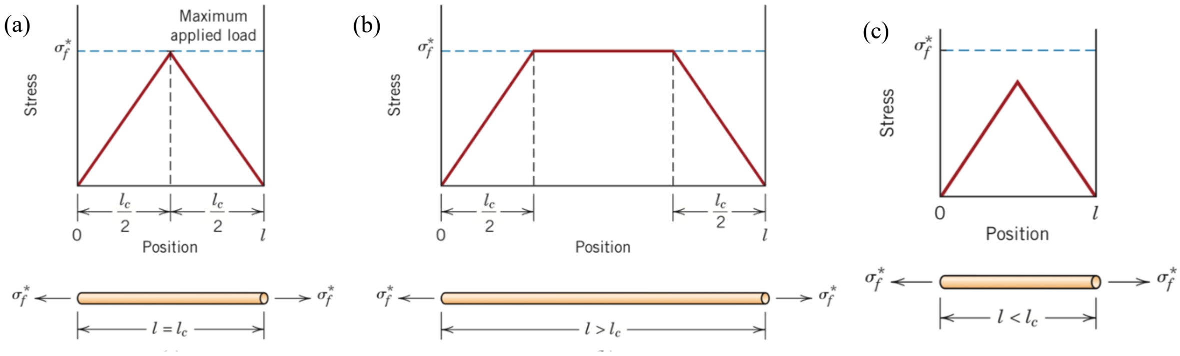

Figure 2.8 : Stress profiles along a loaded fibre when (a) fibre length = critical length (b) fibre length > critical length (c) fibre length < critical length (Callister and Rethwisch, 2011)

These principles were applied to graphene flakes by Gong et al, who used shear-lag equations to find the critical length of reinforcement of a single layer of graphene. This was done by placing pristine monolayer graphene sheet upon a PMMA substrate where the two materials are interacting through Van-der-Waals forces alone (Gong *et al.*, 2010a). The interfacial stress transfer was determined through uniaxial loading of the PMMA substrate and tracking the changes to the graphene structure with Raman spectroscopy. Carbon materials has a well-defined Raman spectra, which show clear shifts to characteristic G' peak when under load (Cooper, Young and Halsall, 2001). This relationship allowed the stress transfer of to be determined through monitoring the graphene spectra when the PMMA substrate was under load (figure 2.9a). The sample was subjected to a 0.4% strain the gradient of which was mapped along the length of the graphene monolayer as displayed in figure 2.9b. 0.4% strain was used as it was found to be low enough to maintain a good interface over the entire graphene layer, as higher levels of strain resulted with the graphene sheet to slip over the surface. The critical length of reinforcement was determined to be 3µm, but in real-life applications, 8-10 times this value should be used to ensure good reinforcement, concluding that flakes should be 25-30µm in planar size (Papageorgiou, Kinloch and Young, 2017).

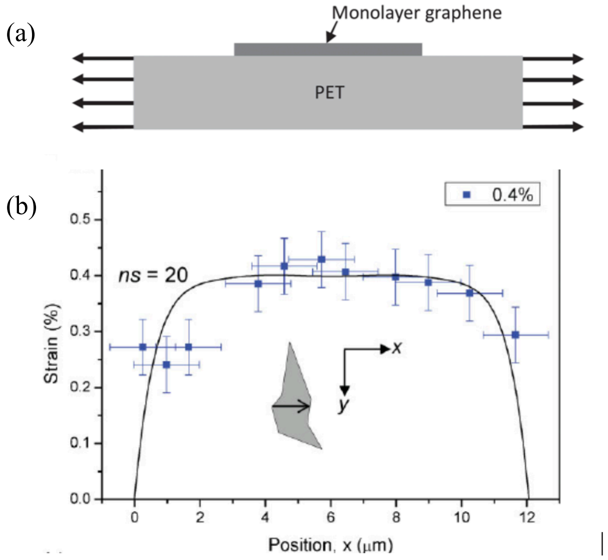

Figure 2.9 : (a) monolayer graphene placed onto a graphene substrate under load (b) strain gradient determined from across the monolayer graphene under 0.4% strain (Gong *et al.*, 2010a)

Further investigation into this relationship was performed by (Wang et al., 2016), who applied these principles on functionalised monolayer graphene sheets on a PMMA substrate. A O3/H2O gaseous mixture was used to form hydrogen bonds to the graphene surface. It was concluded that the alteration of the graphene structure caused the interface to become stiffer and stronger, improving the stress transfer efficiency.

2.2.3 Interfacial Factors

Many studies have shown that graphene functionalisation is necessary to effectively enhance composite properties with graphene fillers, as agglomerations and poor interfacial interactions have a negative impact on properties (Punetha et al., 2017)(Chandrasekaran, Seidel and Schulte, 2013)(Jin, Duan and Mu, 2016). The presence of functional groups causes disruption to the strong sp^2 carbon network, resulting in degradation to the exceptional graphene properties (Georgantzinos, Katsareas and Anifantis, 2012). This highlights the need to strike a balance between having adequate levels of functionalisation to improve interfacial properties, but without causing too much disruption to the graphene structure in order to preserve mechanical performance. A study performed by (Vallés et al., 2016) investigated how C/O ratio of graphene oxide materials affected the overall degree of reinforcement when combined with epoxy resins. It was determined that samples with higher oxygen contents produced stronger interfaces and improved overall composite Young’s modulus, regardless of the alteration to the graphene structure.

Graphene surface texture plays a role in overall mechanical performance. For a single sheet of graphene, it is common to find small out of plane rippling as a result of thermal fluctuations.

However, other environmental factors can also affect the surface texture. For example, it is common for nanoscale wrinkling to occur in graphene produced through CVD (Li et al., 2015), as a result of both uneven surface texture of copper substrate and rapid changes in temperature during production. Folding and crumpling can also occur through physical handling as a result of the high flexibility of graphene (Fasolino, Los and Katsnelson, 2007).

It has been shown that wrinkled graphene surface can improve interfacial stress transfer and reduce the affect of shear displacement between stacked graphene sheets through geometrical interlocking, improving overall mechanical properties (Androulidakis et al., 2017)(Qin et al., 2016)(Deng and Berry, 2016). Androulidakis et al examined the tensile response of mono, bi and tri-layer graphene deposited on a polymer substrate with the use of Raman spectroscopy. This was performed on graphene flakes which had no wrinkling and small wavelength wrinkling, to show the role of surface texture on reinforcement. Samples were attached to a bi-axial jig allowing tensile deformations to be performed under analysis through Raman spectroscopy. The shift rate of Raman spectra peaks were recorded with applied stress, allowing the response behaviour to be investigated across the samples. It was concluded that the presence of wrinkling did not compromise the mechanical performance of monolayer graphene and was found to enhance mechanical performance for both bi and tri-layer graphene. Raman shift rates for both bi and tri-layer graphene were determined to be higher in the wrinkled state than the flat counterpart, indicative of improved stress transfer due to better shear strength across the graphene / epoxy interface (Androulidakis et al., 2017). These results are based on monolayer graphene with continuous contact with the polymer substrate along the length of the wrinkles (figure 2.10) Conversely, graphene with delaminated wrinkles can cause decreased properties as each ripple behaves as an isolated flake and would need to fulfil shear lag parameters to adequately provide stress transfer (Li et al., 2015). Additionally, it was determined that the effect of interlocking is only seen in monolayer graphene and properties begin to decline with stacked graphene sheets (Androulidakis et al., 2017). The graphene used in this study has been deemed to be flat with little wrinkling compared with other commercially available graphene powders and surface texture will not be investigated with respect to mechanical reinforcement (Chong, Hinder and Taylor, 2016).

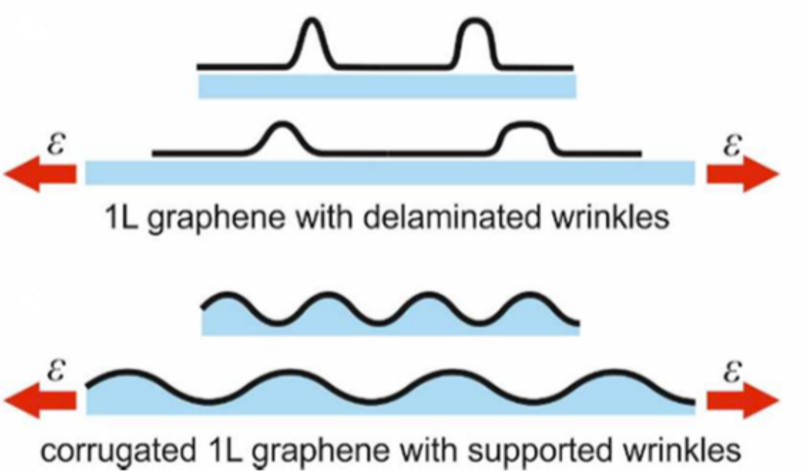

Figure 2.10: monolayer graphene with delaminated and supported wrinkles (Androulidakis et al., 2017)

2.3 *Quantifying Dispersion*

2.3.1 *Image-Based Characterisation*

Dispersion state is most commonly characterised through visual methods, with electron microscopy being hailed as the 'gold-standard' technique (Yu and Li, 2017)(Abdullah and Ansari, 2015). The issue with qualitative analysis is that results are based on opinion and become unreliable. Previous studies have developed methods of quantitively describing nanoparticle dispersion, mostly using statistical analysis or imaging software with TEM or SEM images. These studies can be categorised into either particle based or matrix based quantification. Particle based quantification can manifest in the following ways; measurement of particle size distribution, particle density or distance between particles (Luo and Koo, 2008).

Notably, Khare & Burris developed the 'free-space length' method of characterisation (figure 2.11) (Khare and Burris, 2010), which analyses matrix characteristics. This technique is used on TEM image of a 2D cross-section and analyses the unfilled spaces in the matrix between nanoparticles. The reasoning behind this being that 'good' dispersion is determined by three factors; filler size, filler loading and agglomeration – each of which have an effect on the interparticle distance. This method repeatedly places a square of known size over the image at random and counts the number of particles which fall inside. This is done with squares of statistically significant length, the largest square which has the highest probably of containing zero particles over all instances is determined to be the free-space length. Smaller values, and therefore smaller squares, are indicative of better dispersion. The method was cross referenced with TEM images and corresponding tensile measurements presented by Chen et al (Chen, Jian and Yen, 2009) and confirmed the link between free-space length and mechanical performance. This demonstrates the effectiveness of this quantitative method and reinforces the link between dispersion and mechanical properties.

These concepts have been built upon further by Pfeifer & Bandaru who also use statistical based analysis but determine an additional measure of ‘randomness’, allowing the researcher to gauge any dispersion pattern. This allows measurement between the achieved and ideal dispersion state and therefore also mechanical performance (Pfeifer and Bandaru, 2014). Simplified approaches of depicting dispersion graphically, representing particle size and distribution have been developed by (Del Gaudio and Licciardi, 2019), using MATLAB™ software to analyse binary microscopy images. These methods all focus on the characterisation of particle size and homogeneous distribution, confirming that these two factors are important when considering dispersion state.

Other novel visualisation techniques through elemental mapping using energy dispersive spectroscopy analysis (EDS), to determine dispersion state have been employed by Mohan et al (Mohan, Haalboom and Bhattacharyya, 2020). A series of map scans were performed on polished cross-sections of cured graphene / epoxy samples and repeated over varied polymer compositions. Elemental scans for carbon, oxygen and nitrogen were constructed, carbon mapping determined the base state of the image, displaying the carbon atoms which both graphene flake and polymer matrix are consisted of. The dual blend polymer matrix was comprised of carbon, hydrogen, oxygen and nitrogen atoms. Due to the low molecular weight of hydrogen deeming EDS analysis unsuitable, scans were performed each for oxygen and nitrogen. Each scan was binarised before the oxygen and nitrogen maps were ‘subtracted’ from the base carbon map, leaving areas which could contain graphene. A MATLAB script was used to measure both the percentage of the image covered by resulting carbon and the average distance between particles, to gauge dispersion state. Whilst this remains an innovative use of EDS spectroscopy, this would be better suited to analysis of a 2-phase system with different elemental composition for enhanced precision. Similar mapping methods have also been performed by (Shojaee et al., 2013), utilising confocal Raman spectroscopy.

Most post-processing techniques first convert images to binary, meaning they consist only of two colours. In this case the colours correspond to being either matrix or nanoparticle. Thresholding is used to determine the point in tonal range, whereby the limit of what is classified as matrix or nanoparticle is determined. This process is generally done manually and therefore is difficult to standardise, even more so as brightness and contrast settings can vary massively, not only between equipment but also different sessions using the same equipment. It must also be considered that microscopy techniques represent a 2D slice of material, which may not embody 3D properties. This is especially true when characterising irregular shapes such as graphene which have high aspect ratio.

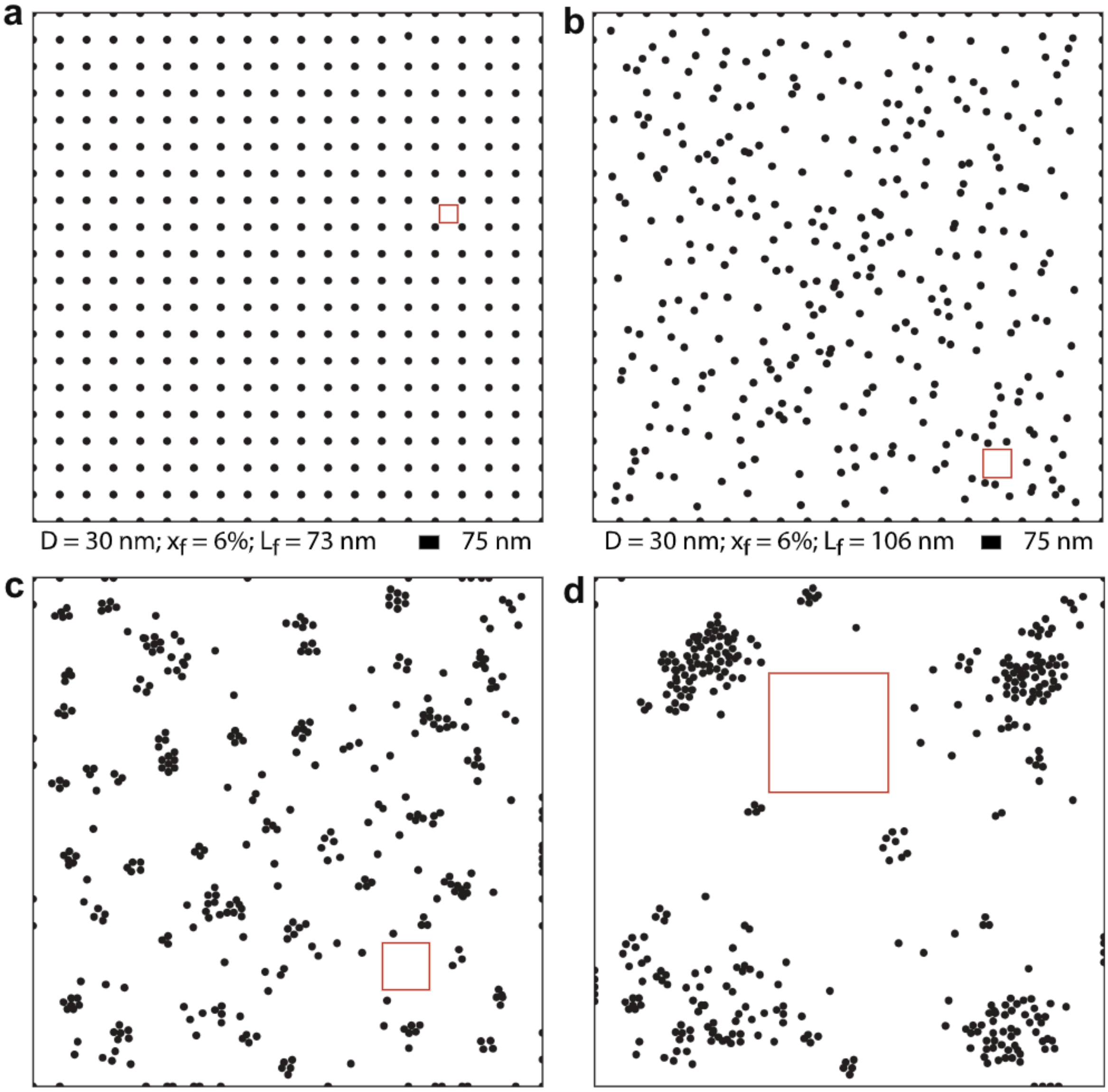

Figure 2.11 : Quadratic sampling method used by Khare & Burris (Khare and Burris, 2010)

It is clear from literature that TEM is essential to accurately visualise dispersion state due to the size of graphene flakes, and so far has been the preferred method to do so. However, when considering this analysis within an industrial setting, it is not feasible to use TEM due to sample preparation and imaging being very time consuming, costly and requiring trained technicians to operate equipment. Additionally, the small sample area that is imaged does not necessarily represent the bulk behaviour. Similar image processing techniques could be applied to optical microscopy images, which are quickly generated and easily accessible however, accuracy and representation is lost due to the higher magnification.

2.3.2 Bulk Material Characterisation

Extensive research using non-visual methods has been undertaken to quantitively assess dispersion state in bulk samples, including rheology, x-ray diffraction spectroscopy (XRD)(Praveen, Pramod and Neogi, 2017), and dynamic light scattering (DLS)(Nolte, Schilde and Kwade, 2012). These methods are desirable as analysis is based on a larger quantity of material, giving representation of bulk properties.

The relationship between polymer nanocomposites and rheological behaviour is much researched and well understood. In simple shear viscosity testing of filled polymers, the following parameters directly alter viscosity; polymer chain length, polymer / filler interactions, filler loading, morphology and dispersion state (Liu et al., 2009). This means that if all other parameters can be controlled, data regarding dispersion state can determined through viscosity measurements. Viscosity is defined as a materials resistance to flow, in the case of graphene / epoxy materials, these flow properties are determined from the mobility of the polymer chains. The presence of graphene restricts the mobility of the polymer chains, increasing internal molecular friction, resulting with increased viscosity. As deagglomeration and exfoliation occurs, the number of graphene sites rises and provides higher levels of restriction to chain mobility. This phenomenon allows comparisons to be made between dispersion states for each given system (Throckmorton and Palmese, 2015). However, the resulting internal friction experienced is dependent also on the particle size in relation to the polymer chain geometry, with smaller particles having reduced effect on the bulk flow (Grabowski and Mukhopadhyay, 2014). This may limit the effectiveness of this technique for smaller sized graphene flakes.

The act of enhancing dispersion is based on changing graphene powder morphology, primarily through two mechanisms; firstly breaking down agglomeration and secondly, exfoliation of graphene layers. Exfoliation to few layers increases each particles aspect ratio which enhances mechanical performance, therefore quantifying graphene layering would give insight to overall reinforcement capabilities (Morimune-Moriya, Goto and Nishino, 2019). XRD provides analysis of crystal structure and atomic spacing through examination of diffracted x-rays and interference patterns produced when bombarding a crystalline material with x-rays. When these values coincide to satisfy Bragg's law ($n\lambda=2d \sin \theta$), measurements for both diffraction angle and lattice spacing can be resolved and material determined (Dutrow and Clark). The amount of each occurrence is counted and an intensity for each spacing determined. Characteristic peak of graphite interlayer spacing is found at ~26.5°, figure 2.12 shows how the intensity drastically drops with fewer layers when comparing with spectra collected for graphene. This technique is commonly used to monitor flake thickness and assess quality of dispersion state achieved (Wan et al., 2013)(Ahmadi-Moghadam et al., 2015)(Liang et al., 2009).

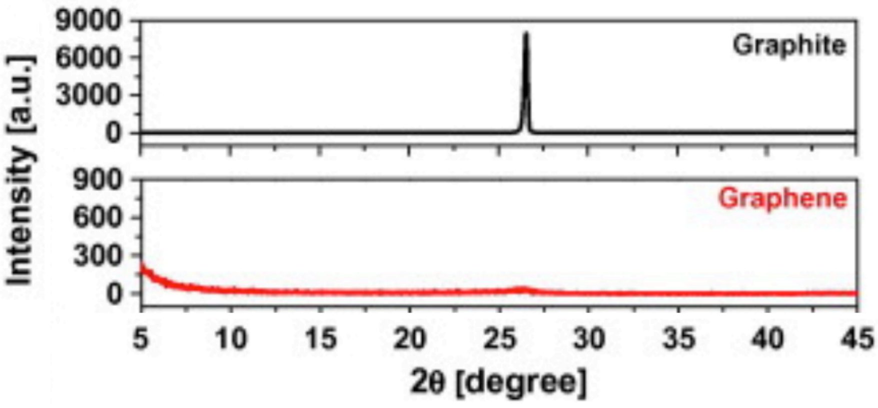

Figure 2.12: XRD spectra illustrating the characteristic graphitic interlayering peak for graphite and monolayer graphene (Wan et al., 2013)

Large scale particle sizing has been achieved through DLS, which analyses intensity of light scattered after being directed at a particle. This intensity is dependent on the Brownian motion of these particles in suspension, meaning by using a light source of fixed wavelength, a light intensity is detected unique to each particle size. Through the Stoke-Einstein relationship values of particle size can be determined. This measurement is performed in low viscosity solution such as deionised water (Stetefeld, McKenna and Patel, 2016). However, there are some limitations of this method, firstly, the analysis is based on spherical particles meaning accuracy is lost with irregularly shaped particles such as graphene. Secondly, due to this method relying on the free movement of particles, this results in analysis being only possible for instances where graphene has been mixed in low viscosity material such as a solvent. This project is focussed on all mixing being performed after incorporation with epoxy resins, meaning an additional step to dissolve away any resin is required before analysis. Whilst this is achievable, this results with waste materials and additional steps to the manufacturing process. Additionally, this leads to uncertainty of whether measurements are representative of the graphene / epoxy batch.

These procedures can all successfully be used to describe changes in dispersion state after analysing relatively large samples, giving good representation of the bulk sample. As these techniques do not involve any level of visual investigation, it becomes difficult to objectively determine dispersion quality from any given method alone. This requires a level of preliminary investigation to be carried out to determine how each dispersion state correlates to measurements, likely involving visual methods and mechanical testing to be performed alongside. This would need to be performed for each unique graphene powder / epoxy system as we have seen the effect of flake morphology, filler loading and polymer system.

2.4 Mixing and Dispersion

2.4.1 De-agglomeration & Exfoliation

As previously discussed, the graphene formation has great influence on the overall ability to provide reinforcement. Due to the tendency of graphene sheets to stack and then aggregate into large agglomerates, it is necessary to include a process during manufacture that facilitates de-agglomeration and exfoliation, whilst also creating a homogeneous dispersion. De-agglomeration refers to breaking-down aggregated stacked graphene, whereas exfoliation involves the shearing of individual graphene sheets. De-agglomeration requires much less energy than exfoliation, as the forces responsible for aggregation are much weaker than the interlayer pi-pi interactions which cause stacking (Paton et al., 2014). In order to produce exfoliation, shear forces exceeding that of the interlayer shear stresses (ISS) of the graphene must be used during mixing. Throckmorton and Palmese (2018) investigated this relationship and found the ISS can vary based on graphitic crystal structure. It was concluded that in the case of pristine AB stacked graphite, shear stresses above 140MPa (Liu et al., 2012) would be required to achieve exfoliation, but in the case of 'real graphite', which contain impurities and grain boundaries, the ISS can be reduced as low as 0.5MPa.

In order to break-down agglomerates, enough shear stress must be applied to the system to overcome the weak interparticle bonds which hold them together. The magnitude of these forces has been labelled as the agglomerate cohesive strength which are largely dependent on the geometry of the stacked graphene particulates and overall agglomerate size. Graphene flakes with larger planar size give increased cohesive strength as a result of increased surface area and therefore having a higher proportion of interactions. Agglomerates decrease in cohesive strength as they become larger (Scurati, Feke and Manas-Zloczower, 2005). The two mechanism of de-agglomeration are defined as either 'rupture' or 'erosion', which occur based on the relationship between the shear stress applied into a system and the cohesive strength of the agglomerates present. If shear stress is smaller than the cohesive stress, erosion is the main mechanism occurring and on the other hand, if the shear stress is larger than the cohesive strength then rupture is occurring (Hansen, Khakhar and Ottino, 1998). A study performed by (Kasaliwal et al., 2010) demonstrated these mechanisms through twin screw compounding of multiwall carbon nanotubes (MWCNT) into polycarbonate, as displayed in figure 2.13. Rupture refers to fast breakdown of agglomerates into large sub-agglomerates, whereas erosion is the shearing of small sections from the agglomerate surface. These mechanisms were investigated for GNPs mixed into polypropylene through twin-screw extruding by (He et al., 2017), the shear stress and residence time were analysed to understand the effect on de-agglomeration. It was found that better dispersion was produced when erosion mechanism was dominant, for longer mixing durations. This highlights the need for mixing parameters to be fully investigated in order to improve efficiency when producing dispersion states.

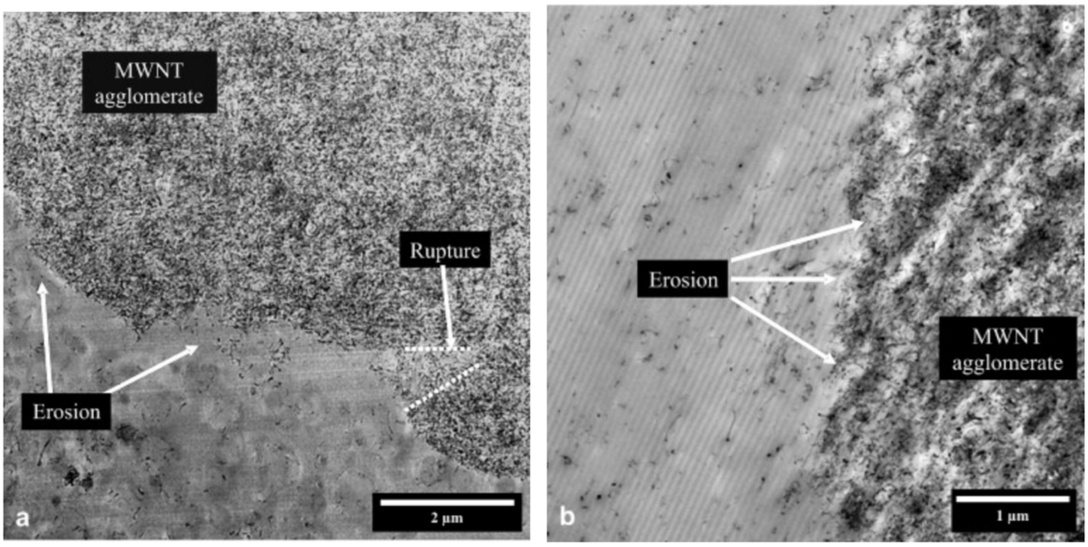

Figure 2.13 : Images displaying the erosion and rupture mechanisms of de-agglomeration of MWCNT after twin screw compounding (Kasaliwal et al., 2010)

2.4.2 Mixing methods

A wide range of techniques have been developed to create graphene dispersions, with mixing procedures ranging from minutes to days to complete (Kilic, Sherif and Ozbulut, 2019). This process is important to investigate when aspiring to optimise the dispersion process within an industrial setting, where fewer steps, resources and short mixing durations are favoured.

Sonication is a popular method of dispersing graphene, where much research has centred around optimising processing parameters (Zhang and Chen, 2019)(Tyurnina et al., 2020)(Cai et al., 2018). Sonication uses both ultrasonic sound waves and physical vibrations to break down agglomerates. The ultrasonic sound waves produce cycles of high and low pressure, causing microscopic bubbles to form and collapse. Figure 2.14 illustrates how the formation of cavitation induced bubbles and liquid jets are produced and exert high shear forces on the graphene particles, resulting in de-agglomeration and exfoliation of graphene sheets (Lin et al., 2017). Sonication is a very quick but aggressive method, whilst this results in efficient de-agglomeration, the process becomes difficult to control and in some cases causes damage and fragmentation of graphene flakes which is detrimental to mechanical properties (Ye and Feng, 2016). Sonication is commonly followed by centrifugation to separate graphene flakes by size, helping to retain graphene quality (Turner et al., 2019).

This process is usually performed within water or solvent medium, as chemical compatibility and the low viscosity medium facilitates the cavitation process. Mixing with the aid of solvents becomes inefficient as additional steps are then required to remove either before or after incorporation with the epoxy matrix, prolonging mixing times in addition to creating a negative environmental impact through the use of chemicals.

A study conducted by (Chong, Hinder and Taylor, 2016) used sonication to disperse a variety of graphene powders directly within epoxy resin, before analysing the mechanical properties. This research included analysis of the same epoxy resin and Haydale Ltd O_2-plasma treated GNP, which have been investigated in this project. It was concluded that the sonication process resulted in fragmentation of the GNPs which resulted with little improvement to mechanical performance, therefore sonication will not be investigated in this project.

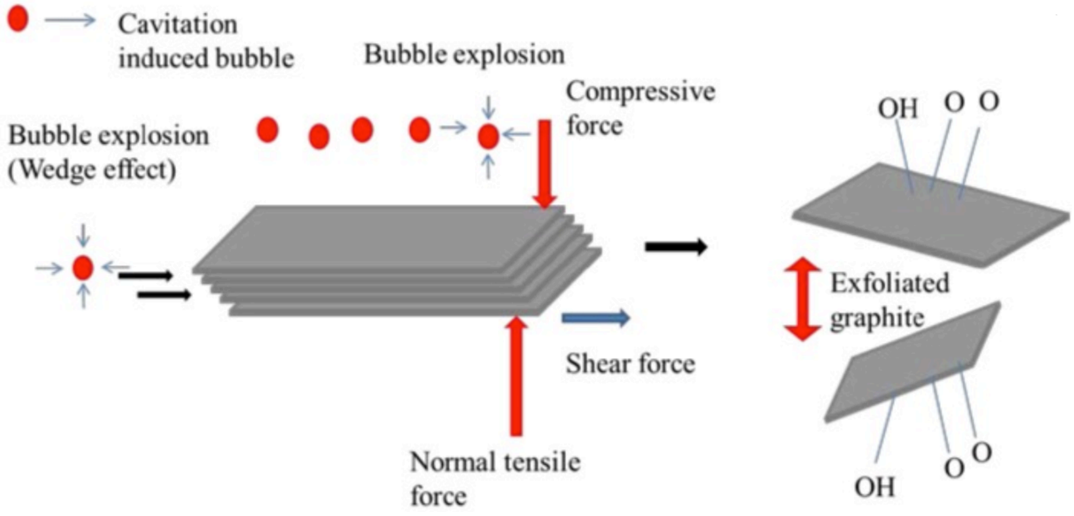

Figure 2.14 : Exfoliation of graphene sheets through sonication (Lin et al., 2017)

The two high shear mixing methods investigated in this project are overhead rotor-stator, high shear mixing (OHM) and three roll milling (3RM). These methods have been selected as they can be used directly with graphene / epoxy materials, are commonplace within industrial settings and have good scope for processing quantities to be scaled up. Both of these methods use shear forces to de-agglomerate and homogenise mixtures, but have key differences in setup which affect the overall effectiveness of each system.

Overhead rotor-stator mixers are commonly used in both research laboratories and industry. This equipment utilises a rotor-stator mixing probe to de-agglomerate, homogenise and emulsify batches of material through high shear forces. Material is drawn into the work head, due to the high speed rotation of the rotor, before being pushed out through the holes in the stator. The high shear forces exerted through this motion cause collisions between particles and the equipment, resulting in de-agglomeration. These particles are then redistributed into the material batch, as displayed in figure 2.15. It has been determined that shear forces up to 10,000s^{-1} are achievable through the Silverson LM5 equipment. Convection currents form in the material batch, which are responsible for the circulation of material through the mixing head (Silverson, 2020). This can result in an uneven effect of de-agglomeration across the material batch as agglomerates either get drawn into the streams following convection currents or settle in areas of low shear, this effect is further exacerbated in systems with high viscosity (Tamminen and Koiranen, 2015)(Utomo, Baker and Pacek, 2009).

Jet cavitation can also contribute to de-agglomeration, this is caused by velocity changes generated by fast currents produced by the quick rotation of the rotor. However, this is most effective in a low viscosity matrix (Capelo-Martinez, 2009), due to the high viscosity of epoxy resins compared with solvents, it is unlikely for this mechanism to occur during mixing of materials used in this report.

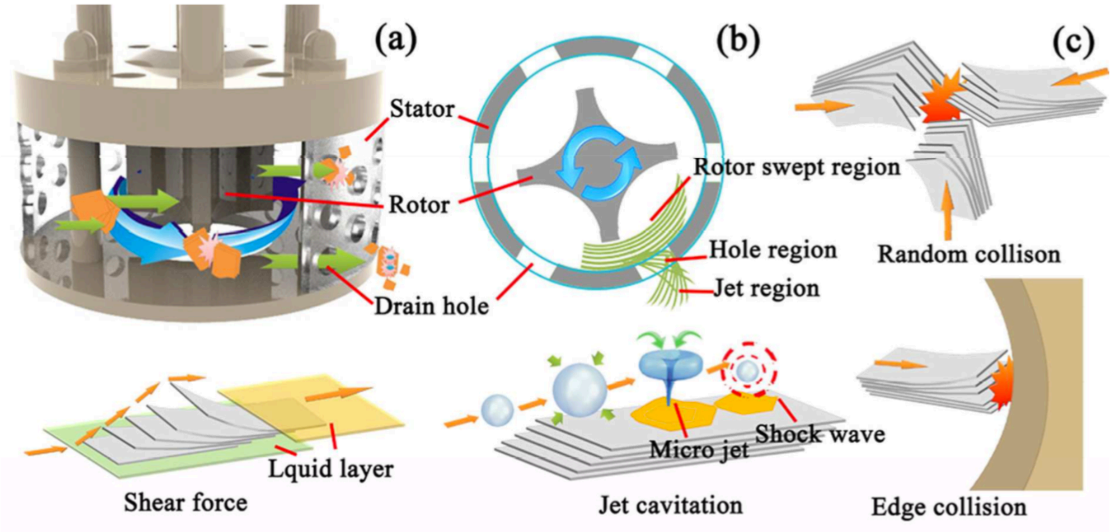

Figure 2.15 : De-agglomeration mechanism through rotor-stator equipment (Liu et al., 2014)

A study performed by (Liu et al., 2014), investigating the use of rotor-stator mixing methods on the exfoliation of graphene nanosheets in IPA-water, determined that graphene with smaller lateral dimensions are easier to exfoliate, as the overall force causing layering is also smaller and therefore easier to overcome. It was also hypothesised that particles with fewer stacked sheets are more likely to be torn by the high shear force, resulting with undesirable decrease in lateral dimensions. Rotor-stator mixing is an attractive method of de-agglomeration for use within an industrial setting, due to low maintenance use and ability to be scaled up with large quantities of material. The main drawback of this method is the uneven mix profile which may lead to the requirement of longer processing times, however, recirculating pump systems can be utilised with large quantities of material which would mitigate this effect. A key drawback of this method is the tendency of the material to heat as a result of the high energy mixing, this effect needs to be monitored when used with polymer resins to avoid degradation of the material.

3RM equipment consists of three alternatively rotating cylinders, spinning at incrementally increased speeds. Material is poured into the gap between the first two rollers, drawn out to then pass through a smaller gap between the second and third roller, and finally scraped off the last roller and deposited, as displayed in figure 2.16a. This process is usually repeated multiple times. The high shear is experienced as it twice passes between rollers, the differential in roller speed causes a gradient in shear stress across the nip gap, resulting with de-agglomeration, as demonstrated in figure 2.16b. This high shear force can be controlled by altering the roller speed, nip gap and material viscosity. It is common to use multiple passes for each batch of material processed, changing processing parameters to increase the high shear forces with further mixing (Li et al., 2016).

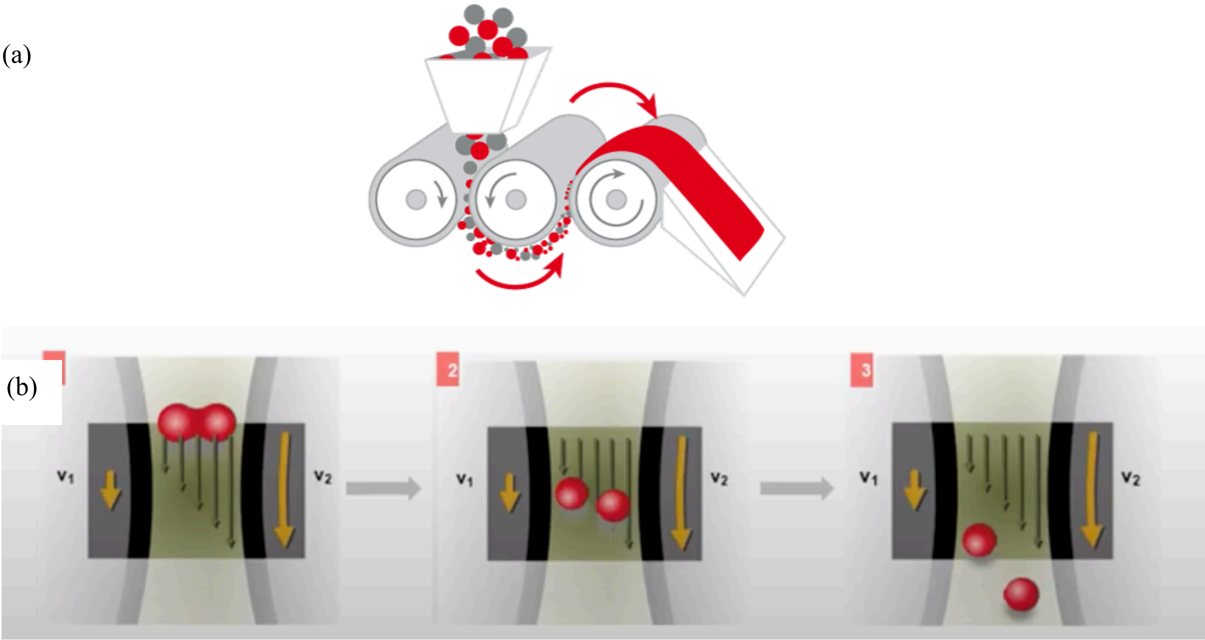

Figure 2.16 : (a) Process of mixing through the 3RM (Exakt Technologies Inc, 2020) (b) the process of de-agglomeration through 3RM, illustrating the velocity gradient between each nip-gap (Exakt Technologies Inc, 2018)

3RM is advantageous over OHM is the even distribution of shear force applied over the material batch, leaving a homogeneous effect of de-agglomeration. High filler loadings can also be used giving higher throughput of material, however, the close proximity of graphene at high loadings can lead to re-agglomeration once high shear force has been removed. Mixing by 3RM does have shorter processing times increasing efficiency, but the process does require a technician to operate the equipment.

2.4.3 Maintaining Dispersion State

Due to the nano-size and potential toxicity of graphene, the marketing of graphene in powder form is limited to consumers with specialist equipment with which nanomaterials can be safely handled. In order to maximise the versatility of marketing, graphene is combined into the host material at high filler loadings, called ‘masterbatches’. By compounding the hazardous nanomaterials into polymer, the batch materials can be safely handled and used in a wider variety of environments. Because of the high tendency for graphene to agglomerate, the longevity of dispersion state after mixing is an extremely useful parameter to industry to understand when commercialising graphene / epoxy materials.

The presence of functional groups aid de-agglomeration through improvement of graphene solubility with in polar, non-polar mediums and some polymeric mediums. The enhanced wettability undermines the weak forces which promote interactions with other graphene flakes and undermine agglomeration (Speranza, 2019)(Wypych, 2019)(Dai et al., 2015). The ability to re-agglomerate can still exist based on the levels of alteration to surface energy (Kazi et al., 2015a). As agglomeration can affect mechanical performance, it is important to understand this behaviour. Work conducted by (Santos et al., 2018), investigated the effect of morphology and functionalisation on the dispersion and re-agglomeration behaviour of GNP / polypropylene composites, prepared through an extensional mixer. Material was tested at various stages along the extensional mixer, with the expectation that re-agglomeration would occur during the stress-relaxation period. It was determined that re-agglomeration was experienced at a slower rate for larger graphene flakes, with functionalisation delaying this behaviour even further.

Generally, it is expected that if re-agglomeration were to occur it would happen during the relaxation period after mixing. However, many studies have document settling behaviour where graphene dispersions have been left over extended periods of time (Johnson, Dobson and Coleman, 2015). Therefore it can be assumed these motions which occur over time can facilitate re-agglomeration and therefore must be tracked over engineering timescale.

2.4.4 Manufacturing Hybrid Composites

Once the graphene has been effectively dispersed within the matrix material, it can be further combined with long fibres to produce hybrid composites. Fibre composites are comprised layers of aligned fibres, housed within a matrix material. Examples of commonly used manufacturing methods are discussed further in this section, however they have not been explored in this research.

Resin infusion techniques use vacuum pressure to draw the matrix material through the fibre arrangement to ensure full wetting, figure 2.17 illustrates the resin infusion method. The process begins with the fibre arrangement being laid upon a mould of the desired component shape and covered over with a vacuum bag with an airtight seal, with an inlet an outlet attached. The inlet pipe is placed within a pot contain the matrix resin and the outlet pipe is connected to a vacuum pump. Firstly, the inlet pipe is clamped off whilst the vacuum pump removes all the air from within the fibre layup. Once a vacuum is achieved, the inlet pipe is opened to allow the resin to be drawn through the fibres, aided by the vacuum pressure. Once the resin has penetrated through all of the fibres, the inlet and outlet are closed and the resin is allowed to cure.

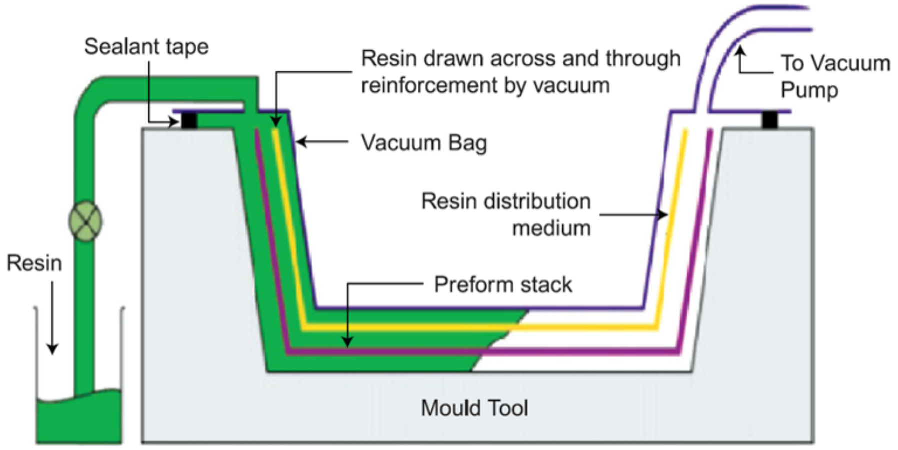

Figure 2.17: Schematic illustrating vacuum assisted resin infusion technique (Verma *et al.*, 2014)

Wet layup or hand layup is a simple but labour intensive method of fibre composite manufacture. This techniques involves the placement of each layer of fibres which are then manually wetted with resin, commonly with the aid of a tool such as a roller (figure 2.18). This is then repeated for each subsequent layer until the desired component has been formed. To improve laminate quality the component is often placed within a vacuum bag once the lamination process is complete.

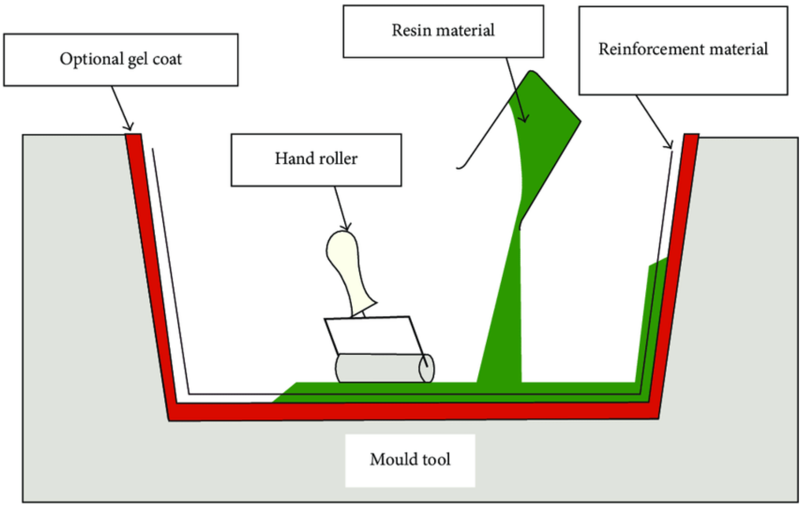

Figure 2.18: Schematic illustrating the wet or hand layup techniques (Udupi and Lester Raj Rodrigues, 2016)

Pre-preg (figure 2.19) refers to reinforcing long fibres which have already been impregnated with an uncured resin system, or resin / graphene system in the case of hybrid composites. This technique consists of the pre-preg layers being placed upon the mould tool to the desired configuration, before being placed within a vacuum bag and placed under vacuum in order to ensure the lay-up forms to the shape of the mould. The component is then ready to be cured, usually within an autoclave which applied both high pressure and heat. Manufacturing components with pre-preg materials is advantageous as they have a high resin to fibre ratio, which improves the final component properties, this is difficult to achieve in hand layup techniques. The process is generally easier, cleaner, with less waste material and results with a higher quality component.

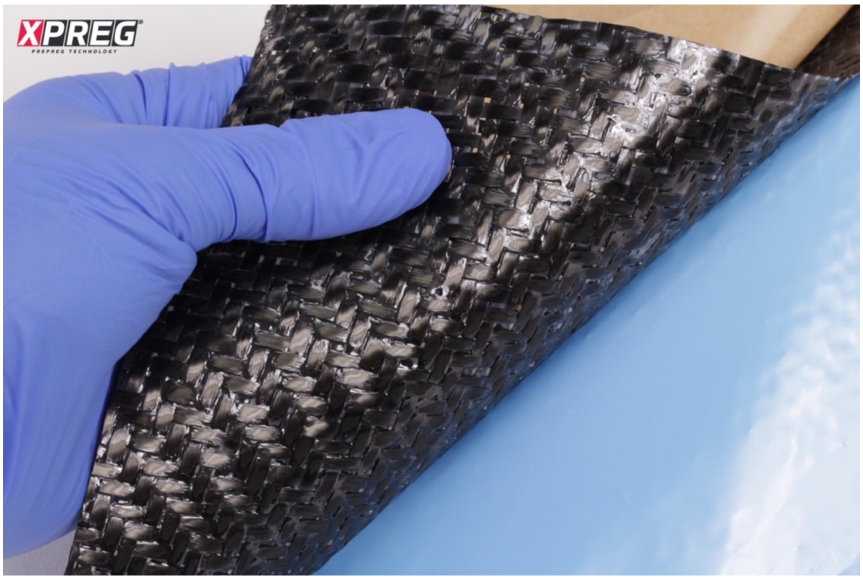

Figure 2.19 : A sheet of carbon fibre / epoxy resin pre-preg material (Easy Composites, 2021)

2.5 Mechanical Performance

It is well documented that achieving good dispersion is a primary obstacle when producing carbon based nanocomposites, with much research acknowledging that high levels of dispersion results in improved mechanical properties (Tang et al., 2013)(Gudarzi and Sharif, 2012)(Liang et al., 2018). Agglomeration is undesirable in mechanical purposes as they behave as stress concentrators, encouraging crack initiation and propagation leading to premature failure. Highly disperse systems have been shown to improve strength, stiffness and fracture toughness properties (Tang et al., 2013)(Wei et al., 2015)(Song et al., 2011). It is accepted that processes need to be undertaken to ensure a homogenous mixture, however there is limited research exploring the extent of the effect of dispersion state. Further research is needed to fully determine what constitutes good dispersion and the best method to quantify this in an industrial setting.

Work conducted by (Tang et al., 2013), showed great improvements to composite properties where highly dispersed RGO was used, the good dispersion state was produced through a combination of sonication and ball milling of the RGO in ethanol. The mixture was then combined into epoxy resin and degassed at temperature in a vacuum oven to remove the solvent. The poor dispersion state was sonicated in the same way but not receive ethe additional ball milling. This trend was maintained across various filler loadings. Improved properties were measured for glass transition temperature (Tg), fracture toughness, electrical conductivity and tensile and flexural strength and modulus. Table 2.2 displays the percentage increase in measured values of the good dispersion state compared with the poor, for the respective properties for materials at the highest filler loading studied (0.2% by weight). The most notable increase has been seen in electrical conductivity, due to an increase in flake contact points easing the flow of electrical current in the highly insulating epoxy matrix (Marsden et al., 2018). The large increase in tensile and flexural strength are owing to the improved graphene network effectively dissipating applied load and improved fracture toughness the result of propagating cracks required more energy, as illustrated in figure 2.20 (Domun et al., 2017)(Atif, Shyha and Inam, 2016). Samples representative of both low and high dispersion state underwent sonication within ethanol, further planetary ball milling was performed to produce high dispersion state suggesting that an element of high shear mixing is needed for adequate mixing (Tang et al., 2013).

Table 2.2 : Calculated percentage increase to properties of well-dispersed samples over the poorly disperse, based on samples produced at 0.2 wt%. Values have been calculated from data presented in study by (Tang et al., 2013)

	Glass Transition Temp, Tg	Fracture Toughness	Tensile Modulus	Tensile Strength	Flexural Modulus	Flexural Strength	Electrical Conductivity
% Increase	6.3	25.0	1.3	35.9	3.7	53.3	2024.3

(Pullicino et al., 2017) investigated how high shear mixing parameters may affect composite properties. Research focused on altering mixing duration and intensity achieved through an overhead high shear mixer. Optical microscopy and tensile testing were used to gauge agglomerate size and mechanical properties for each instance. It was concluded that the instance which exhibited the smallest average agglomerate size, gave the highest tensile strength. There did not appear to be any correlation between either mixing duration or mixing speed with mechanical performance. It was suggested that these fluctuations where a result of a combination of factors including agglomeration distribution size and lack of interfacial bonding. This highlights that understanding dispersion state will allow greater control of final mechanical properties and the need for a standardised method of quantifying dispersion.

An in-depth study into the optimisation of graphene dispersion into epoxy resin and the resulting effects on tensile properties was carried out by (Kilic, Sherif and Ozbulut, 2019). This research investigated the combined use of sonication and high shear mixing for varied mixing times and at different stages of the manufacturing process. Furthermore, two different epoxy systems were considered, where mixing in either resin or hardener was explored. In terms of manufacturing considerations, the study concluded that samples mixed through both sonication and high shear attained higher fracture strains, compared to samples mixed through sonication alone. Additionally, the dispersion of graphene into hardener resulted in decreased fracture strain. The dispersion quality of graphene was determined through qualitative analysis of microscopy images. Whilst microscopy gives good microscale visualisation of the dispersion state achieved, it is difficult to confidently asses the overall dispersion state using this method. As the sonication and high shear mixing has been performed using probe and overhead setup respectively, de-agglomeration is likely to be inhomogeneous across the material batch, further reducing the effectiveness of microscopy.

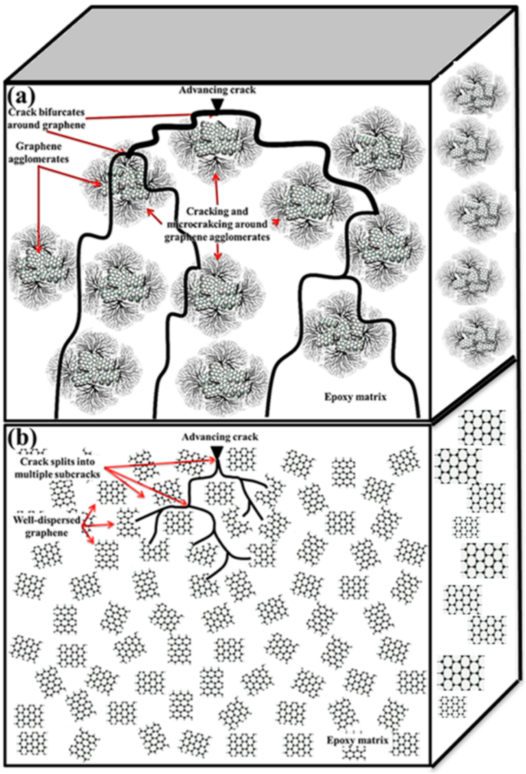

Figure 2.20 : mechanisms of crack propagation in poor (above) and good (below) dispersion states (Atif, Shyha and Inam, 2016)

These studies demonstrate the relationship between material properties and dispersion state, however there is scope for this to be understood further. Different mixing methods have been shown to de-agglomerate and homogenise to varying extents, highlighting improvement of properties are vastly dependent on method of mixing. Mixing programs need to be understood further as it has been shown that higher degrees of mixing time or intensity do not correlate to mechanical properties (Pullicino et al., 2017), emphasising the importance of being able to characterise dispersion state.

2.5.1 *Thermomechanical and Cure*

Thermomechanical properties of composite materials are important to investigate. The physical properties of thermoset polymers drastically change upon heating from hard and rigid within the 'glassy' region to soft and malleable within the 'rubbery' region. Due to the high interest for composite materials within the aerospace sector, where tolerance to high temperature is imperative, the thermomechanical properties of graphene / epoxy composites are of high interest (Topal *et al.*, 2016). The glass transition temperature (Tg) is taken from the range of temperatures over which the polymer transitions between these two states and are the subject of many research studies.

Published research has shown both improvements and deterioration of Tg with the addition of graphene.

The properties of thermoset polymers are highly influenced by their internal structure. Where the degree of crosslinking is highly influential on the overall composite strength and stiffness, leaving curing cycles and the effect of the addition of fillers important parameter to understand (Chakraborty *et al.*, 2018). A study conducted by (Vryonis et al., 2019) investigated the effect of graphene oxide (GO) on the epoxy resin curing process. It was determined that the hydroxyl groups present in GO are capable of forming bonds with the epoxy resin during the post-cure process. This occurred in sites which would have normally reacted with the hardener material, causing disruption to the resin stoichiometry. This led to a lower degree of crosslinking and a reduction to Tg. The addition of 2% GO by weight caused Tg to reduce by 8.74%, compared with neat epoxy after undergoing full cure and post-cure cycles. However, these reactions result to improvements in interfacial properties and overall composite mechanical performance (Bao *et al.*, 2011), highlighting the need to understand the relationship between these factors and overall composite performance.

2.6 Aims

This work aims to fully investigate the link between manufacture, dispersion state and mechanical performance, with strong consideration to industry practices and capabilities. The efficacy of dispersion characterisation methods have been investigated and compared to in order to develop an accurate and efficient, quantitative method which can be adopted into industrial quality control processes.

Various high-shear methods which are commonplace in an industrial setting have been assessed to determine the quality of dispersion state produced and the resultant effect on mechanical properties. Varied levels of functionalisation intensity has been assessed to understand the extent to which this aids the de-agglomeration process as well improvement to interfacial properties. Furthermore, studies into the effect of dispersion, functionalisation and flake size with relation to curing procedure has been assessed.

Finally, this research conducted in this report aims to look at re-agglomeration behaviour of uncured graphene / epoxy masterbatches over the space of 4 weeks, investigating the role of functionalisation, filler loading and storage temperature. This work would be hugely beneficial in the understanding of the product needs over real-life timescales.

3 Materials & Experimental Methods

The materials and equipment used in this project are detailed in this chapter. A brief overview of parameters and the purpose of each method has been detailed.

3.1 Materials

All materials were provided by Haydale Ltd. There were two geometries of graphene investigated through this project, with dimensions quoted in table 3.1. The powders have been classified as Graphene Nanoplatelet (GNP) and Few Layer Graphene (FLG) as per ISO/TD 80004-13 and will be referred to as such through this report. These two materials are distinguished by the planar size and number of layers as discussed in section 2.2.1.

Each graphene powder has undergone two plasma functionalisation treatments performed by Haydale Ltd, using procedure described in section 2.1.2. All treatments were performed in an oxygen atmosphere, with each graphene powder undergoing functionalisation to two levels of intensity; 'standard' and 'high'. The 'standard' treatment refers to the process which is used commercially in Haydale products. The 'high' intensity treatment is an experimental treatment which was performed with increased processing time, plasma power and gas pressure, with the aim of enhancing the proportions of functional groups attached to the graphene surface. The increase of carboxylic functional group content was particularly desirable for its reactive properties, enhancing both dispersion state and interfacial properties (Williams *et al.*, 2013).

Through this report the three functionalisation states will be referred to as the following; U (unfunctionalised), S (standard treatment) or H (high intensity treatment). Both flake morphology and effects of functionalisation are explored further in chapter 4.

Table 3.1 : Dimensions of graphene investigated in this work

	Number of Layers	Planar Size
Graphene Nanoplatelet (GNP)	15-20	5 µm
Few Layer Graphene (FLG)	1-4	>200 nm

Huntsman Araldite LY1564 is a low viscosity, modified bisphenol-A epoxy resin. This was used as the matrix material with Aradur 2954 hardener. Information and properties relevant to this project are detailed in table 3.2, further information on the curing procedure is described in chapter 3.5.2.

Table 3.2: Overview of information for epoxy resin system used throughout this project, values have been taken from the material data sheet

Property		Value
Viscosity (Araldite LY1564 only)		1200 – 1400 mPas
Mix ratio (parts by weight)	Araldite LY1564	100
	Aradur 2954	35
Curing cycle		1 hr 80 °C + 4 hr 140 °C
Tensile test	Tensile modulus	2550 – 2650
	Tensile strength	71 – 77 MPa
	Strain at break	4.5 – 5.5 %
Flexural test	Flexural modulus	2600 – 2800 MPa
	Flexural strength	120 – 124 MPa
	Strain at break	6.5 – 7.5 %
Glass transition temperature (Tg)		129 – 134 °C

3.2 Powder & Chemical Characterisation

Experiments detailed in this section were performed on all graphene powders, with the following intentions; to understand the differences in chemistry after functionalisation, visualise the two flake morphologies and measure initial agglomerate size distribution. These questions are investigated further in chapter 4.

3.2.1 X-Ray Photoelectron Spectroscopy (XPS)

Measurements were performed on each graphene powder to characterise the chemical changes caused by plasma functionalisation. XPS fires high energy X-Rays which interact with the atoms held on the surface of the material, this causes electrons to be released from their atomic orbitals and detected by the machine. The energy required to release each electron is measured, this value is known as binding energy (eV). Each electron possesses a unique binding energy dependent on the position and atom it is held inside, allowing for chemical compositions to be ascertained (Zambonin and Desimoni, 1987).

As the oxygen based functional groups were attached, scans were focussed on detecting carbon and oxygen atoms using an Thermo K-alpha XPS. The scans were performed under vacuum with chamber pressure was set to ~$1x10^{-9}$ Torr with core levels set to binding energy 284.8eV, which correlates to C 1s. The powder sample was placed directly onto the sample plate and held in place with copper clips. Once spectra had been produced, curve fitting was performed to determine the proportions of each functional group present using CasaXPS software with a Shirley background settings. A Scofield sensitivity factor was employed to scale the measured peaks, ensuring peak areas are representative of the amount of material present within a sample surface (Morgan, 2017).

3.2.2 Raman Spectroscopy

Raman Spectroscopy was performed on all graphene powders to compliment XPS data and assess how the functionalisation process affected chemical and atomic composition. In this technique, light of known wavelength is shone onto a sample and causes molecular vibrations to occur. This interaction causes the light to change in frequency before it is scattered back and detected. The shift in frequency is analysed to gain information about the molecular structure (Laserna, 2014). Scans were performed with a Renishaw InVia in the spectrum range of 500-3500 cm^{-1}, which adequately captures the vibration modes of the graphene samples. The equipment was fitted with a 514nm Edge Laser performing at 10% laser power. Accumulation was set to 5 with an exposure time of $10s^{-1}$, these settings were determined to give good spectra resolution whilst minimising scan duration. The laser exposure on the material was minimised and cosmic ray removal was engaged. Three scans were performed for each powder to ensure repeatability.

3.2.3 ZetaSizer

Zeta potential and electrical conductivity were measured for each graphene particle using a Malvern ZetaSizer nano ZS. Zeta potential is the measure of electrostatic attraction or repulsion between particles (Ferraris et al., 2018), these measurements were conducted to understand the stability of graphene powders in dispersion and the effect of functionalisation on this behaviour. 0.1g of each powder was hand mixed into 10ml of distilled water. Tests were performed at room temperature and zeta potential was calculated through Malvern software using the Smoluchowski equation.

3.2.4 Scanning electron microscopy (SEM)

Scanning Electron Microscopy (SEM) images were collected for each graphene powder in order to visualise the morphology and agglomerate size. SEM imaging was performed for all graphene powders using a Quanta 3D FEG, at spot size 3.5nm, and 20kV beam current. These settings allowed better resolution at low magnification. Samples were held onto conductive carbon sticky pads, mounted onto steel holders. Excess powder was removed using compressed air spray. Images were taken at low magnification to determine initial agglomerate size and again at high magnification to study the flake morphology. Post processing using ImageJ software was used for measurements for agglomerate size and also planar size.

3.2.5 Sample Preparation for Transmission Electron Microscopy (TEM)

3.2.5.1 Powder Imaging

TEM imaging was performed only on GNP-S and FLG-S powders, this was done to clarify measurements of planar size and number of graphene layers therefore deagglomeration was essential. Each powder was mixed into acetone and ultrasonicated using a fisher scientific S-Series ultrasonic bath at frequency 37kHz for 5 mins. The solution was then dropped onto TEM grids and allowed to dry out before imaging.

3.2.5.2 Microtome cured samples

The use of microtome equipment and TEM imaging detailed in section 3.2.6.2 was facilitated by Manchester University and the Henry Royce PhD access scheme. These samples were imaged to determine dispersion state of graphene after undergoing mixing and curing. TEM samples were prepared from previously tested flexural test samples which were first ground down to a square point, approximately 1mm x 1mm as shown in figure 3.1, using a grinding table. A Leica EM VC6 microtome with glass knife was used to further reduce the dimensions of the flat surface to approximately 0.5mm square and then across the flat surface to ensure it was level. Finally an oscillatory diamond knife was used to cut the TEM samples. Films of 100nm thickness were shaved off at a speed 0.4mm/s, with knife operating at 3V and frequency 28kHz. The cut films were then deposited into a bath of distilled water and picked up onto copper mesh TEM grids. It was determined during initial optimisation of setup parameters that the GNPs were not suitable for preparation in this method. It was found that the optimum sample thickness was too thin to adequately encase the graphene flakes, resulting in them being pulled out and tearing the epoxy resin during cutting. It was not feasible to increase the film thickness as this decreased the ability of TEM electron beam to penetrate through the sample.

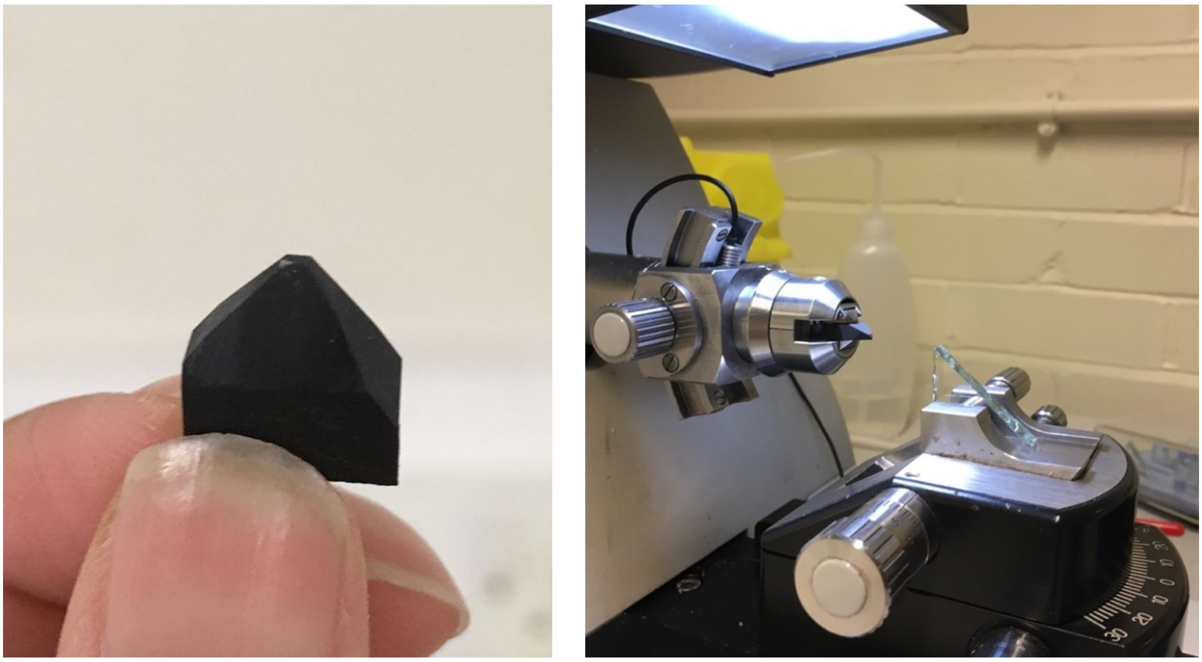

Figure 3.1 (left) sample geometry from which TEM samples were cut from (right) sample mounted in microtome ready to be cut with glass blade

3.2.6 *Transmission Electron Microscopy (TEM)*

3.2.6.1 *Powder imaging*

TEM imaging was conducted on FEI Tecnai 12 Biotwin microscope with Gatan Orius SC1000A CCD camera. This was performed on GNP-S and FLG-S samples, prepared as described in section 3.2.5.1.

3.2.6.2 *Graphene / epoxy imaging*

An Oxford Instruments Technai G3 TEM was used to image dispersion state of graphene embedded into epoxy resin. These bright field images were taken at 80kV HT acceleration voltage at spot size 3. The condenser aperture was set to 100µm and objective aperture to 20µm. This method of imaging was performed on select cured FLG / epoxy samples, prepared as described in section 3.2.5.2, analysis of these samples is detailed in section 6.4.

3.3 *Mixing Methods*

This section will outline the parameters used for each mixing method, the primary aim was to assess the dispersion quality produced through different mixing methods and the benefit of long mixing times. Selected mixing equipment are typically used in industry and parameters have been chosen to be achievable within this setting. All mixing has been performed before cure, with a mixture of graphene and epoxy resin only. This was done to further streamline the mixing process.

3.3.1 High Speed Mixing

SpeedMixer DAC 800.1 allows high speed, double rotation of sample held within a container. This motion is described as ‘dual asymmetric centrifuge’ and uses centrifugal forces to quickly homogenise mixtures as demonstrated in figure 3.2. De-agglomeration does not occur during this process meaning this method of mixing alone is not sufficient to achieve a good dispersion state. Due to material being mixed within removable containers, material losses during mixing are minimal. This technique is ideal for initial combination of graphene and epoxy, in addition to the incorporation of hardener.

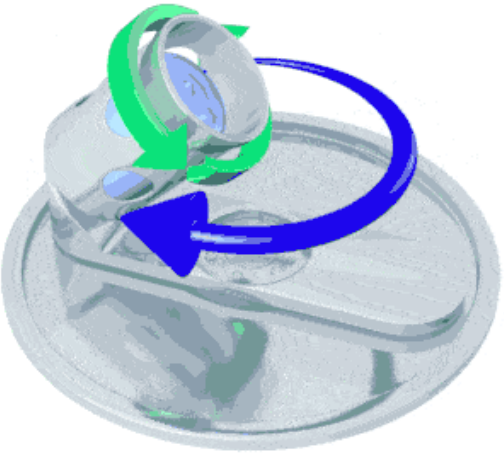

Figure 3.2 : Dual motion of the high speed mixer (FlackTek Inc, 2018)

High speed mixing has been used to create material masterbatches, this describes the process of wetting high concentrations of graphene into the epoxy resin. The purpose of this is to combine and contain the hazardous graphene powders into epoxy resin, resulting in no risk of inhalation of graphene. This allows safe transportation and handling of graphene outside of a fume hood. Masterbatches were produced for each graphene powder at 10% fill weight. As high speed mixing quickly combines graphene into the epoxy with no effect of de-agglomeration, this method was used to produce samples representative of the ‘unmixed’ state. These samples were mixed at 1950 rpm for 5 minutes, with powders comprising of 1% fill weight. This mixing program adequately facilitates the combining of the graphene within the epoxy resin. This equipment was used throughout the casting process, as described in section 3.5.2.

3.3.2 Over Head High-Shear Mixing

Silverson LM5 overhead mixer (figure 3.3) uses a high-shear rotor blade to de-agglomerate and homogenise material. Masterbatched material (at 10 wt% fill) was diluted with epoxy resin to achieve graphene content of 1% fill weight and roughly combined through hand mixing. Mixing speed was slowly ramped up to 6000rpm so as not to exceed 2 volts and overload the equipment. As mixing began, the mixture heated up, reducing the viscosity and a drop in the voltage used by the equipment. It took approximately 2 minutes to reach the target rpm. Initial mixing was performed with 1248g of material, with 180g of material being removed after 15, 30, 60 & 90 minutes of mixing. Material was kept in a water bath with temperature monitored to ensure it did not rise above 60°C and degrade the resin. Mixing was performed in 15 minute bursts to allow sample to cool and water bath to be changed.

This high shear method has the capacity to de- agglomerate graphene sheets, which is essential to produce good dispersion state. This method operates on relatively small batches of material, but has the potential to be scaled up. This method relies on convection currents within the material batch to draw material through the rotor-stator, leaving an inhomogeneous mixing profile and inconsistencies in dispersion of each batch.

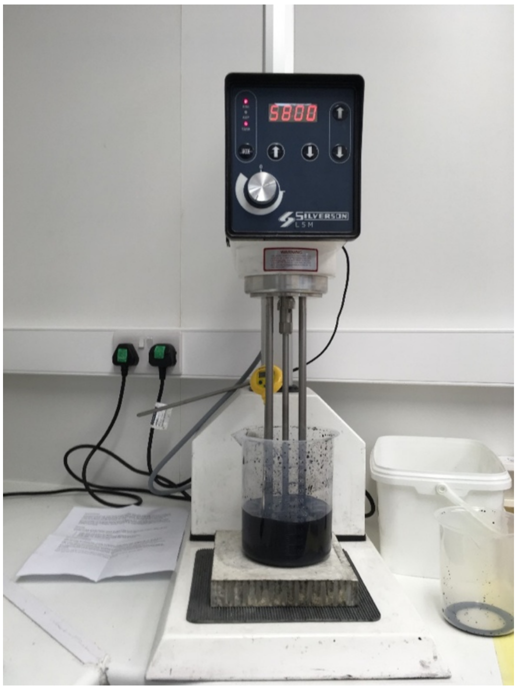

Figure 3.3 : Silverson LM5 overhead high-shear rotor-stator mixer

3.3.3 Three Roll Mill (3RM)

Exakt 80E equipment was used to de-agglomerate samples through high-shear forces. This batch processing method passes material between 3 horizontal rollers rotating in alternate directions at a speed ratio of 9 : 3 : 1. Material was processed at 10% weight fill to increase material viscosity and subsequent shear forces. Material was processed for 2, 5 10 & 15 passes to parameters defined in table 3.2. The initial 2 passes through the 3RM are performed at lower roller speed with wider nip gaps in order to facilitate a gradual effect of de-agglomeration, these mixing parameters are referred to as '3RM-P1'. Subsequent passes are carried out with narrower nip gap and higher roller speed, these parameters have been referred to as '3RM-P2' as detailed in table 3.3.

Table 3.3 : 3RM processing parameters

	Passes	Nip Gap 1 (µm)	Nip Gap 2 (µm)	Roller Speed (rpm)
3RM-P1	1-2	45	15	380
3RM-P2	3-15	15	5	450

Similarly to the LM5 Silverson mixer this equipment uses high-shear forces essential for de-agglomeration and exfoliation, but ensures even distribution of force is applied to material. This method is ideal for mixing high viscosity material, allowing effective mixing to be performed at high filler loadings. 3RM has the capacity to scale up, allowing for the possibility of high volume of throughput material.

3.4 Microscopy & Agglomerate Sizing

The equipment and parameters used to characterise dispersion state are outlined in this section. These methods are further discussed in Chapter 5.

3.4.1 Hegman Gauge

This equipment was used to perform fineness of grind measurements with accordance to ASTM D1210, using a double channel TQC grindometer. The Hegman gauge consists of a tapered channel machined along the length of a stainless steel block. The depth of the channel ranges from 0-25µm which is denoted in increments of 2.5µm. Approximately 1g of uncured graphene / epoxy sample was placed at the top of each channel and scraped down in a single motion, ensuring contact between the scraper and equipment over the length of the channel. Resultant streaks were formed in the material at the depth of the channel which corresponded to the agglomerate size.

Measurements were recorded for the largest agglomerate size and the point of break, as illustrated in figure 3.4. The point of break corresponds to the average agglomerate size and is determined as the point from where streaks are formed across the channel. Although this measurement effectively displays general average size trends, it is very subjective leaving repeatability low. Values for each were taken as an average over 10 measurements. This test is predominantly used with inks and pigments to assess the dispersion of particles in suspension.

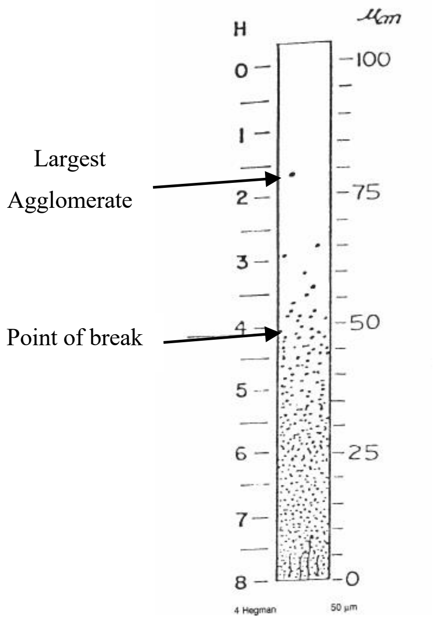

Figure 3.4 : Illustration of the determination of 'break' and ‘largest agglomerate’ values ASTM D1210

3.4.2 *Optical Microscopy*

Optical microscopy was used to observe FLG within epoxy resin. A Nikon eclipse LV100 Microscope was used in light transmission mode at x10 magnification and Nis-Elements software was used to size and measure agglomerates. Samples were prepared by placing a drop of material onto a clean glass slide with a glass cover slip placed on top and allowed to settle. Samples used for agglomerate sizing were diluted down to 0.1% filler loading to ensure they were clearly identified under the microscope. Thresholding techniques were performed through Nikon Nis-Elements software to identify agglomerates in each image and values for equivalent diameter. This method is discussed further in chapter 5.1.1. Analysis was based on measurements taken for between 800-1000 agglomerates.

3.4.3 *Rheology*

Tests were performed on uncured samples, with Bohlin Instruments rheometer according to BS ISO 6721-10. Measurements were executed using 40mm parallel plates with a gap size of 0.5mm, a water bath was utilised to control the temperature of the base plate and ensure that each measurement was performed at 25ºC. Viscometry tests were conducted to find material viscosity at a filler loading of 1% by weight. Viscometry measurements were based on 20 data points taken logarithmically over a shear rate of 0.1-1000s^{-1}.

3.5 Sample Production

3.5.1 Mold design and manufacture

Molds were fabricated from aluminium T24 tooling plate, in two separate designs. The first, as seen in figure 3.5a, allowed the manufacture of 4mm x 210 mm x 220mm (approx.) boards which were subsequently machined for mechanical test specimens. This sandwich mold was constructed from a 4mm thick centre plate and two 8mm thick outer plates, held together by steel nuts and bolts. The second mold was used for the fabrication of DMA test samples, a sandwich mold with centre and outer plates measuring 2mm & 4mm in thickness respectively. The plates were held together by stainless steel screws which fit into threaded holes machined into the bottom plate, as shown in figure 3.5b and c The mold produced samples with dimensions 2mm x 5mm x 15mm.

3.5.2 Casting procedure

Araldite LY 1564 was cured with Aradur 2954 hardener at ratio of 100:35 by weight respectively. The calculation of graphene fill weight was based on the percentage of the overall weight of the final part (the combined weight of resin, hardener and graphene).

Following any mixing, the uncured graphene / epoxy mixtures were placed into a vacuum chamber and held at -1 bar for 1 hour. This was done to remove air bubbles from the sample and ensure the quality of casted samples. The hardener was then added and combined for 3 minutes at 1950rpm in SpeedMixer equipment and then returned to the vacuum chamber for a further 30 minutes.

Material was decanted into both plate and DMA molds. The plate molds was held upright and slightly tilted as sample was slowly poured along the edge of the centre cavity to ensure no air was introduced to the mixture during this process. Material was slowly pipetted into each cavity of the DMA mold, again ensuring no air was trapped within. Samples were then left to cure at room temperature for 18 hours. Samples were then post cured in pre heated oven for 1 hour at 80ºC and a further 4 hours at 140ºC (Huntsman, 2011).

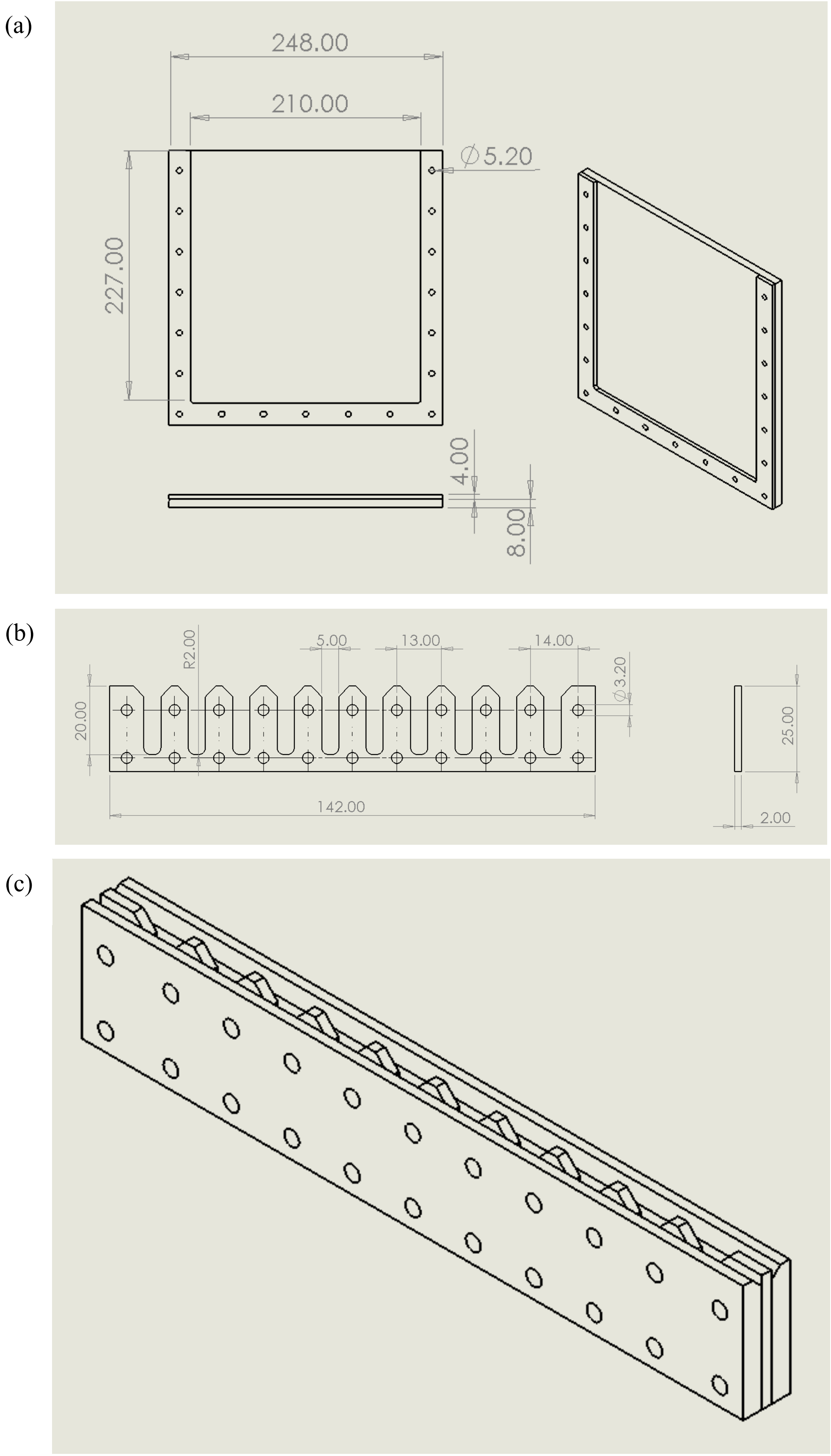

Figure 3.5 Technical drawings of manufactured molds (a) plaque mold (b) DMA mold centre geometry (c) DMA mold assembled

3.6 Mechanical Testing

The mechanical testing methods and procedures are outlined in this chapter. All tests were performed on materials produced at 1wt% fill loading.

3.6.1 Dynamic Mechanical Analysis (DMA)

Perkin Elmer D8000 Dynamic Mechanical Analyser was used in single cantilever mode to run temperature sweep tests on samples manufactured by method outlined in section 3.5. The test parameters were set after an initial strain sweep test was conducted on pure epoxy samples to determine the Linear Viscoelastic Region (LVR), where samples were setup in single cantilever mode and subjected to deformation over the range 0 – 100 microns, at frequency 1Hz at 25^{o}C.

The aim of this test is to find the region where the relationship between the applied stress and resultant strain is linear, meaning the polymer structure is not permanently deformed when under load. It is important to set further test parameters from within this region as there will be no rearrangement within the polymer structure and ensures the accuracy of software calculations of structural properties (Menard, 1999).

Figure 3.6 shows the relationship between displacement and storage modulus for each graphene sample. The point at which the storage modulus is changeable with displacement amplitude indicates the displacement is large enough to cause permanent deformation and the end of the LVR. The end of the linear region for all samples is denoted by the dashed line as shown in figure 3.6, leaving the displacement amplitude (strain) to be selected as 0.01mm.

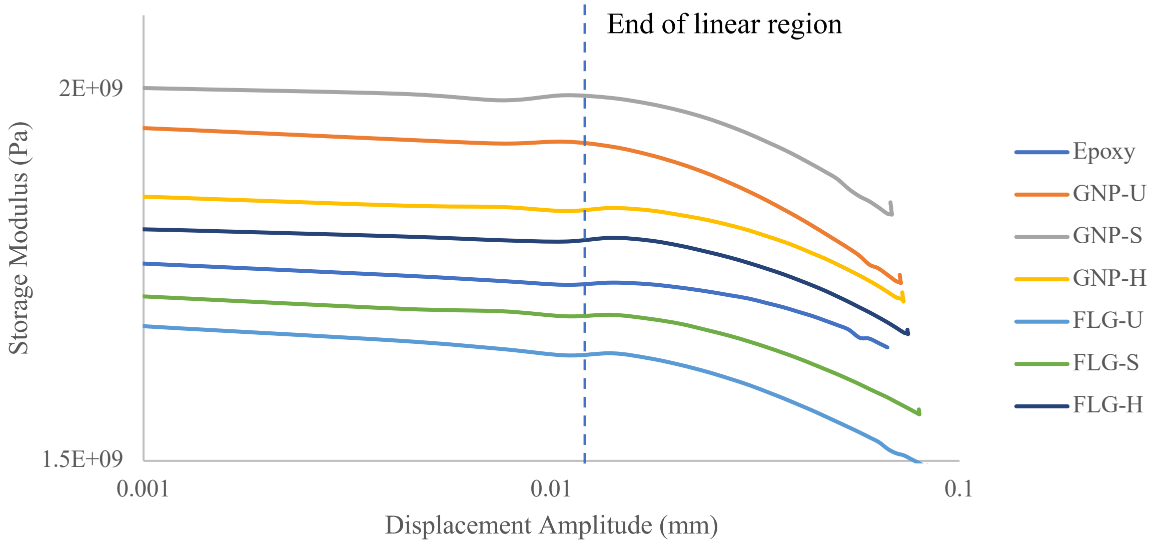

Figure 3.6 : LVR tests performed for each material at 1 wt% fill

Temperature scans were performed in single cantilever mode, with the parameters defined in table 3.4. The curves generated for tanδ, storage and loss modulus were investigated further, to ascertain information regarding the cure behaviour and viscoelastic properties. Values for glass transition temperature (Tg) were taken at the peak of the tanδ curve, loss modulus curves have been compared numerically with the curve peak height. Storage modulus values have been taken at 40°C unless otherwise stated, as demonstrated in figure 3.7.

Table 3.4 : Tests parameters used during DMA test

Start Temperature (ºC)	End Temperature (ºC)	Displacement / Strain (mm)	Frequency (Hz)	Heating Rate (ºC/min)
25	200	0.01	1	3

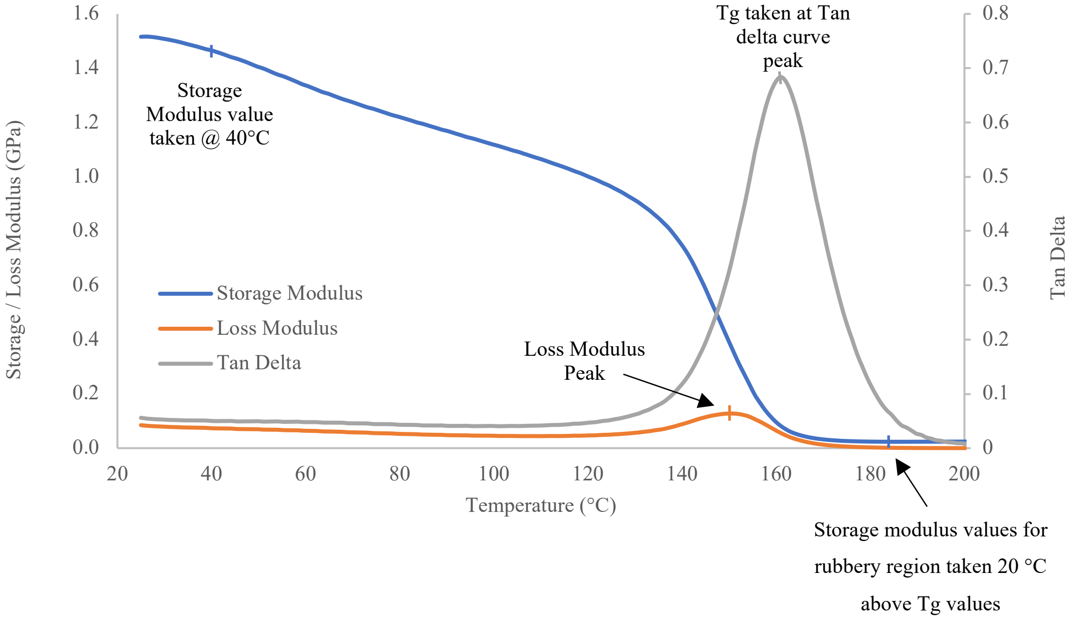

Figure 3.7: Illustration of how values have been determined from DMA curves

3.6.2 Tensile Testing

Type 1BA dumbbell shaped small specimens were machined from cast plaques in accordance to BS EN ISO 527, as shown in figure 3.8. 10 samples were machined and tested for each material using Shimadzu Autograph equipment, fitted with 20kN load cell. A plastic guide was fabricated to ensure each sample was held in the same position within the clamps. Video Strain Gauge (VSG) equipment was used to track elongation across the sample gauge length, which was used to calculate strain in samples. Load applied was recorded through the VSG as a direct output from Shimadzu equipment.

As per BS EN ISO 527-1, samples were then tested until failure, at 2mm/min load rate. Due to noise in load data caused by the connection between Shimadzu load output and VSG input, computational post processing was used to smooth presented curves. This was done using the moving average function in excel over a set of 30 data points. Values for tensile modulus were determined using the 'chord slope' method as defined in section 10.3.2 of BS EN ISO 527. Strength and strain at break measurements were taken at the stress and strain at failure, respectively.

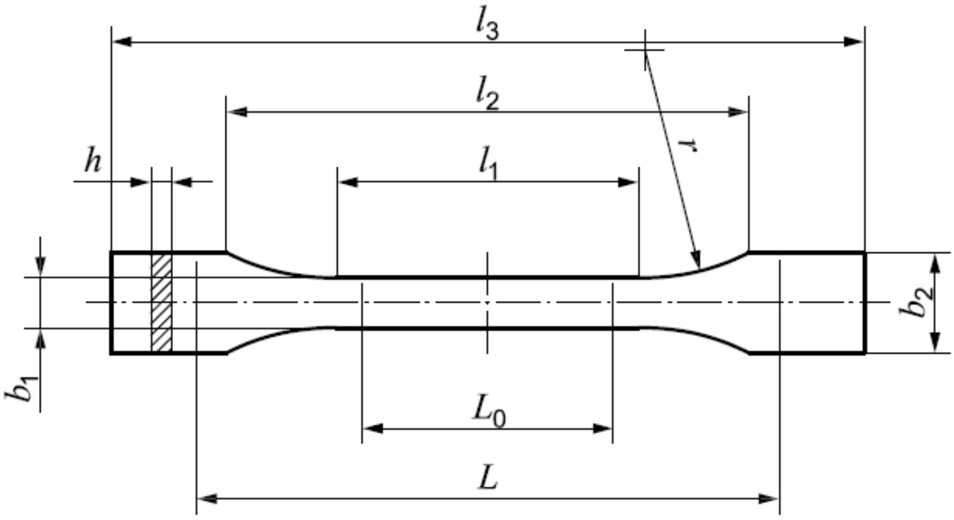

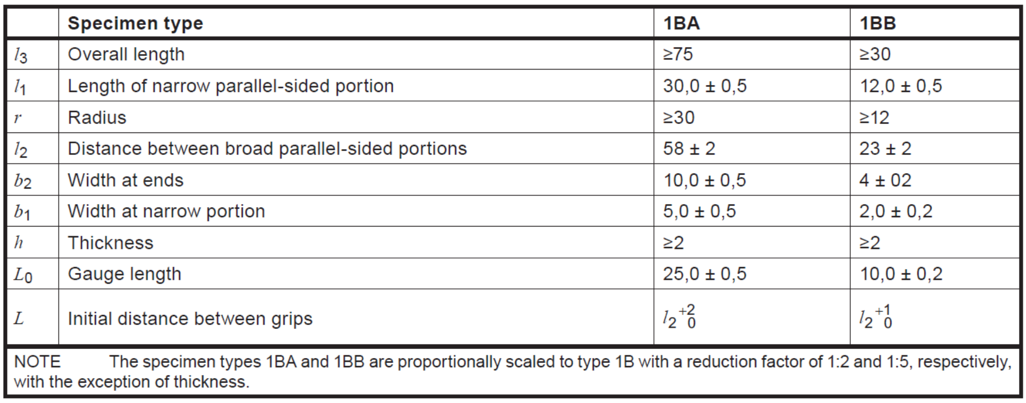

	Specimen type	1BA	1BB
l_3	Overall length	≥75	≥30
l_1	Length of narrow parallel-sided portion	30,0 ± 0,5	12,0 ± 0,5
r	Radius	≥30	≥12
l_2	Distance between broad parallel-sided portions	58 ± 2	23 ± 2
b_2	Width at ends	10,0 ± 0,5	4 ± 02
b_1	Width at narrow portion	5,0 ± 0,5	2,0 ± 0,2
h	Thickness	≥2	≥2
L_0	Gauge length	25,0 ± 0,5	10,0 ± 0,2
L	Initial distance between grips	$l_2{}^{+2}_{\ 0}$	$l_2{}^{+1}_{\ 0}$

NOTE The specimen types 1BA and 1BB are proportionally scaled to type 1B with a reduction factor of 1:2 and 1:5, respectively, with the exception of thickness.

Figure 3.8 : Tensile specimen geometry as per BS ISO 527-1, type 1BA specimens were used

3.6.3 Flexural Testing

Samples were machined from cast plaques manufactured through process outlined in section 3.5 in accordance to BS ISO 178. Rectangular samples were produced to measurements 4mm x 10mm x 90mm. The radius of supports and loading edge was 5mm, arranged to give a span width of 64mm with loading edge directly in the centre. Measurements were conducted in compression using a Zwick Roell 50 fitted with a 50kN load cell. VSG apparatus was used to measure the sample deflection under load, which was later used to calculate strain values. Load applied was recorded through the VSG as a direct output from Zwick equipment. Pre-load was applied at 1mm/min up to 5N of force, loading rates of 2mm/min and 10mm/min were used to determine flexural modulus and flexural strength, respectively. Values for Flexural stress, strain and modulus were calculated as per section 9 of BS ISO 178.

4 Graphene Characterisation

Characterisation methods have been performed on each graphene powder to define the fundamental differences. Microscopy and sizing methods have been used to visualise differences in geometry and particle size distribution (PSD). Chemical characterisation techniques have been employed to fully understand the effect of each functionalisation process.

4.1 Morphology

Figures 4.1 to 4.4 show SEM and TEM images taken for both graphene powders. GNPs have been quoted as having a planar size of approximately 5µm with 15-25 layers, translating to aspect ratio of 597 – 995 (figures 4.1 and 4.2). Sheets appear to be large and flat with low levels of wrinkling, suggesting interfacial stress transfer through mechanical interlocking will not occur (Qin et al., 2016). Flakes show a range of planar sizes, therefore it is difficult to say whether these are stacked flakes with irregular planar dimensions or agglomerated flakes.

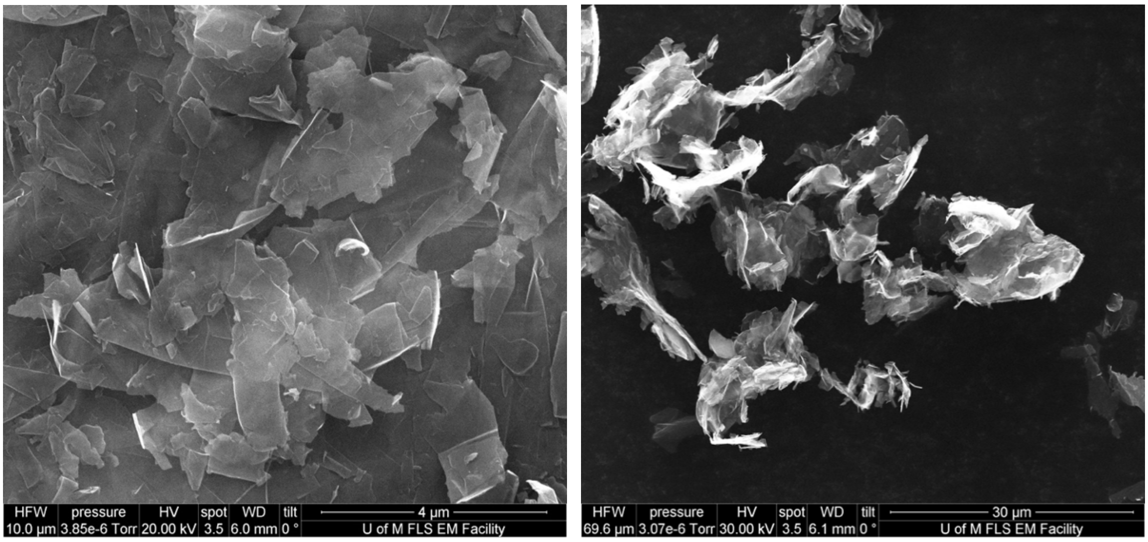

Figure 4.1 : SEM images of GNP-U powder

The right image shows GNP agglomerates in the initial state, comprised of many graphene flakes. These measure much larger than the initial quoted dimensions and maintain a flaky appearance. Figure 4.2 confirms the quoted number of layers to be accurate. Figure 4.3 displays FLG powder, illustrating the stark difference in morphology between the two graphene flakes. High levels of agglomeration is apparent and appear to be textured and spherical in shape. FLG is quoted to have a planar size <200nm and consist of 1-4 layers, giving an aspect ratio of 149 - 597.

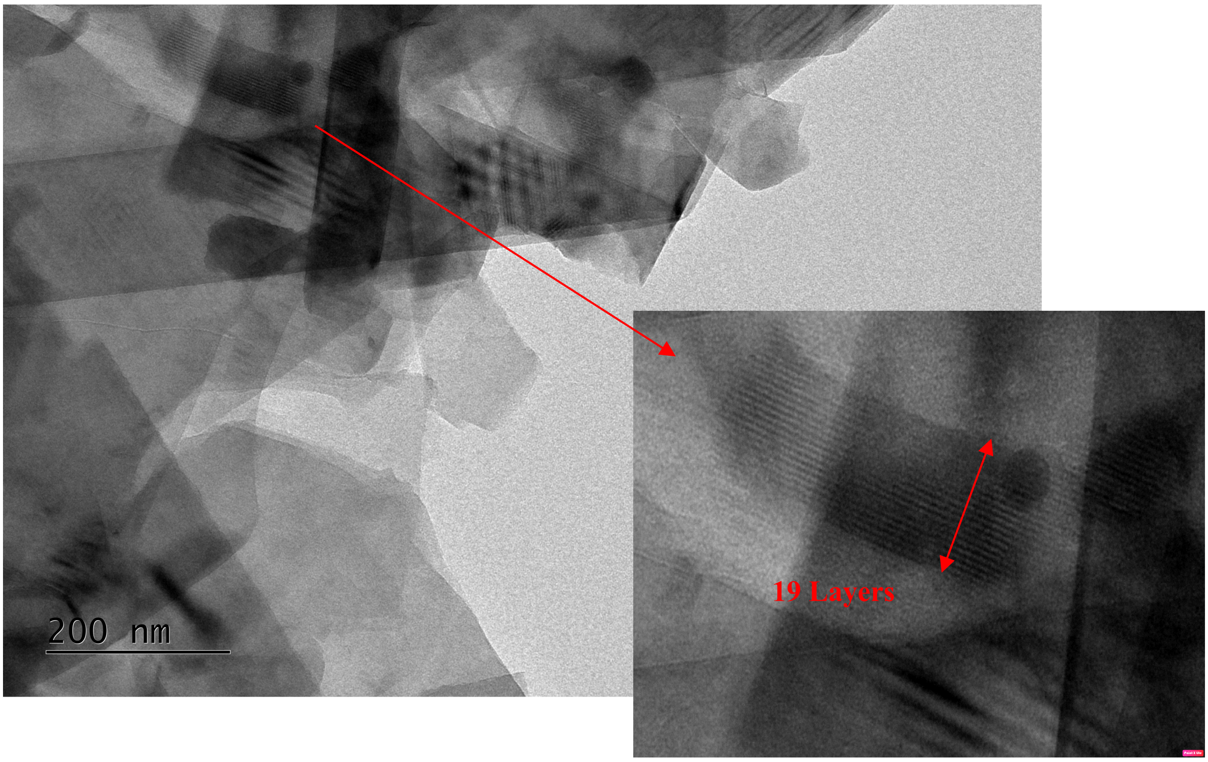

Figure 4.2 : TEM image of GNP-U flake and number of layers in a particulate

It is clear that deagglomeration is vital in order to achieve these quoted values. Figure 4.4 shows TEM images of FLG, samples were prepared from FLGs with had undergone ultrasonication in acetone, showing a wide range of planar sizes. It is not possible to determine the number of graphene layers from these images, this could be due to the low quoted number. Other methods such as ellipsometry may be necessary to determine this.

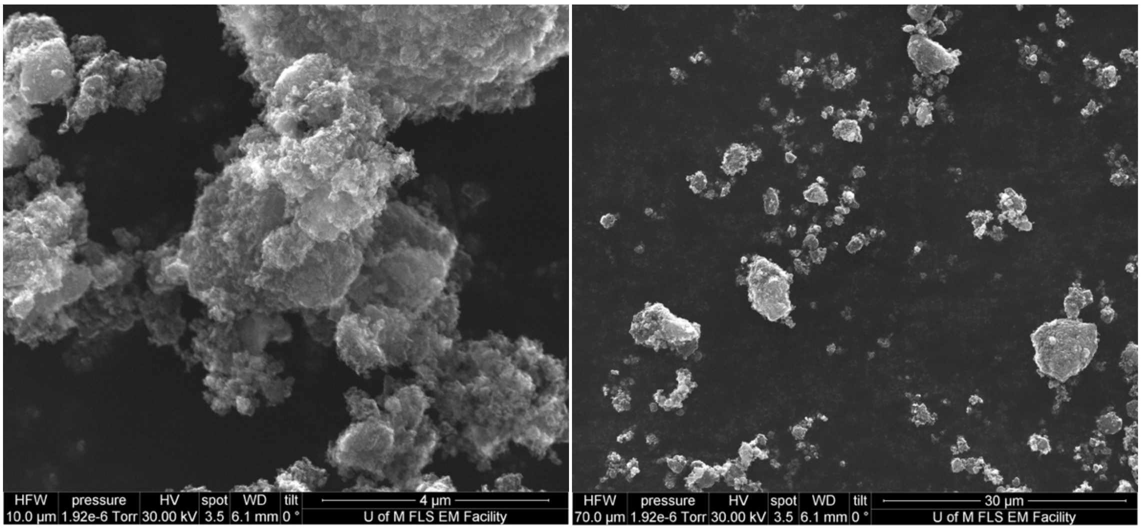

Figure 4.3 : SEM images of FLG-U powder

Both Graphene powders have been determined to possess planar sizes much lower than the length required to provide adequate reinforcement in composite materials (25 – 30µm) (Papageorgiou, Kinloch and Young, 2017), however these calculations have been based on pristine monolayer graphene. Functionalisation performed on these flakes should improve interfacial properties, meaning that planar sizes smaller than this quoted value could still provide beneficial improvements to mechanical performance. FLG has a much higher surface area than GNP, which could be an explanation for the larger degree of agglomeration (Papageorgiou, Kinloch and Young, 2017).

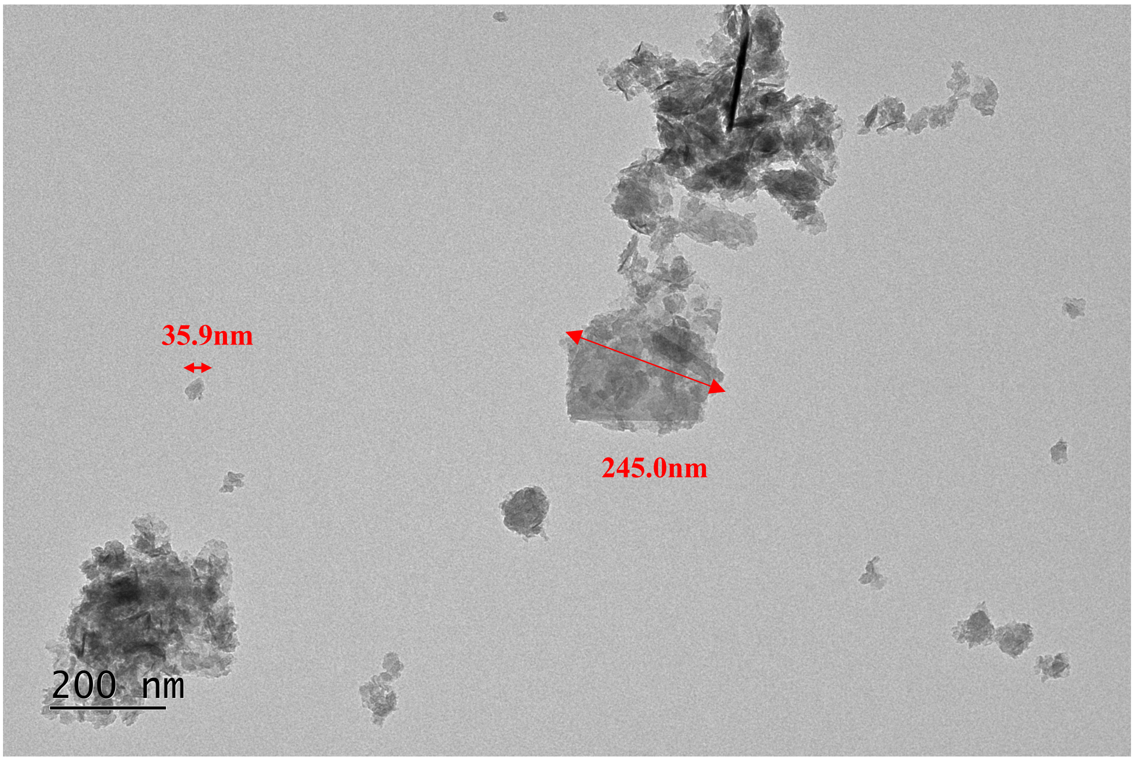

Figure 4.4 : TEM image of FLG powder

4.2 *Chemical Analysis*

This section employs techniques to understand the atomic disposition of each powder and the differences caused by each functionalisation treatment. These results will help to explain differences in mechanical performance and ability to disperse.

4.2.1 XPS

XPS analysis data presented in table 4.1 reveals the atomic ratio (at.%) of carbon to oxygen for each graphene powder. It should be noted here that there is a low level of oxygen present on the graphene surface prior to the plasma functionalisation process. The presence of surface functionalisation aids dispersion state through increased polarity and chemical reactiveness, promoting hydrophilic behaviour through repulsive electrostatic forces between agglomerates and encouraging interactions with the epoxy matrix (Taira, Yamanaka and Okada, 2017). The higher disruption to the sp^2 structure however degrades the mechanical performance of the graphene sheets.

It was expected that higher intensity treatments would attach a higher proportion of oxygen functional groups to the surface of the graphene powders, increasing chemical reactivity and improving interfacial properties whilst making de-agglomeration and dispersion more efficient (Vallés et al., 2016). Additionally, the aim of higher intensity functionalisation was to increase the proportions of reactive carboxylic groups. Table 4.1 shows that the FLGs follow this trend, where oxygen content increased with intensity of treatment suggesting a greater proportion of functional groups present. It is expected that the high oxygen content of the FLG-H samples will result in easier de-agglomeration and the highest proportions of interfacial interactions. GNPs display similar oxygen contents after both standard and high intensity treatments indicating the saturation point for the addition of oxygen groups was achieved after the standard functionalisation treatment. FLGs have a higher saturation point due to the small flake size having a higher proportion of chemically reactive flake edges, available for bonding with functional groups (Sharma et al., 2010).

Table 4.1 : Atomic ratios determined for graphene powders

FLG Type	Functionalisation	Carbon (at.%)	Oxygen (at.%)
GNP	None	97.5	2.5
	Standard	92.6	7.4
	High	93.2	6.8
FLG	None	98.4	1.6
	Standard	90.5	9.5
	High	88.1	11.9

Figure 4.5 shows the carbon satellite peaks for functionalised GNPs, these have been fitted and analysed to give representation of the bonding mechanisms present. The area beneath each peak can be calculated to give the proportion of each type of bond detected within each sample. There is a clear change in the intensity of the peaks found at binding energies ~284.5eV, showing that although the levels of oxygen detected in the bulk powders are similar, there is variation in proportions of bonding type.

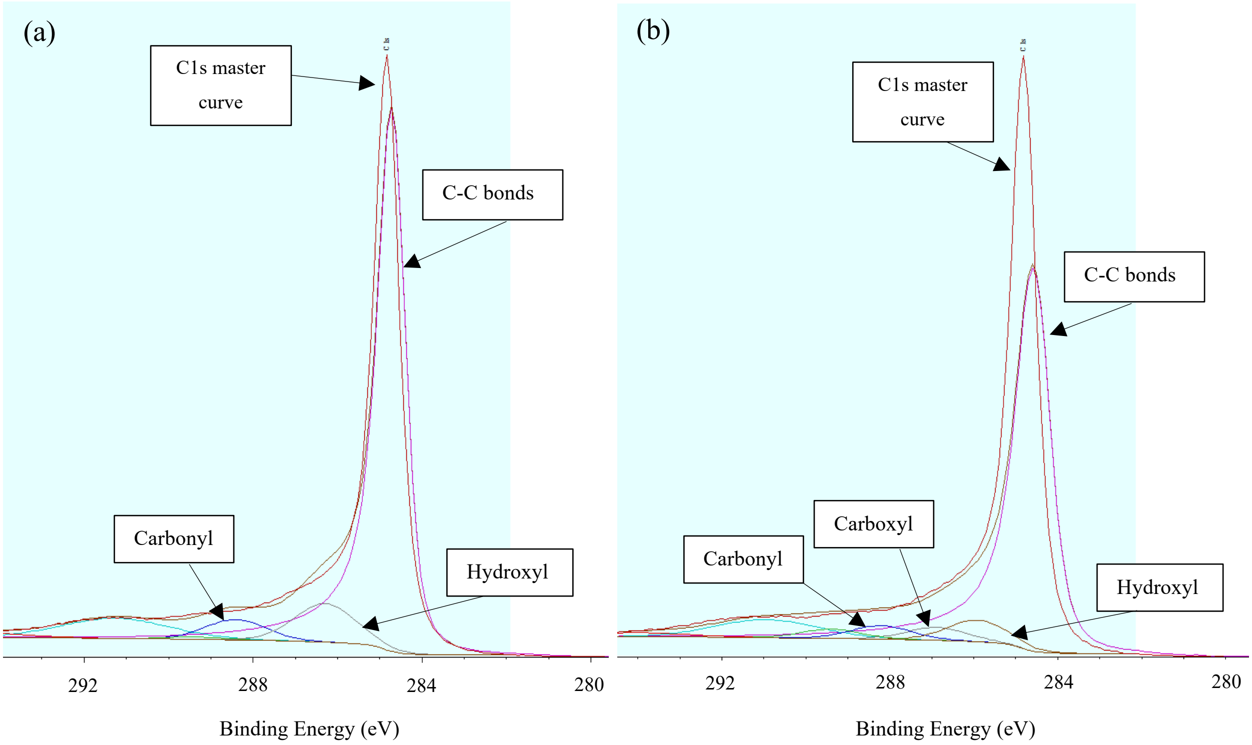

Figure 4.5 : Fitted satellite curves for Carbon peaks determined for (a) GNP-S and (b) GNP-H

Table 4.2 details variations in bonding chemistry present in the two samples. Both functionalised GNP powders are primarily comprised of carbonyl, carboxyl and hydroxyl groups, which have strong interactions with polymer polar groups. These groups are generally associated with bonding to the edges of GNP sheets, however they may also be found attached to any planar defect sites. In terms of exfoliation, it is desirable to have some disruption to the basal plane as alteration of the sp^2 aromatic network leads to a net weakening of Van-der-Waals interactions responsible for the stacking of graphene (Li et al., 2008)(Dobrota et al., 2016). The main differences in functionalised GNP's are as follows (Jimenez-Cervantes et al., 2016)(Chen, Feng and Li, 2012);

- As anticipated, GNP-H has a higher proportion of chemically reactive carboxyl groups which promote interactions between GNP and polymer chains, increasing stability and interfacial properties (Li et al., 2008).
- GNP-S powder has a higher proportion of polar hydroxyl and carbonyl groups, which provide a greater barrier between GNP interactions, enhancing stability.
- GNP-H powders also contain 5.52% of sp^3 bonds which could indicate material degradation and decreased mechanical performance (Yang et al., 2018)(Zhang et al., 2011) (Ito and Okamoto, 2013).

Table 4.2 : Satellite curve breakdown for functionalised GNPs

Bond Type	Binding Energy (eV)	Atomic ratio. %	
		GNP-S	GNP-H
C sp^2	284 – 285 (Kang and Khondaker, 2014)	76.27	75.60
C sp^3	286 (Zhang, Huang and Liu, 2016)	0	5.52
Carbonyl (C=O)	288 (Zhang, Huang and Liu, 2016)	4.67	3.46
Hydroxyl (C-O)	286-287 (Zhou et al., 2011)	8.85	3.32
Carboxyl (O-C=O)	289 (Zhou et al., 2011)	0.51	2.41

4.2.2 Raman Spectroscopy

Raman spectroscopy was performed to visualise the proportions of sp^2 bonds against edge and defect sites, to aid in understanding the mechanisms behind the efficiency of these powders as reinforcement. As depicted in figure 4.6, certain peaks correlate to various bonding structures. The G-Band peak (~1580cm^{-1}) is a result of in-plane vibrations caused by C-C, sp^2 bonds. The D-Band (~1350cm^{-1}) corresponds to out of plane vibrations or the level of disorder within the material; referring to flake edges and any defects across the plane (Jorio, 2012). Taking the ratio of D/G intensity peaks can display the level of disruption to sp^2 bonds present within each powder, as shown in table 4.3. 2D peak (or G’) can indicate number of graphene layers present, with pristine monolayer graphene displaying a narrow peak with high intensity.

Figure 4.6 shows the comparative peaks between unfunctionalised flake morphologies, the G-band peak gives higher intensity in GNP compared to FLG, indicating a higher proportion of in-plane sp^2 bonds. FLG shows higher intensity in D-band peak, indicating a higher proportions of defect sites or out of plane bonding. This is likely owed to GNP powder having larger planar dimensions and therefore fewer flake edge sites (Bellunato et al., 2016). The calculated disorder density shown in table 4.3 shows that the level of ‘disorder’ is 0.208 and 0.727, for GNP and FLG respectively. This again confirms the idea that FLGs have a smaller proportion of sp^2 bonds. The 2D peak found in GNP-U spectra, shows to have almost a ‘double-peak’ shifted over a higher frequency range, characteristic of graphitic samples which are comprised of more than 4 layers (Bottari et al., 2017).

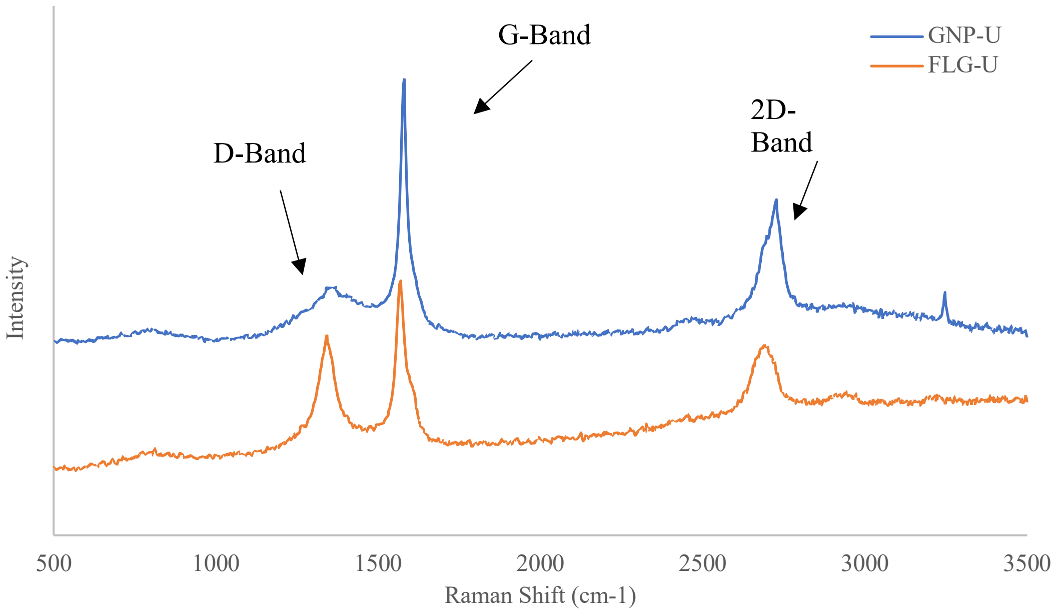

Figure 4.6 : Unfunctionalised graphene Raman spectra

Figure 4.7a displays Raman spectra for all GNP samples. An increase in D-band peak is seen with the addition of functionalisation, suggesting additional disruption to the sp^2 network with treatment. This could be indicative of a smaller proportion of sp^2 bonds caused by plasma treatment. This is reflected in data shown in table 4.3 where there is an increase in disorder density with functionalisation. The degree of disorder is similar between the standard and high levels of functionalisation, which is as expected after XPS analysis showed similar levels of attached oxygen groups. There is a blue shift in peaks (decrease in wavelength) with the addition of functionalisation, which could be attributed to the atomic structural change causing differing vibrational frequencies of the atomic bonds. Spectra collected for FLG samples, shown in figure 4.7b, display minimal changes in peaks, again, reflected in table 4.3 where the calculated density disorder is similar for all three samples. This could indicate that the functionalisation process has caused minimal disruption to existing sp^2 graphene structure. Due to the small planar size, there is already a high proportion of edge defect sites available for bonding. This could be an explanation for the lack of disruption to the sp^2 network.

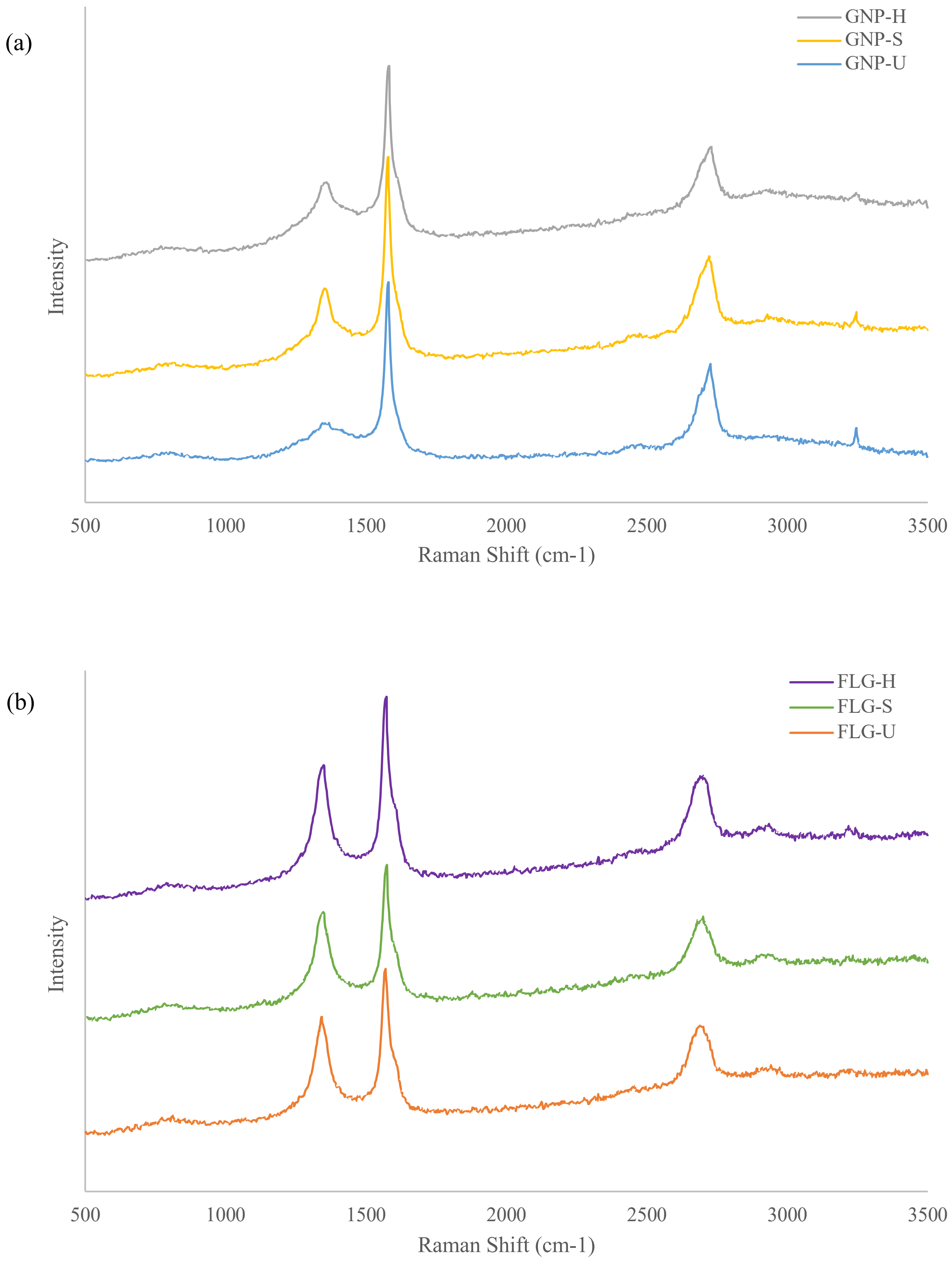

Figure 4.7 : Raman spectra produced for (a) GNPs (b) FLGs

Table 4.3 : Calculated values of disorder density from Raman curves

	Functionalisation	Disorder Density
GNP	None	0.208
	Standard	0.395
	High	0.365
FLG	None	0.719
	Standard	0.689
	High	0.647

4.2.3 Zeta Potential

Zeta potential measurements were performed to quantify powder stability in solution and the effect of functionalisation. Zeta potential is derived using DVLO theory from electrostatic potential close to the surface of a particle in solution, referring to the amount of energy required to move a single point charge towards the particle. Large zeta potential values correlate to high required forces, meaning agglomeration is unlikely and therefore good stability is achieved. It is accepted that ±30-35mV is the threshold of good stability and improving with increased value (Lu et al., 2010)(Malvern Instruments, 2000).

FLG-U powder has zeta potential measured at -23.18mV (table 4.4), suggesting low stability and therefore a high presence of short range attractive forces such as Van-der-Waals, which agrees with large agglomerate size, with respect to planar size visualised in figure 4.3. Similarly, GNP-U zeta potential has been determined to be at the threshold of good stability, suggesting potential for agglomeration to occur but better stability than its FLG counterpart. This is due to FLG having higher surface area to volume ratio, which leaves higher surface energy promoting interactions with neighbouring particles (Nanda et al., 2003).

For both morphologies, the presence of functionalisation has resulted with increased zeta potential suggesting enhanced stability, due to the presence of hydrophilic functional groups. However, the increased values still measure on the threshold of stability for FLG-S & FLG-H suggesting that agglomeration may still occur but to a lesser degree (Kazi et al., 2015b). These measurements suggest that GNPs, especially after functionalisation, may hold their dispersion state better than FLGs.

Table 4.4 : Zeta potential measurements

	Zeta Potential (mV)	
	GNP	FLG
Unfunctionalised	-32.0	-23.2
Standard	-42.3	-30.9
High	-45.1	-30.9

4.3 Powder Size Distribution

Agglomerate size distribution was determined from SEM images of graphene powders to determine the initial state of agglomeration. ImageJ was used to measure the largest diameter of 80 - 100 randomly chosen agglomerates. Figure 4.8 show cumulative frequency for all powders. As expected, FLG powders show a smaller range in particle diameter compared to GNPs. A similar trend is seen with functionalisation where GNP-S and FLG-S both show an increased proportion of smaller agglomerates, compared to their unfunctionalised counterparts. FLG-H however shows a similar distribution curve to FLG-U. Both functionalised GNP powders interestingly show an increase in the proportion of both the smallest and largest size agglomerates. SEM images captured for each graphene powder are shown in figure 4.9, improved de-agglomeration is evident in functionalised samples.

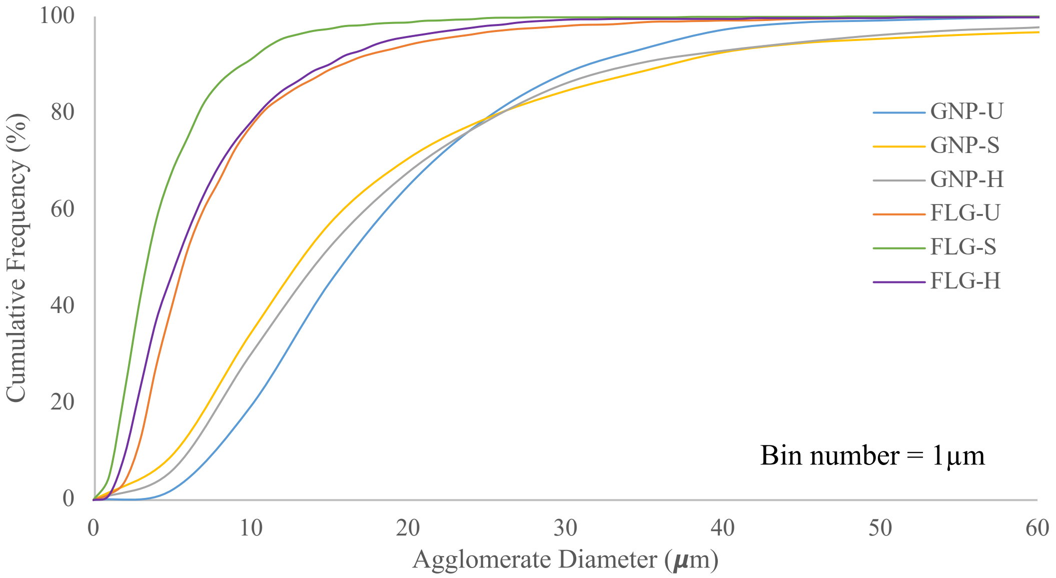

Figure 4.8 : Cumulative agglomerate frequency of all powders

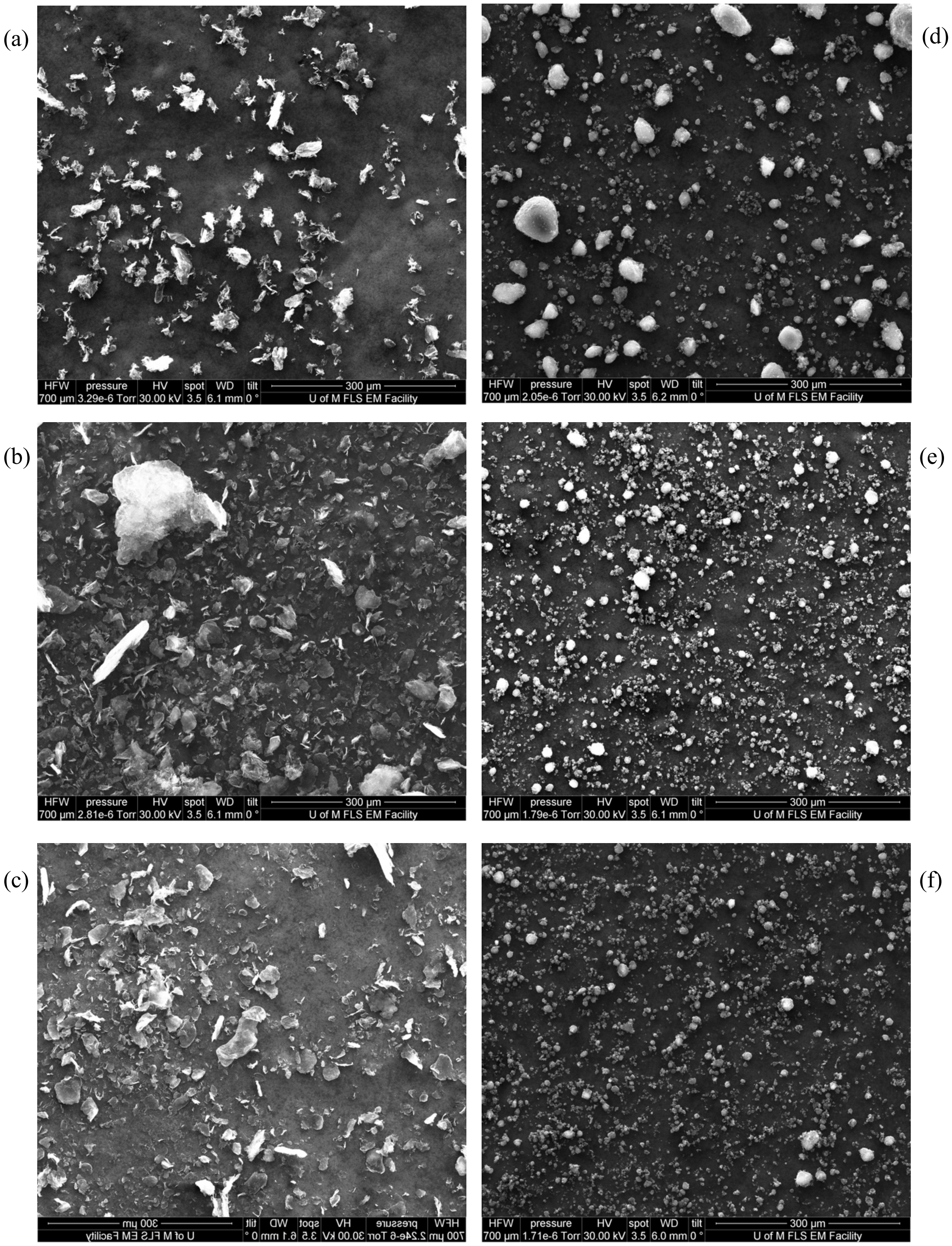

Figure 4.9: SEM images of each graphene powder (a) GNP-U (b) GNP-S (c) GNP-H (d) FLG-U (e) FLG-S (f) FLG-H

5 *Describing Dispersion*

The various methods available to assess graphene dispersion state within uncured epoxy resin are outlined and discussed in this chapter. When classifying a good dispersion, there must be evidence of minimal agglomeration and homogenous distribution of graphene. The distribution of graphene has been deemed to be good as the initial incorporation of graphene into the epoxy matrix was performed using centrifugal mixing, leaving these methods to primarily assess the levels of de-agglomeration achieved. Both visual and bulk methods have been utilised and critiqued for relevance within an industrial setting. Each method has been discussed with examples of poor and good dispersion. The parameters used to achieve each dispersion state is detailed in table 5.1. The effect of functionalisation and mixing parameters are investigated further in section 6.

Table 5.1 : Mixing parameters used for samples discussed in this chapter

Dispersion Quality	Mixing Method	Parameters
Poor	SpeedMixer	5 minutes 1950 rpm
Good	3RM	5 passes Please refer to section 3.3.3 for further detail

A short investigation into the effect of filler loading on mechanical properties was performed to ensure the optimisation of mechanical performance. Figure 5.1 displays the flexural modulus and strength for unfunctionalised GNP and FLG samples, mixed to produce a good dispersion state (table 5.1). Both samples gave optimised results at filler loadings of 1% fill by weight and have therefore been selected for use in this project. The methods discussed in this chapter relate to materials produced at 1% fill by weight.

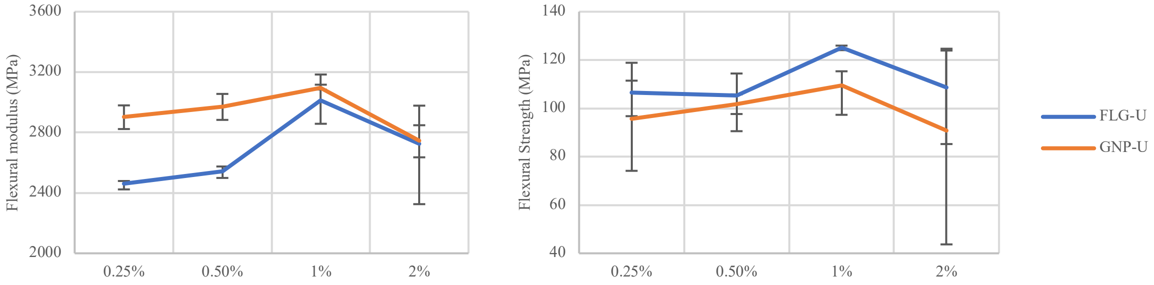

Figure 5.1 : Flexural modulus and strength measurements for FLG-U and GNP-U at varied filler loadings

5.1 Visual methods

When questioning whether good dispersion has been attained post-mixing, visualisation is an instinctive response. Images are an effective way to depict dispersion state, however, visually analysing small changes becomes more difficult and therefore subjective which encourages the use of quantitative methods to describe trends.

5.1.1 Optical Microscopy

Many laboratories have an optical microscopy as staple equipment, due to its versatility, ease of use and low maintenance. Sample preparation is quick and inexpensive, and a variety of image processing software exists to allow fast quantitative interpretation of an image. Relatively low magnification is the main drawback of this method, meaning it is not possible to view individual flakes. However, it is possible to accurately depict and size larger flakes and agglomerates, making optical microscopy a good microscale technique. Post-processing methods are popular when analysing dispersion state and can focus on analysis of matrix material or added particles.

Matrix based methods consist of measuring the proportion of matrix visible, where less matrix is visible with high levels of dispersion state. Figure 5.2 shows this method performed with ImageJ software and table 5.2 shows data collected using this method for GNP-U samples. Whilst this remains an effective measurement to generally describe dispersion state, there are factors which severely affect the accuracy of these measurements. Firstly, the use of coverslips result in aggregation of particles as the material spreads through the confined space between slide and coverslip, leaving high saturation of graphene towards the edges of the slide (figure 5.3). Coverslips are necessary to control the depth of each sample and ensure adequate transmission of light through the slide. However, they appear to promote agglomeration and therefore misrepresent the dispersion state of the bulk material, as demonstrated by the variation in values displayed in table 5.2. This is especially visible for samples with poor dispersion state. This could be controlled by controlling the volume of each sample and capturing multiple images from the same areas across each slide. The poorly dispersed sample has shown high values and large variation, however as previously discussed this effect is exacerbated by slide preparation. Conversely, the sample with good dispersion has shown lower % area values in addition to smaller variation in results. As found with any image processing method including thresholding techniques, there is a degree of inaccuracy caused by the innate subjectivity of personal judgement. This is difficult to overcome due to microscope brightness and contrast settings changing between sessions causing thresholding limits to also change. This could be due to environmental factors such as, changing light levels inside the laboratory or changes in preparation between slides. Small deviations in sample thickness, filler loading and dispersion state will all influence the light transmission through the sample.

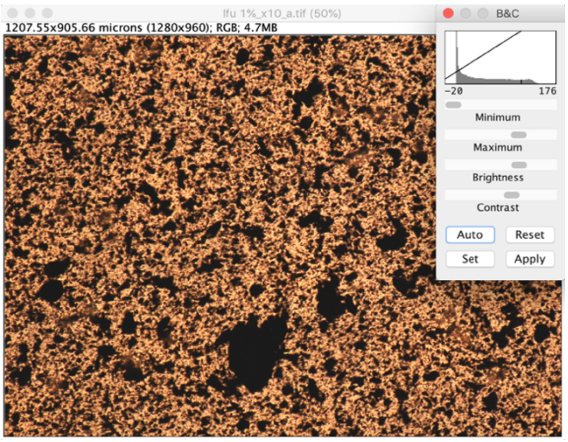

1. Brightness and contrast levels are adjusted to illustrate the difference between graphene and epoxy more clearly

2. Image is converted to an ‘8-bit’ image

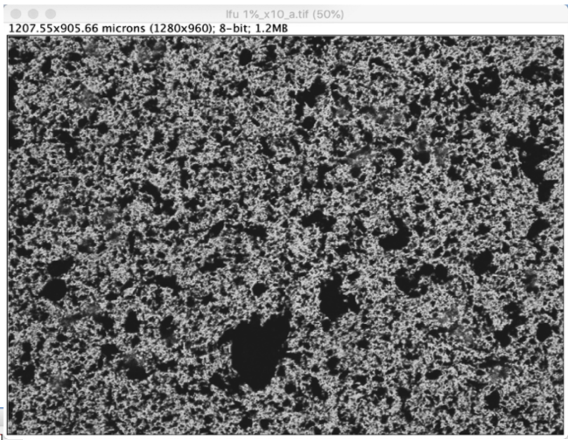

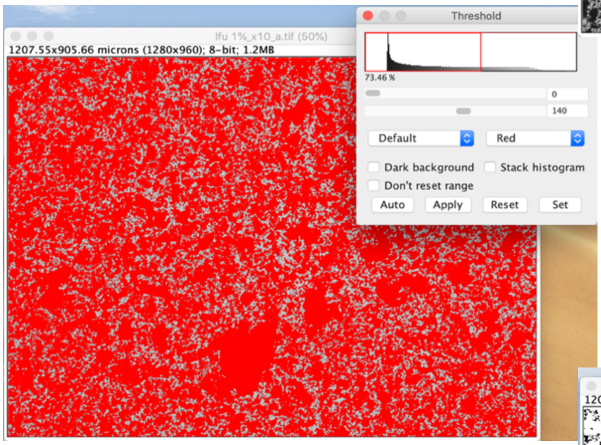

3. Thresholding is conducted by eye to define the limit of which shades constitute graphene and epoxy

4. Areas of epoxy resin are shown in black and graphene shown in white. Percentage area of epoxy resin represented in this image is calculated

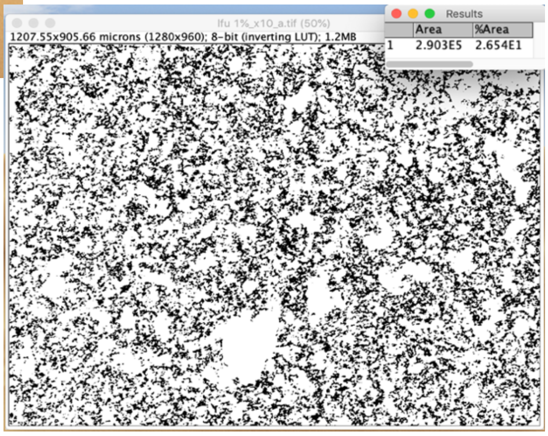

	Area	%Area
1	2.903E5	2.654E1

Figure 5.2 : Method of determining % area of matrix using ImageJ software

Table 5.2 : % area calculated from different areas across the slide (arbitrarily as denoted as A-C) of GNP-U samples mixed through different techniques, images were taken at 1% filler loading

		Poor Dispersion	Good Dispersion
% Area	A	39.1	17.0
	B	26.5	26.2
	C	45.4	21.3

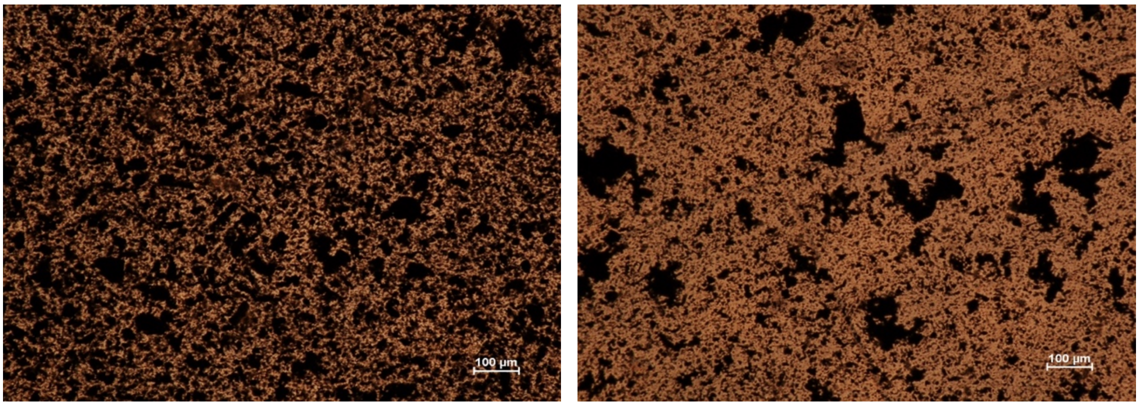

Figure 5.3 : Optical microscopy images of GNP-U at 1% filler loading by weight in poor dispersion state (left) image taken from centre of slide (right) image taken from edge of slide

Post-processing methods are also used for particle-based analysis which involve measuring size distribution of particles. For this method, it is important that each graphene agglomerate can be wholly visualised, meaning an extra step to dilute filler loading is required. Figure 5.4 shows an example of this method for GNP-U samples at a filler loading of 0.1% by weight. Images have been captured at relatively low magnification (x10); however, this has been selected to maintain focal depth across the image. Higher magnifications left large proportions out of focus, making the thresholding process more difficult.

This post-processing method firstly uses thresholding techniques to define the graphene agglomerates against epoxy matrix. The lower filler loading allows for clear definition between the two elements making thresholding easier. The area of each graphene agglomerate is determined and equivalent diameter calculated by modelling each particle as a circle which allows comparisons to be made across irregularly shaped particles. These values are then output and presented as examples shown in figure 5.5 to give the particle size distribution (PSD).

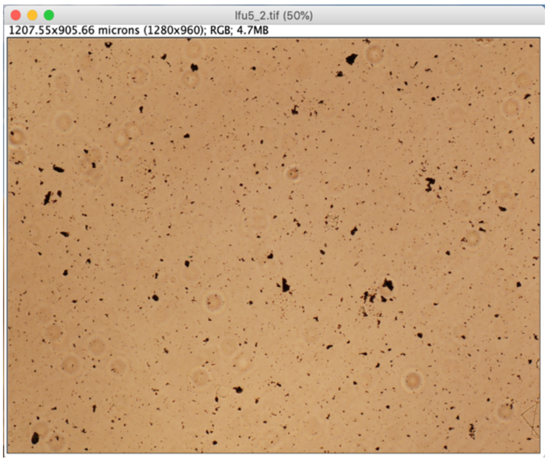

1. Image is converted to a binary image and threshold limit is determined.

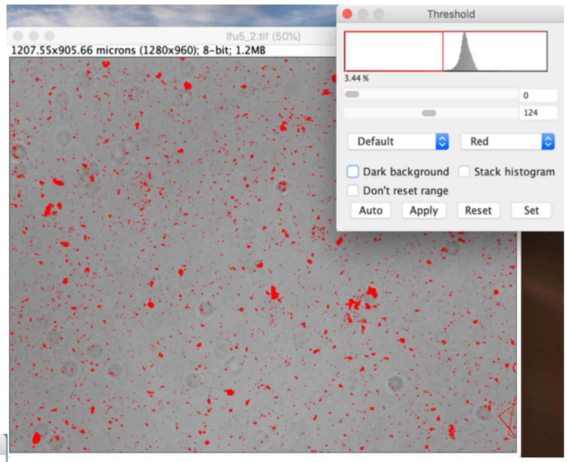

2. Image is converted to a binary

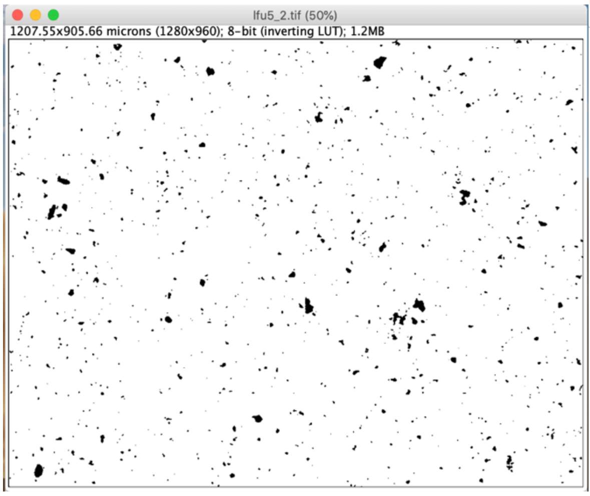

3. Equivalent diameter is calculated for each agglomerate (black) and values output

Figure 5.4 : Particle sizing based analysis method using image processing software with optical microscopy images

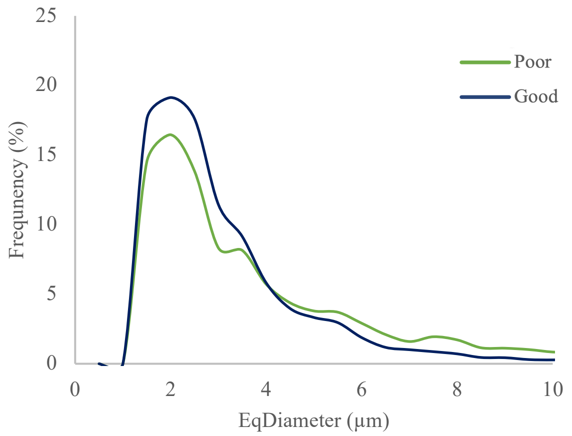

Figure 5.5 : Examples of how agglomerate size distribution have been displayed through this report

Similar thresholding obstacles are faced in this technique, but the low filler loading makes interpretation easier through the clearer distinction between matrix and graphene. Additionally, the aggregation affect during slide preparation is mitigated by the low filler loading, giving greater homogeneity across the slide. Generally, between 800-1000 particles were analysed from multiple images taken across the slide, giving good representation of the PSD.

The main downside of optical microscopy is the low magnification. With the microscope setup used in this work, each pixel measured 1µm^2. To eliminate the effect of background noise, particles which were smaller than 3x3 pixels were not measured. This left the smallest equivalent diameter measurable to be 3µm, leaving this technique incompatible with graphene flakes with very small dimensions. GNP flakes were determined to possess an average planar flake size of 5µm, which is towards the lower end of this scale, but these can still be depicted under the optical microscope.

FLGs hold a planar size <200nm which would not be visible at high levels of dispersion. However, as FLGs form agglomerates several microns in diameter, this technique is still useful to measure these particles and allows inference into trends relating to de-agglomeration. Data collected in this way is more accurately used to show comparisons between dispersion states, rather than as direct measurements of PSD. Figure 5.6 shows an optical microscope image of FLG-U after thresholding and PSD distribution curve.

Dispersion quantification based on the positioning of particles in relation to one another (Khare and Burris, 2010), is not suitable for optical images taken in this project due to the high filler loadings used. 1% filler loading is too high to effectively discern individual particles (refer to figure 5.2 and 5.3). Diluting to smaller filler loadings is a possibility, but as particle positioning is being measured there is uncertainty as to whether any patterns correlate to higher filler loadings.

Alternatively, equipment with the capacity to image at higher magnifications such as electron microscopy could be used with this technique. The use of dilution to measure particles is valid as the size of the agglomerates is unlikely to change during this process.

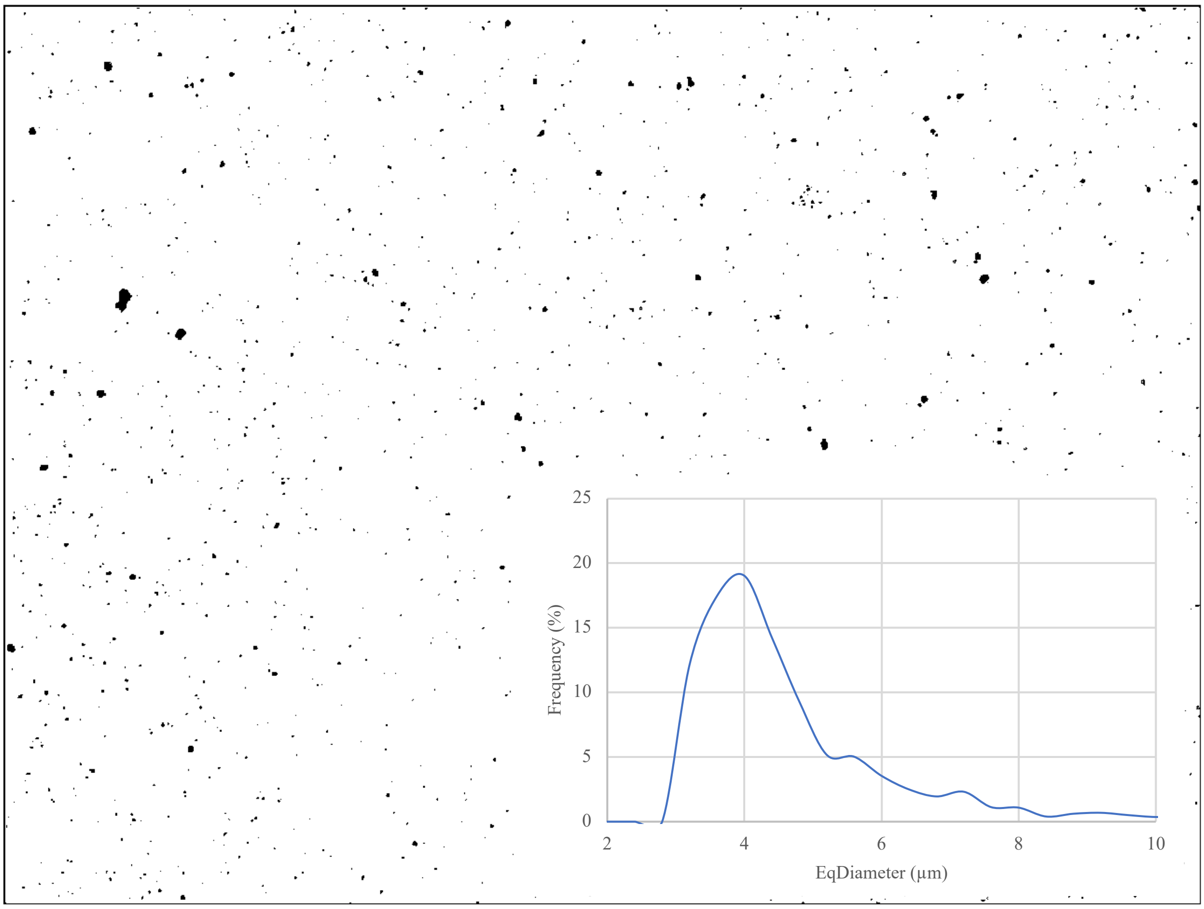

Figure 5.6 : Microscopy image of 3RMilled FLG-U at 0.1% fill weight post thresholding and histogram produced from calculated equivalent diameter

Whilst optical microscopy remains a useful tool to quickly visualise dispersion and quantify graphene particle size, the accuracy of the data produced is largely influenced by the magnification of images. This method is not suitable to accurately describe all particle sizes but does give good representation of the larger sized agglomerates, which can be useful to make comparisons between samples. Graphene powders which consist of a high proportion of flakes smaller than 3µm, such as FLG, may not be suitable for this type of analysis, however due to a significant number of agglomerates measuring larger than this threshold, some comparative based conclusions could still be drawn from this method. Nevertheless, due to the ease of capturing images and versatility in post processing methods, optical microscopy could easily be implemented into a quality control process.

5.1.2 Electron Microscopy

TEM is generally the 'go-to' method to visualise dispersion, due to high magnification allowing nanoscale imaging. This method provides high resolution flake imaging and definitive proof of successful de-agglomeration. However, due to the high magnification, the sample area is very small and therefore not necessarily representative of the bulk sample. For accurate representation, graphene must be visualised after being cured in epoxy resin. However, this process requires specialist expertise and equipment to produce samples, which makes it both time-consuming and expensive.

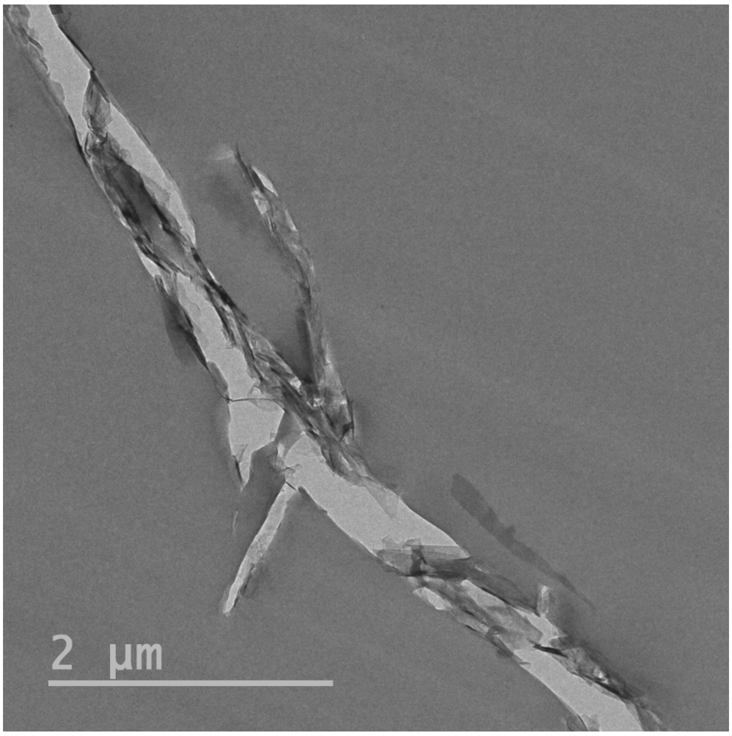

Figure 5.7 : TEM image displaying site where GNP-U flake has been torn from epoxy resin during sample preparation

It was discovered that ultramicrotome was not suitable for preparing samples containing GNP flakes, due to the large planar size. A maximum sample thickness was determined to be 200nm to allow adequate penetration of the electron beam, which is significantly smaller than the average GNP planar size. This resulted in larger flake sizes being pulled from the sample, shown in figure 5.7, misrepresenting the distribution of sizes. FLG flakes however, were small enough to be successfully embedded into microtomed samples and imaged through TEM. A selection of 6 TEM images were processed through ImageJ software to measure agglomerate diameter, as demonstrated in figure 5.8. A note was taken of the number of agglomerates measured and statistical analysis was performed to determine the d10, d50 and d90 values for each set of images. These values denote an agglomerate diameter which 10%, 50% and 90% of all measured diameters are lower than, respectively. This gave a good indication of the distribution of agglomerate sizes found over the nanoscale.

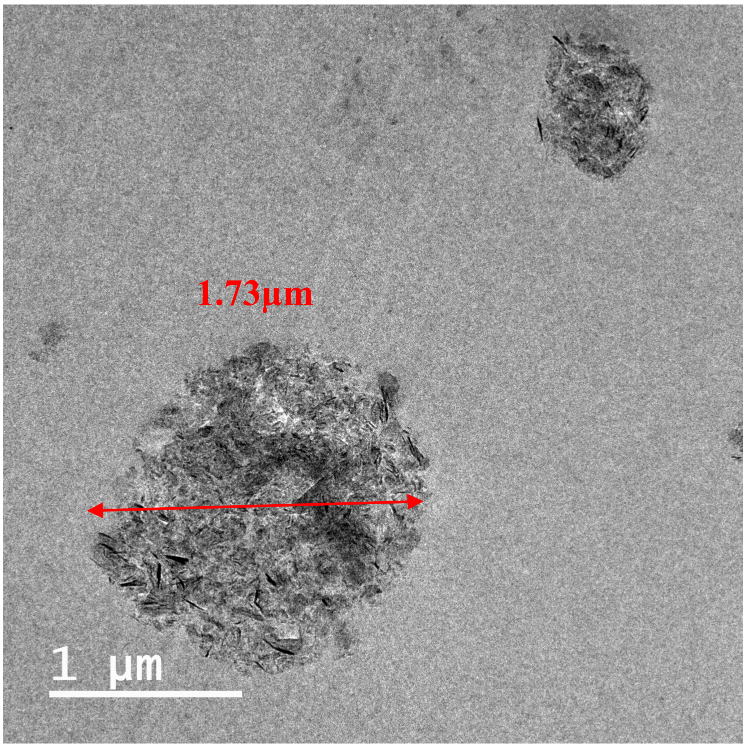

Figure 5.8: Example of FLG-U agglomerate measurement, using ImageJ

Whilst TEM remains the most accurate method of visualising graphene flakes, it is not feasible for it to be used as the sole method of confirming dispersion state. This is primarily due to long processing times, high cost and low representation of bulk samples. For the epoxy systems investigated in this research, TEM analysis was limited to graphene with dimensions smaller than that determined to be necessary to provide adequate stress transfer (Papageorgiou, Kinloch and Young, 2017), concluding, this would not be a universal imaging technique. TEM is beneficial for understanding de-agglomeration behaviour, however due to the high operating cost and long processing times this may not be feasible for batch quality assessment.

5.2 Bulk Material Methods

This section examines methods performed on bulk material to assess dispersion state. These techniques focus on measurements which are affected by dispersion state to infer changes in bulk material.

5.2.1 Hegman Gauge

Measuring dispersion using a Hegman gauge can ensure homogeneity of suspension-based material and is commonly used with paints and ink. This practice provides rapid detection of any large agglomerates prior to curing. The gauge operates over the scale of 0-25µm, with each 2.5µm increment denoted, meaning the recorded values are less accurate than other methods. The Hegman gauge is highly effective at quickly illustrating the presence of any large agglomerates as well as a rough indication of size. Further details on the operation of the Hegman gauge is define in section 3.4.1.

Figure 5.9 illustrates the difference in how dispersion state is depicted between mixing methods. The gauge illustrating good dispersion shows no ‘streaking’, indicating successful de-agglomeration of large agglomerates and homogenisation through high-shear mixing. There is high confidence that these conclusions are representative of the batch material, as sample sizes are relatively high volume (~1ml) and repeat tests were also performed. It is difficult to infer exact values for agglomerate size with confidence due to the low accuracy of this method.

In conclusion, the Hegman gauge is a useful method of quick determination of bulk dispersion state and range of agglomeration size. The equipment is inexpensive and does not require any specialist training to be used effectively. Due to the imprecision in measurements, this method would serve best to compare against large changes in dispersion state and to measure upper limits of agglomerate size. This is especially useful where improvements to strength and strain at failure are required, as large ‘stress raising’ particles can be quickly identified.

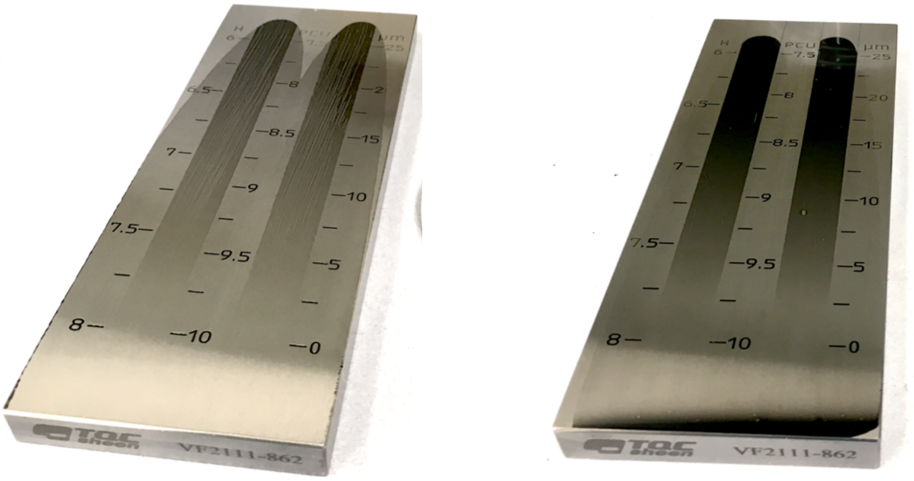

Figure 5.9 : Hegman gauge tests performed on FLG-U samples at 1% fill loading by weight (Left) poor dispersion (Right) good dispersion

5.2.2 Rheology

Viscometry measurements can be very effective in demonstrating dispersion. Properties relating to viscosity with respect to shear rate are calculated on materials prior to cure. The addition of graphene to epoxy resin causes an increase in viscosity due to the graphene flakes physically restricting the flow of epoxy chains. As de-agglomeration occurs, the number of graphene particles increases, resulting in more sites of epoxy chain restriction which again increases viscosity. With this knowledge, the level of de-agglomeration achieved can be gauged.

There are numerous additional parameters which affect viscosity, including flake size and filler loading. For this reason, it is difficult to attribute a general value for dispersion state, meaning individual parameters should be determined for each material composition. Figure 5.10 displays viscosity calculated from the average of three repeat measurements and includes error bars to show maximum and minimum values. After high shear mixing, there is a noticeable increase in viscosity which is indicative of de-agglomeration. Additionally, the error bars cover a smaller range showing the dispersion state is also more homogeneous.

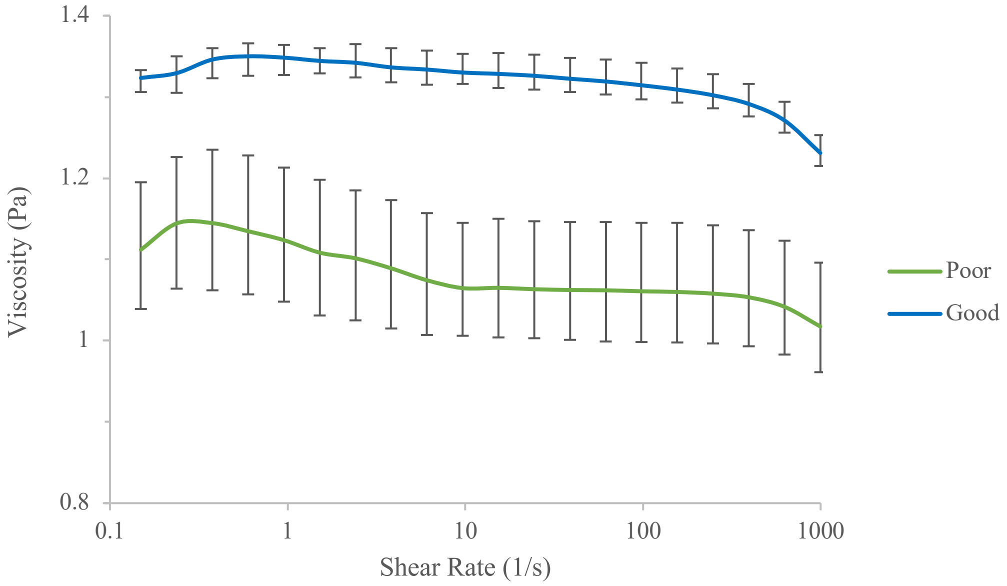

Figure 5.10 : Material response of FLG-U at 1% filler loading by weight, with good and poor dispersion

Rheology is a useful tool for quick dispersion analysis, showing good representation of bulk material with repeat measurements. When examining dispersion state, rheology should be used comparatively for each graphene / epoxy system, as flake morphology, filler loading and epoxy brand will impact the measured viscosity (Grabowski and Mukhopadhyay, 2014). To use this as the sole method of determining dispersion, an initial investigation using multiple sizing techniques should be performed to fully understand the correlation to viscosity. Due to the quick output of data and minimal sample preparation post-mixing, rheology is a very effective tool to analyse dispersion state in an industrial environment.

5.2.3 X-Ray Diffraction

Since graphene is comprised of crystallographic in-plane structures arranged over a number of layers, XRD can be used to determine structural characteristics. These measurements were performed on cured graphene / epoxy samples. The characteristic diffraction peak relating to the graphitic layering is shown at ~26.5º, where high intensity correlates to increased layering. Reduction in peak intensity indicates exfoliation has occurred, which is desirable as better mechanical properties are seen with fewer layers. XRD is a bulk technique and gives data corresponding broadly to the material. Figure 5.11 shows spectra collated from cured samples at poor dispersion, where the characteristic graphitic peak is not seen for FLG flakes. This indicates a lack of stacking morphology and can be explained by low number of layers found in FLG (between 1-4).

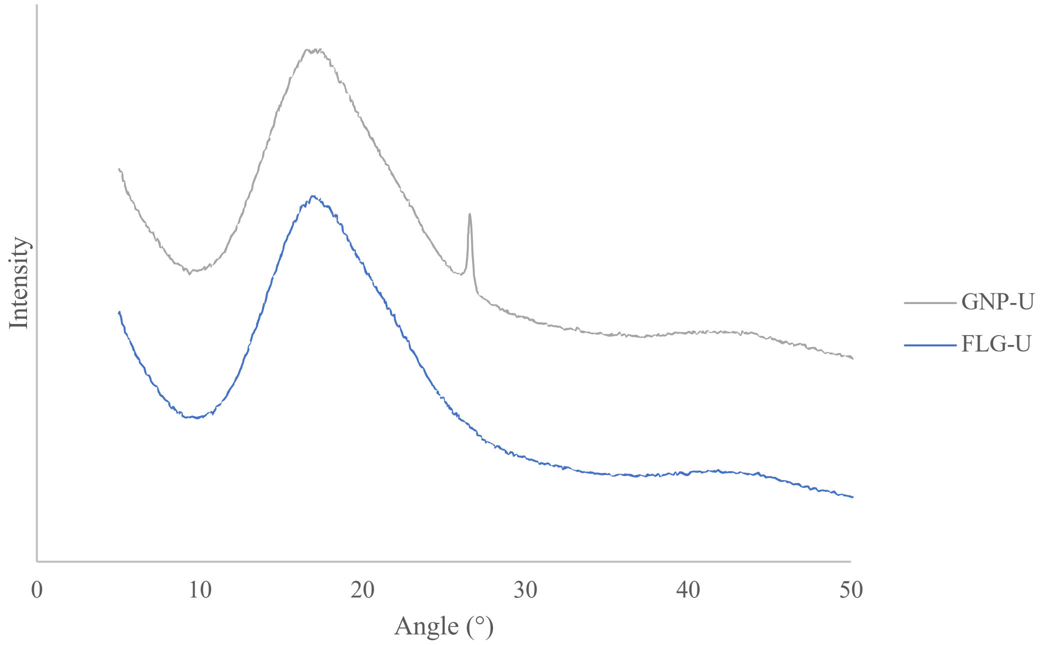

Figure 5.11 : XRD spectra for materials at poor dispersion state

Compared with other techniques discussed, XRD is unique as direct information relating to flake thickness can be determined. This is useful when investigating the material response to a given mixing method and helps develop a comprehensive understanding of each graphene powder. However, the efficacy of XRD is not equal across all morphologies as seen in FLG powders. The lack of peak present shows that the number of layers is small but this does not help when characterising dispersion state where there are high levels of agglomeration present.

Due to mixing being performed directly onto the graphene / epoxy mixture, samples would need to be cured prior to XRD analysis, significantly increasing the time in which these tests can be performed. Additionally, high operating costs of equipment and specialist training required to perform tests leaves XRD unsuitable for use as part of a quality control process. As exfoliation is closely linked to the levels of shear stress used during mixing, this analysis would be extremely useful as part of the initial development of mixing parameters rather than as a fixed part of quality control process (Throckmorton and Palmese, 2015).

5.3 Quality Control Considerations

In order for a quality control process to be considered effective, measurements of dispersion state need to be determined efficiently and accurately, with a method that is low cost, easy to interpret and compatible with a range of graphene morphologies. All methods discussed successfully provide useful data relating to dispersion state, but each come with individual advantages and disadvantages.

Firstly, there is a trade-off between the accuracy of measurements and ease of equipment operation. The Hegman gauge is by far the quickest and easiest technique, but only allows macroscale measurements to be made to an accuracy of 2.5µm. In contrast, TEM allows measurements over the nanoscale but results in high operating costs and prolonged analysis times. Of these two techniques, the Hegman gauge would better suit incorporation into the manufacturing procedure. This highlights the question of how much influence agglomeration has on mechanical properties and therefore how accurately it needs to be measured to ensure good levels have been achieved.

The described particle sizing techniques span the nano, micro and macro scales, through TEM, optical microscopy and Hegman gauge, respectively. The cost, analysis time and difficulty of each method decreases as the scale becomes larger, leaving analysis over the micro or macro scale most desirable. It is unclear whether the relationship between mixing and de-agglomeration is universal over each size category, which is critical to understand as this will affect the mechanical properties. Macro scale analysis is essential to ensure the largest agglomerates are broken down to improve strength properties, but analysis over the nano scale is also important to ensure that full de-agglomeration is achieved to optimise reinforcement. The trends over each size category need to be analysed to ensure de-agglomeration trends are universal and therefore allow confident inference of bulk dispersion state from low accuracy methods.

It is difficult to interpret indirect dispersion measurements such as viscometry. Although analysis is quick and representative of a relatively large amount of sample, it is difficult to make conclusive statements about dispersion state. Viscosity is affected by many other factors such as temperature, flake size and filler loading. Additionally, each polymer matrix used will have a different viscosity. This would require comprehensive analysis of viscosity changes with dispersion state for each graphene / polymer system to be analysed before viscometry could be adapted into the quality control process. As viscosity itself is also an important manufacturing parameter in the production of hybrid composites, it would be beneficial to be able to deduce multiple conclusions from a single measurement.

The efficacy of XRD, TEM and to a lesser extent optical microscopy, have been shown to vary based on graphene morphology, making them unsuitable for use as a universal tool. As these techniques still provide useful information relating to dispersion, it is beneficial to understand if trends such as exfoliation can be deciphered from other measurements.

6 Mixing Methods

Methods discussed in chapter 5 have been used to investigate the change to dispersion state through each high shear mixing method. The aim is to create a homogeneous dispersion state, whilst maintaining high aspect ratio and minimising agglomeration. Several procedures have been employed for each mixing method and assessed to determine their effectiveness at producing good dispersion with respect to;

- Mixing method
- Mixing duration
- Flake size
- Functionalisation intensity

The use of SM, OHM and 3RM equipment are examined in this section. Detailed mixing parameters can be found in chapter 3.3.

6.1 De-agglomeration Mechanisms

The cohesion strength has been calculated for each graphene morphology over the initial measured PSD. This has been compared against the shear stress produced through each mixing method, in order to evaluate de-agglomeration mechanisms and fully understand the effectiveness of each mixing method.

6.1.1 *Shear Stress*

The shear stress produced by each mixing method was calculated through equation 2,

$$\sigma = \dot{\gamma}\eta \tag{2}$$

Where $\dot{\gamma}$ = shear rate and η = sample viscosity. Viscosity values were determined through viscometry measurements. The shear rate produced through OHM was determined using the equation 3

$$\dot{\gamma} = \frac{\pi N D}{\Delta R} \tag{3}$$

Where N = mixing speed (RPS), D = rotor diameter (m) and ΔR = gap between rotor and stator (m) (Tamminen and Koiranen, 2015). Values used are detailed in table 6.1. Equation 4 was used to calculate the shear rate achieved through 3RM.

Table 6.1: Values used in equation 3 to calculate the shear stress produced through OHM

Mixing Program	Mixing speed, N (RPS)	Rotor diameter, D (m)	Rotor / stator gap, ΔR (m)
OHM	100	2.82×10^{-2}	1.75×10^{-4}

$$\dot{\gamma} = \frac{(u_2 - u_1)}{L} \tag{4}$$

Where, u = roller velocity (ms^{-1}) and L = nip gap (m) (Njuguna, 2013). Shear rate has been calculated using values in table 6.2, describing conditions across the 2nd nip gap of the 3RM.

Table 6.2: Values used in equation 4 to calculate shear rate produced through 3RM

Mixing program	Last roller velocity, u_2 (ms^{-1})	Middle roller velocity, u_1 (ms^{-1})	2nd nip gap, L (m)
3RM – P1	1.59	0.53	15×10^{-6}
3RM – P2	1.88	0.63	5×10^{-6}

All values used and calculated with equation 2 are displayed in table 6.3. Viscosity values were measured with respect to strain rate using a rheometer, with setup detailed in chapter 3.4.3. The rheometer was found to test over a range of 0.1-1000 s^{-1} for shear rate, which is much lower than the calculated values experienced through each mixing method. Therefore is was not possible to perform viscosity measurements under the exact shear rate produced during mixing.

Table 6.3 : Values determined through equations 2-4 and viscosity measurements for each mixing method

		Shear Rate, $\dot{\gamma}$ (s^{-1})	Viscosity, η (Pa.s)	Shear Stress, σ (kPa)
FLG	OHM	5×10^4	1.25	63
	3RM-P1	7.1×10^4	2.8	199
	3RM-P2	25×10^4	2.7	675
GNP	OHM	5×10^4	1.5	75
	3RM-P1	7.1×10^4	0.8	57
	3RM-P2	25×10^4	0.9	225

However, measurements of samples at 1 wt% loading and representative of material mixed through OHM, was found to display Newtonian behaviour, which is characterised by no change to viscosity with respect to shear rate (Zaman et al., 2011). This leaves confidence that the viscosity will not change at shear rates above the bounds of the equipment and at levels produced through OHM. This concludes measured viscosity values can be used reliably. Material at 10 wt% loading displayed shear thinning behaviour as a result of the increase to viscoelastic behaviour with the addition of filler (Nobile et al., 2016). These materials exhibit the relationship displayed in figure 6.1a, in order to be confident of the material viscosity under each shear rate, the upper Newtonian region must be attained over the range of shear rates measured. Measured data displayed in figure 6.1b, shows FLGs begin to plateau after ~100s^{-1}, whereas GNPs display a less defined transition and noisy data at high shear rate. It is difficult to discern whether this is indicative of transition into the plateau region or noise created by the tests being performed towards the limits of equipment capabilities. Nevertheless, an average of the final measured data point will be taken from three repeat measurements and used as the viscosity value for calculations in equation 2. These values are adequate for these purposes as they are being used to give an general idea of shear stress levels in relation to other methods.

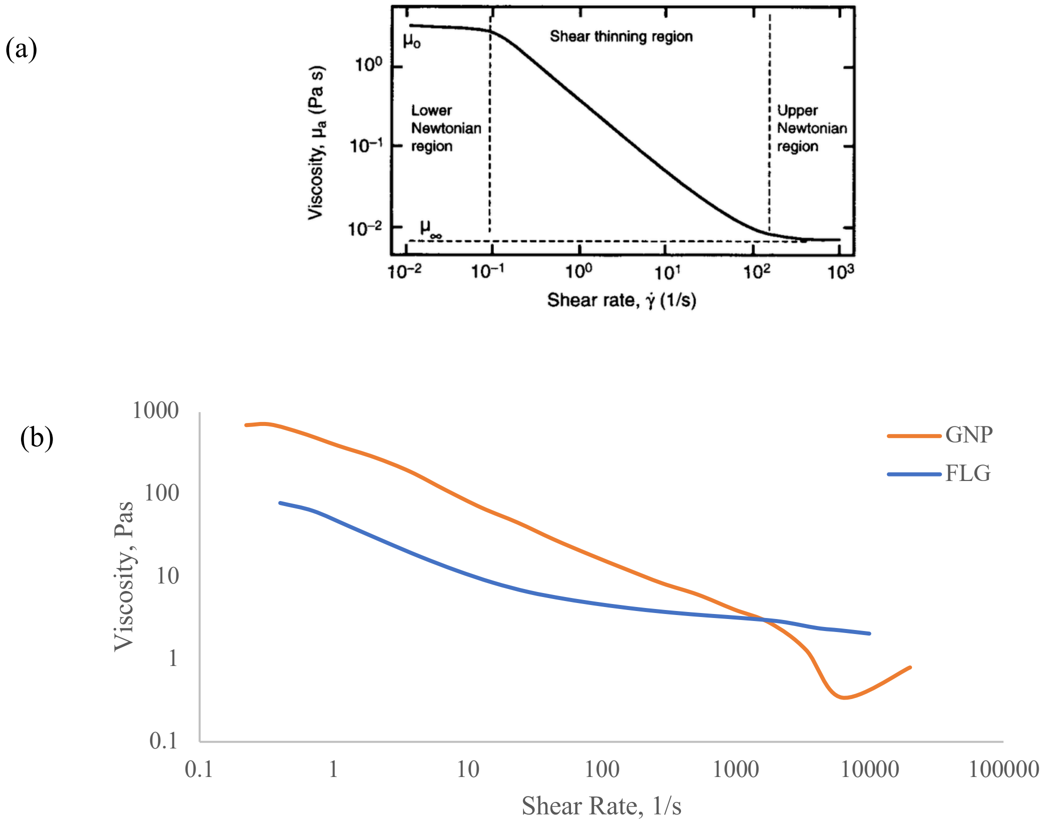

Figure 6.1 : (a) Example of shear thinning behaviour with respect to shear rate (Risum and Friis, 2009) (b) measured viscosity at 10 wt% fill

6.1.2 Cohesion Strength

De-agglomeration mechanisms were investigated using methods previously outlined in work by (He et al., 2017). Agglomerates are comprised of randomly orientated, clusters of stacked graphene sheets (figure 6.2). These clusters partially interact and form amorphous, weakly bonded agglomerates. The cohesion strength refers to the internal interactions holding agglomerates together and can influence the rate and mechanism of de-agglomeration, under a given shear stress. These calculations predict whether rupture or erosion will be the dominant mechanism of de-agglomeration for a particle of a given size. (Kasaliwal et al., 2010). The cohesion strength was calculated using the Rumpf equation (equation 5)

$$\sigma_c = (1-\varepsilon)\varepsilon^{-1}d^{-2}F \tag{5}$$

where σc = agglomerate cohesive strength, ε = porosity (taken as 0.85 (He et al., 2017)), d = agglomerate diameter and F = van der Waals force between particles. This was calculated using equation 6.

$$F = -\frac{Aab}{6\pi d^3} \tag{6}$$

Van der Waals force was calculated by modelling graphene sheets as square prisms, where A = Haymaker constant (2.38×10^{-19} (He et al., 2017)), a and b = flake planar dimensions (5 µm and 200nm where used for GNP & FLG respectively) and d = layer separation for graphite layers. Sonntag and Russel investigated the break-down of aggregates and concluded the minimum separation distance of aggregated GNPs is 2.58nm (Sonntag and Russel, 1987). As these calculations aim to predict break-down of aggregated graphene stacks rather than exfoliation, this value was used over the interlayer spacing of 0.314nm.

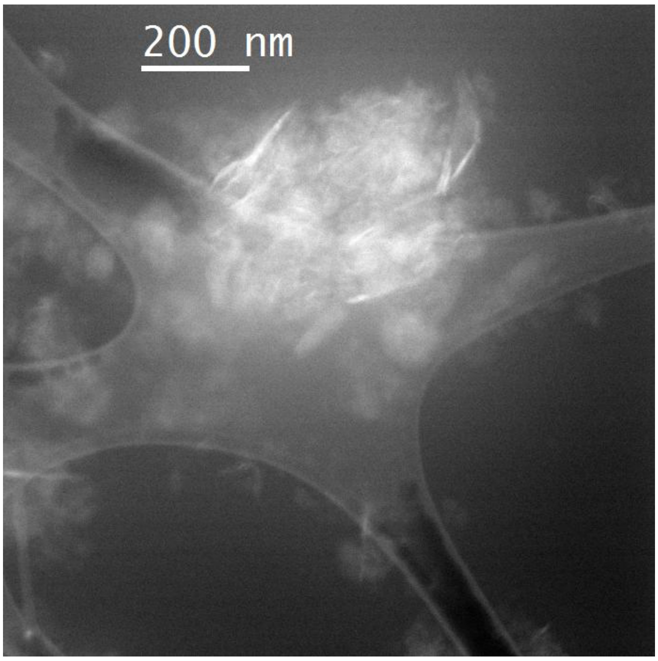

Figure 6.2: SEM image of FLG agglomerate within uncured epoxy resin

Figure 6.3 display the calculated shear stress for each mixing method against agglomerate cohesion strength. These values have been compared against the initial PSD of each graphene power, determined through SEM measurements (section 4.3). There is a clear linear relationship between cohesion strength and agglomerate size, showing less shear stress is required to break down larger agglomerates. The rate of de-agglomeration also increases where the ratio of shear stress to cohesion strength is high, leaving the rate of de-agglomeration changeable with dispersion state (Scurati, Feke and Manas-Zloczower, 2005). GNP flakes have higher cohesion strengths than FLGs, showing that agglomerates comprised of larger flake dimensions require more force to break down, due to the higher degree of interaction (Yi and Shen, 2015). Functionalised samples have been included in these predictions as plasma-functionalisation is a surface technique (Kondratowicz et al., 2018), leaving the internal agglomerate structure unaltered by functionalisation and therefore still exhibiting similar de-agglomeration behaviour (Williams et al., 2013).

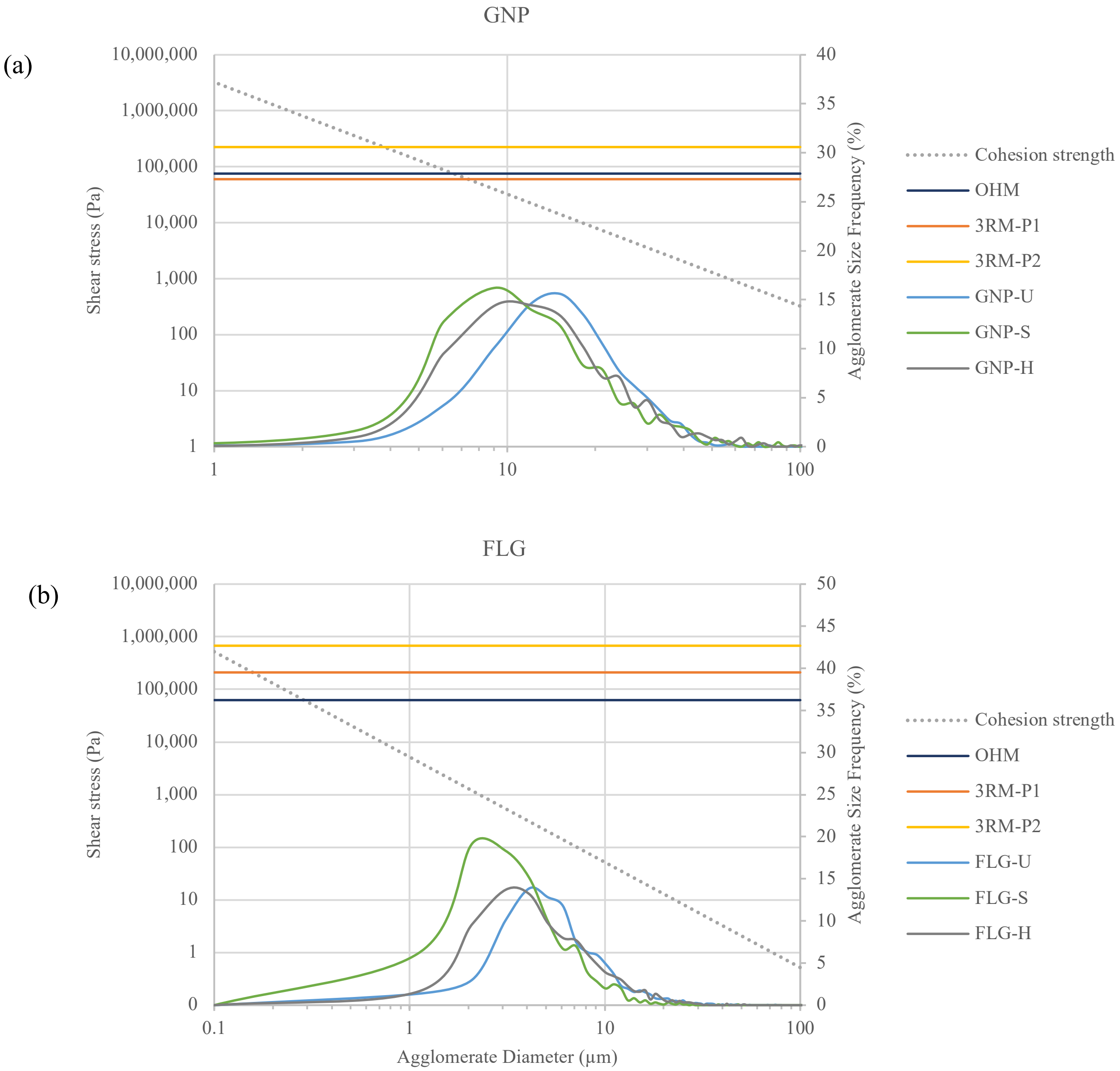

Figure 6.3: Cohesion strength of agglomerates in comparison against shear stress produced through each mixing method (a) GNPs (b) FLGs

The differing levels of shear stress produced for each flake size highlights the importance of tailoring the mixing method and parameters to the individual material. Mixing conditions where high levels of rupture take place are advantageous as mixing times can be reduced an therefor improve manufacturing efficiency. Erosion can also be beneficial as shearing mechanism ensures smaller particle sizes, but this mechanism results in longer mixing times (He et al., 2017).

GNPs undergo similar levels of shear stress with OHM and 3RM-P1 mixing (figure 6.3a), predicting de-agglomeration mechanisms for each GNP will be similar under these two conditions. The overall effect is expected to be more homogeneous after mixing by 3RM due to the even application of shear force over the material batch. 3RM-P2 outputs the highest shear stresses resulting in the highest proportion of agglomerate sizes undergoing rupture.

GNP-U samples have the largest initial agglomerate sizes. Rupture is expected to be the dominant mechanism to break down agglomerates sized >7µm during OHM and 3RM-P1. Rupture is then expected to act upon all GNP-U agglomerates during 3RM-P2. The rate of de-agglomeration is expected to slow as the net PSD becomes smaller, due the changing ratio of cohesion strength to shear stress (Scurati, Feke and Manas-Zloczower, 2005). Functionalisation has reduced the size of the initial agglomerates, resulting in a higher proportion of the PSD measuring >7µm for both functionalised GNPs. Erosion will be more significant during OHM and 3RM-P1, which will result in overall larger agglomerate sizes. Rupture becomes the dominant mechanism during 3RM-P2.

The shear stresses presented in figure 6.3b all significantly exceed the cohesion strength of all FLG agglomerates, showing rupture to be the dominant mechanism of de-agglomeration under all cases of mixing. The rate of de-agglomeration will increase with higher shear stresses, leaving 3RM-P2 projected to be the most efficient mixing method. FLG-U and functionalised FLGs were determined to be ‘unstable’ and on the border of ‘stability’ respectively, through analysis of zeta potential (section 4.2.3), leaving the possibility of FLG re-agglomeration (Cha et al., 2016)(Vilaverde et al., 2015).

6.1.3 Exfoliation

The interlayer shear stress (ISS) of graphite has been predicted to be 500 kPa (Throckmorton and Palmese, 2015), meaning a shear stress exceeding this value would be required to achieve exfoliation of stacked graphene sheets. This mechanism would be applicable to the clusters of stacked graphene which aggregate to form agglomerates. Exfoliation is desirable as this increases graphene aspect ratio and improves mechanical performance. Table 6.3 shows the only mixing procedure to achieve the conditions for exfoliation is 3RM-P2 of FLGs. The same mixing procedure for GNPs is much lower than this value suggesting exfoliation is not possible. However, the disruption to C-C bonded network caused through functionalisation, may further decrease the ISS and aid the exfoliation process (Cheng et al., 2019). There is potential to see fragmentation where shear forces are large enough to achieve exfoliation. This is detrimental to mechanical performance due to decreased planar size and damage to graphene sheets. Shorter mixing times may be able to minimise this effect (Yi and Shen, 2015a)(Yoon, Lee and Yoon, 2018).

6.2 Hegman gauge

The Hegman gauge was used to measure agglomerates over the macroscale, average values for the largest measured agglomerate and break are presented in figures 6.4 and 6.5 GNP-U samples were expected to show fast de-agglomeration under the dominant rupture mechanism. This trend is demonstrated in both measurements for each mixing method. Values show a steep drop upon high shear mixing and continue to slowly decrease for the duration of mixing time. Mixing through 3RM gave faster reduction to net agglomerate size, which is attributed to the even distribution of high-shear force. The higher shear forces generated through 3RM-P2 did not appear to significantly impact de-agglomeration. Both mixing methods have produced error bars spanning similar sizes, showing large agglomerates up to ~20μm are present in both mixtures after mixing had been completed. Longer mixing times could be used to further break down these agglomerates, however this becomes inefficient and undesirable.

Both functionalised GNPs were predicted to experience erosion for a larger proportion of the initial agglomerates, during OHM and 3RM-P1. As a result of this, both GNP-S and GNP-H have reduced the average agglomerate size by a smaller degree. Firstly, the GNP-S break values show an initial drop after 15 minutes of mixing, to approximately 7μm and fluctuates around this value over the remaining mixing time. This is the critical size at which the dominant mechanism of de-agglomeration switches, showing a significant proportion of agglomerates undergoing slow erosion. The largest measured agglomerate similarly shows a slow gradual decrease over the mixing time. The error bars are consistently wide and measuring at the highest end of the scale, indicating agglomerates even larger than 25μm are present within the batch. The larger average values and presence of larger agglomerates (>25μm), when compared to the GNP-U counterpart, are the result of fewer agglomerates undergoing rupture, combined with the uneven OHM mix profile. GNP-H measurements from OHM mixed samples have followed a similar trend to GNP-S. GNP-H has produced break measurements similar to that of GNP-U, but high values for largest agglomerate (>25μm). This broad range of agglomerate sizes is reflective of the inhomogeneous distribution of shear stress through the mixing batch. Both functionalised GNPs have given similar trends over the course of 3RM mixing, where a drop in values is displayed after 3RM-P1 and again with the increased shear stress after 3RM-P2. This is reflective of the increasing influence of rupture upon mixing through each profile. The largest measured agglomerate values are smaller and span and narrower area than those measured through OHM, showing better de-agglomeration through 3RM.

These measurements show that faster de-agglomeration was achieved where rupture was the dominant mechanism, highlighting better efficiency with techniques using higher levels of shear stress. Large agglomerates (>25µm) were observed in OHM samples where erosion was significant, correlating to less aggressive de-agglomeration and inhomogeneous application of shear stress. Large agglomerates are undesirable in composite materials as they provide little reinforcement and behave as stress concentrators when under loading, resulting in the degradation of mechanical performance (Tang et al., 2013). In order to reduce the impact of these, longer mixing times or higher shear stresses can be employed.

Rupture was determined to be the dominant mechanism of de-agglomeration for all FLG samples. 3RM-P2 gave the highest shear stress and therefore is expected to produce the quickest rate of de-agglomeration. OHM produced the lowest shear stress and is expected to provide the slowest rate of de-agglomeration. Additionally, FLG-S is comprised of the smallest agglomerates and are therefore expected to have a slower rate of de-agglomeration. A large consideration of using Hegman gauge with small agglomerate sizes is the incompatibility in scale. The FLGs were found to have their average agglomerate size range between 2-4µm (figure 6.3b). As the Hegman gauge measures over 2.5-25µm, to an accuracy of 2.5µm, it becomes difficult to visualise trends to the bulk of FLG agglomerates. With this in mind, the data presented in figure 6.5 must be interpreted in relation to the small proportion of agglomerates which size over this scale rather than an indication of bulk agglomerate trends.

Measurements shown in figure 6.5 illustrate a stark contrast between the two mixing methods, where values measured after 3RM mixing are much smaller than OHM. The break values measured after 3RM mixing are similar to the average agglomerate size prior to mixing. This shows a significant proportion of larger sized agglomerates have been broken-down, however agglomerates sized 25µm and potentially higher have been measured in every case of mixing, which could indicate re-agglomeration, due to particle instability (Pacek, Ding and Utomo, 2007). FLG-U and FLG-S mixed by OHM show little change to values over the mixing duration, whereas FLG-H shows a decrease to break values, suggesting high intensity functionalisation had aided the de-agglomeration process. The large break values seen in figures 6.5b and 6.5c are a bit misleading, due to the incompatibility of Hegman gauge scale and the FLG PSD combined with the uneven mix profile of the OHM. These trends cannot be taken as mean values which relate to the bulk material.

These results have highlighted the limitations of the Hegman gauge and the importance of matching the scale of the measurement technique with the agglomerate size. This technique is not suitable for the determination of the bulk trends of FLGs but can effectively identify the presence of large agglomerates. Hegman gauge gives good representation of macro-sized particles and dispersion state of graphene with large planar size.

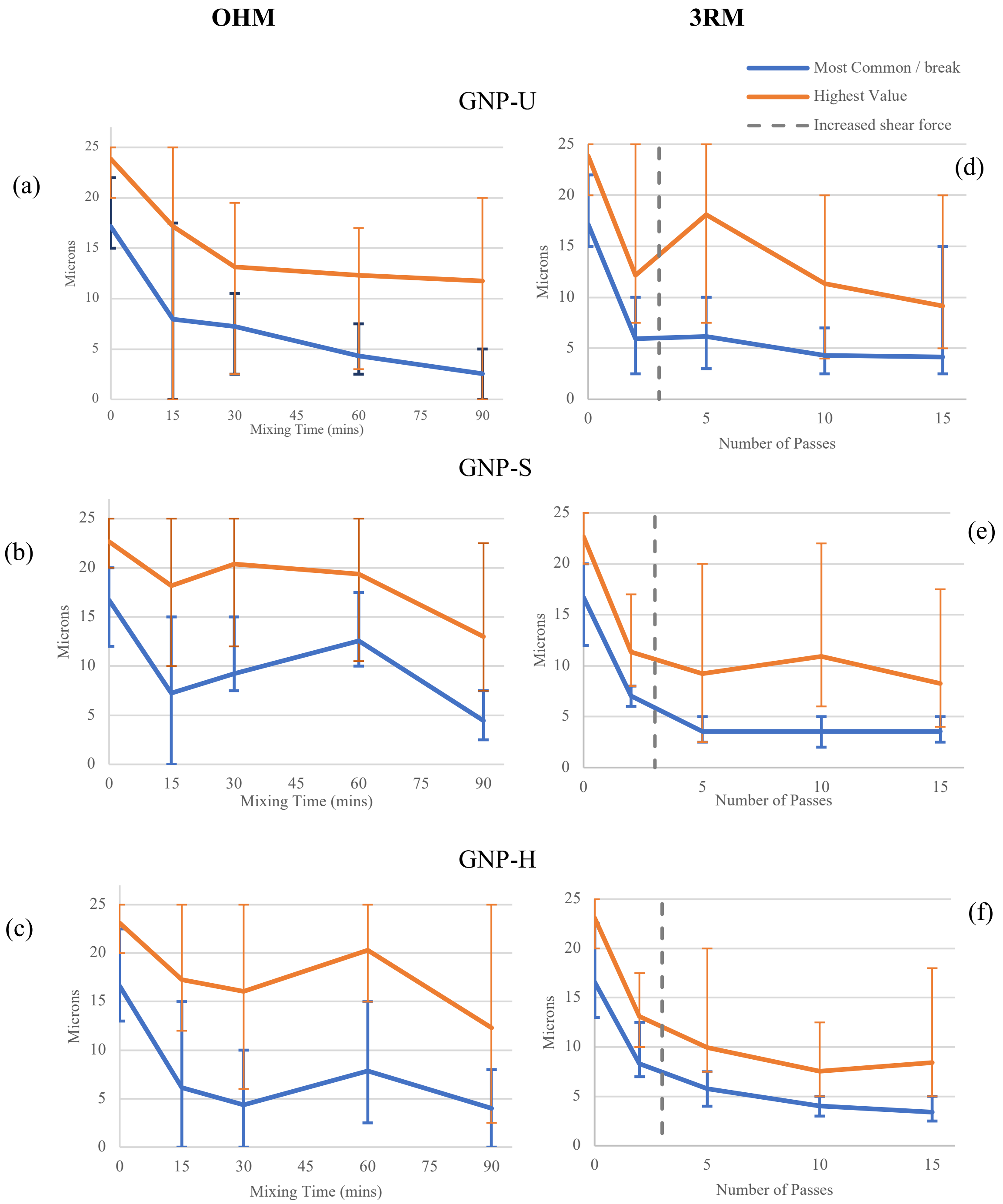

Figure 6.4: Hegman Gauge measurements for GNPs, OHM mixed results are displayed for (a) GNP-U (b) GNP-S (c) GNP-H and 3RM results are displayed for (d) GNP-U (e) GNP-S (f) GNP-H

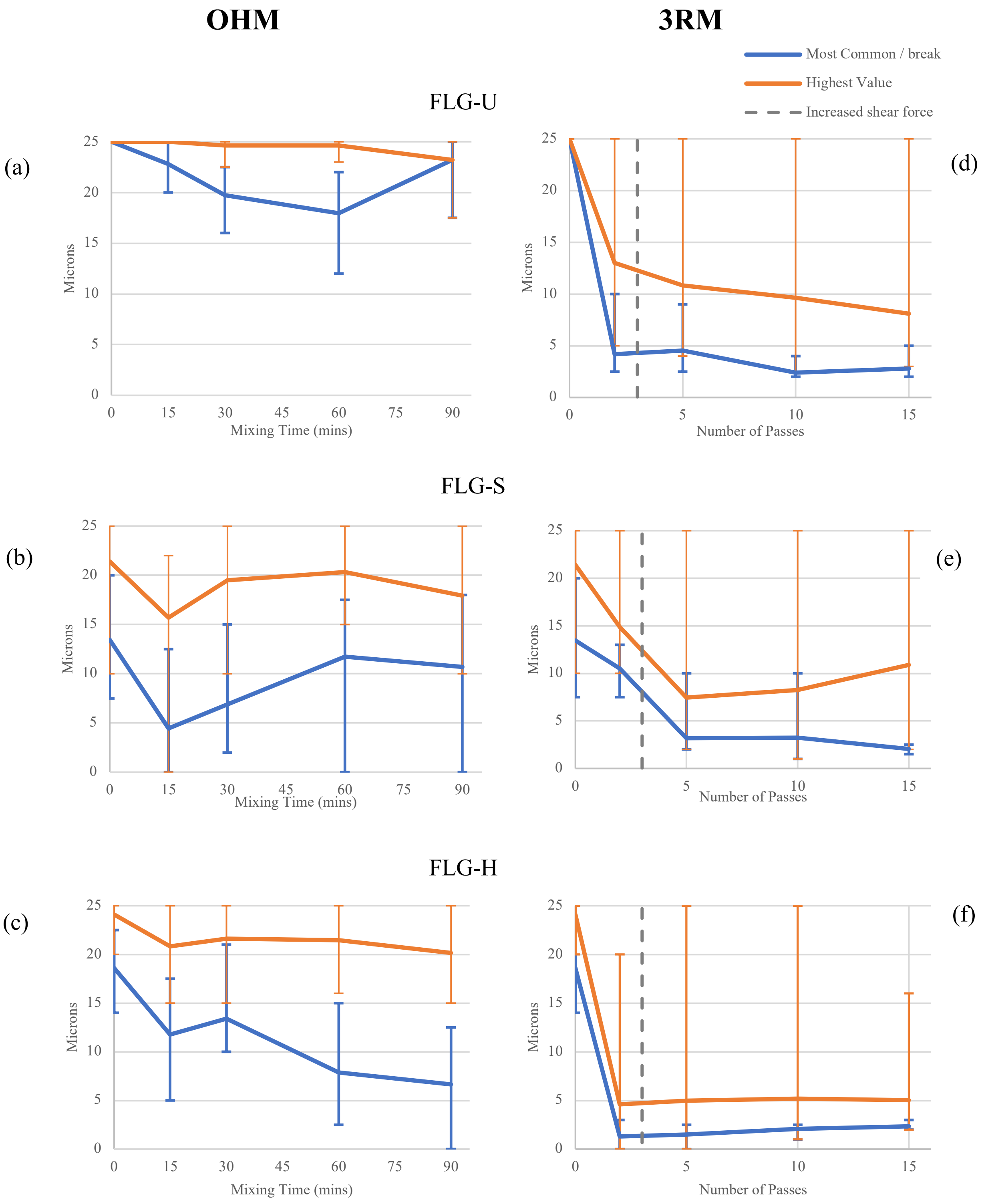

Figure 6.5: Hegman gauge measurements for FLGs OHM mixed results are displayed for (a) FLG-U (b) FLG -S (c) FLG -H and 3RM results are displayed for (d) FLG-U (e) FLG -S (f) FLG -H

6.3 Optical Microscopy

Microscale dispersion was investigated using optical microscopy. Based on the magnification used, this method gives good representation over the range of 3-6µm. Figure 6.6 displays PSD curves and statistical values for GNP samples. Over this scale, the dominant mechanism of de-agglomeration for GNP-U was erosion for OHM and 3RM-P1 and rupture for 3RM-P2. There is no identifiable change to PSD over the course of mixing by OHM. Mixing through 3RM has shown a distinct increase in PSD peak height, which remains similar for the duration of mixing.

Both functionalised GNPs do not show any clear changes to PSD after OHM, which is reflective of the erosion mechanism occurring over this scale in addition to the inhomogeneous mix profile which results in small changes to dispersion state. 3RM mixed GNP-S shows increased peak height of PSD over the course of mixing, indicating a level of de-agglomeration. The PSD peak of GNP-H narrowed after mixing by 3RM and remained consistent over the course of mixing, illustrating immediate effect of de-agglomeration.

Rupture is the de-agglomeration mechanism for all FLG samples. Figure 6.7a shows PSD distribution curves for FLG-U samples mixed through OHM, displaying a general left shift in curve over the mixing period. This illustrates a correlation between de-agglomeration and mixing time. Mixing through 3RM again has produced a clear effect of de-agglomeration, showing a left shift in PSD and increase to peak height after 2 passes. There is little improvement with further passes. Functionalised samples have not shown any clear response to OHM, the PSD are quite varied and display little trend. Conversely, curves produced for 3RM samples show more consistency across curves, reflecting the homogeneity of dispersion.

These data points generally corroborate the trends identified in Hegman gauge analysis. However, the changes to PSD with de-agglomeration are small and therefore can only be interpreted comparatively. This illustrates the difficulty in using this method to interpret changes to dispersion state are not homogeneous, such as with data produced after OHM. Because of these factors, in addition to considerations discussed in (section 5.1.1), the use of optical microscopy alone to measure dispersion state is inaccurate and therefore should be used either comparatively or in conjunction with other methods.

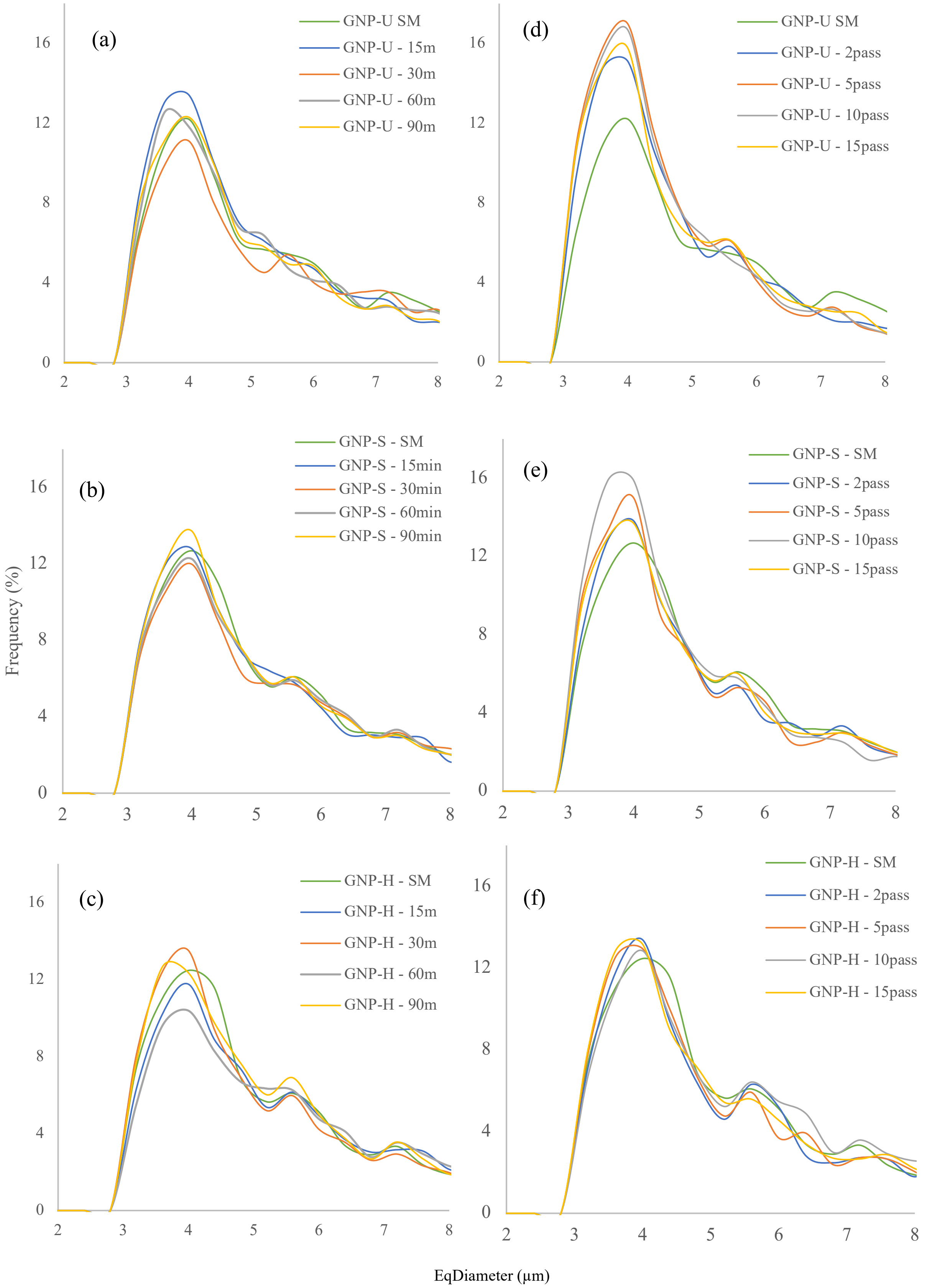

Figure 6.6 : PSD determined from optical microscopy images for GNPs, OHM mixed results are displayed for (a) GNP-U (b) GNP-S (c) GNP-H and 3RM results are displayed for (d) GNP-U (e) GNP-S (f) GNP-H

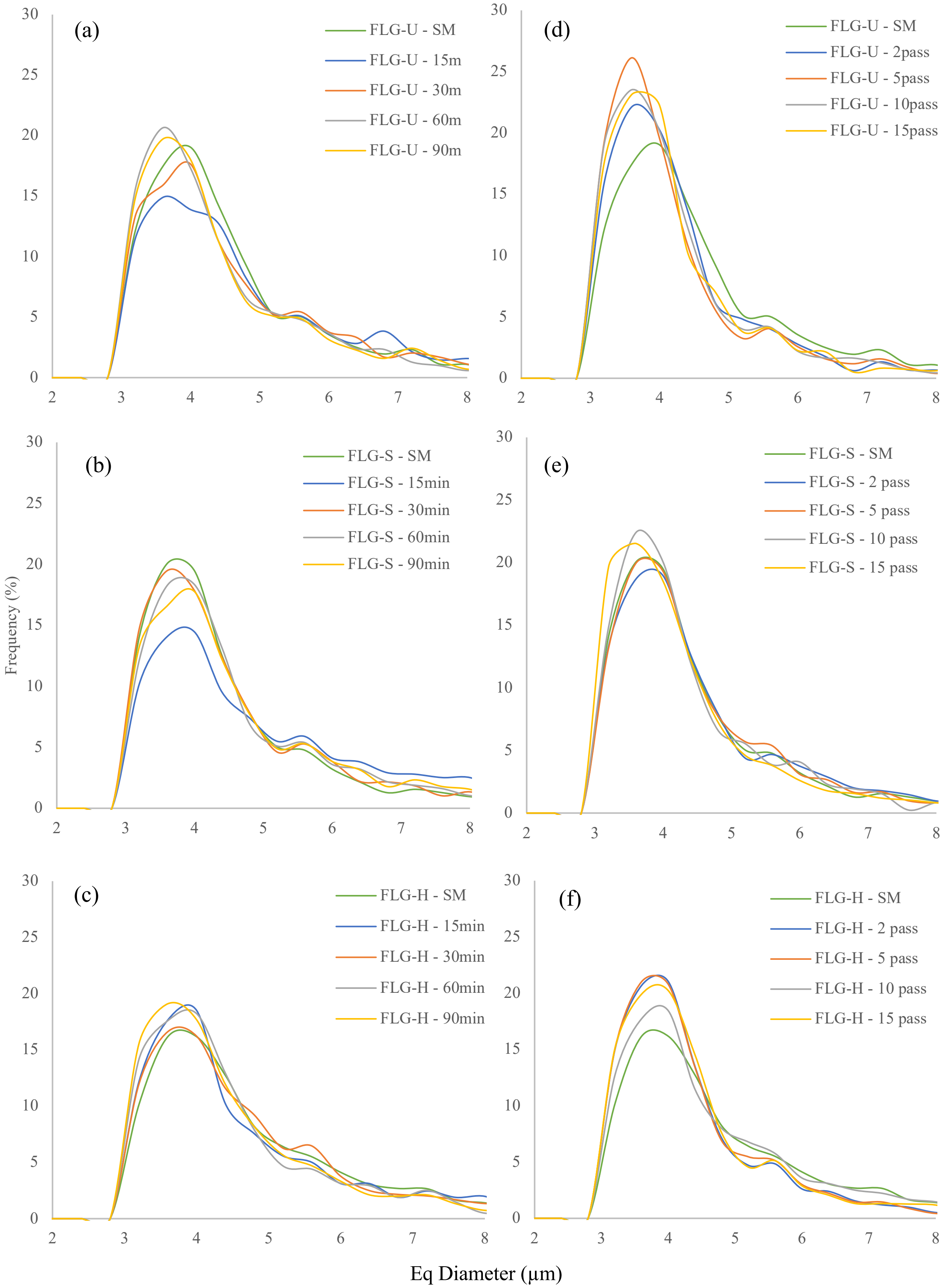

Figure 6.7 : PSD determined from optical microscopy images for FLGs OHM mixed results are displayed for (a) FLG-U (b) FLG -S (c) FLG -H and 3RM results are displayed for (d) FLG-U (e) FLG -S (f) FLG -H

6.4 TEM

Measurements in figure 6.8 represent the nanoscale de-agglomeration for FLG samples. Statistical values were determined based on measurements collected using methods described in section 5.1.2. These samples were prepared and imaged at Manchester University. This package of work was facilitated through the PhD access scheme with the Henry Royce Institute.

TEM measurements are considered to be essential for the visualisation of nanomaterials, as the high magnification allows individual agglomerates and their morphology to be viewed. This is essential for FLGs where all flake dimensions exist over the nanoscale and have low compatibility with other techniques. The operation of TEM is costly and time consuming, leaving select examples of FLGs to be analysed. More focus has been placed with OHM mixed samples due to larger scale methods failing to discern any strong correlation to mixing time, which may be the result of the mixing method in addition to low precision of measuring technique. FLG-H samples mixed through 3RM have not been selected for analysis as previously determined trends were similar to that of FLG-S samples and were expected to give similar results.

Statistical values displayed in figure 6.8, for FLG-U samples show a decrease in agglomerate size with relation to mixing duration for both high shear methods. FLG-S samples mixed through 3RM match previously determined trends where highest levels of de-agglomeration are produced after 3RM-P2. FLG-S samples mixed through OHM have not produced any significant changes to size distribution with mixing time. FLG-H data gives slightly larger values overall but are generally comparable with other data. TEM images taken from OHM mixed samples figure 6.9 illustrate a combination of large particles next to very small particles, which is illustrative of the erosion mechanism present over this range of agglomerate sizes.

The trends produced for 3RM mixed samples line up with the trends determined through optical microscopy and Hegman gauge, indicating the same behaviour across each scale. In terms of quality control, this allows confidence that the trends measured using macroscale techniques are reflective of the whole batch. OHM mixed samples produced similar tendencies with those seen in large scale measurements, however it is difficult to conclude if they are similar as there is little correlation to mixing time. Based on the differences in analysis seen between the two mixing methods, it can be concluded that the dispersion state is poor after OHM mixing. The dispersion state produced after the longest length of mixing for each method is displayed in TEM images in figure 6.9. Samples produced after 3RM give the appearance of areas where full de-agglomeration and / or additional exfoliation has been produced, the original quoted dimensions were <200nm and between 1-4 layers. This is not visible with OHM samples, showing the poorer quality of dispersion state.

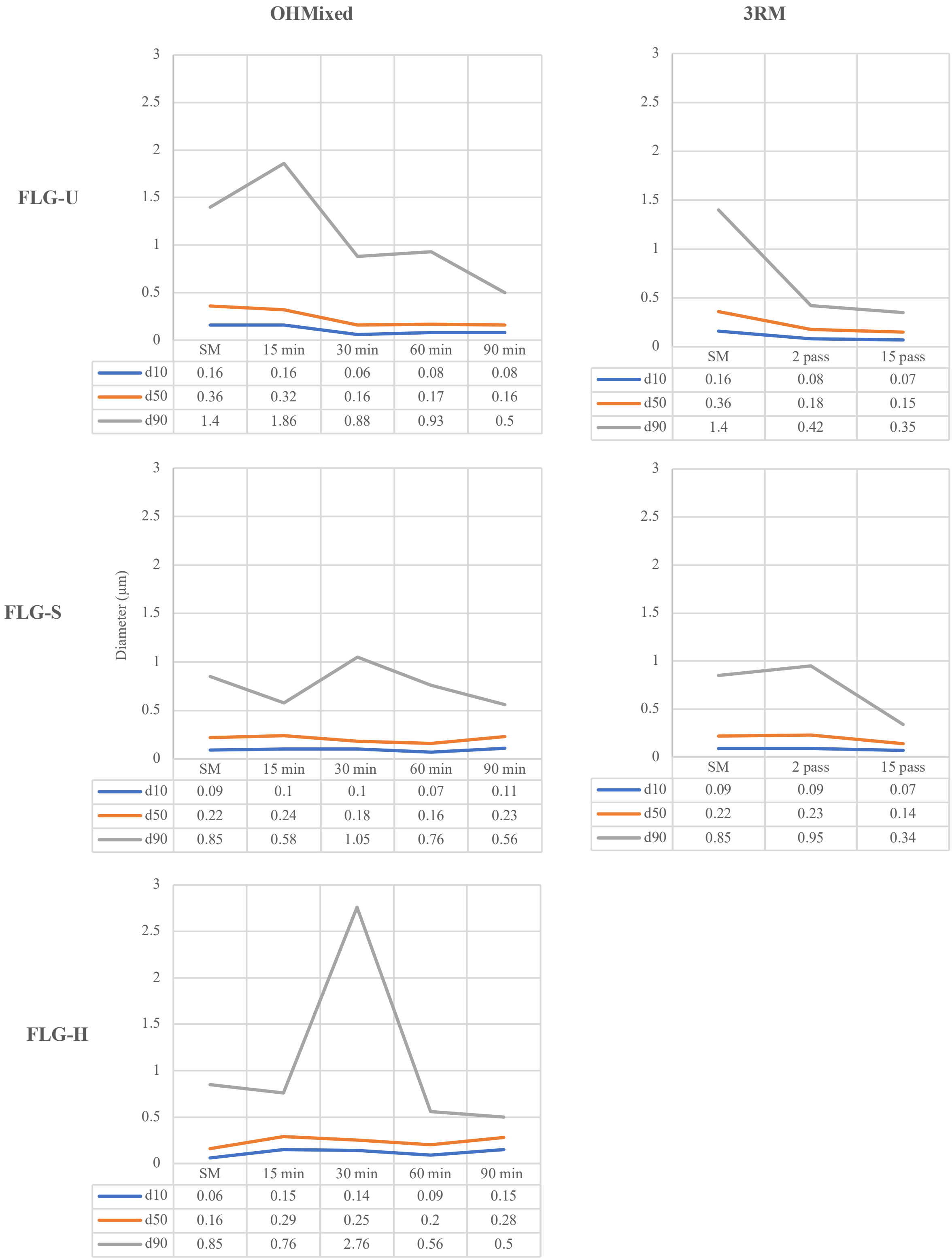

FLG-U, OHMixed:

	SM	15 min	30 min	60 min	90 min
d10	0.16	0.16	0.06	0.08	0.08
d50	0.36	0.32	0.16	0.17	0.16
d90	1.4	1.86	0.88	0.93	0.5

FLG-U, 3RM:

	SM	2 pass	15 pass
d10	0.16	0.08	0.07
d50	0.36	0.18	0.15
d90	1.4	0.42	0.35

FLG-S, OHMixed:

	SM	15 min	30 min	60 min	90 min
d10	0.09	0.1	0.1	0.07	0.11
d50	0.22	0.24	0.18	0.16	0.23
d90	0.85	0.58	1.05	0.76	0.56

FLG-S, 3RM:

	SM	2 pass	15 pass
d10	0.09	0.09	0.07
d50	0.22	0.23	0.14
d90	0.85	0.95	0.34

FLG-H, OHMixed:

	SM	15 min	30 min	60 min	90 min
d10	0.06	0.15	0.14	0.09	0.15
d50	0.16	0.29	0.25	0.2	0.28
d90	0.85	0.76	2.76	0.56	0.5

Figure 6.8: Statistical values for FLGs determined from TEM imaging, determined as explained in section 5.2.1

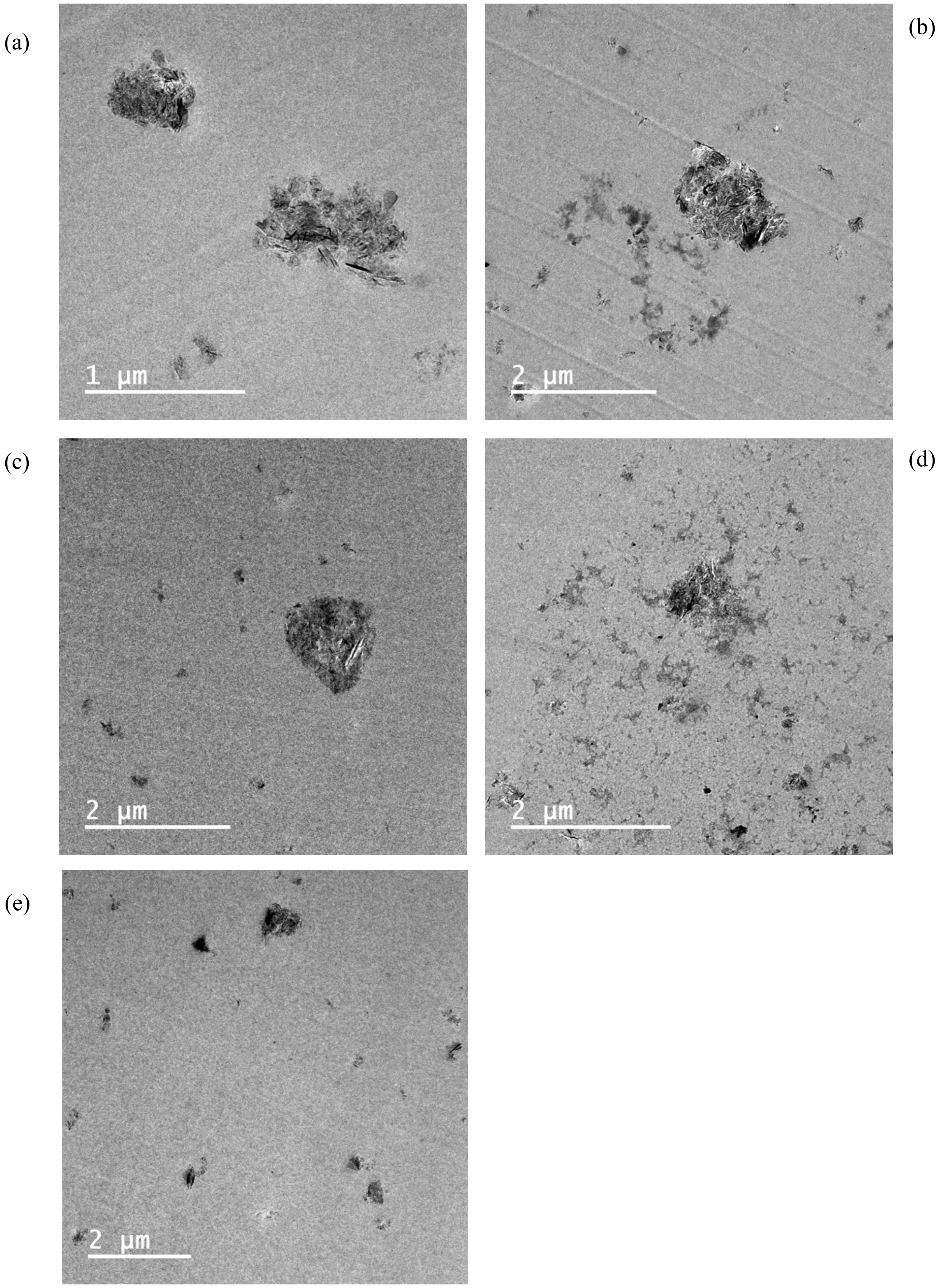

Figure 6.9: TEM images (a) FLG-U OHM 90mins (b) FLG-U 3RM 15passes (c) FLG-S OHM 90mins (d) FLG-S 3RM 15passes (e) FLG-H OHM 90mins

6.5 XRD

The levels of shear stress produced by 3RM were smaller than the critical value of 500kPa (Throckmorton and Palmese, 2015) required to exfoliate graphite sheets leaving it unlikely that exfoliation would be achieved for GNPs. Spectra produced for all GNP-U samples were found to have a peak height of ~1375, for the characteristic graphitic interlayering peak, indicating that no exfoliation occurred over mixing. Peak height was measured at ~1375 for GNP-S SM samples, which decreased to ~850 for spectra produced after 2 and 10 passes, indicating exfoliation had occurred. The level of shear stress present during 3RM-P1 is 70 kPa, which is much lower than the threshold required to achieve exfoliation of graphene sheets, showing functionalisation has altered the graphene surface to the extent that the levels of shear stress required to achieve exfoliation have been significantly reduced, illustrating compatibility in surface energies between O_2 functional groups an polymer chains (Cui et al., 2011). It is possible that the presence of functional groups have sufficiently weakened the $\pi - \pi$ interactions to allow exfoliation to occur at lower shear forces (Quintana, Tapia and Prato, 2014). Studies by (Yi and Shen, 2015) have suggested the surface modification of graphene may lead to a higher exfoliation effect when using mechanical methods. The increased shear stress experienced between 3-15 passes, has not affected the peak intensity showing no further exfoliation has taken place. As plasma functionalisation is a surface treatment, the unfunctionalised sheets become exposed and subsequently require higher levels of force to achieve further exfoliation. This data suggests that functionalisation has facilitated exfoliation, resulting in isolated sheets which can improve reinforcement, however the functionalisation will have degraded the mechanical properties of these sheets.

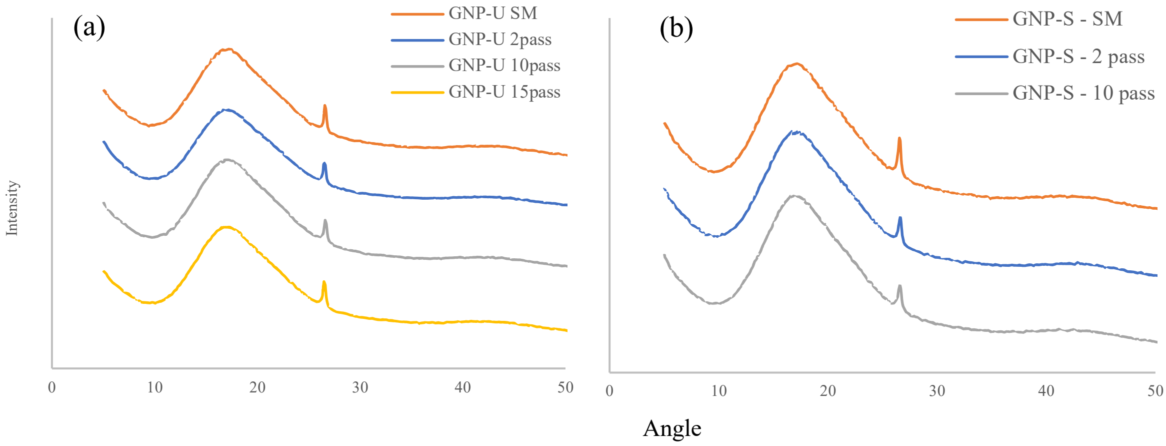

Figure 6.10: XRD spectra for GNPs mixed through 3RM (a) GNP-U (b) GNP-S

6.6 *Viscometry*

Viscosity measurements analyse a relatively large volume of sample, giving good representability of dispersion state. Figure 6.11 displays the viscosity measured at 1s^{-1} shear rate for each mixing procedure. As observed for other measurements of GNPs, there is a clear distinction between the two mixing methods, where mixing through 3RM consistently gives higher viscosity indicating a better dispersion state. Shear rate sweep tests in figures 6.12 and 6.13, display shear thinning behaviour occurring across all GNPs. High viscosity values are observed at low shear rates for GNP-U and GNP-S samples, reflective of the good dispersion state increasing the viscosity through high levels of restriction of chain mobility (Throckmorton and Palmese, 2015). The shear thinning effect is due to the viscoelastic properties of the mix, where 'liquid-like' behaviour is regained at high shear rates. GNP-H samples exhibited interesting behaviour, where a lubrication effect was displayed through the low viscosity measured at high shear rates. This usually indicates there are no interactions between the epoxy and GNP-H functional groups (Amirova et al., 2017).

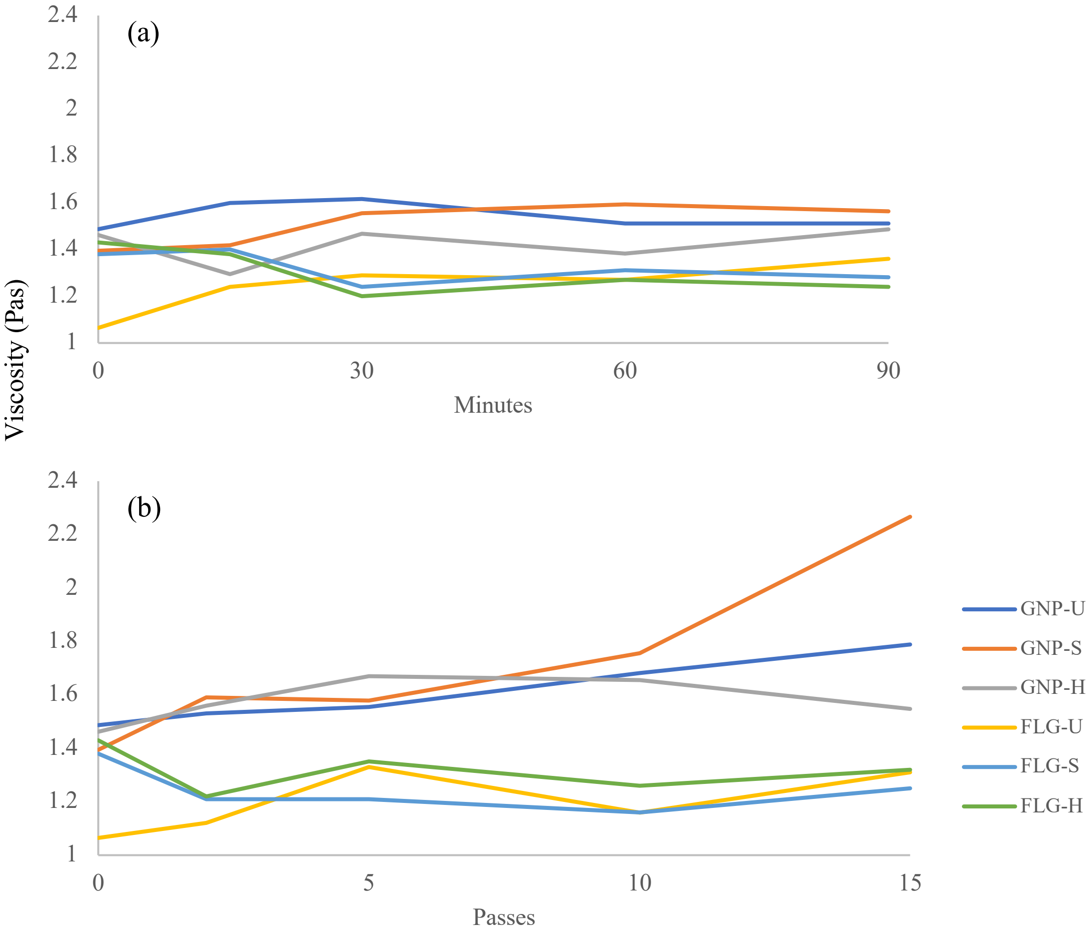

Figure 6.11 : Viscosity measured at 1s^{-1} shear rate with respect to mixing time (a) OHM (b) 3RM

FLG viscosity data does not show any significant trends with mixing method or time. As it has been proven that a level of de-agglomeration has been achieved for FLGs through other characterisation methods, it is concluded that viscometry is not compatible with FLGs as a method of analysing de-agglomeration. Because FLGs have a small planar size and have been used a low filler loadings, the effect of dispersion state on viscosity is less pronounced and consequently reduces the reliability of drawing any substantial conclusions from these measurements. Testing at higher filler loadings may show changes in viscosity and therefore dispersion state more clearly. The FLG low viscosity values do illustrate compatibility of this material with resin fusion techniques for manufacture of hybrid composites.

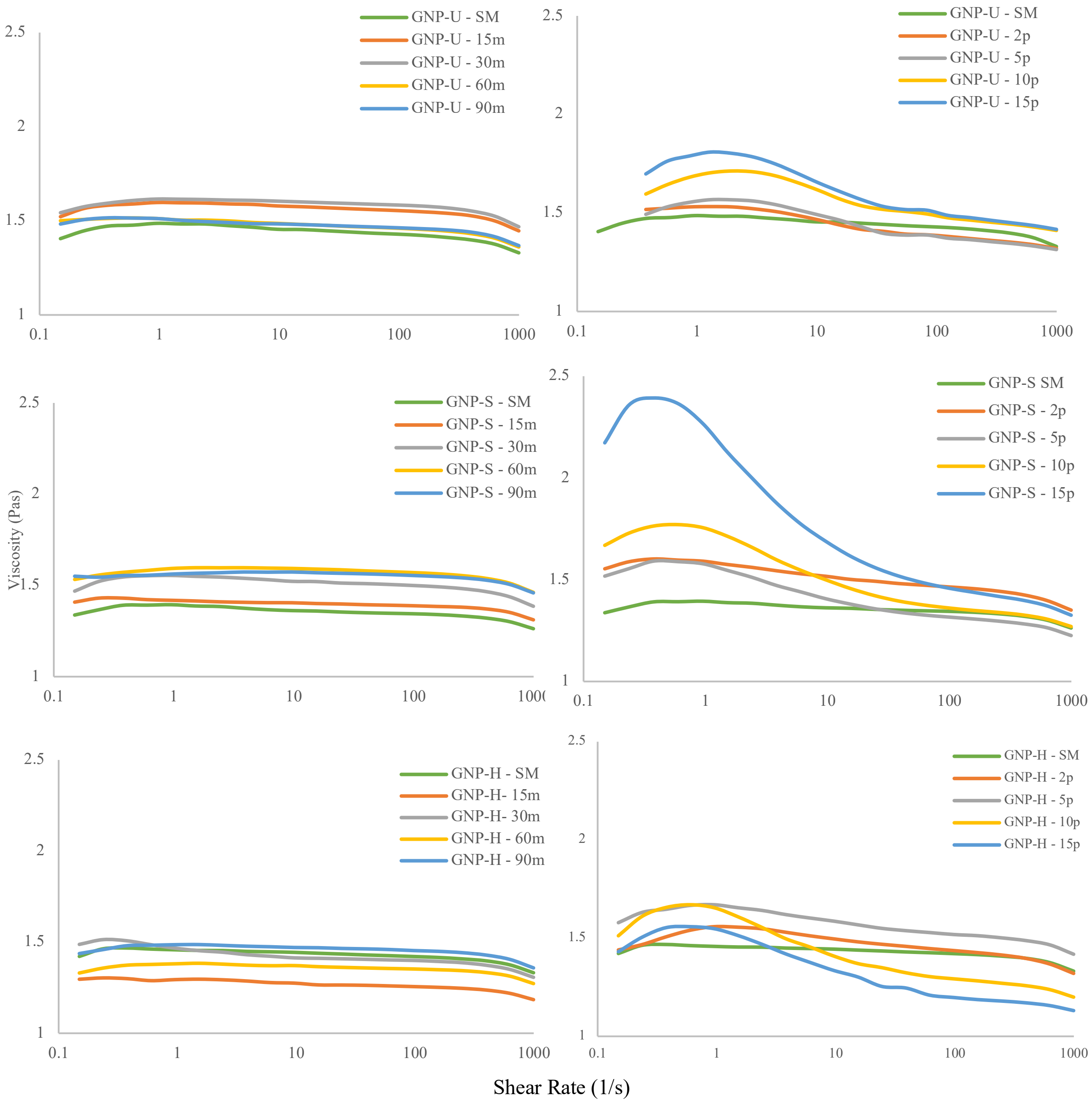

Figure 6.12 : Viscosity measurements for all GNP mixed samples

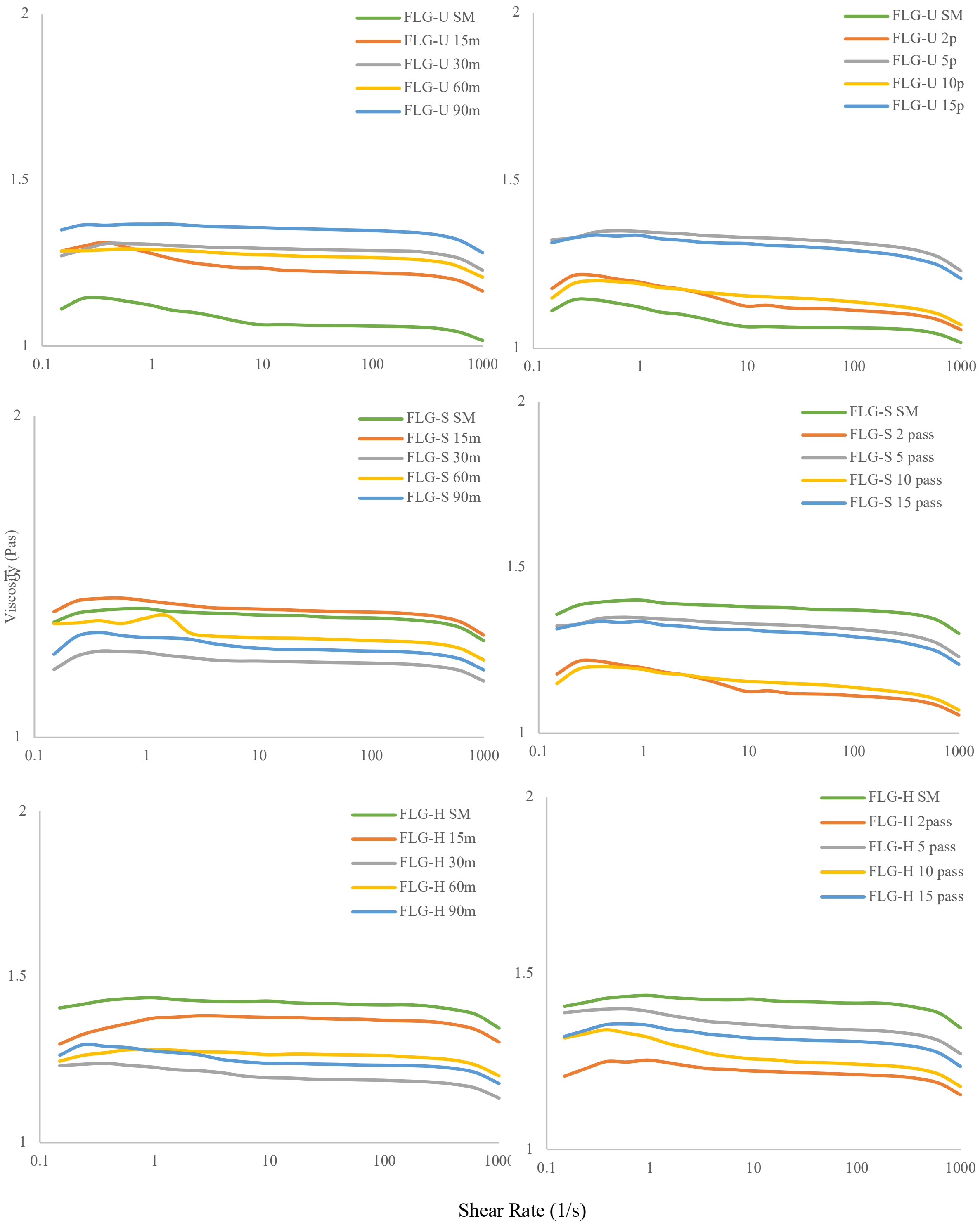

Figure 6.13 : Viscosity measurements for all FLG samples

6.7 Summary

This data unanimously displayed better dispersion state for all materials after mixing through 3RM, highlighting the efficiency of de-agglomeration with evenly distributed shear stress. Samples produced in this way are expected to provide better mechanical reinforcement as a result (Tang et al., 2013). Samples produced through OHM did not de-agglomerate over the bulk material after 90 minutes of mixing, showing this is not an effective method of dispersion.

Mixing by 3RM was found to be effective for both GNP and FLG flakes, with largest changes to dispersion measured after 2-5 passes. This illustrates that short processing times are sufficient to produce good dispersion state. Additionally, good agreement of de-agglomeration trends were seen over the nano, micro and macro scale. This simplifies the quality control process, leaving confidence in the quick analysis produced through the Hegman gauge to be representative of the bulk dispersion state. This is desirable from an industrial viewpoint as this provides an effective and low-cost solution with good representativeness in results.

De-agglomeration appeared to follow predicted mechanisms outlined in section 6.1.2, illustrating the relationship between shear stress, agglomerate size and break-down mechanism. This demonstrates an effective method to predict and modify mixing parameters based on initial agglomerate size. The presence of functionalisation gave a reduction to the initial agglomerate size range, in addition to aiding the exfoliation process. GNP-S samples were exfoliated at low shear stresses showing an affinity between the O_2 functional groups and epoxy chains, both facilitating the dispersion process and forming interactions with the polymer chains. This behaviour was displayed through XRD and viscosity measurements. GNP-H however, did not display any indication of interfacial interactions in the uncured state.

The functionalised FLGs had smaller initial agglomerate sizes and generally performed similarly to FLG-U. FLG samples were found to be difficult to completely break-down and displayed large agglomerates (>25µm) after every case of 3RM mixing, which could indicate a level of re-agglomeration. Zeta potential measurements indicated that FLG-U was unstable, leaving high potential for agglomeration to occur whereas functionalised FLGs showed to be on the border of ‘stability’ showing a lower chance for re-agglomeration to occur. The close proximity of the FLGs at 10 wt% fill and additional SM process used to dilute samples to 1 wt%. fill before analysing, may have facilitated a level of re-agglomeration after undergoing mixing.

7 Mechanical Properties

7.1 Thermomechanical Testing

DMA testing has been explored over this section to investigate how the addition of fillers affects cure behaviour, cross-linking and thermomechanical properties. The role of cure cycle, flake size, dispersion state and functionalisation have been explored to fully understand these relationships and allow optimisation of the manufacturing procedure.

7.1.1 Curing Cycles

A short study into the curing behaviour of the Araldite LY1564 epoxy and Aradur 2954 hardener system was carried out using DMA. The addition of graphene was suspected to have interfered with the epoxy cure based on produced thermomechanical data, leading to further investigation of properties with respect to cure cycle and the addition of GNPs.

The material curing begins after the combination of hardener and epoxy resin, triggering direct reaction and solidification of the two components (Hodd, 1989), the post-cure process then strengthens the structure through the formation of additional crosslinking. It is difficult to decipher whether the addition of graphene has disrupted the initial curing process, the formation of crosslinks or both, therefore changes to the storage modulus over the rubbery state have been investigated.

When heated beyond their glass transition temperature, thermoset polymers enter the rubbery region where polymer chains gain mobility but maintain a level of rigidity due to the formation of crosslinks within the material (Yu et al., 2016). The storage modulus is also influenced by the molecular weight of the polymer chains within this region, and therefore has been used to assess the changes to the epoxy structure over difference cure cycles. As the addition of filler also raises storage modulus values, comparisons have only been made across each material.

The post-cure time and temperature are closely linked to the curing process of epoxy resin. High temperatures increase the energy within the system, allowing interactions to take place more easily. Figure 7.1 show the storage modulus taken from within the rubbery region (20°C above the Tanδ peak height as displayed in figure 3.7), for samples with various post-cure cycles. All samples were initially left to cure for 18 hours at room temperature and post-cured at 80ºC for one hour before undergoing further post-cure at either 140ºC or 160ºC for 4, 8 and 16hrs. Filled samples were produced after mixing through 3RM and therefore have good dispersion state.

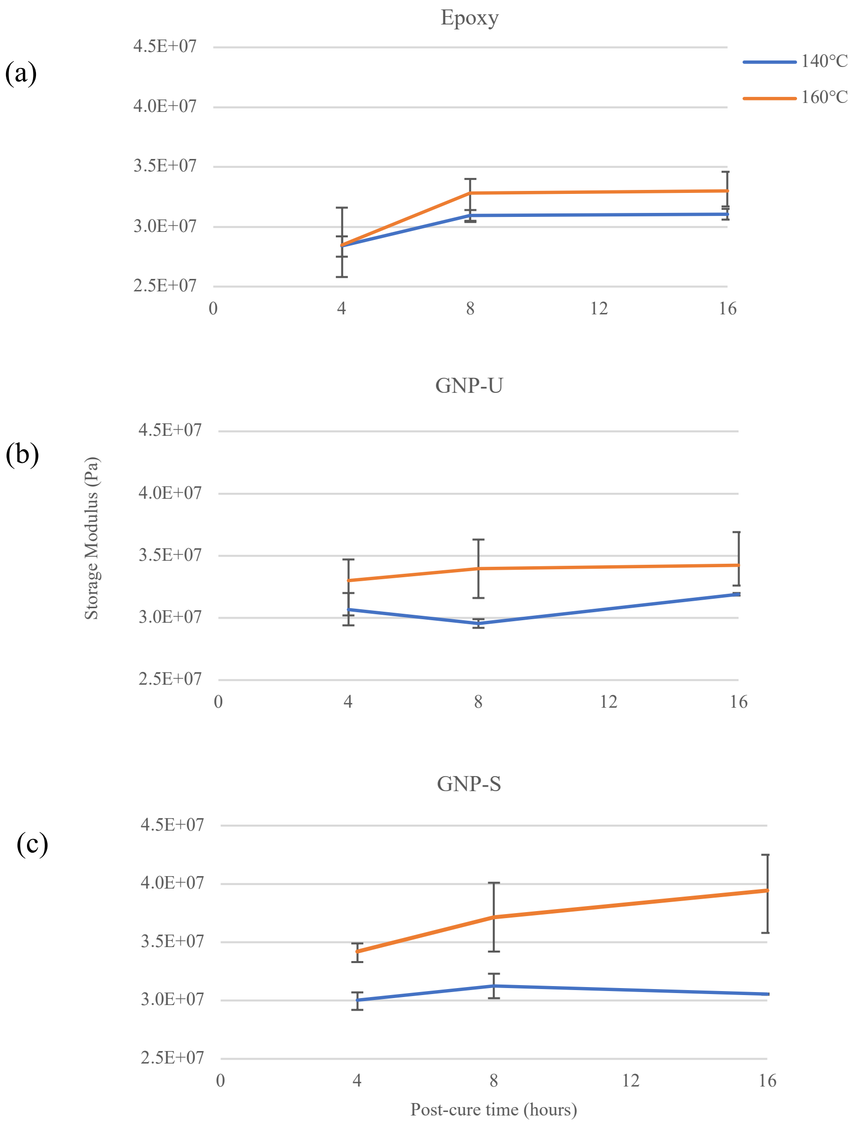

Figure 7.1 : Storage modulus determined from within the rubbery region (taken from 20ºC above the Tg) with relation to cure time for (a) epoxy (b) GNP-U (c) GNP-S

For both investigated temperatures displayed in figure 7.1a, the unfilled epoxy resin reached a plateau in storage modulus after 8 hrs of post-cure, suggesting the curing reaction between epoxy and hardener, and the full extent of crosslinking achievable is realised after this time. A higher storage modulus is developed at elevated cure temperature which suggests a higher degree of crosslinking is produced with higher temperature. GNP-U filled samples show storage modulus continued to increase over the 16hrs of post-cure at 140ºC, suggesting longer post-cure times are required to reach plateau. The higher thermal energy allows crosslink density to reach a plateau after only 8hrs of post-cure at 160ºC. As more energy is required to reach this peak over a shorter period of time, the graphene fillers may slow the rate of cure if the post-cure temperature is not sufficient. The increase in viscosity seen with the addition of fillers will also inhibit the curing process (Wang et al., 2012).

The presence of functionalisation has affected the cure behaviour to a further degree as storage modulus continuously increased over the 16hrs of post-cure at 160ºC. XPS analysis determined high proportions of hydroxyl functional groups attached to the surface of GNP-S flakes which can react with polymer epoxide groups during post-cure and alter the reaction stoichiometry (Vryonis et al., 2019). Incomplete cure and low crosslink density can cause a reduction in Tg through the presence of unreacted epoxy and hardener molecules lowering the molecular weight, and increasing chain mobility through low levels of crosslinking (Menard, 1999).

Figure 7.2 shows the Tg measured for samples after undergoing the extremes of the post cure cycles analysed. After 4hrs post-cure at 140ºC, Tg values for both filled samples are lower than that of epoxy resin whereas after 16hrs post-cure at 160ºC, the presence of graphene filler and functionalisation improves Tg. As the cure cycle used in this project (4hrs at 140 ºC) has been found to be insufficient to show any improvements to Tg properties with the addition of graphene fillers, it is difficult to fully assess the quality of thermomechanical performance. The large improvement to GNP-U Tg at high post-cure temperature shows increased crosslinking within the matrix and additional interfacial crosslinking with GNP-S samples (Bao et al., 2011)(Wang et al., 2012)(Vryonis et al., 2019).

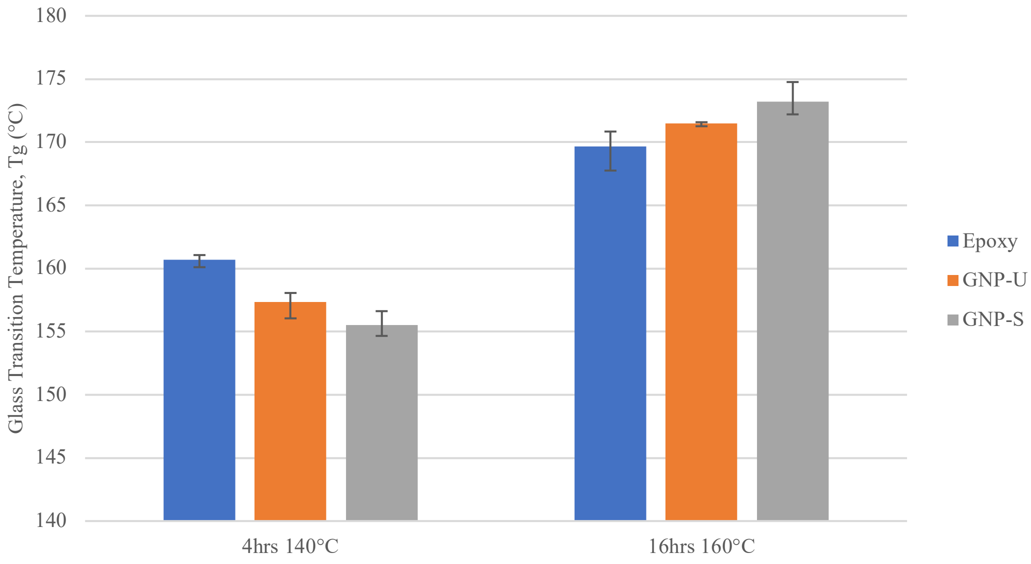

Figure 7.2 : Tg measured for epoxy, GNP-U and GNP-S samples after undergoing the least and most intense curing procedure

The epoxy system used in this investigation is a commercial engineering epoxy resin and has not been specifically manufactured to be used in conjunction with graphene powders. Consequently, the recommended cure cycles do not factor in any effect of fillers on the overall resin properties. This section of work highlights the importance of understanding the effect of both fillers and surface chemistry on the epoxy system cure, in order to effectively tailor overall composite properties.

7.1.2 Filler Geometry

The graphene / epoxy interfacial area increases during de-agglomeration, due to the change in graphene geometry. As the presence of graphene was determined to affect the epoxy structure, the size of the graphene / epoxy interfacial region will influence the degree to which this will occur. Tan delta, storage and loss modulus curves were investigated to understand this relationship.

Epoxy resins exhibit mostly elastic behaviour, due to having a highly crosslinked structure which restricts the physical motion of chains which allows energy to be stored and released upon loading and unloading. The addition of stiff graphene fillers and functionalisation confines chain motion further through physical constraints and interactions between the graphene / epoxy matrix. High levels of dispersion exhibit this behaviour to a high degree as a result of increased interfacial area (Tang et al., 2013), giving increases to both storage modulus and Tg. However, as the addition of highly disperse graphene has been shown to affect the curing process of the epoxy system used, it is difficult to interpret exactly the improvements gained with the addition of graphene fillers. The general trends in tan δ, storage and loss modulus have been examined with relation to dispersion state, flake size and functionalisation.

Firstly, the changes to epoxy with respect to cure cycle have been examined in Figure 7.3. The sample which had undergone longer post-curing time displayed a highly crosslinked structure, visualised through the decreased height and shifted tanδ curve, denoting more elastic behaviour and higher Tg. The loss modulus peak also decreased in height displaying less viscous response upon the onset of transition into the rubbery region, which shows lowered ability to dissipate energy through internal friction (Zhang and Loo, 2009). Additionally, the loss modulus peak height displayed a slight narrowing indicative of a ‘tighter’ structure and lower free volume (Dunson, 2017). The higher storage modulus with longer cure times shows the increased ability to store energy under loading due to higher crosslink density (Surnova et al., 2019).

Table 7.1 presents data collected from selected samples with varied dispersion state and functionalisation for both flake sizes. SM samples have not undertaken any high shear mixing and will be representative of poor dispersion state, whereas 3RM refers to samples produced after 10 passes and represent good dispersion. All samples were post-cured for 4 hours at 140ºC.

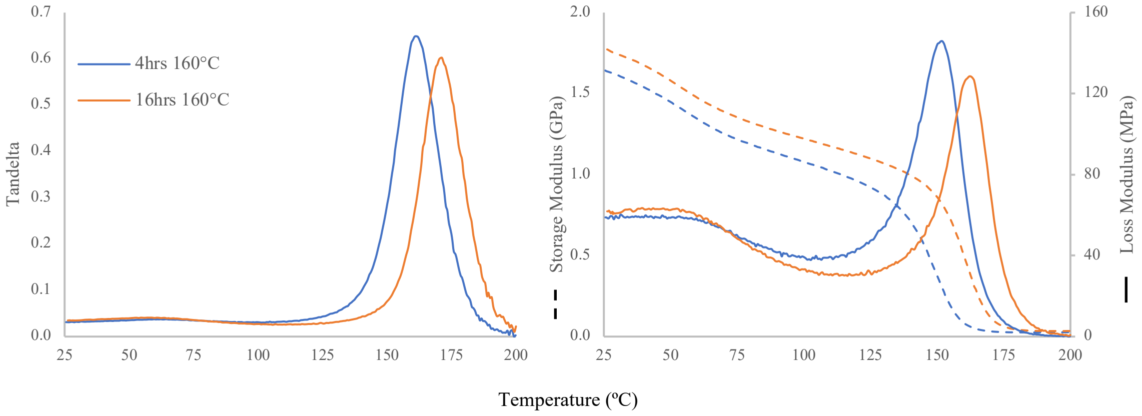

Figure 7.3 : Tan$\boldsymbol{\delta}$, storage and loss modulus curves for epoxy samples after short and long post-cure times

Table 7.1 : Data collated from select DMA measurements illustrated key differences between dispersion state, functionalisation and flake size. Values have been determined as illustrated in figure 3.7.

	Storage Modulus at 40ºC (GPa)	Loss Modulus Peak Height (MPa)	Glass Transition (tanδ peak)
Epoxy	1.60± 0.08	139 ± 2.5	160.7 ± 0.4
GNP-U Unmixed	1.74 ± 0.05	153 ± 2.1	156.1 ± 0.3
GNP-U 3RM	1.85 ± 0.09	157 ± 2.8	157.7 ± 0.8
GNP-S 3RM	1.74 ± 0.06	148 ± 1.6	155.7 ± 0.9
GNP-H 3RM	1.57 ± 0.04	135 ± 3.1	154.1 ± 0.2
FLG-U Unmixed	1.69 ± 0.05	144 ± 1.4	154.8 ± 0.6
FLG-U 3RM	1.77 ± 0.03	142 ± 1.4	158.5 ± 0.1
FLG-S 3RM	1.68 ± 0.04	132 ± 0.5	164.4 ± 0.3
FLG-H 3RM	1.72 ± 0.05	154 ± 2.1	152.0 ± 0.5

Figure 7.4 show tanδ, storage and loss modulus curves for epoxy and GNP-U samples. The presence of GNP-U has been determined to hinder the epoxy cure process over this cure cycle, resulting with low crosslinking and lowered Tg when compared with epoxy, in both dispersion states. Counterintuitively, the storage modulus has not decreased with the disruption to cure and can be explained by the 'crosslinking density effect' (Bao et al., 2011). This is where the effects of low crosslink density are counteracted by restriction to chain motion caused by the physical presence of the graphene sheets, giving both reduced Tg and increased storage modulus. This effect is amplified by the increased interfacial area with high dispersion state and can be visualised by the steep GNP-U 3RM storage modulus gradient upon entering the glass transition region, in addition to the high loss modulus peak showing high dissipation of energy through internal friction (Hossain, Chowdhury and Bolden, 2016). Highly disperse GNP-U can be interpreted as affecting the crosslinking process to a higher degree, but also giving more restriction to chain mobility and therefore improving storage modulus.

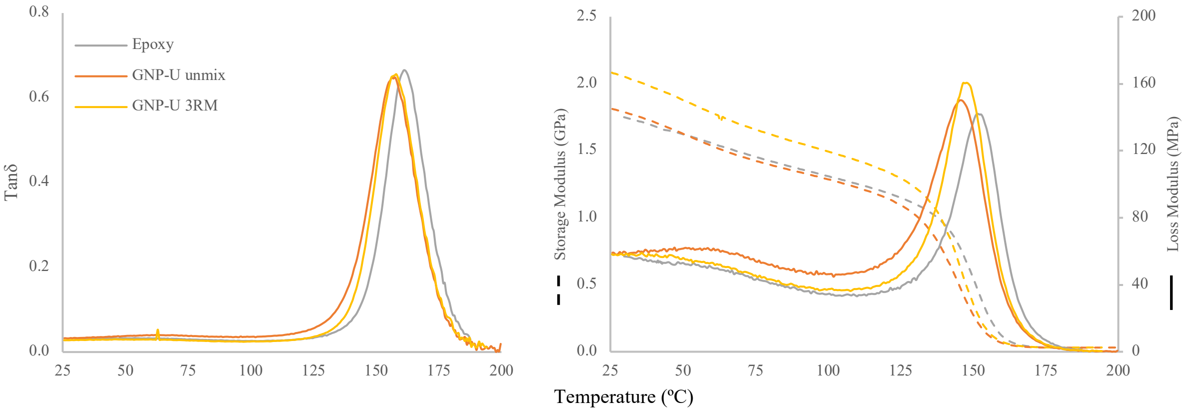

Figure 7.4 : Tan$\boldsymbol{\delta}$, storage and loss modulus curves for epoxy resin, GNP-U unmixed and GNP-U 3RM

Figure 7.5 displays the curves produced for highly disperse, functionalised GNPs. The presence of functionalisation was found to disrupt the resin stoichiometry through interactions between functional groups and epoxy chains forming during post-cure. This results with better properties across the graphene polymer interface, but lowered performance of the epoxy. The Tg decreased with higher intensity functionalisation as a result of lower crosslink density (Surnova et al., 2019), suggesting that GNP-H has formed the highest degree of interactions with the epoxy resin. This can be explained by the high interaction rates of carboxyl and epoxy resin causing a high degree of disruption to resin stoichiometry and overall retardation of epoxy cure (Melro, Pyrz and Jensen, 2016)(Doszlop, Vargha and Horkay, 1978)(Abdalla et al., 2008). This can also explain the decrease to storage modulus and highlight the need for longer cure times. The gradual decrease to loss modulus peak height with functionalisation intensity illustrates increased reduction to dissipative behaviour due to the formation of interfacial bonds.

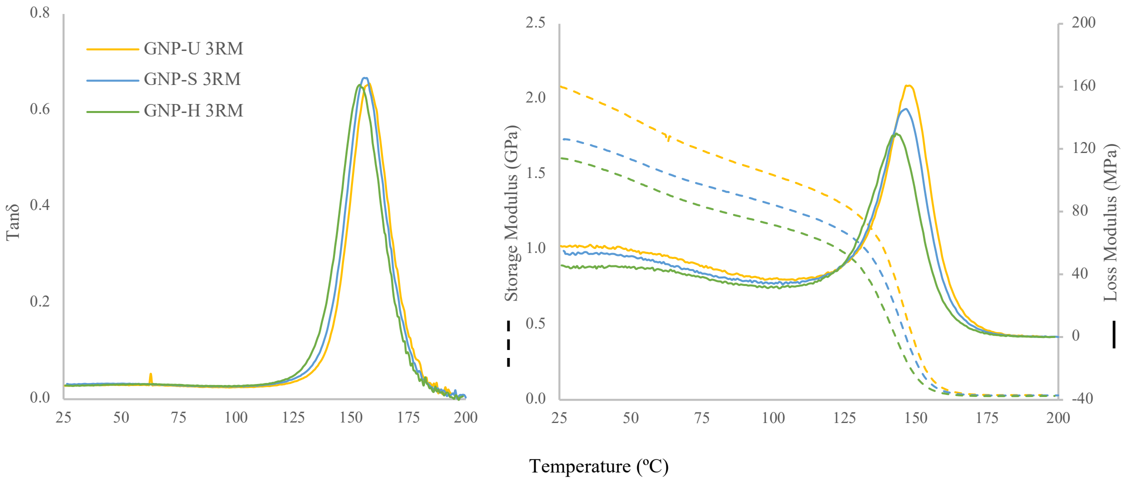

Figure 7.5 : Tan$\boldsymbol{\delta}$, storage and loss modulus curves for each 3RM GNP

Figure 7.6 displays the relationship between epoxy resin and FLG-U in good and poor dispersion state. The Tg has decreased with the addition of FLGs, with SM samples decreasing values to a larger degree suggesting better dispersion state has given less disruption to crosslinking. This is due to the small de-agglomerated FLG particles having less effect on the polymer cure process. FLGs have a planar size comparable to length of epoxy chains (Huang et al., 2017) which leave the effect of physical confinements to chain mobility much smaller than that of GNPs. Agglomerated FLGs have particles measuring over the micro-scale and therefore provide greater barriers to the cure process. There is a small increase to average values of storage modulus and loss modulus peak height with the addition of the FLGs, however when considering the large and overlapping standard deviation of values it can be concluded the effect to viscoelastic behaviour is not significantly affected by the addition of FLG-U.

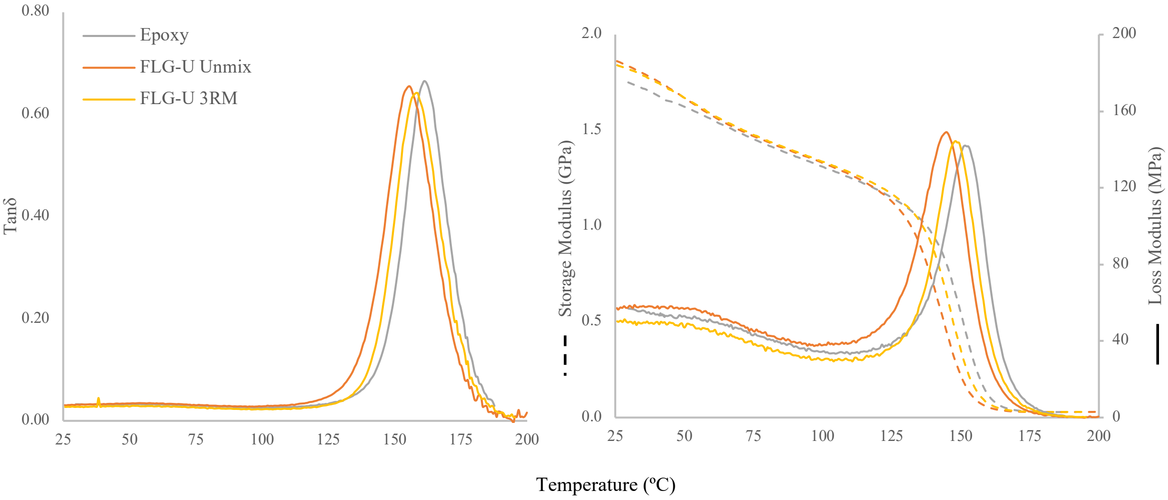

Figure 7.6 : Tan$\boldsymbol{\delta}$, storage and loss modulus curves for epoxy resin, FLG-U unmixed and FLG-U 3RM

Figure 7.7 displays curves for each FLG with good dispersion state. Firstly, the storage modulus was not significantly changed across any case illustrating no effect of reinforcement with the addition of FLGs, due to their low planar size. FLG-H has resulted with the lowest Tg, whilst FLG-S has given a significant increase over that of the epoxy resin. The effect of chain confinement is low as good levels of de-agglomeration have been produced leaving the changes in Tg the result of the varied FLG surface functionality. The oxygen at.% was found to increase with functionalisation content where FLG-U, FLG-S and FLG-H contained 1.6 at.%, 9.5 at.% and 11.9 at.% respectively (table 4.1), illustrating the proportion of functional groups available to interact with the epoxy chains increases with functionalisation intensity. It appears that FLG-S has the optimal properties to allow interfacial bonding whilst causing minimal disruption to the epoxy cure with the curing parameters used (Vryonis et al., 2019). The higher proportion of functional groups present for FLG-H has given a high proportion of interfacial interactions, resulting in retardation of the epoxy cure (Abdalla et al., 2008). This can be visualised through the broad loss modulus peak width and height (Dunson, 2017)

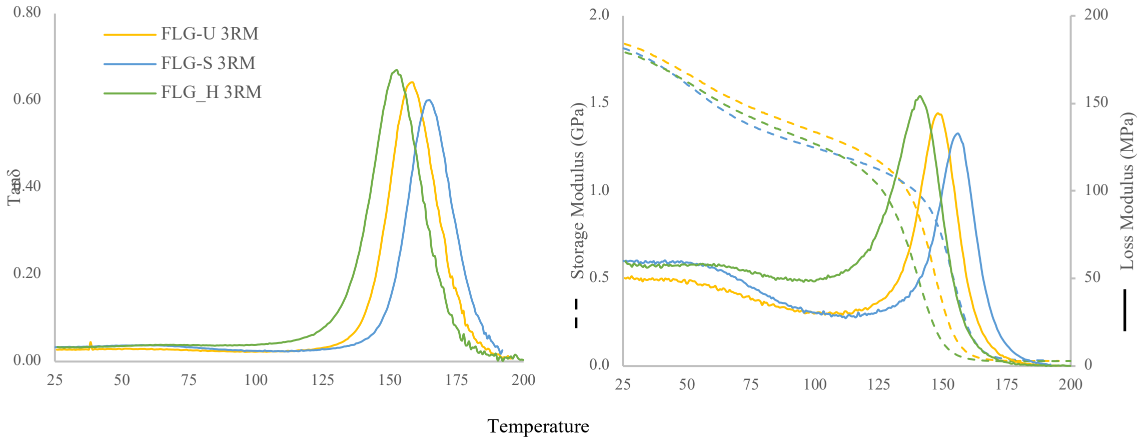

Figure 7.7 : Tan$\boldsymbol{\delta}$, storage and loss modulus curves for each 3RM FLG

Figure 7.8 show the measured Tg values for each mixed sample. Samples mixed through the OHM have given large fluctuations in values with little trend relating to mixing time. This is reflective of the heterogeneity of dispersion state resulting in concentrated areas of all the differing mechanisms discussed within the sample. This implies there will be no batch to batch consistency for Tg measurements, illustrating the importance of good dispersion. These trends are not mirrored in storage modulus values as these measurements are reflective of the bulk sample properties (figures 7.9). GNP-U samples have given higher values of storage modulus after 3RM mixing, indicative of the increased restriction to chain mobility at high levels of dispersion. GNP-H have given lower storage modulus values after 3RM mixing as a result of retardation to polymer cure due to bonding between functional groups and epoxy chains. FLG samples remain give consistent modulus values that are irrespective of dispersion state, with the exception of FLG-U samples mixed through OHM where lower values were seen. Tg values in figure 7.8b show a lowered value for functionalised samples after 15 passes, showing that the FLGs may begin to affect the epoxy cure where high levels of de-agglomeration have been achieved. Lower filler loadings would reduce the interfacial area and mitigate this effect.

These trends illustrate how flake size, functionalisation and dispersion state affect the curing process of epoxy resins, highlighting how all aspects of the manufacturing process influence material properties and the industrial importance of understanding these relationships when defining processing parameters. Although reductions to Tg are not ideal, the lowest measured instance was still high at 151ºC, leaving good scope for use at elevated temperatures. Based on figure 7.2, it is anticipated that improvements to Tg can be achieved with higher temperature of longer curing cycles. The effect of disruption to matrix cure properties on bulk mechanical properties is difficult to predict, with published research declaring both improved and diminished properties (Cook, Mayr and Edward, 1998)(Wu, 1992)(Montazeri et al., 2010). High levels of crosslinking density are particularly detrimental to fracture toughness properties (Atif, Shyha and Inam, 2016), but can improve strength and stiffness at high filler loadings (Vryonis et al., 2019). The effects of these findings with tensile and flexural properties will be further discussed over the next section.

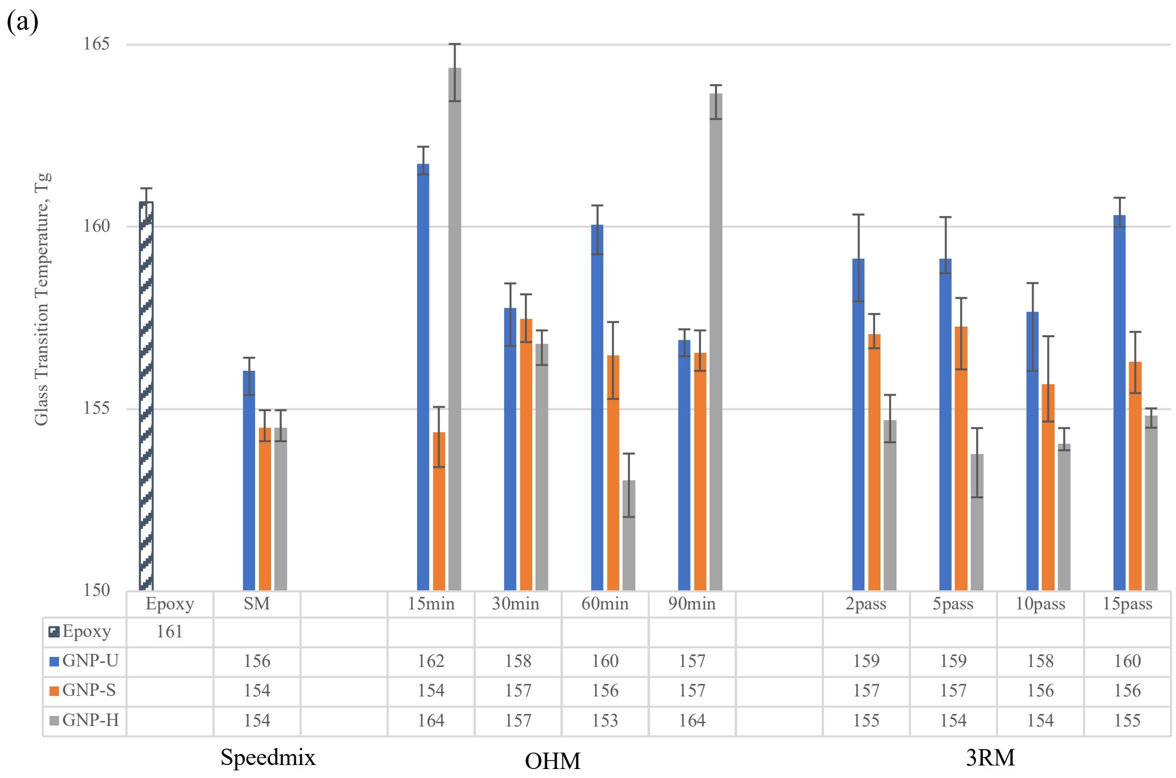

	Epoxy	SM		15min	30min	60min	90min		2pass	5pass	10pass	15pass
▨ Epoxy	161											
🟦 GNP-U		156		162	158	160	157		159	159	158	160
🟧 GNP-S		154		154	157	156	157		157	157	156	156
⬜ GNP-H		154		164	157	153	164		155	154	154	155

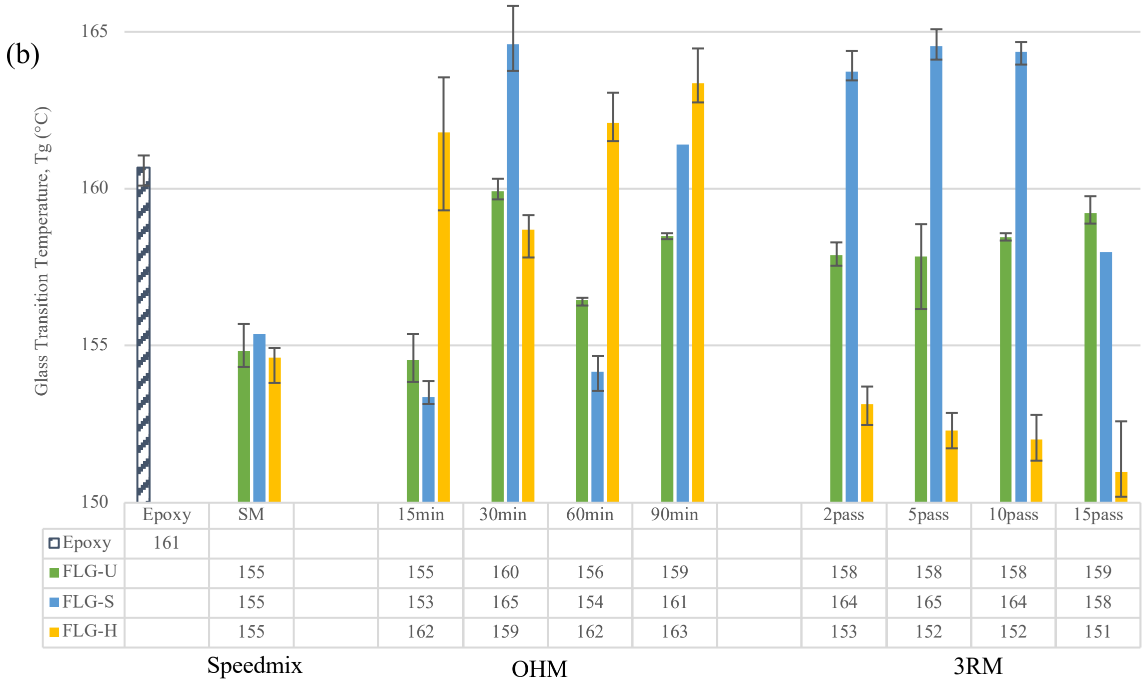

	Epoxy	SM		15min	30min	60min	90min		2pass	5pass	10pass	15pass
☐ Epoxy	161											
🟩 FLG-U		155		155	160	156	159		158	158	158	159
🟦 FLG-S		155		153	165	154	161		164	165	164	158
🟨 FLG-H		155		162	159	162	163		153	152	152	151

Figure 7.8 : Measured Tg values, taken from the tan$\boldsymbol{\delta}$ peak height for (a) GNPs (b) FLGs

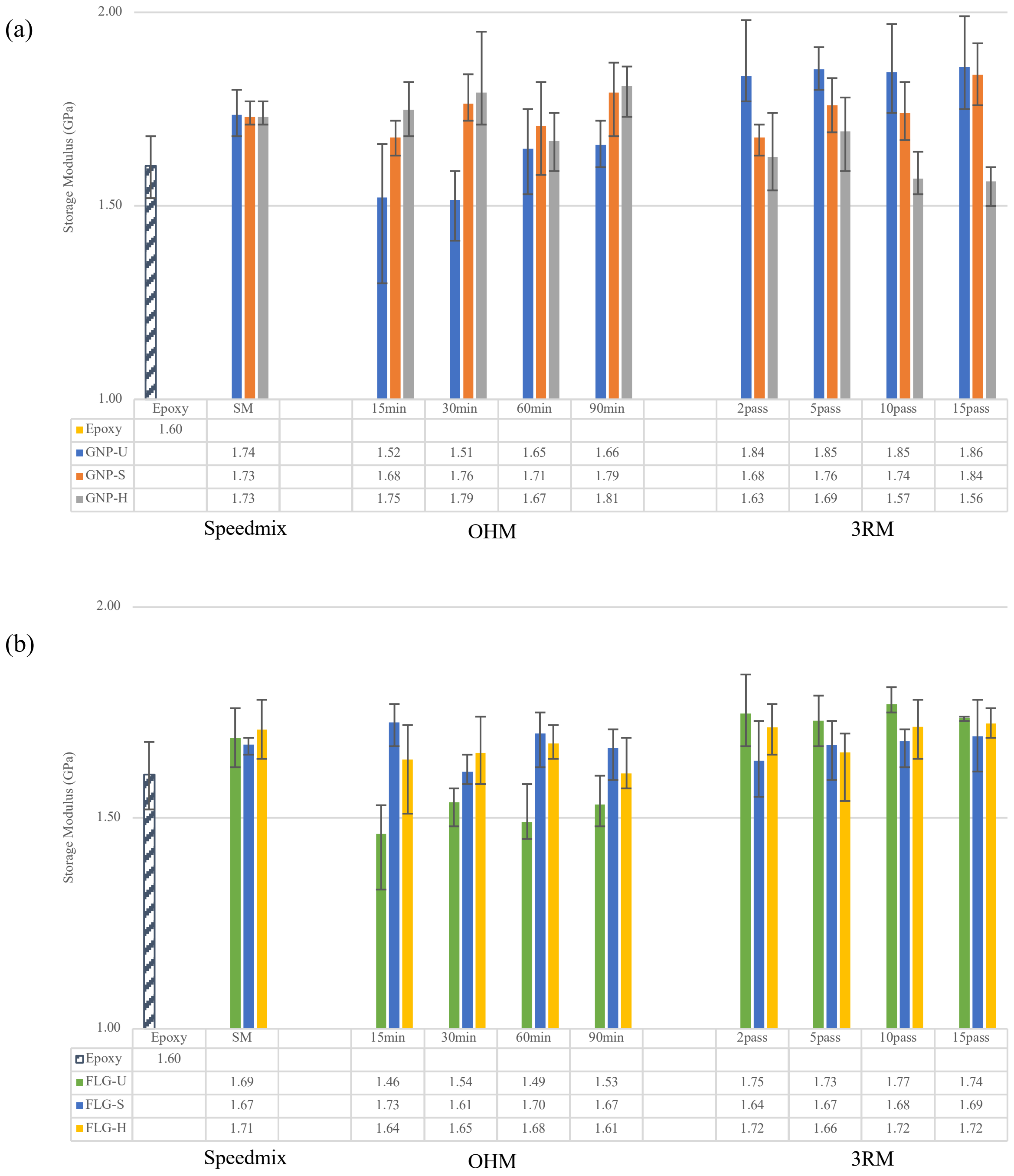

	Epoxy	SM		15min	30min	60min	90min		2pass	5pass	10pass	15pass
Epoxy	1.60											
GNP-U		1.74		1.52	1.51	1.65	1.66		1.84	1.85	1.85	1.86
GNP-S		1.73		1.68	1.76	1.71	1.79		1.68	1.76	1.74	1.84
GNP-H		1.73		1.75	1.79	1.67	1.81		1.63	1.69	1.57	1.56

	Epoxy	SM		15min	30min	60min	90min		2pass	5pass	10pass	15pass
Epoxy	1.60											
FLG-U		1.69		1.46	1.54	1.49	1.53		1.75	1.73	1.77	1.74
FLG-S		1.67		1.73	1.61	1.70	1.67		1.64	1.67	1.68	1.69
FLG-H		1.71		1.64	1.65	1.68	1.61		1.72	1.66	1.72	1.72

Figure 7.9 : Storage modulus values taken from within the glassy state (40ºC) taken from every case of mixing for (a) GNPs (b) FLGs

7.2 Mechanical Testing

Studies into the influence of dispersion state on mechanical properties are detailed in this chapter. This has been performed to fully understand the extent of this relationship, allowing optimisation of mixing method and time. Tensile and flexural tests were performed to find values of stiffness, strength and strain at failure with relation to mixing program, functionalisation and flake size. The exceptional mechanical properties of graphene have not been successfully translated through to composite materials where reinforcement is provided by the graphene alone. The most commercially viable application for these materials is where graphene infused epoxy is used in conjunction with long fibres.

7.2.1 Stiffness

The high stiffness properties of graphene are expected to improve overall modulus values when combined with epoxy resin. The success of providing good reinforcement is closely linked to several factors, including lateral dimension, number of graphene layers and good interfacial interaction. This means that both dispersion state and functionalisation are highly influential on the final composite stiffness. Research performed by (Gong *et al.*, 2010b) used shear-lag theory to characterise stress transfer over a graphene monolayer / polymer interface. It was established that to provide effective reinforcement, graphene sheets must have a critical lateral length of 3µm where graphene and matrix interact fully through Van-der-Waals forces. However, in practical uses it was determined that a planar size 10x larger than this value should be used to provide efficient stress transfer. Both GNPs and FLGs investigated in this work had planar sizes much smaller than this ideal 30µm flake size (5 µm and 200nm, respectively). Large improvements in modulus were not expected to be achieved because of this, but these measurements still illustrate the relationship between dispersion and mechanical performance. The modulus of stacked graphene decreases with increasing layers (Gong et al., 2012) due to poor stress transfer across the weakly bonded graphene sheets. Samples with high levels of de-agglomeration and exfoliation were expected to provide better reinforcement and increase the modulus of the final composite. Functionalised samples were expected to achieve a degree of interaction with the epoxy matrix, improving interfacial stress transfer and further enhancing reinforcement (Chong, Hinder and Taylor, 2016). Higher levels of oxygen content are expected to provide a greater degree of interfacial interactions, leading to improved stress transfer (Vallés et al., 2016). Halpin-Tsai equations have been utilised to explore the role of functionalisation further.

7.2.1.1 Tensile & Flexural Modulus

Tensile and flexural modulus values determined for all GNPs have been presented in figure 7.10. It is important to note that flexural data is generally higher than tensile, but trends between samples are similar. This is due to the variation of stain across samples tested through bending, where half of the material volume is loaded in tension and the other in compression, leaving maximum strains experienced at the top and bottom of the sample and zero strain over the mid-plane. Flexural modulus calculations are based on the surface conditions, where the strain is larger than the rest of the sample. As the rest of the sample is at a lower strain, where the modulus is resultantly lower, the calculated values for flexural modulus appear to the larger than they are (Leguillon, Martin and Lafarie-Frenot, 2015)(Manta, Gresil and Soutis, 2019).

Due to the small variations in modulus values and wide error bars, t-tests have been used to assess whether these changes are statistically significantly different. This has been deemed to be the case if the calculated p-value is lower than the alpha value of 0.05, indicating dispersion state has influenced the modulus value. In this case, the p-value is the calculated probability that the two compared data sets are similar. T-tests have been performed separately for tensile and flexural modulus values and statistical significance has only been confirmed in cases where both p-values are < 0.05 (Saberian et al., 2019). Table 7.2 shows p-values determined for selected data sets. Due to rupture being a mechanism of de-agglomeration for all GNPs, the first comparison made is between the unmixed sample and shortest length of mixing time for each method. Another comparison is made over the shortest and longest mixing time for each method, to assess the degree of improvement with mixing time, and finally, the samples produced after the highest degree of mixing from each method.

The addition of GNPs prior to high-shear mixing have not given any improvement in modulus compared with the epoxy resin. This shows highly agglomerated graphene does not provide any reinforcement in the system used. GNP-U samples have not shown any obvious change to modulus over the duration of OHM mixing. As t-tests are in agreement with this observation, it can be concluded that there has been no improvement to modulus values through mixing with OHM. Both measurements for GNP-U modulus gradually increased with 3RM passes, where greater values were measured for flexural modulus. Modulus values taken after 15passes through the 3RM, were larger than after 90 minutes of OHM mixing, which correlates with the improved dispersion state produced through 3RM and demonstrates better reinforcement with better dispersion state (Tang et al., 2013) (dal Lago et al., 2020).

	Epoxy	SM		15min	30min	60min	90min		2pass	5pass	10pass	15pass
🟩 Tensile Modulus	2656	2655		2697	2724	2701	2705		2878	2806	2985	2944
🟧 Flexural modulus	2864	2840		2780	2811	2753	2898		2844	3096	3134	3172

	Epoxy	SM		15min	30min	60min	90min		2pass	5pass	10pass	15pass
🟩 Tensile Modulus	2656	2651		2536	2646	2420	2473		2949	2994	2985	2959
🟧 Flexural modulus	2864	2615		2945	2811	2740	2874		2892	2946	2945	3024

	Epoxy	SM		15min	30min	60min	90min		2pass	5pass	10pass	15pass
🟩 Tensile Modulus	2656	2694		2770	2827	3104	2567		2993	3138	2993	3028
🟧 Flexural modulus	2864	2837		2645	2820	2846	2733		3176	3252	3139	3123

Figure 7.10 : Tensile and Flexural modulus measurements, in each case of mixing for (a) GNP-U (b) GNP-S (c) GNP-H

The GNP-S flexural modulus increased immediately after mixing through both high-shear methods and remained at similar values with further mixing. Tensile modulus followed the same trend with 3RM mixing only. The modulus produced after 15 passes was not found to be statistically different to that produced after 90 minutes, demonstrating dispersion state produced through both methods improved the modulus value by a similar degree. GNP-H tensile modulus increased with OHM mixing time, reaching a peak after 60 minutes before falling again after 90 minutes. GNP-H was determined to de-agglomerate gradually and unevenly over the course of mixing, as t-tests have indicated no significant change to modulus it was concluded that de-agglomeration was insufficient. Both sets of modulus values rise after 3RM and do not significantly change over the duration of mixing, which corresponds with t-test analysis. GNP-H samples have produced higher modulus values after mixing by 3RM compared with OHM.

Table 7.2 : Calculated p-values for t-test analysis of GNP mixed samples. Data sets considered to be statistically significantly different have been denoted in bold

	GNP-U		GNP-S		GNP-H	
	Tensile Modulus	Flexural Modulus	Tensile Modulus	Flexural Modulus	Tensile Modulus	Flexural Modulus
Unmix & 15 min	0.77	0.01	0.06	2.1e^{-4}	0.20	8.23e^{-3}
15min & 90min	0.83	0.06	0.06	0.31	0.09	0.18
Unmix & 2pass	0.16	0.88	**8.89e^{-3}**	**4.9e^{-4}**	**3.48e^{-4}**	**8.24e^{-7}**
2pass & 15pass	0.11	1.42e^{-5}	0.37	0.06	0.55	0.09
90min & 15pass	**4.67e^{-4}**	**3.5e^{-5}**	5.37e^{-10}	0.05	**8.65e^{-4}**	**3.45e^{-4}**

Figure 7.11 shows the modulus values of all FLG samples do not appear to significantly change under any mixing condition, except for a large increase in FLG-S samples after 90 minutes of mixing by OHM. T-tests agree that the change is significant compared with samples tested after 15 minutes (table 7.3), however in context with the rest of the values measured for FLG-S samples, this increase seems anomalous. Additionally, analysis in chapter 6 demonstrated a better dispersion state was achieved through 3RM which would be expected to improve modulus to a higher degree. Generally, this shows dispersion state has little influence on the ability of FLGs to increase modulus due to the small planar size. Dispersion analysis displayed very large agglomerates in every case of mixing, leaving weakly bound particulates with low modulus present in each sample (Tian et al.,

2016). Additionally, the surface functionalisation did not aid stress transfer to any significant amount.

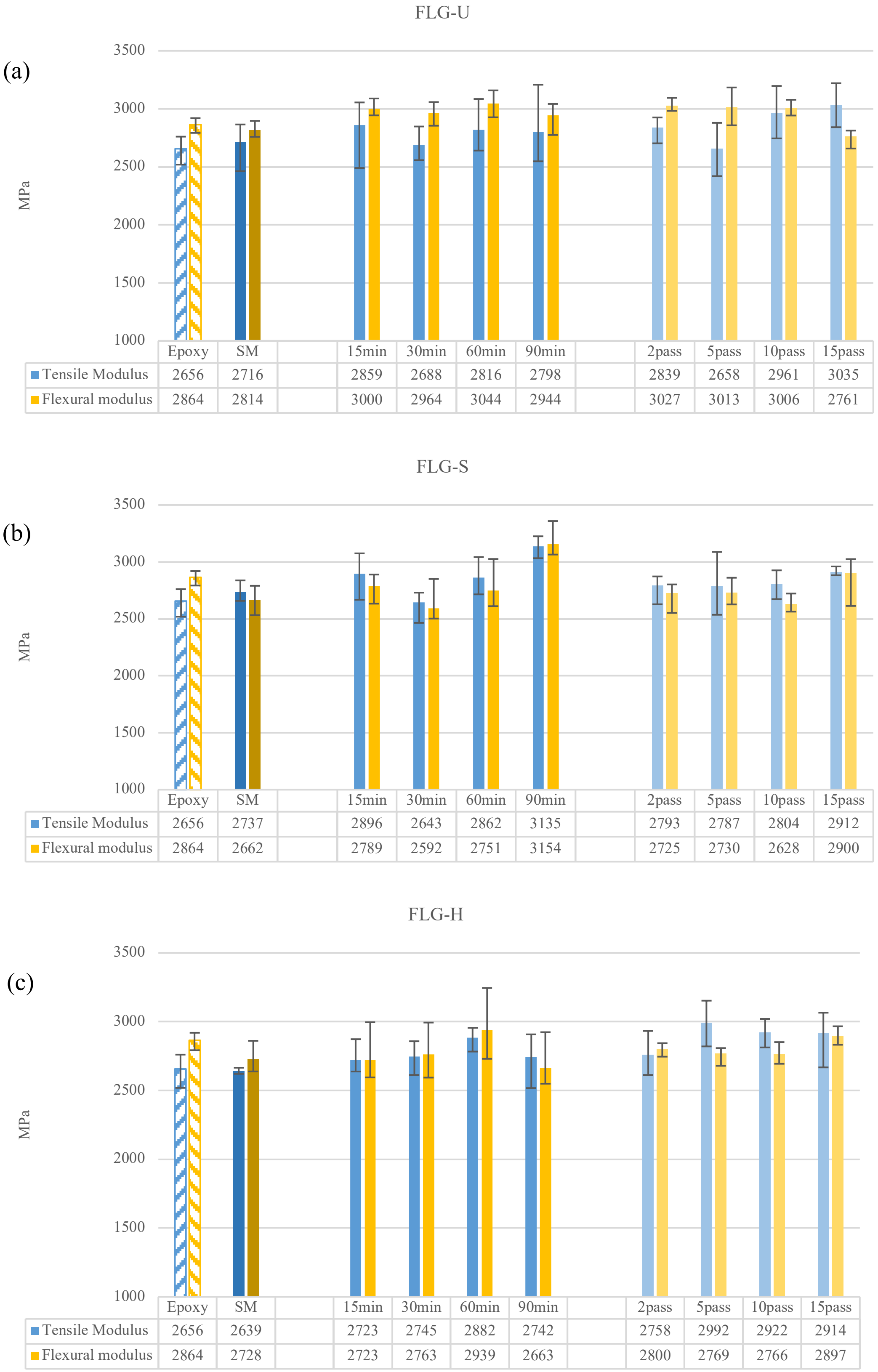

Figure 7.11 : Tensile and Flexural modulus measurements, in each case of mixing for (a) FLG-U (b) FLG-S (c) FLG-H

Table 7.3 : Calculated p-values for t-test analysis of FLG mixed samples. Data sets considered to be statistically significantly different have been denoted in bold

	FLG-U		FLG-S		FLG-H	
	Tensile Modulus	Flexural Modulus	Tensile Modulus	Flexural Modulus	Tensile Modulus	Flexural Modulus
Unmix & 15 min	0.15	$8.46e^{-7}$	**0.01**	**0.02**	0.44	0.89
15min & 90min	0.63	0.10	**$4.62e^{-4}$**	**$1.08e^{-5}$**	0.44	0.22
Unmix & 2pass	0.16	$6.64e^{-10}$	0.55	0.09	0.05	0.01
2pass & 15pass	**$7.69e^{-4}$**	**$2.72e^{-11}$**	0.88	$5.09e^{-3}$	0.29	$1.44e^{-4}$
90min & 15pass	**0.02**	**$4.22e^{-5}$**	0.09	$3.58e^{-4}$	0.27	$1.85e^{-5}$

These results reiterate the need for large planar sizes to effectively increase modulus values, both graphene powders used in this study were too small to significantly change modulus values. This data set however, does illustrate that better dispersion state correlates to improvements in modulus based on larger values found for 3RM samples. The largest changes to measurements were observed upon the onset of mixing and minimal change was found with longer mixing times. This corresponds to the trends of fast acting rupture observed for the majority of samples. GNP-U and GNP-H samples showed higher modulus values after mixing by 3RM, where dispersion state was found to be superior (chapter 6).

7.2.1.2 Halpin-Tsai Equations

The Halpin-Tsai model has been adjusted for randomly orientated, platelet shaped fillers and used to calculate theoretical elastic modulus values of each composite (equations 7-10) (Yang et al., 2013). These values provide the theoretical composite elastic modulus values, where fully de-agglomerated and dispersed graphene stacks are fully bonded over the graphene / epoxy interface. Select measured values have been compared against the ideal theoretical value to assess the quality of the composites produced in this study. It is unlikely that measured modulus values will reach the levels of calculated values as the graphene used is known to have defects, full interfacial bonding is unlikely to be achieved and complete de-agglomeration has not been confirmed in any case of mixing.

$$E_C = E_m\left(\frac{3}{8}.\frac{1+\eta_L\zeta V_f}{1-\eta_L V_f}+\frac{5}{8}.\frac{1+2\eta_T V_f}{1-\eta_T V_f}\right) \quad (7)$$

$$\eta_L = \frac{\frac{E_f}{E_m}-1}{\frac{E_f}{E_m}+\zeta} \quad (8)$$

$$\eta_T = \frac{\frac{E_f}{E_m}-1}{\frac{E_f}{E_m}+2} \quad (9)$$

$$\zeta = \frac{2a_f}{3} \quad (10)$$

where, E_C, E_m and E_f are the elastic modulus of the composite, matrix and graphene respectively, V_f is volume fraction of graphene and a_f is graphene aspect ratio. The measured value of tensile modulus was used for Em (2500MPa) and equation 11 was used to calculate Ef values (Gong et al., 2012).

$$E_f = \frac{E_g}{\left[\frac{N}{2}-k_i\left(\frac{N}{2}-1\right)\right]} \quad (11)$$

where Eg is the in-plane Young's modulus of graphene (1050GPa), ki is the efficiency of stress transfer (taken as 0.6) and N is the number of graphene layers. Due to the decrease of Young's modulus with increasing layers, values have been calculated based on the range of quoted geometry of graphene given by the supplier. Calculated values are as shown in table 7.4

As GNPs generally produced higher modulus values after 3RM and showed no corelation to mixing time, the average value 3RM modulus values for each sample have been taken and compared against the calculated theoretical modulus. All measurements taken for each FLG was used as there was no significant influence of high-shear mixing on modulus value. The percentage of the theoretical modulus attained for each graphene composite is presented in figure 7.12

Table 7.4 : Parameters used in Halpin-Tsai equations and calculated theoretical modulus

	Layers	Aspect ratio, a_f	Graphene modulus, E_f (GPa)	Theoretical composite modulus, E_c (MPa)
GNP	15 - 25	995 - 597	188 - 292	3723 - 4386
FLG	1 - 4	597 - 149	560 - 750	3784 - 6549

Percentages determined for GNPs increased with higher intensity functionalisation. The levels of dispersion were determined to be good for all GNPs mixed by 3RM, but slightly better for GNP-S where exfoliation of graphene sheets was achieved. The improvements in modulus for functionalised GNPs are the result of a combination of good dispersion state and interfacial interactions (Domun et al., 2017)(Williams et al., 2013). DMA analysis found that interfacial interactions were present for both functionalised GNPs, but the epoxy crosslinking density reduced with higher intensity fuctionalisation. The increased modulus found for GNP-H can be explained by the high proprtion of carbonyl and carboxyl functional groups which form stronger interactions with epoxy than hydroxyl groups (Melro, Pyrz and Jensen, 2016), leaving GNP-H to have a higher interfacial shear strength than GNP-S and therefore improve modulus values to a larger degree (Young et al., 2012). There is no significant improvement to FLG percentages with functionalisation, showing no change to modulus values despite finding evidence of interfacial interaction with functionalised FLGs. The variation in theoretical composite modulus is very wide, due to the rapid decrease in modulus properties between monolayer, bilayer and trilayer graphene (Gong et al., 2012), which the FLG powder is comprised of. Additionally, the small planar size is unlikely to facilitate any significant improvement to modulus making it difficult to assess interfacial properties using this method.

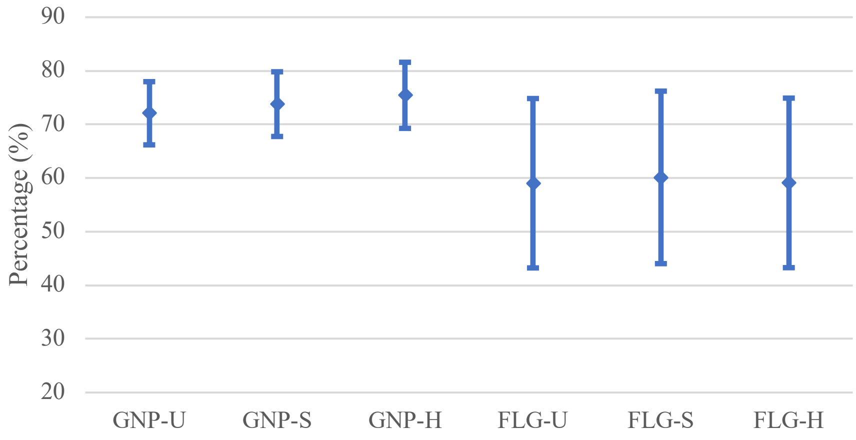

Figure 7.12 : Percentage of calculated theoretical composite modulus attained by measured samples

7.2.2 Strength

The inclusion of graphene into polymer materials can improve strength (Young et al., 2012) and is an effective way of increasing composite strength whilst maintaining low weight. Premature failure of graphene based composites is largely the result of agglomeration and poor interfacial properties, leaving the graphene to behave as stress concentrators rather than reinforcement (Yi and Shen, 2015a). It was expected that samples with good dispersion and interfacial properties will provide increased overall strength (Rafiee et al., 2010).

Figure 7.13 displays measured tensile and flexural strength for all GNPs, where the trends in relation to functionalisation, mixing method and time are consistent over the two measurements. The epoxy resin however was found to be much smaller in tensile strength than flexural strength, in relation to the filled samples. When comparing measured data to the data sheet, the measured flexural strength is much closer to the quoted value (120-124MPa), than measured tensile strength (71-77MPa), leaving comparisons against epoxy resin to be made based on flexural data only.

The addition of each unmixed GNP has lowered the overall strength due to the high levels of agglomeration. Large agglomerates have poor internal strength due to the weak bonds which hold them together (Chandrasekaran et al., 2014), additionally, the polymer chains cannot penetrate the agglomerate structure leading to low levels of reinforcement (Yang et al., 2011). Both tensile and flexural measurements displayed increased strength after high-shear mixing, where highest values were produced after 3RM mixing. This illustrates that strength improves with higher quality dispersion state. Strength measurements for all GNPs mixed through OHM do not improve with mixing time, showing that the changes to dispersion state over this time were inadequate to increase the strength. As shear stresses are not evenly distributed through the material batch when mixing by OHM, there is a higher proportion of large agglomerates present in the bulk sample leading little change with mixing time.

Mixing through 3RM has shown strength values to increase with increased mixing reflecting continuous improvement to dispersion state. This was trend however was not observed for 3RM GNP-S samples tested under tension. GNP-S samples appear to consistently show the lowest strength values, which could be the result of a few factors. Firstly, as the dispersion state and interfacial interactions were determined to be good, this could be the result of decreased cross-linking density of the epoxy resin (Yu et al., 2016). Although, GNP-H were additionally found to have decreased crosslinking density, the interfacial shear strength is stronger as a result of higher levels of interactions between the epoxy chains and carboxyl and carbonyl functional groups (Melro, Pyrz and Jensen, 2016)(Abdalla et al., 2008), which comparatively will improve overall material strength. Secondly, GNP-S samples mixed by 3RM have given a wide range in tensile strength, with average values slowly decreasing with higher levels of mixing. These GNP-S sheets experienced exfoliation after 3RM giving high interfacial area, which would further exacerbate the detrimental effect of poor interfacial properties or impediment to cure (Watson et al., 2017). However, the same trend is not mirrored in the flexural strength measurements, this could be an effect of the increased values and low variation produced through flexural testing. Only half of the sample tested under flexure experiences a bending stress, whereas samples which are tested in tension have stress acting across the whole volume, giving more area for stress concentrators to exist, resulting in failure at lower stresses. GNP-H has marginally higher values than GNP-U in most cases, but the improvement is not considered to be significantly larger.

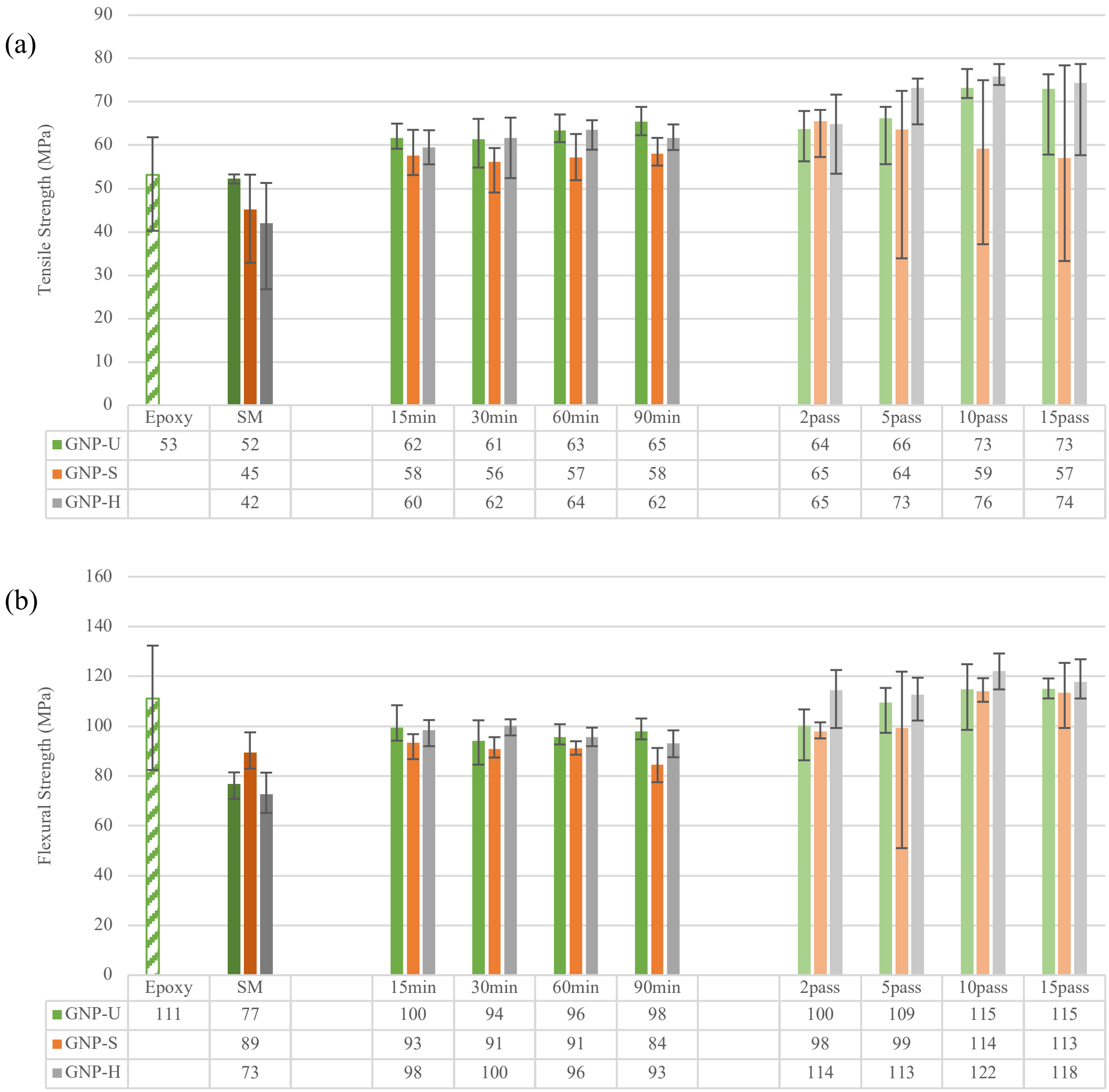

Figure 7.13 : Strength measurements taken for each GNP (a) Tensile strength (b) Flexural strength

These data sets show that mixing method has a visible effect on GNP / epoxy strength, where 3RM mixing gave highest strength values due to better levels of dispersion state. The number of passes appeared to improve the strength, illustrating the relationship between dispersion and strength.

The addition of highly agglomerated FLGs has resulted in a reduction of tensile and flexural strength compared with epoxy resin (figure 7.14). The unmixed FLGs have given similar tensile strength and slightly higher flexural strength values compared with GNPs. This is likely due to a combination of the difference in stress distributions between the two testing methods and FLGs being smaller and therefore having lower stress raising behaviour (Manta, Gresil and Soutis, 2019)(Wang, Jin and Song, 2013). Additionally, FLGs were found to have less disruption to epoxy curing when good dispersion was achieved.

Both high-shear mixing methods have improved strength to similar values. Flexural strength data shows the majority of tested samples have larger strength than the epoxy resin, based on average values. The main difference between the mixing methods is the variation in strength across the mixing time, where mixing through 3RM gave lower variability than OHM. This is reflective of the difference in homogeneity of application of high-shear stress through each method. Although the difference in strength between the two mixing methods is not massive, the 3RM has the added benefit of predictability in strength values. FLG-H samples show slightly higher tensile strength values, which could indicate improved interfacial properties, but the trend is not clearly seen in flexural strength and therefore becomes difficult to conclude this behaviour.

FLGs have increased overall strength values to a larger degree, showing smaller particles improve strength to a greater degree (He et al., 2019). The fundamental problem found with FLGs was that they were very difficult to de-agglomerate through the methods used in this study, as agglomerates measuring at the highest end of the investigated scale were found in every instance of mixing. This suggests that if better dispersion was achieved for FLGs, the strength could potentially be even higher. The small planar size and improvement to epoxy strength seen with the addition FLGs is very attractive when considering their use with addition to long fibres, as the small planar size allows easier infiltration between fibres, providing a homogeneous effect of improved strength.

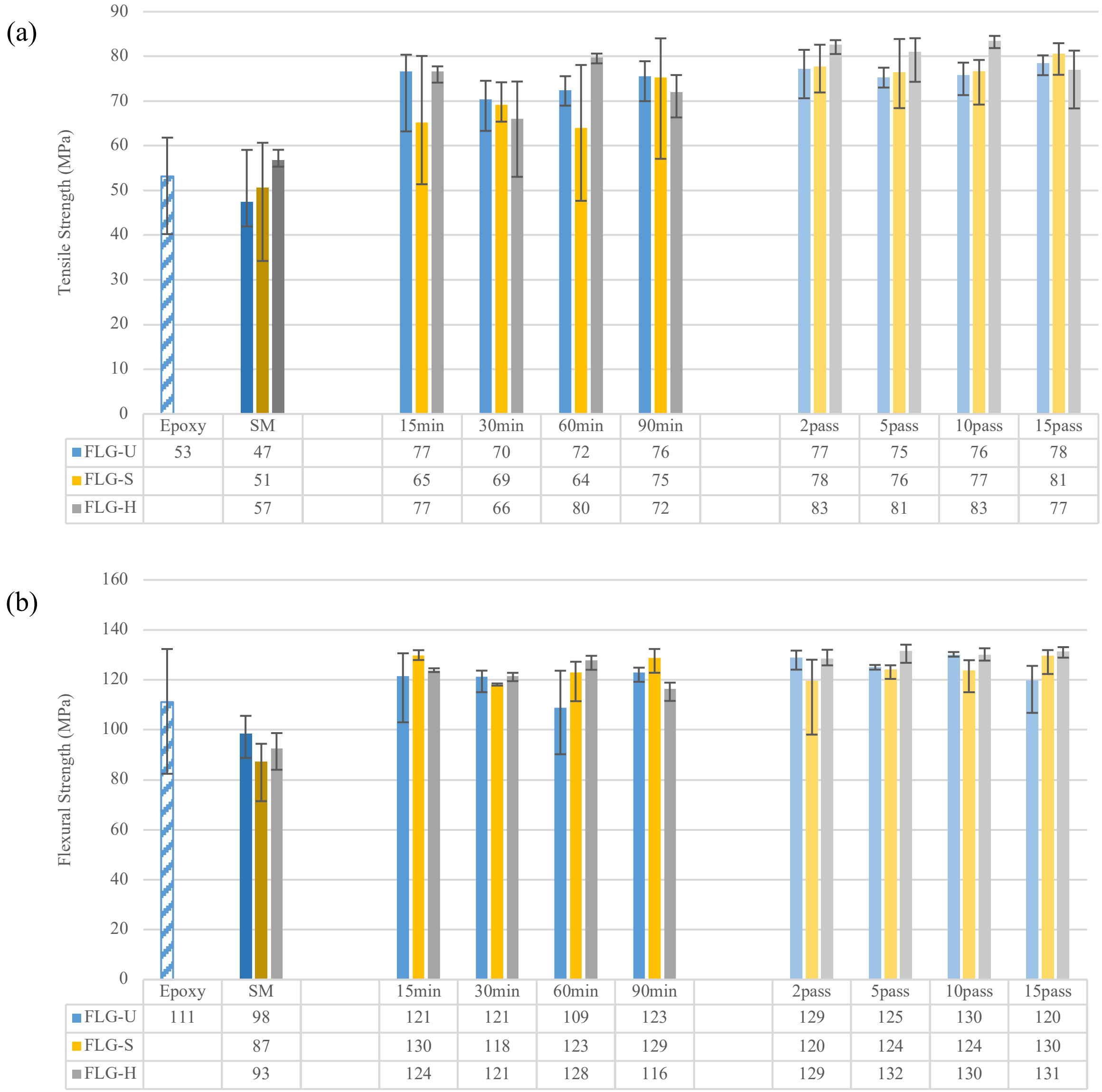

(a)

	Epoxy	SM		15min	30min	60min	90min		2pass	5pass	10pass	15pass
■ FLG-U	53	47		77	70	72	76		77	75	76	78
■ FLG-S		51		65	69	64	75		78	76	77	81
■ FLG-H		57		77	66	80	72		83	81	83	77

(b)

	Epoxy	SM		15min	30min	60min	90min		2pass	5pass	10pass	15pass
■ FLG-U	111	98		121	121	109	123		129	125	130	120
■ FLG-S		87		130	118	123	129		120	124	124	130
■ FLG-H		93		124	121	128	116		129	132	130	131

Figure 7.14 : Strength measurements taken for each FLG (a) Tensile strength (b) Flexural strength

7.2.3 Strain at break

The strain at break has been analysed to show how the addition of fillers, functionalisation and dispersion state affects the ductility of the final composite. Increased strain at break is a sign of improved ability to plastically deform, increasing ductile behaviour. This is associated with good dispersion and interfacial properties between graphene / epoxy matrix, resulting from the reduced effect of filler stress concentration (Akhina et al., 2018)(Joy et al., 2020).

Figures 7.15 and 7.16 display the strain at break determined from tensile and flexural measurements, where the trends are generally similar to those seen in strength values. The addition of unmixed graphene has resulted in lower values than epoxy due to the high levels of agglomerates. Highest values have been obtained in samples mixed through 3RM, where the dispersion state was better. FLGs have given larger strain at break values than GNPs after high-shear mixing, this could be due to their smaller size and therefore lowered tendency to behave as a stress concentrators. Additionally, lower levels of disruption to the epoxy structure were found with FLG-U and FLG-S samples when highly disperse as well as the presence of interfacial interaction with functionalisation. The error bars are considerably wide for FLGs which could be reflective of the wide range of agglomerates found in these samples.

In some cases the strain at break appears to increase with longer mixing times, this is more visible with the 3RM mixed samples showing the strain at break is receptive to small changes in dispersion state. This is due to failure being initiated by the weakest point within the material and therefore highly influenced agglomerate size and dispersion, explaining why the inhomogeneous de-agglomeration produced through OHM does not alter the values much over the mixing time. The FLG-H mixed samples have consistently shown high values for all samples post high-shear mixing, this illustrates again that the interfacial properties are good.

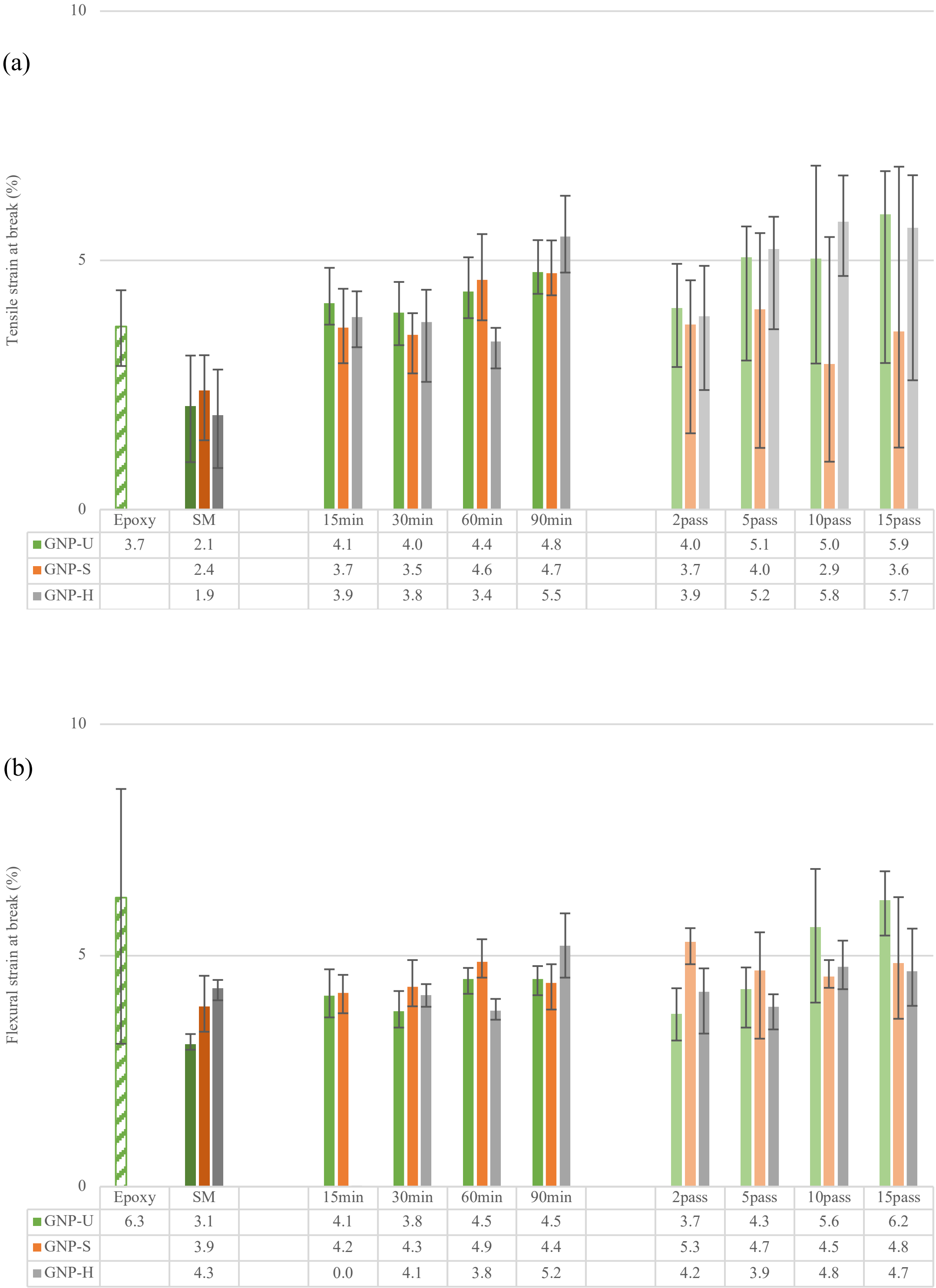

	Epoxy	SM		15min	30min	60min	90min		2pass	5pass	10pass	15pass
🟩 GNP-U	3.7	2.1		4.1	4.0	4.4	4.8		4.0	5.1	5.0	5.9
🟧 GNP-S		2.4		3.7	3.5	4.6	4.7		3.7	4.0	2.9	3.6
■ GNP-H		1.9		3.9	3.8	3.4	5.5		3.9	5.2	5.8	5.7

	Epoxy	SM		15min	30min	60min	90min		2pass	5pass	10pass	15pass
🟩 GNP-U	6.3	3.1		4.1	3.8	4.5	4.5		3.7	4.3	5.6	6.2
🟧 GNP-S		3.9		4.2	4.3	4.9	4.4		5.3	4.7	4.5	4.8
■ GNP-H		4.3		0.0	4.1	3.8	5.2		4.2	3.9	4.8	4.7

Figure 7.15 : Strain at break measurements taken for each GNP (a) tensile strain at break (b) flexural strain at break

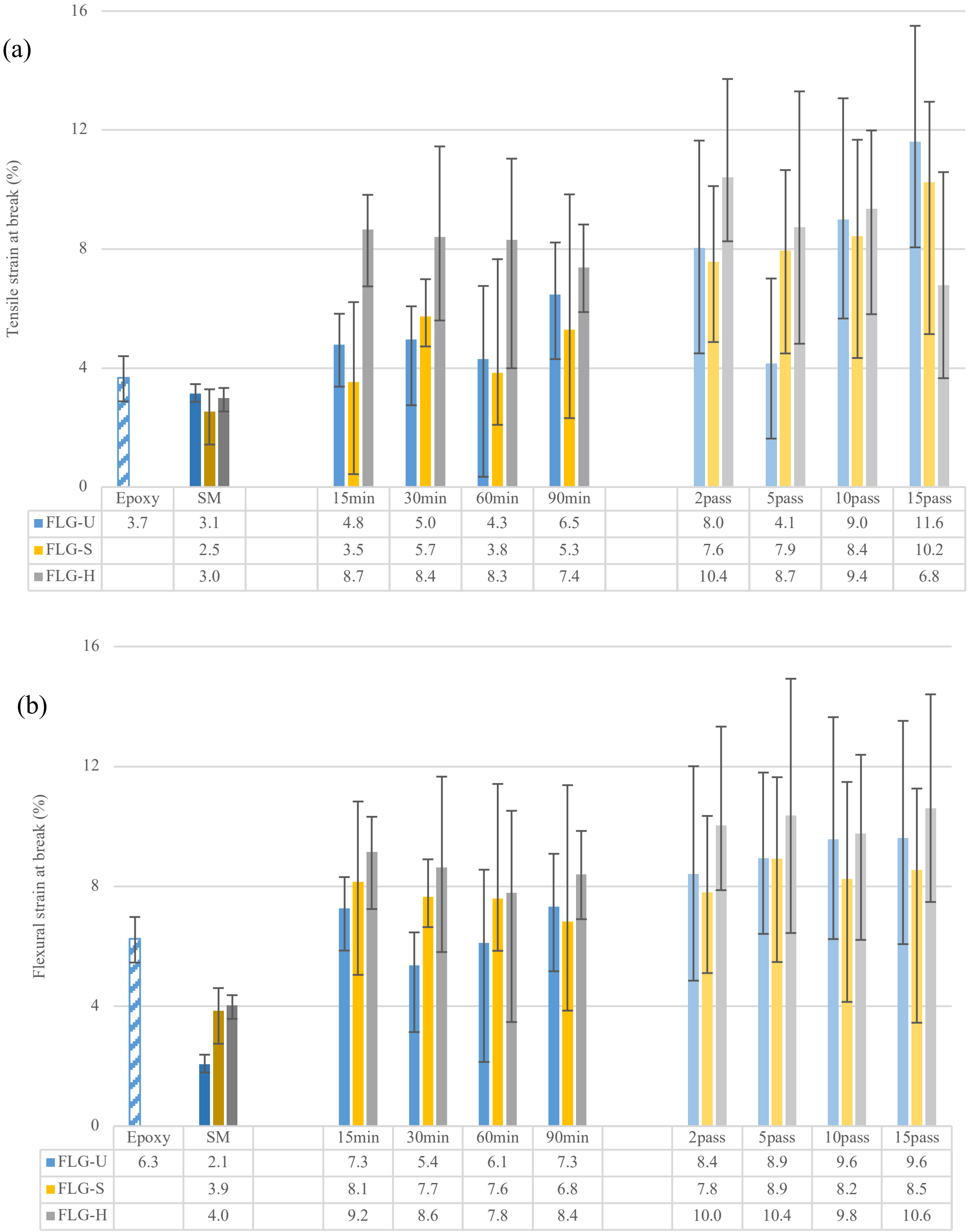

(a)

	Epoxy	SM		15min	30min	60min	90min		2pass	5pass	10pass	15pass
■ FLG-U	3.7	3.1		4.8	5.0	4.3	6.5		8.0	4.1	9.0	11.6
■ FLG-S		2.5		3.5	5.7	3.8	5.3		7.6	7.9	8.4	10.2
■ FLG-H		3.0		8.7	8.4	8.3	7.4		10.4	8.7	9.4	6.8

(b)

	Epoxy	SM		15min	30min	60min	90min		2pass	5pass	10pass	15pass
■ FLG-U	6.3	2.1		7.3	5.4	6.1	7.3		8.4	8.9	9.6	9.6
■ FLG-S		3.9		8.1	7.7	7.6	6.8		7.8	8.9	8.2	8.5
■ FLG-H		4.0		9.2	8.6	7.8	8.4		10.0	10.4	9.8	10.6

Figure 7.16 : Strain at break measurements taken for each GNP (a) tensile strain at break (b) flexural strain at break

7.3 Summary

The produced data has highlighted the correlation between dispersion state and mechanical properties, where every high-shear mixing example gave an improvement upon the SM state. This emphasises the importance of good dispersion as well as incorporating high-shear mixing methods to optimise graphene mechanical performance (Tang et al., 2013). The main difference observed between mixing through OHM and 3RM, was the variability in results with relation to mixing time. Generally, samples mixed through 3RM gave consistent values or showed a general trend with relation to mixing time, whereas OHM gave more fluctuation with relation to mixing time. This correlates to the study performed by (Pullicino et al., 2017), where the same OHM equipment was used to disperse GNPs into epoxy resin for varied mixing times and compared with mechanical properties. Pullicino et al displayed there was no strong relationship, showing that OHM cannot reliably produce repeatable results under a given mixing profile, which is highly undesirable from a manufacturing perspective.

The highest values for GNP samples were measured after mixing through 3RM. There was a clear correlation between mixing time, strength and strain at break measurements. Samples tested after 15 passes gave the highest values, which is reflective of a higher degree of de-agglomeration with longer mixing times and leading to a reduction in the influence of stress raisers. This highlights that there is an improvement to properties with longer mixing times. The presence of functionalisation gave small improvements to the modulus values, where higher intensity treatments gave better reinforcement. GNP-H gave the highest modulus and strength values of all GNPs as a result of the increased interfacial shear strength. The degradation of GNP-H detected through the presence of sp^3 bonds did not negatively impact the ability to provide reinforcement (Bu et al., 2019).

A study performed by (Domun et al., 2017) examined the tensile properties of the same epoxy system and GNP-S graphene used in this study, samples were mixed through magnetic stirring of GNPs in methanol solvent. This was done to disrupt Van-der-Waals forces and promote de-agglomeration. The epoxy resin was then slowly added to the solution before being placed within a vacuum oven the remove the solvent, before being cured and post-cured at a temperature higher than used in this study. The measured tensile values for samples manufactured at 1% filler loading by weight, are shown in table 7.5 and compared to the values collected in this study after 15 passes through the 3RM. The differences observed in epoxy measurements between the two studies, is the result of the different cure cycles used. Domun *et al* concluded that agglomeration was the reason for low improvement to properties when filler loadings of 1 wt% and higher were used. The large degree of increase shown in this work can be attributed to improvements in dispersion state. Tg was found to increase with the addition of GNP-S in the Domun *et al* study, indicating a higher degree of crosslinking was achieved in their materials as a result of the higher cure temperature used. This may have led to the low levels of enhancement to properties, which would corroborate findings by (Montazeri et al., 2010). This study investigated the effect of increasingly intense cure cycles for epoxy / MWCNT (0.5 wt% fill) composites and the resultant effect on tensile properties. The same epoxy resin was used in this study, but cured with a different hardener. It was found that measured values for tensile modulus and UTS both increased with more crosslinking, but had mixed effects on the strain at break. The effect of reinforcement seen with the addition MWCNT decreased with higher crosslinking, leaving little need for the addition of MWCNT where more intense cure cycles were used. Further investigation into the effect of curing parameters and mechanical properties would be required to understand this relationship further.

Table 7.5 : Comparison of measured tensile values between study conducted by Domun et al and this study

	(Domun *et al.*, 2017)			Present study		
Cure cycle	1hr at 80°C, 4 hrs at 160°C			1hr at 80°C, 4 hrs at 140°C		
	Epoxy	1wt% GNP-S	**% increase**	Epoxy	1wt% GNP-S	**% increase**
Tensile Modulus (MPa)	2490	2590	**4.0**	2656	2944	**10.8**
Tensile Strength (MPa)	71	72	**1.4**	53	57	**7.5**
Strain at break (%)	6.5	7.1	**9.2**	3.7	5.9	**59.5**
Glass transition temp (°C)	161	166	**3.1**	161	160	**-0.6**

Other researchers investigating dispersion and using the same epoxy system have produced results showing larger improvements to tensile modulus. (Poutrel et al., 2017) tested GNPs with 25µm planar size and 18 layers, in the raw state and after treatment with surfactant Triton X-100 to improve interfacial properties. Samples underwent functionalisation through the addition of the GNPs and Triton X-100 into acetone, which was sonicated for 2 hours. The mixture was then added into the epoxy resin and underwent high shear mixing for a further 2 hours to ensure complete de-agglomeration. Further alignment of GNPs was performed under an electric field during cure. Poutrel *et al* measured a 6.6% and 23.9% increase in tensile modulus for the poorly disperse raw sample and highly disperse, functionalised and aligned sample respectively. GNP-H produced an average of 14% improvement in tensile modulus after 3RM mixing, which is much lower due to the smaller planar size and random orientation (Young et al., 2012).

FLGs have shown a distinct improvement in strain at break after mixing through 3RM, whereas both mixing methods performed similarly for modulus and strength and did not significantly improve with mixing time. FLG-H gave the highest strain at break values indicating good dispersion and interfacial properties, promoted by the increased O_2 content (Vallés et al., 2016)(Zaman et al., 2011). The modulus values of composites containing FLGs did not significantly improve over that of the epoxy resin, due to the small planar size, however this is less of a concern as these materials are primarily being considered for use in hybrid composites. Long fibres made from materials like carbon or glass are high in both stiffness and strength, therefore, improvements to the matrix strength and strain at break would be most beneficial (Okoli and Smith, 1998). Demonstration of improvement to these parameters is extremely desirable as long fibre composites such as carbon fibre are limited by their matrix strength. The extremely small particles isolated through 3RM (figure 6.9) are desirable, as they are able to effectively infiltrate fibre tows, providing homogeneous reinforcement. However, FLGs were also found to contain large agglomerates in every case of mixing, which is the reason for the wide error bars displayed for strain at break measurements. This may indicate a further process is required to remove the larger agglomerates and optimise overall performance, however this increases processing times and becomes inefficient and undesirable.

8 Shelf Life Investigation

As dispersion state is influential to composite properties, it is commercially important to understand how this may change with time. The specialist high shear mixing equipment used in this project is not likely to be accessible to every potential consumer, leaving analysis of long-term dispersion state essential to understand. This section summarises a study performed to understand how dispersion state changes over time, closely monitoring any re-aggregation behaviour and the resultant effect on storage modulus. The following variables were assessed;

- Functionalisation
- Storage temperature
- Filler loading

The materials were initially prepared by 3RM as previously described in section 3.2.4, for a total of 5 passes. As GNP-H samples were both easy to de-agglomerate and improved mechanical performance, they were investigated in this section. There were four storage conditions monitored, as described in table 8.1. Instance 1 describes the control sample, instance 2 uses GNP-U fillers to assess the role of 'high' intensity functionalisation. Instance 3 and 4 uses increased matrix viscosity, through low temperature and filler loading respectively, to limit the motion of fillers in attempt to prevent re-aggregation. Zeta potential results placed GNP-U samples within the region of 'stability' suggesting re-aggregation is not likely to occur. Room temperature was monitored and recorded once each day and was found to vary between 20-23ºC. Cold temperature conditions were measured to be consistent at 8°C, this complies with recommended storage conditions outlined by material data sheet. Experiments ran over the space of 4 weeks, with measurements being taken immediately after, 1 day, 1 week and 4 weeks post initial mixing. At each interval, Hegman measurements and optical microscopy were carried out to assess changes to dispersion state and DMA was performed to analyse any changes to physical properties.

Table 8.1 : Summary of storage conditions used in this study

Instance	Functionalisation	Filler Loading (% wt.fill)	Temperature
1	O_2-High	1	RT
2	None	1	RT
3	O_2-High	1	Fridge
4	O_2-High	10	RT

Particle sizing through the Hegman gauge (figure 8.1) has shown a small increase to break values for all samples over the 28 day period to comparable levels (between ~4.5-5.8µm), GNP-U largest agglomerate increases, but to a slower rate as time passes. GNP-U have all initially increased with time before universally showing a decrease after 28 days. These results suggest that all samples have experienced a level of re-aggregation, with average agglomerate size all measuring similar sizes. GNP-H samples stored at room temperature have shown the most rapid increase to largest agglomerate size over the first 7 days, suggesting high degrees of re-aggregation. Care was taken to mix samples prior to testing in attempt to redisperse any settled GNPs, but the drop in largest agglomerate measured for all GNP-H samples could be indicative of this occurrence.

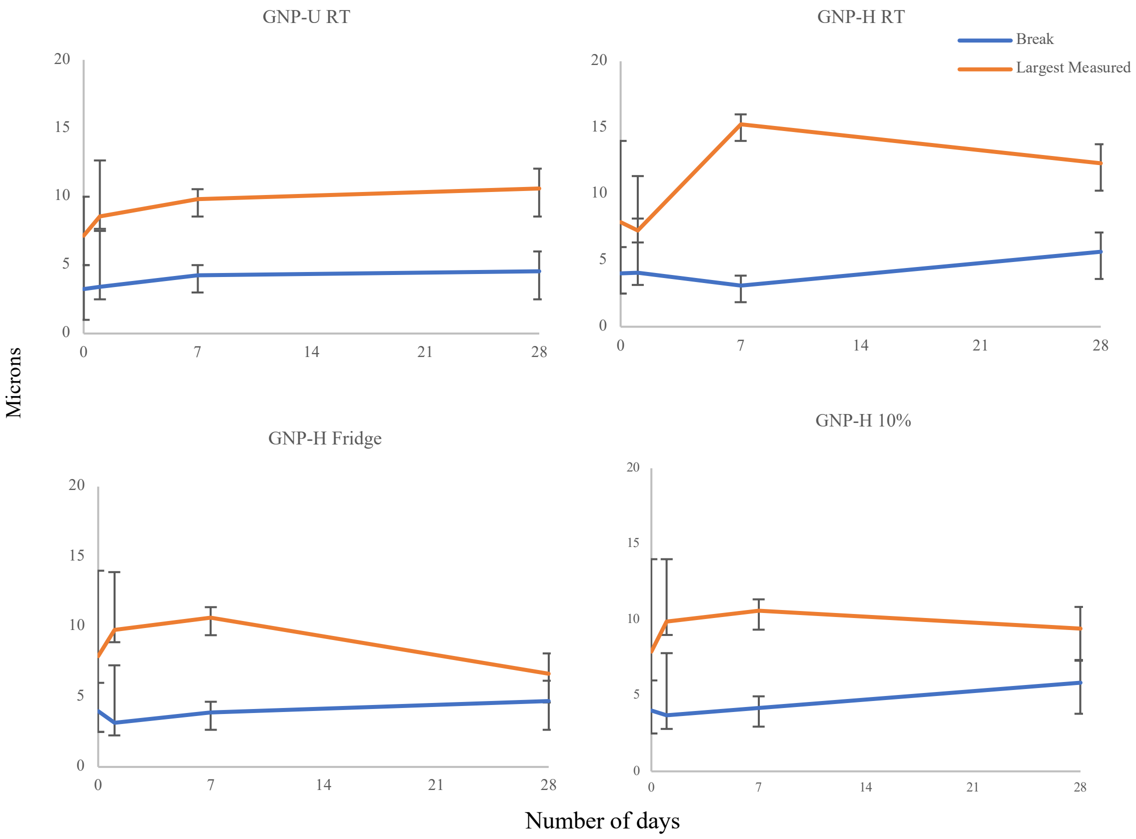

Figure 8.1 : Hegman gauge measurements for each storage condition over the course of 28 days

Optical microscopy is in general agreement with this trend, showing a shift to larger particle sizes as time progresses (figure 8.2). The largest increase in agglomerate size is observed by GNP-H stored at room temperature at high filler loading, this could be the result of the graphene flakes being held in closer proximity within the epoxy matrix increasing the ease of re-agglomeration. PSD curves for GNP-H samples stored at low temperatures have generally shown consistent curves, with the exception of 14 days which suggested an improvement in dispersion state. It should be noted that the epoxy resin crystallised after 28 days of being held at low temperatures and required heating to (60ºC) for 20 minutes to reverse this phenomenon. It appears the energy supplied heating process has not had any noticeable effect to the dispersion state. GNP-U samples have given the most consistent values, with the exception of PSD measured after 1 day, displaying the slowest rate of re-aggregation.

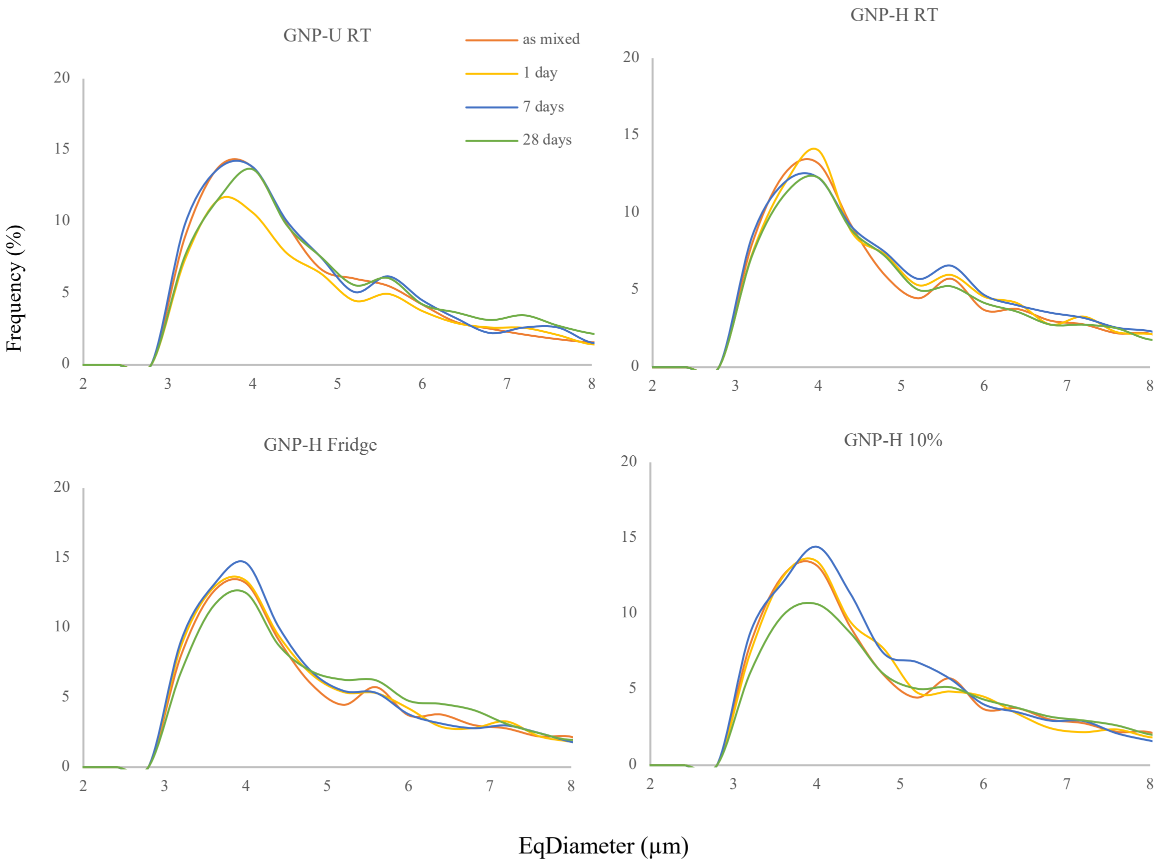

Figure 8.2 : PSD curves for each storage condition

Storage modulus values are displayed in figure 8.3, to gauge an idea of the resultant effect on mechanical properties. As storage modulus values have been shown to produce wide error bars it is difficult to conclude anything with certainty. For measurements taken after 28 days, the lowest modulus was measured for GNP-H stored at high filler loading and at room temperature, which does loosely correlate with samples showing higher levels of re-aggregation. However the large fluctuations seen for the other two samples detracts somewhat from those trends. Previous studies have concluded that small changes to dispersion state have not correlated in any meaningful way to bulk properties, suggesting the observed trends cannot be considered reliable.

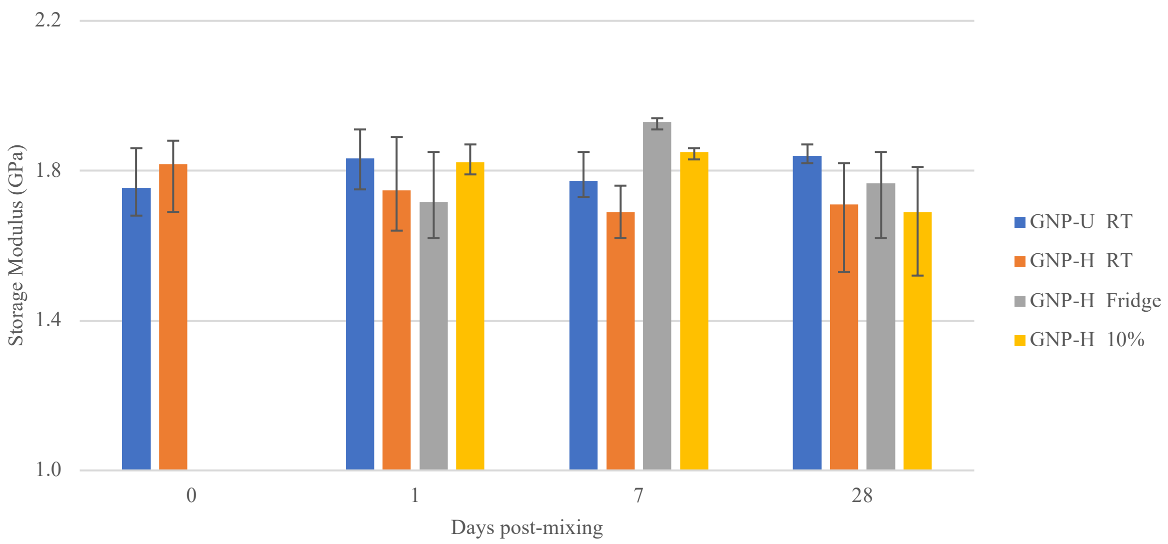

Figure 8.3 Storage modulus values for each storage condition over time

This short study has determined that the presence of ‘high’ intensity functionalisation has not significantly maintained dispersion state over the period of 28 days. Although re-aggregation appears to be steadily occurring over this time frame, it has not significantly impacted bulk mechanical performance. Storing at high filler loadings appears to increase the rate of re-aggregation. Low temperature storage appears to be effective at maintaining dispersion state but may induce crystallisation.

9 Conclusions

This body of work has confirmed the strong influence between manufacture, dispersion state and mechanical properties, illustrating how all the choices made during manufacture can influence the final material performance. This work has given a comprehensive assessment of the manufacturing process of graphene / epoxy composites, methods which are currently used within industry have been compared and explored further through optimisation of processing parameters.

It has been demonstrated that different methods of high-shear mixing can produce very different effects on dispersion state and therefore mechanical properties. Many studies refer generally to the use of high-shear methods to produce good dispersion, however there is little consideration to the high-shear mixing equipment used. This work has demonstrated how different dispersions are produced with mixing method, showing all high-shear mixing methods do not perform equally.

The de-agglomeration process was found to follow predictions based on calculations of cohesion strength through the Rumpf equation. These methods have been used to model the de-agglomeration behaviour of carbon nanotubes (Kasaliwal *et al.*, 2010) and by (He *et al.*, 2017) to understand the de-agglomeration behaviour of graphene when mixed through a twin-screw compounder, but these techniques are not commonplace when discussing de-agglomeration methods. This work has demonstrated the effective use of these simple calculations to numerically link processing parameters to de-agglomeration behaviours.

The effect of de-agglomeration was present over the nano, micro and macro scale allowing inferences to be made on each material batch, based on macro-scale measurements. This is ideal when considering methods of quality control to ensure dispersion state. The fast, low cost and ease of use of macro-scale measurements like the Hegman gauge, can be easily adopted into mixing procedures. The largest effect of de-agglomeration was found to be towards the beginning of mixing, illustrating that short mixing times are sufficient to create a good dispersion state. This confidently proves that quality of dispersion state can be produced over short mixing times, which allows processing times to be cut shorter and the overall mixing process to be optimised.

Mechanical properties were found to increase after high-shear mixing, with largest improvements seen with samples produced through 3RM. Extended mixing times were found to give small improvements to strength and strain at break measurements. GNPs gave small improvements to modulus values with 3RM mixing, however was limited by the small planar size. The small planar size of FLGs did not provide any improvements to modulus but increased values of strength and strain at break, illustrating ideal properties for use in hybrid composites. The presence of functionalisation led to improvements of interfacial properties, which were demonstrated through mechanical performance. GNP-S and GNP-H both gave higher modulus values over that of GNP-U and the presence of high levels of carboxyl and carbonyl functional groups present of the GNP-H surface allowed increased interfacial strength. Functionalised FLGs increased the strength and strain at break, with FLG-H giving the largest degree of improvements.

DMA analysis has illustrated the impact of dispersion, functionalisation and flake size upon curing kinetics of the epoxy matrix, leading to reductions in glass transition temperature and highlighting the importance of selecting the correct curing cycles. This effect is industrially important to understand as reductions to Tg can limit the range of suitable applications. For example, the aerospace industry, where composite materials are becoming increasingly popular, require that materials can withstand elevated temperatures.

Analysis of GNP-H dispersion state over 28 days has indicated that re-agglomeration is occurring over long timescales, despite functionalisation, where storing materials at high filler loadings has facilitated this re-agglomeration process. As it has been demonstrated that good dispersion enhances overall mechanical performance, it is important to have knowledge of the period of time over which this applies post-mixing. From an industrial and commercial standpoint, this knowledge can help to organise the day-to-day operation within the workspace and improve the support given to consumers.

10 Further Work

Further investigation into the fracture toughness properties would be beneficial in building a comprehensive picture of the improvements to mechanical properties, where dispersion state and interfacial properties are enhanced. It is anticipated that improvements to graphene dispersion and interfacial properties have the largest impact to fracture toughness and therefore would be interesting to explore further. This is especially useful to measure for matrix materials considered for use in hybrid composites, as fracture is initiated within the matrix.

Additional work researching the improvement to the mechanical properties of fibre composites, with the addition of graphene to the matrix material would be complimentary to the current project. The implementation of methods to improve dispersion and interfacial properties of the graphene / epoxy matrix, as investigated in the current work, to observe the scale of improvement to the final composite properties would also be interesting to investigate.

Furthermore, the impact of graphene and functionalisation on polymer cure could be further understood. Investigations correlating the disruption to resin stoichiometry and the resultant impact on overall mechanical properties would be beneficial to understand from a material quality viewpoint. Studying the impact of higher intensity curing cycles could be undertaken to determine a practical method of mitigating this effect. The relationship between Tg, curing cycles and the bulk mechanical properties could be further understood in order to better optimise manufacturing parameters.

Additional analysis of dispersion state over longer periods of time, which are more representative of ‘real-world’ scenarios, would be beneficial to fully assess the dispersion shelf-life. It would also be of interest to assess the glass transition and mechanical properties under various storage conditions and over time. This would allow a full assessment of the impact of re-agglomeration to mechanical performance as well as gaining insight into the effectiveness of various storage conditions to prolong dispersion state.

11 Bibliography

A350 XWB Family - Passenger aircraft - Airbus (no date). Available at: https://www.airbus.com/aircraft/passenger-aircraft/a350xwb-family.html (Accessed: 23 May 2020).

Abdalla, M. *et al.* (2008) ‘Cure behavior of epoxy/MWCNT nanocomposites: The effect of nanotube surface modification’, *Polymer*. Elsevier BV, 49(15), pp. 3310–3317. doi: 10.1016/j.polymer.2008.05.016.

Abdullah, S. I. and Ansari, M. N. M. (2015) ‘Mechanical properties of graphene oxide (GO)/epoxy composites’, *HBRC Journal*. Informa UK Limited, 11(2), pp. 151–156. doi: 10.1016/j.hbrcj.2014.06.001.

Ahmadi-Moghadam, B. *et al.* (2015) ‘Effect of functionalization of graphene nanoplatelets on the mechanical response of graphene/epoxy composites’, *Materials and Design*. Elsevier Ltd, 66(PA), pp. 142–149. doi: 10.1016/j.matdes.2014.10.047.

Akhina, H. *et al.* (2018) ‘Plasticized PVC graphene nanocomposites: Morphology, mechanical, and dynamic mechanical properties’, *Polymer Engineering and Science*, 58, pp. E104–E113. doi: 10.1002/pen.24711.

Alam, A., Wan, C. and McNally, T. (2017) ‘Surface amination of carbon nanoparticles for modification of epoxy resins: plasma-treatment vs. wet-chemistry approach’, *European Polymer Journal*. Elsevier Ltd, pp. 422–448. doi: 10.1016/j.eurpolymj.2016.10.004.

Ali Charfi, M. *et al.* (2020) ‘Effect of Graphene Additive on Flexural and Interlaminar Shear Strength Properties of Carbon Fiber-Reinforced Polymer Composite’, *Journal of Composites Science*, 4(4), p. 162. doi: 10.3390/jcs4040162.

Amirova, L. *et al.* (2017) ‘Homogeneous Liquid Phase Transfer of Graphene Oxide into Epoxy Resins’, *ACS Applied Materials and Interfaces*. American Chemical Society, 9(13), pp. 11909–11917. doi: 10.1021/acsami.7b02243.

Androulidakis, C. *et al.* (2017) ‘Wrinkled Few-Layer Graphene as Highly Efficient Load Bearer’, *ACS Applied Materials and Interfaces*, 9(31), pp. 26593–26601. doi: 10.1021/acsami.7b07547.

Atif, R. and Inam, F. (2016) ‘Reasons and remedies for the agglomeration of multilayered graphene and carbon nanotubes in polymers’, *Beilstein Journal of Nanotechnology*. Beilstein-Institut Zur Forderung der Chemischen Wissenschaften, 7(1), pp. 1174–1196. doi: 10.3762/bjnano.7.109.

Atif, R., Shyha, I. and Inam, F. (2016) ‘Mechanical, thermal, and electrical properties of graphene-epoxy nanocomposites-A review’, *Polymers*, 8(8). doi: 10.3390/polym8080281.

Avouris, P. and Dimitrakopoulos, C. (2012) ‘Graphene: synthesis and applications’, *Materials Today*. Elsevier, 15(3), pp. 86–97. doi: 10.1016/S1369-7021(12)70044-5.

Bachmann, J., Hidalgo, C. and Bricout, S. (2017) ‘Environmental analysis of innovative sustainable composites with potential use in aviation sector—A life cycle assessment review’, *Science China Technological Sciences*. Springer Verlag, pp. 1301–1317. doi: 10.1007/s11431-016-9094-y.

Bao, C. *et al.* (2011) ‘In situ preparation of functionalized graphene oxide/epoxy nanocomposites with effective reinforcements’, *Journal of Materials Chemistry*, 21(35), pp. 13290–13298. doi: 10.1039/c1jm11434d.

Bellunato, A. *et al.* (2016) ‘Chemistry at the Edge of Graphene’, *ChemPhysChem*, 17(6), pp. 785–801. doi: 10.1002/cphc.201500926.

Boaretti, C. *et al.* (2020) 'Investigation of plasma-assisted functionalization of graphitic materials for epoxy composites', *Nanomaterials*, 10(1). doi: 10.3390/nano10010078.

Bottari, G. *et al.* (2017) 'Chemical functionalization and characterization of graphene-based materials', *Chemical Society Reviews*. Royal Society of Chemistry, pp. 4464–4500. doi: 10.1039/c7cs00229g.

Bu, H. *et al.* (2019) 'The role of sp 2 and sp 3 hybridized bonds on the structural, mechanical, and electronic properties in a hard BN framework', *RSC Advances*. Royal Society of Chemistry, 9(5), pp. 2657–2665. doi: 10.1039/c8ra09636h.

Cai, X. *et al.* (2018) 'Effects of Tip Sonication Parameters on Liquid Phase Exfoliation of Graphite into Graphene Nanoplatelets', *Nanoscale Research Letters*. Springer New York LLC, 13(1), p. 241. doi: 10.1186/s11671-018-2648-5.

Callister, W. D. and Rethwisch, D. G. (2011) *Materials Science and Engineering*. 8th edn. John Wiley & Sons, Ltd.

Capelo-Martinez, J.-L. (2009) *Ultrasound in Chemistry: Analytical Applications*. John Wiley & Sons. Available at: https://books.google.co.uk/books?id=G-N5goiAFMcC&pg=PA5&lpg=PA5&dq=cavitation+in+high+viscosity+matrix&source=bl&ots=5ZbHTF_ql0&sig=ACfU3U0VzPWc3Yps70z9iWJDgHt9ABfRKQ&hl=en&sa=X&ved=2ahUKEwjQitbx473qAhWGXxUIHXXaBqYQ6AEwCXoECAkQAQ#v=onepage&q=cavitation in high viscosity matrix&f=false (Accessed: 8 July 2020).

Castarlenas, S. *et al.* (2014) 'Few-layer graphene by assisted-exfoliation of graphite with layered silicate', *Carbon*. Pergamon, 73, pp. 99–105. doi: 10.1016/J.CARBON.2014.02.044.

Cha, J. H. *et al.* (2016) 'Quantitative Evaluation of the Dispersion of Graphene Sheets With and Without Functional Groups Using Molecular Dynamics Simulations', *Nanoscale Research Letters*. Springer New York LLC, 11(1). doi: 10.1186/s11671-016-1336-6.

Chakraborty, S. *et al.* (2018) 'Interfacial interaction and the fracture toughness (K_{IC}) trends in epoxy nanocomposites filled with functionalized graphene-based fillers', *Polymer Composites*. John Wiley and Sons Inc., 39(S4), pp. E2356–E2369. doi: 10.1002/pc.24675.

Chandrasekaran, S. *et al.* (2014) 'Fracture toughness and failure mechanism of graphene based epoxy composites', *Composites Science and Technology*. Elsevier BV, 97, pp. 90–99. doi: 10.1016/j.compscitech.2014.03.014.

Chandrasekaran, S., Seidel, C. and Schulte, K. (2013) 'Preparation and characterization of graphite nano-platelet (GNP)/epoxy nano-composite: Mechanical, electrical and thermal properties', *European Polymer Journal*. Pergamon, 49(12), pp. 3878–3888. doi: 10.1016/j.eurpolymj.2013.10.008.

Chen, C. H., Jian, J. Y. and Yen, F. S. (2009) 'Preparation and characterization of epoxy/γ-aluminum oxide nanocomposites', *Composites Part A: Applied Science and Manufacturing*, 40(4), pp. 463–468. doi: 10.1016/j.compositesa.2009.01.010.

Chen, D., Feng, H. and Li, J. (2012) 'Graphene oxide: Preparation, functionalization, and electrochemical applications', *Chemical Reviews*. American Chemical Society, pp. 6027–6053. doi: 10.1021/cr300115g.

Chen, J. *et al.* (2013) 'An improved Hummers method for eco-friendly synthesis of graphene oxide', *Carbon*. Elsevier Ltd, 64(1), pp. 225–229. doi: 10.1016/j.carbon.2013.07.055.

Cheng, C. *et al.* (2019) 'Tandem chemical modification/mechanical exfoliation of graphite: Scalable synthesis of high-quality, surface-functionalized graphene', *Carbon*. Elsevier Ltd, 145, pp. 668–676. doi: 10.1016/j.carbon.2019.01.079.

Chong, H. M., Hinder, S. J. and Taylor, A. C. (2016) 'Graphene nanoplatelet-modified epoxy: effect of aspect ratio and surface functionality on mechanical properties and toughening mechanisms', *Journal of Materials Science*. Springer New York LLC, 51(19), pp. 8764–8790. doi: 10.1007/s10853-016-0160-9.

Chua, C. K. and Pumera, M. (2013) 'Chemical reduction of graphene oxide: a synthetic chemistry viewpoint', *Chemical Society Reviews*. The Royal Society of Chemistry, 43(1), pp. 291–312. doi: 10.1039/C3CS60303B.

Cook, W. D., Mayr, A. E. and Edward, G. H. (1998) 'Yielding behaviour in model epoxy thermosets - II. Temperature dependence', *Polymer*, 39(16), pp. 3725–3733. doi: 10.1016/S0032-3861(97)10335-4.

Cooper, C. A., Young, R. J. and Halsall, M. (2001) 'Investigation into the deformation of carbon nanotubes and their composites through the use of Raman spectroscopy', *Composites Part A: Applied Science and Manufacturing*, 32(3–4), pp. 401–411. doi: 10.1016/S1359-835X(00)00107-X.

Cooper, D. R. *et al.* (2012) 'Experimental Review of Graphene', *ISRN Condensed Matter Physics*, 2012, pp. 1–56. doi: 10.5402/2012/501686.

Cui, X. *et al.* (2011) 'Liquid-phase exfoliation, functionalization and applications of graphene', *Nanoscale*. The Royal Society of Chemistry, pp. 2118–2126. doi: 10.1039/c1nr10127g.

Dai, J. F. *et al.* (2015) 'Surface properties of graphene: Relationship to graphene-polymer composites', *Reviews on Advanced Materials Science*, 40(1), pp. 60–71.

dal Lago, E. *et al.* (2020) 'Influence of different carbon-based fillers on electrical and mechanical properties of a PC/ABS blend', *Polymers*, 12(1). doi: 10.3390/polym12010029.

Dassi (2019) *Graphene | Innovative road bike materials*. Available at: https://dassi.com/dassi-innovation/graphene (Accessed: 10 April 2020).

Deng, S. and Berry, V. (2016) 'Wrinkled, rippled and crumpled graphene: An overview of formation mechanism, electronic properties, and applications', *Materials Today*. Elsevier B.V., pp. 197–212. doi: 10.1016/j.mattod.2015.10.002.

Dey, A. *et al.* (2016) 'Plasma engineering of graphene', *Applied Physics Reviews*, 3(2). doi: 10.1063/1.4947188.

Dobrota, A. S. *et al.* (2016) 'A general view on the reactivity of the oxygen-functionalized graphene basal plane', *Physical Chemistry Chemical Physics*. Royal Society of Chemistry, 18(9), pp. 6580–6586. doi: 10.1039/c5cp07612a.

Domun, N. *et al.* (2017) 'Improving the fracture toughness properties of epoxy using graphene nanoplatelets at low filler content', *Nanocomposites*. Taylor and Francis Inc., 3(3), pp. 85–96. doi: 10.1080/20550324.2017.1365414.

Doszlop, S., Vargha, V. and Horkay, F. (1978) 'Reactions of Epoxy With Other Functional Groups and the Arising Sec-Hydroxyl Groups.', *Periodica Polytechnica Chemical Engineering*, 22(3), pp. 253–275.

Dunson, D. (2017) *Characterization of Polymers using Dynamic Mechanical Analysis (DMA)*. Available at: https://www.eag.com/wp-content/uploads/2017/09/M-022717-Characterization-of-Polymers-using-Dynamic-Mechanical-Analysis.pdf (Accessed: 30 August 2019).

Dutrow, B. L. and Clark, C. M. (no date) *X-ray Powder Diffraction (XRD)*. Available at: https://serc.carleton.edu/research_education/geochemsheets/techniques/XRD.html (Accessed: 10 June

2020).

Easy Composites (2021) *XC130 450g 2x2 Twill 12k Prepreg Carbon Fibre 1.25m - Easy Composites*. Available at: https://www.easycomposites.co.uk/xc130-450g-22-twill-12k-prepreg-carbon-fibre (Accessed: 11 September 2021).

Eitan, A. *et al.* (2003) 'Surface Modification of Multiwalled Carbon Nanotubes: Toward the Tailoring of the Interface in Polymer Composites', *Chemistry of Materials*. American Chemical Society, 15(16), pp. 3198–3201. doi: 10.1021/CM020975D.

Eqra, R., Janghorban, K. and Manesh, H. D. (2015) 'Effect of number of graphene layers on mechanical and dielectric properties of graphene–epoxy nanocomposites', *Plastics, Rubber and Composites*. Maney Publishing, 44(10), pp. 405–412. doi: 10.1179/1743289815Y.0000000037.

Exakt Technologies Inc (2018) *Three Roll Mill EXAKT 80E PLUS Dispersing + Analysing (Dreiwalzwerk)*. Available at: https://www.youtube.com/watch?v=jL3nEPLPt98 (Accessed: 8 July 2020).

Exakt Technologies Inc (2020) *The New 80E Plus | Exakt Technologies*. Available at: https://exaktusa.com/80e-plus/ (Accessed: 8 July 2020).

Fasolino, A., Los, J. H. and Katsnelson, M. I. (2007) 'Intrinsic ripples in graphene', *Nature Materials*, 6(11), pp. 858–861. doi: 10.1038/nmat2011.

Felten, A. *et al.* (2005) 'Radio-frequency plasma functionalization of carbon nanotubes surface O 2, NH 3, and CF 4 treatments', *Journal of Applied Physics*, 98(7). doi: 10.1063/1.2071455.

Ferraris, S. *et al.* (2018) 'Zeta Potential Measurements on Solid Surfaces for in Vitro Biomaterials Testing: Surface Charge, Reactivity Upon Contact With Fluids and Protein Absorption', *Frontiers in Bioengineering and Biotechnology*. Frontiers Media S.A., 6(MAY), p. 60. doi: 10.3389/fbioe.2018.00060.

Fiore, V. and Valenza, A. (2013) 'Epoxy resins as a matrix material in advanced fiber-reinforced polymer (FRP) composites', *Advanced Fibre-Reinforced Polymer (FRP) Composites for Structural Applications*. Woodhead Publishing, pp. 88–121. doi: 10.1533/9780857098641.1.88.

Del Gaudio, C. and Licciardi, G. A. (2019) 'A simple tool for two-dimensional quantification of filler dispersion: A proposal', *Fullerenes Nanotubes and Carbon Nanostructures*. Taylor & Francis, 27(5), pp. 446–452. doi: 10.1080/1536383X.2019.1594199.

Geim, A. K. (2011) 'Nobel Lecture: Random walk to graphene', *Reviews of Modern Physics*, 83(3), pp. 851–862. doi: 10.1103/RevModPhys.83.851.

Geim, A. K. and Novoselov, K. S. (2007) 'The rise of graphene', *Nature Materials*, 6(3), pp. 183–191. doi: 10.1038/nmat1849.

Georgakilas, V. *et al.* (2012) 'Functionalization of graphene: Covalent and non-covalent approaches, derivatives and applications', *Chemical Reviews*. American Chemical Society, pp. 6156–6214. doi: 10.1021/cr3000412.

Georgantzinos, S. K., Katsareas, D. E. and Anifantis, N. K. (2012) 'Limit load analysis of graphene with pinhole defects: A nonlinear structural mechanics approach', *International Journal of Mechanical Sciences*. Pergamon, 55(1), pp. 85–94. doi: 10.1016/j.ijmecsci.2011.12.006.

Gong, L. *et al.* (2010a) 'Interfacial stress transfer in a graphene monolayer nanocomposite', *Advanced Materials*, 22(24), pp. 2694–2697. doi: 10.1002/adma.200904264.

Gong, L. *et al.* (2010b) 'Interfacial Stress Transfer in a Graphene Monolayer Nanocomposite', *Advanced*

Materials, 22(24), pp. 2694–2697. doi: 10.1002/adma.200904264.

Gong, L. *et al.* (2012) ‘Optimizing the reinforcement of polymer-based nanocomposites by graphene’, *ACS Nano*. UTC, 6(3), pp. 2086–2095. doi: 10.1021/nn203917d.

Grabowski, C. A. and Mukhopadhyay, A. (2014) ‘Size effect of nanoparticle diffusion in a polymer melt’, *Macromolecules*. American Chemical Society, 47(20), pp. 7238–7242. doi: 10.1021/ma501670u.

Gudarzi, M. M. and Sharif, F. (2012) ‘Enhancement of dispersion and bonding of graphene-polymer through wet transfer of functionalized graphene oxide’, *Express Polymer Letters*, 6(12), pp. 1017–1031. doi: 10.3144/expresspolymlett.2012.107.

Hamerton, I. *et al.* (2014) ‘Towards the rational design of polymers using molecular simulation: Predicting the effect of cure schedule on thermo-mechanical properties for a cycloaliphatic amine-cured epoxy resin’, *Reactive and Functional Polymers*. Elsevier, 74(1), pp. 1–15. doi: 10.1016/J.REACTFUNCTPOLYM.2013.10.005.

Hansen, S., Khakhar, D. V. and Ottino, J. M. (1998) ‘Dispersion of solids in nonhomogeneous viscous flows’, *Chemical Engineering Science*. Elsevier Sci Ltd, 53(10), pp. 1803–1817. doi: 10.1016/S0009-2509(98)00010-4.

Hawkins, D. A. and Haque, A. (2014) ‘Fracture toughness of carbon-graphene/epoxy hybrid Nanocomposites’, *Procedia Engineering*. Elsevier B.V., 90, pp. 176–181. doi: 10.1016/j.proeng.2014.11.833.

Haydale (2019) *Automotive Applications – Haydale*. Available at: https://haydale.com/applications/automotive/ (Accessed: 28 August 2021).

He, S. *et al.* (2017) ‘Study on the morphology development and dispersion mechanism of polypropylene/graphene nanoplatelets composites for different shear field’, *Composites Science and Technology*. Elsevier Ltd, 153, pp. 209–221. doi: 10.1016/j.compscitech.2017.10.024.

He, S. *et al.* (2019) ‘Effect of primary particle size and aggregate size of modified graphene oxide on toughening of unsaturated polyester resin’, *Polymer Composites*. John Wiley and Sons Inc., 40(10), pp. 3886–3894. doi: 10.1002/pc.25248.

Hodd, K. (1989) ‘Epoxy Resins’, in *Comprehensive Polymer Science and Supplements*. Elsevier, pp. 667–699. doi: 10.1016/B978-0-08-096701-1.00178-6.

Hossain, M. K., Chowdhury, M. M. R. and Bolden, N. W. (2016) ‘Processing and Performance Evaluation of Amine Functionalized Graphene Nanoplatelet Reinforced Epoxy Composites’, *Journal of Materials Science and Engineering A*, 6(3), pp. 117–130. doi: 10.17265/2161-6213/2016.5-6.001.

Huang, Y. *et al.* (2017) ‘High mechanical properties of epoxy networks with dangling chains and tunable microphase separation structure’, *RSC Advances*. Royal Society of Chemistry, 7(77), pp. 49074–49082. doi: 10.1039/c7ra08886h.

Huntsman (2011) ‘Araldite ® LY564 Aradur ® 2954 Advanced Materials Araldite ® LY 564* / Aradur ® 2954* HOT CURING EPOXY SYSTEM’, (January), pp. 1–5.

Hussein, A. and Kim, B. (2018) ‘Graphene/polymer nanocomposites: The active role of the matrix in stiffening mechanics’, *Composite Structures*, 202(January), pp. 170–181. doi: 10.1016/j.compstruct.2018.01.023.

Inc, F. (2018) *SpeedMixer Technology | FlackTek Inc.* Available at: https://speedmixer.com/speedmixer-technology/ (Accessed: 19 June 2020).

Iso, P. D. (2017) ‘PD ISO / TS 80004 - 13 : 2017 BSI Standards Publication Nanotechnologies — Vocabulary’.

Ito, A. and Okamoto, S. (2013) ‘Mechanical Properties of Single- and Quadruple-Crystalline Graphites Containing Interlayer sp3 Bonds Using Molecular Dynamics Simulations’, *GSTF International Journal of Engineering Technology*, 2(1), pp. 15–21.

Jimenez-Cervantes, E. *et al.* (2016) ‘Graphene-Based Materials Functionalization with Natural Polymeric Biomolecules’, in *Recent Advances in Graphene Research*. InTech. doi: 10.5772/64001.

Jin, Y., Duan, F. and Mu, X. (2016) ‘Functionalization enhancement on interfacial shear strength between graphene and polyethylene’, *Applied Surface Science*. Elsevier B.V., 387, pp. 1100–1109. doi: 10.1016/j.apsusc.2016.07.047.

Johnson, D. W., Dobson, B. P. and Coleman, K. S. (2015) ‘A manufacturing perspective on graphene dispersions’, *Current Opinion in Colloid and Interface Science*. The Authors, 20(5–6), pp. 367–382. doi: 10.1016/j.cocis.2015.11.004.

Jorio, A. (2012) ‘Raman Spectroscopy in Graphene-Based Systems: Prototypes for Nanoscience and Nanometrology’, *ISRN Nanotechnology*, 2012(2), pp. 1–16. doi: 10.5402/2012/234216.

Joy, J. *et al.* (2020) ‘Effect of filler loading on polymer chain confinement and thermomechanical properties of epoxy/boron nitride (h-BN) nanocomposites’, *New Journal of Chemistry*. Royal Society of Chemistry, 44(11), pp. 4494–4503. doi: 10.1039/c9nj05834f.

Kalita, G. and Tanemura, M. (2017) ‘Fundamentals of Chemical Vapor Deposited Graphene and Emerging Applications’, in *Graphene Materials - Advanced Applications*. InTech. doi: 10.5772/67514.

Kang, N. and Khondaker, S. I. (2014) ‘The impact of carbon sp2 fraction of reduced graphene oxide on the performance of reduced graphene oxide contacted organic transistors’, *Applied Physics Letters*. American Institute of Physics Inc., 105(22), p. 223301. doi: 10.1063/1.4902881.

Kasaliwal, G. R. *et al.* (2010) ‘Analysis of agglomerate dispersion mechanisms of multiwalled carbon nanotubes during melt mixing in polycarbonate’, *Polymer*. Elsevier Ltd, 51(12), pp. 2708–2720. doi: 10.1016/j.polymer.2010.02.048.

Kazi, S. N. *et al.* (2015a) ‘Investigation on the use of graphene oxide as novel surfactant to stabilize weakly charged graphene nanoplatelets’, *Nanoscale Research Letters*. Springer New York LLC, 10(1), p. 212. doi: 10.1186/s11671-015-0882-7.

Kazi, S. N. *et al.* (2015b) ‘Investigation on the use of graphene oxide as novel surfactant to stabilize weakly charged graphene nanoplatelets’, *Nanoscale Research Letters*. ???, 10(1), pp. 16–18. doi: 10.1186/s11671-015-0882-7.

Khare, H. S. and Burris, D. L. (2010) ‘A quantitative method for measuring nanocomposite dispersion’, *Polymer*. Elsevier Ltd, 51(3), pp. 719–729. doi: 10.1016/j.polymer.2009.12.031.

Kilic, U., Sherif, M. M. and Ozbulut, O. E. (2019) ‘Tensile properties of graphene nanoplatelets/epoxy composites fabricated by various dispersion techniques’, *Polymer Testing*. Elsevier Ltd, 76, pp. 181–191. doi: 10.1016/j.polymertesting.2019.03.028.

Kondratowicz, I. *et al.* (2018) ‘Tailoring properties of reduced graphene oxide by oxygen plasma treatment’, *Applied Surface Science*. Elsevier B.V., 440, pp. 651–659. doi: 10.1016/j.apsusc.2018.01.168.

Laserna, J. (2014) *An Introduction to Raman Spectroscopy: Introduction and Basic Principles - 2014 - Wiley Analytical Science*, *Wiley Analytical Science*. Available at: https://analyticalscience.wiley.com/do/10.1002/sepspec.1882education/full/ (Accessed: 3 January 2021).

Laurenzi, S. *et al.* (2014) ‘Fracture mechanisms in epoxy composites reinforced with carbon nanotubes’, in *Procedia Engineering*. Elsevier Ltd, pp. 157–164. doi: 10.1016/j.proeng.2014.11.139.

Lavin-Lopez, M. del P. *et al.* (2016) ‘Influence of Different Improved Hummers Method Modifications on the Characteristics of Graphite Oxide in Order to Make a More Easily Scalable Method’, *Industrial and Engineering Chemistry Research*. American Chemical Society, 55(50), pp. 12836–12847. doi: 10.1021/ACS.IECR.6B03533.

Lee, C. *et al.* (2008) ‘Measurement of the elastic properties and intrinsic strength of monolayer graphene’, *Science*. American Association for the Advancement of Science, 321(5887), pp. 385–388. doi: 10.1126/science.1157996.

Leguillon, D., Martin, É. and Lafarie-Frenot, M. C. (2015) ‘Flexural vs. tensile strength in brittle materials’, *Comptes Rendus - Mecanique*. Elsevier Masson SAS, 343(4), pp. 275–281. doi: 10.1016/j.crme.2015.02.003.

Li, X. *et al.* (2008) ‘Highly conducting graphene sheets and Langmuir-Blodgett films’, *Nature Nanotechnology*. Nature Publishing Group, 3(9), pp. 538–542. doi: 10.1038/nnano.2008.210.

Li, Y. *et al.* (2016) ‘Optimization of Three-Roll Mill Parameters for In-Situ Exfoliation of Graphene’, in *MRS Advances*. Materials Research Society, pp. 1389–1394. doi: 10.1557/adv.2016.191.

Li, Z. *et al.* (2015) ‘Deformation of Wrinkled Graphene’, *ACS Nano*, 9(4), pp. 3917–3925. doi: 10.1021/nn507202c.

Li, Z. *et al.* (2018) ‘Effect of functional groups on the agglomeration of graphene in nanocomposites’, *Composites Science and Technology*. Elsevier, 163, pp. 116–122. doi: 10.1016/J.COMPSCITECH.2018.05.016.

Liang, A. *et al.* (2018) ‘Recent developments concerning the dispersion methods and mechanisms of graphene’, *Coatings*, 8(1). doi: 10.3390/coatings8010033.

Liang, J. *et al.* (2009) ‘Molecular-Level Dispersion of Graphene into Poly(vinyl alcohol) and Effective Reinforcement of their Nanocomposites’, *Advanced Functional Materials*, 19(14), pp. 2297–2302. doi: 10.1002/adfm.200801776.

Lin, Z. *et al.* (2017) ‘Simple technique of exfoliation and dispersion of multilayer graphene from natural graphite by ozone-assisted sonication’, *Nanomaterials*. MDPI AG, 7(6). doi: 10.3390/nano7060125.

Liu, F. *et al.* (2019) ‘Synthesis of graphene materials by electrochemical exfoliation: Recent progress and future potential’, *Carbon Energy*. John Wiley & Sons, Ltd, 1(2), pp. 173–199. doi: 10.1002/CEY2.14.

Liu, J. *et al.* (2009) ‘Static, rheological and mechanical properties of polymer nanocomposites studied by computer modeling and simulation’, *Physical Chemistry Chemical Physics*. The Royal Society of Chemistry, 11(48), pp. 11365–11384. doi: 10.1039/b913511a.

Liu, L. *et al.* (2014) ‘A green, rapid and size-controlled production of high-quality graphene sheets by hydrodynamic forces’, *RSC Advances*, 4(69), pp. 36464–36470.

Liu, Z. *et al.* (2012) ‘Interlayer shear strength of single crystalline graphite’, in *Acta Mechanica Sinica/Lixue Xuebao*. Springer, pp. 978–982. doi: 10.1007/s10409-012-0137-0.

Lu, J. *et al.* (2010) ‘Stable aqueous suspension and self-assembly of graphite nanoplatelets coated with various polyelectrolytes', *Journal of Nanomaterials*, 2010. doi: 10.1155/2010/186486.

Luo, Z. P. and Koo, J. H. (2008) 'Quantification of the layer dispersion degree in polymer layered silicate nanocomposites by transmission electron microscopy', *Polymer*. Elsevier BV, 49(7), pp. 1841–1852. doi: 10.1016/j.polymer.2008.02.028.

Ma, P. C. *et al.* (2010) 'Dispersion and functionalization of carbon nanotubes for polymer-based nanocomposites: A review', *Composites Part A: Applied Science and Manufacturing*. Elsevier Ltd, pp. 1345–1367. doi: 10.1016/j.compositesa.2010.07.003.

Malvern Instruments (2000) 'Zeta potential: An Introduction in 30 minutes', *Zetasizer Nano Serles Technical Note. MRK654-01*, 2, pp. 1–6. Available at: http://scholar.google.com/scholar?hl=en&btnG=Search&q=intitle:Zeta+Potential+An+Introduction+in+30+Minutes#0.

Manta, A., Gresil, M. and Soutis, C. (2019) 'Tensile and flexural behaviour of a graphene/epoxy composite: experiments and simulation', *Journal of Physics: Materials*. IOP Publishing, 3(1), p. 014006. doi: 10.1088/2515-7639/ab52d8.

Marsden, A. J. *et al.* (2018) 'Electrical percolation in graphene-polymer composites', *2D Materials*, 5(3). doi: 10.1088/2053-1583/aac055.

Massingill, J. S. and Bauer, R. . (2000) *EPOXY RESINS*. Pergamon. doi: 10.1016/B978-008043417-9/50023-4.

McEvoy, N. *et al.* (2013) 'Functionalisation of graphene surfaces with downstream plasma treatments', *Carbon*, 54(1), pp. 283–290. doi: 10.1016/j.carbon.2012.11.040.

Melro, L. S., Pyrz, R. and Jensen, L. R. (2016) 'A molecular dynamics study on the interaction between epoxy and functionalized graphene sheets', in *IOP Conference Series: Materials Science and Engineering*. Institute of Physics Publishing. doi: 10.1088/1757-899X/139/1/012036.

Menard, K. P. (1999) *DYNAMIC MECHANICAL ANALYSIS A Practical Introduction*. Available at: www.crcpress.com (Accessed: 24 February 2019).

Mohan, V. B., Haalboom, M. and Bhattacharyya, D. (2020) 'Novel dispersion analysis and selective quantification of particulate components in graphene nanoplatelets-polymer-polymer hybrid composites', *Journal of Applied Polymer Science*. John Wiley and Sons Inc., p. 49296. doi: 10.1002/app.49296.

Montazeri, A. *et al.* (2010) 'The Effect of Curing Cycle on the Mechanical Properties of MWNT/Epoxy Nanocomposite', *International Journal of Polymer Analysis and Characterization*. Taylor & Francis Group , 15(3), pp. 182–190. doi: 10.1080/10236661003671744.

Morgan, D. J. (2017) 'Cluster cleaned HOPG by XPS', *Surface Science Spectra*, 24(2), p. 024003. doi: 10.1116/1.4993771.

Morimune-Moriya, S., Goto, T. and Nishino, T. (2019) 'Effect of aspect ratio of graphene oxide on properties of poly (vinyl alcohol) nanocomposites', *Nanocomposites*. Taylor and Francis Inc., 5(3), pp. 84–93. doi: 10.1080/20550324.2019.1647688.

Naebe, M. *et al.* (2014) 'Mechanical Property and Structure of Covalent Functionalised Graphene/Epoxy Nanocomposites', *Scientific Reports*. Nature Publishing Group, 4(1), pp. 1–7. doi: 10.1038/srep04375.

Nanda, K. K. *et al.* (2003) 'Higher Surface Energy of Free Nanoparticles', *Physical Review Letters*, 91(10), pp. 1–4. doi: 10.1103/PhysRevLett.91.106102.

Nixon, R., Cahill, J. and Jolanki, R. (2012) ‘Epoxy Resins’, *Kanerva’s Occupational Dermatology, Second Edition*. Springer, Berlin, Heidelberg, 1, pp. 559–581. doi: 10.1007/978-3-642-02035-3_51.

Njuguna, J. (2013) *Structural Nanocomposites: Perspectives for Future Applications*. Springer Science & Business Media.

Nobile, M. R. *et al.* (2016) ‘Rheological and morphological properties of graphene-epoxy nanocomposites’, in *AIP Conference Proceedings*. American Institute of Physics Inc., p. 020143. doi: 10.1063/1.4949718.

Nolte, H., Schilde, C. and Kwade, A. (2012) ‘Determination of particle size distributions and the degree of dispersion in nanocomposites’, *Composites Science and Technology*. Elsevier, pp. 948–958. doi: 10.1016/j.compscitech.2012.03.010.

Okoli, O. I. and Smith, G. F. (1998) ‘Failure modes of fibre reinforced composites: The effects of strain rate and fibre content’, *Journal of Materials Science*. Springer Netherlands, 33(22), pp. 5415–5422. doi: 10.1023/A:1004406618845.

Pacek, A. W., Ding, P. and Utomo, A. T. (2007) ‘Effect of energy density, pH and temperature on de-aggregation in nano-particles/water suspensions in high shear mixer’, *Powder Technology*. Elsevier, 173(3), pp. 203–210. doi: 10.1016/J.POWTEC.2007.01.006.

Papageorgiou, D. G., Kinloch, I. A. and Young, R. J. (2017) ‘Mechanical properties of graphene and graphene-based nanocomposites’, *Progress in Materials Science*, 90, pp. 75–127. doi: 10.1016/j.pmatsci.2017.07.004.

Paton, K. R. *et al.* (2014) ‘Scalable production of large quantities of defect-free few-layer graphene by shear exfoliation in liquids’, *Nature Materials*. Nature Publishing Group, 13(6), pp. 624–630. doi: 10.1038/nmat3944.

Pfeifer, S. and Bandaru, P. R. (2014) ‘A methodology for quantitatively characterizing the dispersion of nanostructures in polymers and composites’, *Materials Research Letters*. Taylor & Francis, 2(3), pp. 166–175. doi: 10.1080/21663831.2014.886629.

Poutrel, Q. A. *et al.* (2017) ‘Effect of pre and Post-Dispersion on Electro-Thermo-Mechanical Properties of a Graphene Enhanced Epoxy’, *Applied Composite Materials*. Applied Composite Materials, 24(2), pp. 313–336. doi: 10.1007/s10443-016-9541-0.

Praveen, M., Pramod, M. and Neogi, S. (2017) ‘Dispersion study of clay nanoparticles in vinylester resin’, *Journal of Vinyl and Additive Technology*. John Wiley and Sons Ltd, 23, pp. E51–E57. doi: 10.1002/vnl.21577.

Pullicino, E. *et al.* (2017) ‘The Effect of Shear Mixing Speed and Time on the Mechanical Properties of GNP/Epoxy Composites’, *Applied Composite Materials*, 24(2), pp. 301–311. doi: 10.1007/s10443-016-9559-3.

Punetha, V. D. *et al.* (2017) ‘Functionalization of carbon nanomaterials for advanced polymer nanocomposites: A comparison study between CNT and graphene’, *Progress in Polymer Science*. Elsevier Ltd, pp. 1–47. doi: 10.1016/j.progpolymsci.2016.12.010.

Qin, H. *et al.* (2016) ‘Mechanical properties of wrinkled graphene generated by topological defects’, *Carbon*. Elsevier Ltd, 108, pp. 204–214. doi: 10.1016/j.carbon.2016.07.014.

Qin, W. *et al.* (2020) ‘Synergistic effects of graphene/carbon nanotubes hybrid coating on the interfacial and mechanical properties of fiber composites’, *Materials*, 13(6). doi: 10.3390/ma13061457.

Quintana, M., Tapia, J. I. and Prato, M. (2014) ‘Liquid-phase exfoliated graphene: functionalization, characterization, and applications’, *Beilstein Journal of Nanotechnology*. Beilstein-Institut Zur Forderung der Chemischen Wissenschaften, 5(1), pp. 2328–2338. doi: 10.3762/bjnano.5.242.

Rafiee, M. A. *et al.* (2010) ‘Fracture and fatigue in graphene nanocomposites’, *Small*. John Wiley & Sons, Ltd, 6(2), pp. 179–183. doi: 10.1002/smll.200901480.

Rooyanian, S. *et al.* (2018) ‘A simple route to surface functionalization of graphene nanosheets by benzoic acid and its application toward Pb(ii) sensing’, *New Journal of Chemistry*. Royal Society of Chemistry, 42(21), pp. 17371–17378. doi: 10.1039/C8NJ04110E.

Saberian, M. *et al.* (2019) ‘Investigation on tensile properties of epoxy/graphene nano-platelets/carboxylated nitrile butadiene rubber ternary nanocomposites using response surface methodology’, *Nanomaterials and Nanotechnology*. SAGE Publications Ltd, 9, p. 184798041985584. doi: 10.1177/1847980419855842.

Saeed, M. *et al.* (2020) ‘Chemical Vapour Deposition of Graphene—Synthesis, Characterisation, and Applications: A Review’, *Molecules*, 25(17). doi: 10.3390/molecules25173856.

Santos, R. *et al.* (2018) ‘Effects of Particle Size and Surface Chemistry on the Dispersion of Graphite Nanoplates in Polypropylene Composites’, *Polymers*. MDPI AG, 10(2), p. 222. doi: 10.3390/polym10020222.

Scurati, A., Feke, D. L. and Manas-Zloczower, I. (2005) ‘Analysis of the kinetics of agglomerate erosion in simple shear flows’, *Chemical Engineering Science*. Elsevier Ltd, 60(23), pp. 6564–6573. doi: 10.1016/j.ces.2005.05.059.

Sharma, R. *et al.* (2010) ‘Anomalously large reactivity of single graphene layers and edges toward electron transfer chemistries’, *Nano Letters*. American Chemical Society, 10(2), pp. 398–405. doi: 10.1021/nl902741x.

Sharma, R., Sharma, A. K. and Sharma, V. (2015) ‘Synthesis of carbon nanotubes by arc-discharge and chemical vapor deposition method with analysis of its morphology, dispersion and functionalization characteristics’, *http://www.editorialmanager.com/cogenteng*. Cogent, 2(1), p. 1094017. doi: 10.1080/23311916.2015.1094017.

Shojaee, S. A. *et al.* (2013) ‘Raman spectroscopic imaging of graphene dispersion in polymer composites’, *Carbon*. Elsevier Ltd, pp. 510–513. doi: 10.1016/j.carbon.2013.05.068.

Silverson (2020) *Lab Mixer | High Shear Industrial Laboratory Mixers Homogenisers*. Available at: https://www.silverson.co.uk/en/products/laboratory-mixers/ (Accessed: 7 July 2020).

Singh, S., Srivastava, V. K. and Prakash, R. (2015) ‘Influences of carbon nanofillers on mechanical performance of epoxy resin polymer’, *Applied Nanoscience (Switzerland)*, 5(3), pp. 305–313. doi: 10.1007/s13204-014-0319-0.

Sohail, M. *et al.* (2017) ‘Modified and improved Hummer’s synthesis of graphene oxide for capacitors applications’, *Modern Electronic Materials*. Elsevier, 3(3), pp. 110–116. doi: 10.1016/J.MOEM.2017.07.002.

Song, P. *et al.* (2011) ‘Fabrication of exfoliated graphene-based polypropylene nanocomposites with enhanced mechanical and thermal properties’, *Polymer*. Elsevier Ltd, 52(18), pp. 4001–4010. doi: 10.1016/j.polymer.2011.06.045.

Sonntag, R. C. and Russel, W. B. (1987) ‘Structure and breakup of flocs subjected to fluid stresses. III.

Converging flow', *Journal of Colloid And Interface Science*. Academic Press, 115(2), pp. 390–395. doi: 10.1016/0021-9797(87)90054-3.

Speranza, G. (2019) 'The Role of Functionalization in the Applications of Carbon Materials: An Overview', *C — Journal of Carbon Research*, 5(4), p. 84. doi: 10.3390/c5040084.

Stetefeld, J., McKenna, S. A. and Patel, T. R. (2016) 'Dynamic light scattering: a practical guide and applications in biomedical sciences', *Biophysical Reviews*. Springer Verlag, pp. 409–427. doi: 10.1007/s12551-016-0218-6.

Subrahmanyam, K. S. *et al.* (2009) 'Simple Method of Preparing Graphene Flakes by an Arc-Discharge Method', *Journal of Physical Chemistry C*. American Chemical Society, 113(11), pp. 4257–4259. doi: 10.1021/JP900791Y.

Surnova, A. *et al.* (2019) 'Fully exfoliated graphene oxide accelerates epoxy resin curing, and results in dramatic improvement of the polymer mechanical properties', *Composites Part B: Engineering*. Elsevier, 162(June 2018), pp. 685–691. doi: 10.1016/j.compositesb.2019.01.020.

Taira, R., Yamanaka, A. and Okada, S. (2017) 'Electronic structure and electric polarity of edge-functionalized graphene nanoribbons', *Japanese Journal of Applied Physics*. Japan Society of Applied Physics, 56(8), p. 085103. doi: 10.7567/JJAP.56.085103.

Tamminen, J. and Koiranen, T. (2015) 'Mixing performance comparison of milliscale continuous high-shear mixers', *Canadian Journal of Chemical Engineering*, 93(12), pp. 2245–2252. doi: 10.1002/cjce.22327.

Tan, H., Wang, D. and Guo, Y. (2018) 'Thermal growth of graphene: A review', *Coatings*, 8(1). doi: 10.3390/coatings8010040.

Tang, L. C. *et al.* (2013) 'The effect of graphene dispersion on the mechanical properties of graphene/epoxy composites', *Carbon*. Pergamon, 60, pp. 16–27. doi: 10.1016/j.carbon.2013.03.050.

Throckmorton, J. and Palmese, G. (2015) 'Direct preparation of few layer graphene epoxy nanocomposites from untreated flake graphite', *ACS Applied Materials and Interfaces*. American Chemical Society, 7(27), pp. 14870–14877. doi: 10.1021/acsami.5b03465.

Tian, Y. *et al.* (2016) 'High strain rate compression of epoxy based nanocomposites', *Composites Part A: Applied Science and Manufacturing*. Elsevier Ltd, 90, pp. 62–70. doi: 10.1016/j.compositesa.2016.06.008.

Topal, E. *et al.* (2016) 'Investigation of mechanical properties of graphene and reduced graphene oxide reinforced epoxy matrix composites', *Journal of Testing and Evaluation*. ASTM International, 45(4), pp. 1182–1191. doi: 10.1520/JTE20160124.

Topkaya, T., Çelik, Y. H. and Kilickap, E. (2020) 'Mechanical properties of fiber/graphene epoxy hybrid composites', *Journal of Mechanical Science and Technology*, 34(11), pp. 4589–4595. doi: 10.1007/s12206-020-1016-4.

Turner, P. *et al.* (2019) 'Controlled Sonication as a Route to in-situ Graphene Flake Size Control', *Scientific Reports*. Nature Publishing Group, 9(1), pp. 1–8. doi: 10.1038/s41598-019-45059-5.

Tyurnina, A. V. *et al.* (2020) 'Ultrasonic exfoliation of graphene in water: A key parameter study', *Carbon*. Elsevier Ltd, 168, pp. 737–747. doi: 10.1016/j.carbon.2020.06.029.

Udupi, S. R. and Lester Raj Rodrigues, L. (2016) 'Detecting Safety Zone Drill Process Parameters for Uncoated HSS Twist Drill in Machining GFRP Composites by Integrating Wear Rate and Wear Transition Mapping', *Indian Journal of Materials Science*. Hindawi Limited, 2016, pp. 1–8. doi:

10.1155/2016/9380583.

Utomo, A., Baker, M. and Pacek, A. W. (2009) 'The effect of stator geometry on the flow pattern and energy dissipation rate in a rotor-stator mixer', *Chemical Engineering Research and Design*. Elsevier, 87(4), pp. 533–542. doi: 10.1016/j.cherd.2008.12.011.

Valentini, L. *et al.* (2005) 'Sidewall functionalization of single-walled carbon nanotubes through CF4 plasma treatment and subsequent reaction with aliphatic amines', *Chemical Physics Letters*. Elsevier, 403(4–6), pp. 385–389. doi: 10.1016/j.cplett.2005.01.042.

Vallés, C. *et al.* (2016) 'Effect of the C/O ratio in graphene oxide materials on the reinforcement of epoxy-based nanocomposites', *Journal of Polymer Science Part B: Polymer Physics*. John Wiley and Sons Inc., 54(2), pp. 281–291. doi: 10.1002/polb.23925.

Verma, K. K. *et al.* (2014) 'Challenges in Processing of a Cocured Wing Test Box Using Vacuum Enhanced Resin Infusion Technology (VERITy)', *Procedia Materials Science*. Elsevier BV, 6, pp. 331–340. doi: 10.1016/J.MSPRO.2014.07.042.

Vilaverde, C. *et al.* (2015) 'Dispersion and re-agglomeration of graphite nanoplates in polypropylene melts under controlled flow conditions', *Composites Part A: Applied Science and Manufacturing*. Elsevier Ltd, 78, pp. 143–151. doi: 10.1016/j.compositesa.2015.08.010.

Vryonis, O. *et al.* (2019) 'Understanding the cross-linking reactions in highly oxidized graphene/epoxy nanocomposite systems', *Journal of Materials Science*. Springer US, 54(4), pp. 3035–3051. doi: 10.1007/s10853-018-3076-8.

Wan, Y. J. *et al.* (2013) 'Improved dispersion and interface in the graphene/epoxy composites via a facile surfactant-assisted process', *Composites Science and Technology*. Elsevier, 82, pp. 60–68. doi: 10.1016/j.compscitech.2013.04.009.

Wang, G. *et al.* (2016) 'Tuning the Interfacial Mechanical Behaviors of Monolayer Graphene/PMMA Nanocomposites', *ACS Applied Materials and Interfaces*. American Chemical Society, 8(34), pp. 22554–22562. doi: 10.1021/acsami.6b03069.

Wang, X., Jin, J. and Song, M. (2013) 'An investigation of the mechanism of graphene toughening epoxy', *Carbon*, 65, pp. 324–333. doi: 10.1016/j.carbon.2013.08.032.

Wang, Y. T. *et al.* (2012) 'Carboxyl-terminated butadiene-acrylonitrile-toughened epoxy/carboxyl-modified carbon nanotube nanocomposites: Thermal and mechanical properties', *Express Polymer Letters*, 6(9), pp. 719–728. doi: 10.3144/expresspolymlett.2012.77.

Wang, Z., Soutis, C. and Gresil, M. (2021) 'Fracture Toughness of Hybrid Carbon Fibre/Epoxy Enhanced by Graphene and Carbon Nanotubes', *Applied Composite Materials 2021*. Springer, pp. 1–15. doi: 10.1007/S10443-021-09906-X.

Watson, G. *et al.* (2017) 'Tensile and Flexural Properties of Hybrid Graphene Oxide / Epoxy Carbon Fibre Reinforced Composites', *IOP Conference Series: Materials Science and Engineering*, 195(1). doi: 10.1088/1757-899X/195/1/012009.

Wei, D. and Liu, Y. (2010) 'Controllable Synthesis of Graphene and Its Applications', *Advanced Materials*. John Wiley & Sons, Ltd, 22(30), pp. 3225–3241. doi: 10.1002/ADMA.200904144.

Wei, J. *et al.* (2015) 'Graphene Nanoplatelets in Epoxy System: Dispersion, Reaggregation, and Mechanical Properties of Nanocomposites', *Journal of Nanomaterials*, 2015. doi: 10.1155/2015/561742.

Williams, J. *et al.* (2013) ‘Plasma treatment as a method for functionalising and improving dispersion of carbon nanotubes in epoxy resins’, *Journal of Materials Science*, 48(3), pp. 1005–1013. doi: 10.1007/s10853-012-6830-3.

Wu, C. S. (1992) ‘Influence of post-curing and temperature effects on bulk density, glass transition and stress-strain behaviour of imidazole-cured epoxy network’, *Journal of Materials Science*. Kluwer Academic Publishers, 27(11), pp. 2952–2959. doi: 10.1007/BF01154105.

Wypych, G. (2019) *Graphene: Important Results and Applications*. Available at: https://books.google.co.uk/books?id=eQ6LDwAAQBAJ&pg=PA158&lpg=PA158&dq=graphene+stacking+and+agglomeration&source=bl&ots=21_P9bKc-N&sig=ACfU3U0fze_iDpolLYDD-rGcEvL8RPROtg&hl=en&sa=X&ved=2ahUKEwj83sOen7HqAhUEaRUIHSClCZMQ6AEwCHoECAsQAQ#v=onepage&q=graphene stacking and agglomeration&f=false (Accessed: 3 July 2020).

Xia, Z. *et al.* (2016) ‘Electrochemical Functionalization of Graphene at the Nanoscale with Self-Assembling Diazonium Salts’, *ACS Nano*. American Chemical Society, 10(7), pp. 7125–7134. doi: 10.1021/acsnano.6b03278.

Yang, G. *et al.* (2018) ‘Structure of graphene and its disorders: a review’, *Science and Technology of Advanced Materials*. Taylor & Francis, 19(1), pp. 613–648. doi: 10.1080/14686996.2018.1494493.

Yang, S. Y. *et al.* (2011) ‘Synergetic effects of graphene platelets and carbon nanotubes on the mechanical and thermal properties of epoxy composites’, *Carbon*. Pergamon, 49(3), pp. 793–803. doi: 10.1016/j.carbon.2010.10.014.

Yang, Y. *et al.* (2013) ‘Enhancing graphene reinforcing potential in composites by hydrogen passivation induced dispersion’, *Scientific Reports*. Nature Publishing Group, 3(1), pp. 1–7. doi: 10.1038/srep02086.

Ye, S. and Feng, J. (2016) ‘The effect of sonication treatment of graphene oxide on the mechanical properties of the assembled films’, *RSC Advances*. Royal Society of Chemistry, 6(46), pp. 39681–39687. doi: 10.1039/c6ra03996k.

Yi, M. and Shen, Z. (2015a) ‘A review on mechanical exfoliation for the scalable production of graphene’, *Journal of Materials Chemistry A*. Royal Society of Chemistry, pp. 11700–11715. doi: 10.1039/c5ta00252d.

Yi, M. and Shen, Z. (2015b) ‘A review on mechanical exfoliation for the scalable production of graphene’, *Journal of Materials Chemistry A*, pp. 11700–11715. doi: 10.1039/c5ta00252d.

Yoon, H. J., Lee, J. Y. and Yoon, T. H. (2018) ‘Millstone Exfoliation: a True Shear Exfoliation for Large-Size Few-Layer Graphene Oxide’, *Nanoscale Research Letters*. Springer New York LLC, 13(1), p. 186. doi: 10.1186/s11671-018-2598-y.

Young, R. J. *et al.* (2012) ‘The mechanics of graphene nanocomposites: A review’, *Composites Science and Technology*. Elsevier, pp. 1459–1476. doi: 10.1016/j.compscitech.2012.05.005.

Yu, J. W. *et al.* (2016) ‘Enhancement of the crosslink density, glass transition temperature, and strength of epoxy resin by using functionalized graphene oxide co-curing agents’, *Polymer Chemistry*. Royal Society of Chemistry, 7(1), pp. 36–43. doi: 10.1039/c5py01483b.

Yu, S. and Li, S. (2017) ‘Effects of surface-modification on properties of Graphene/Epoxy composites’, in *ICEMPE 2017 - 1st International Conference on Electrical Materials and Power Equipment*. Institute of Electrical and Electronics Engineers Inc., pp. 490–493. doi: 10.1109/ICEMPE.2017.7982136.

Zaaba, N. I. *et al.* (2017) ‘Synthesis of Graphene Oxide using Modified Hummers Method: Solvent

Influence’, *Procedia Engineering*. Elsevier, 184, pp. 469–477. doi: 10.1016/J.PROENG.2017.04.118.

Zaman, I. *et al.* (2011) ‘Epoxy/graphene platelets nanocomposites with two levels of interface strength’, *Polymer*. Elsevier Ltd, 52(7), pp. 1603–1611. doi: 10.1016/j.polymer.2011.02.003.

Zambonin, P. G. and Desimoni, E. (1987) ‘X-Ray Photoelectron Spectroscopy: Principles, Instrumentation, Data Processing and Molten Salt Applications’, in *Molten Salt Chemistry*. Springer Netherlands, pp. 425–445. doi: 10.1007/978-94-009-3863-2_21.

Zhang, B. and Chen, T. (2019) ‘Study of Ultrasonic Dispersion of Graphene Nanoplatelets’, *Materials*. MDPI AG, 12(11), p. 1757. doi: 10.3390/ma12111757.

Zhang, X., Huang, Y. and Liu, P. (2016) ‘Enhanced Electromagnetic Wave Absorption Properties of Poly(3,4-ethylenedioxythiophene) Nanofiber-Decorated Graphene Sheets by Non-covalent Interactions’, *Nano-Micro Letters*. SpringerOpen, 8(2), pp. 131–136. doi: 10.1007/s40820-015-0067-z.

Zhang, X. and Loo, L. S. (2009) ‘Study of glass transition and reinforcement mechanism in polymer/layered silicate nanocomposites’, *Macromolecules*. American Chemical Society, 42(14), pp. 5196–5207. doi: 10.1021/ma9004154.

Zhang, Y. Y. *et al.* (2011) ‘Mechanical properties of bilayer graphene sheets coupled by sp3 bonding’, *Carbon*. Pergamon, 49(13), pp. 4511–4517. doi: 10.1016/j.carbon.2011.06.058.

Zhou, J. *et al.* (2011) ‘Magnetite/graphene nanosheet composites: Interfacial interaction and its impact on the durable high-rate performance in lithium-ion batteries’, *RSC Advances*. Royal Society of Chemistry, 1(5), pp. 782–791. doi: 10.1039/c1ra00402f.